INNATE IMMUNITY PATHWAYS IN AUTOIMMUNE DISEASES

EDITED BY: Moncef Zouali and Antonio La Cava
PUBLISHED IN: Frontiers in Immunology

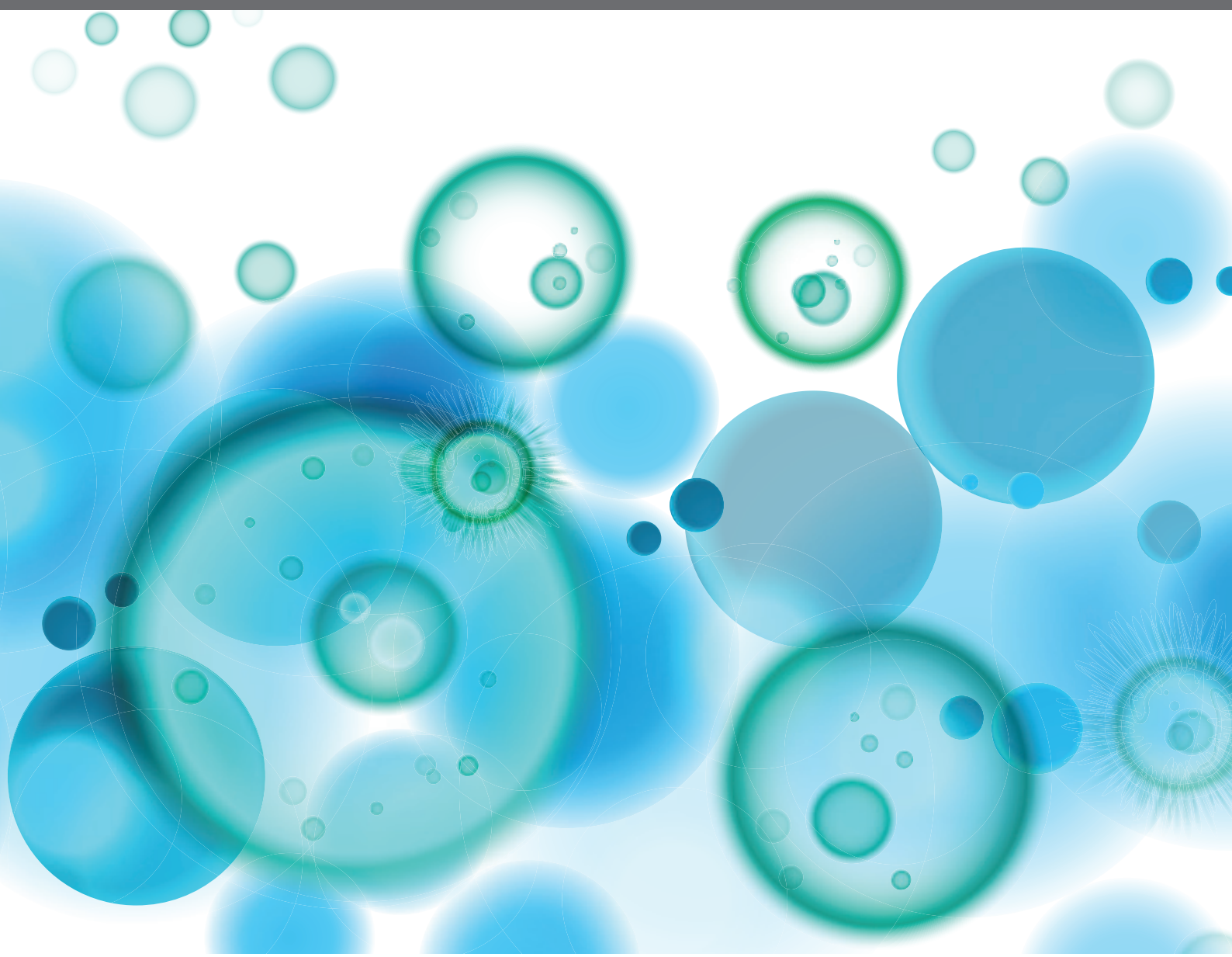

frontiers Research Topics

frontiers

ISSN 1664-8714
ISBN 978-2-88963-236-7
DOI 10.3389/978-2-88963-236-7

About Frontiers

Frontiers is more than just an open-access publisher of scholarly articles: it is a pioneering approach to the world of academia, radically improving the way scholarly research is managed. The grand vision of Frontiers is a world where all people have an equal opportunity to seek, share and generate knowledge. Frontiers provides immediate and permanent online open access to all its publications, but this alone is not enough to realize our grand goals.

Frontiers Journal Series

The Frontiers Journal Series is a multi-tier and interdisciplinary set of open-access, online journals, promising a paradigm shift from the current review, selection and dissemination processes in academic publishing. All Frontiers journals are driven by researchers for researchers; therefore, they constitute a service to the scholarly community. At the same time, the Frontiers Journal Series operates on a revolutionary invention, the tiered publishing system, initially addressing specific communities of scholars, and gradually climbing up to broader public understanding, thus serving the interests of the lay society, too.

Dedication to Quality

Each Frontiers article is a landmark of the highest quality, thanks to genuinely collaborative interactions between authors and review editors, who include some of the world's best academicians. Research must be certified by peers before entering a stream of knowledge that may eventually reach the public - and shape society; therefore, Frontiers only applies the most rigorous and unbiased reviews.
Frontiers revolutionizes research publishing by freely delivering the most outstanding research, evaluated with no bias from both the academic and social point of view. By applying the most advanced information technologies, Frontiers is catapulting scholarly publishing into a new generation.

What are Frontiers Research Topics?

Frontiers Research Topics are very popular trademarks of the Frontiers Journals Series: they are collections of at least ten articles, all centered on a particular subject. With their unique mix of varied contributions from Original Research to Review Articles, Frontiers Research Topics unify the most influential researchers, the latest key findings and historical advances in a hot research area! Find out more on how to host your own Frontiers Research Topic or contribute to one as an author by contacting the Frontiers Editorial Office: researchtopics@frontiersin.org

INNATE IMMUNITY PATHWAYS IN AUTOIMMUNE DISEASES

Topic Editors:
Moncef Zouali, Institut National de la Santé et de la Recherche Médicale (INSERM), France
Antonio La Cava, University of California, Los Angeles, United States

Citation: Zouali, M., La Cava, A., eds. (2019). Innate Immunity Pathways in Autoimmune Diseases. Lausanne: Frontiers Media SA.
doi: 10.3389/978-2-88963-236-7

Table of Contents

frontiers in Immunology

EDITORIAL
published: 04 June 2019
doi: 10.3389/fimmu.2019.01245

Editorial: Innate Immunity Pathways in Autoimmune Diseases

Moncef Zouali[1]* *and Antonio La Cava*[2]

[1] Graduate Institute of Biomedical Sciences, China Medical University, Taichung City, Taiwan, [2] Department of Medicine, University of California, Los Angeles, Los Angeles, CA, United States

Keywords: toll-like receptor, dendritic cells, innate-like B cells, extracellular vesicle, semaphorin, lupus, arthritis, calcium-dependent peptidyl-arginine deiminase

Editorial on the Research Topic

Innate Immunity Pathways in Autoimmune Diseases

The immune system has evolved to protect the organism against infectious threats and to prevent the emergence of tumors, while preserving homeostatic immune integrity. Moreover, to avoid destruction of its own tissues, the immune system undergoes developmentally ordered processes that create the basis of immune tolerance to self. Autoimmune diseases develop when regulatory mechanisms of self-tolerance become impaired and/or deregulated.

Since immune tolerance is not innate, but is established during fetal life and postnatal development through an array of sophisticated mechanisms, unraveling the pathways that underlie the generation of pathogenic autoimmune reactions has typically focused on the adaptive branch of the immune system. Recently, however, it has been demonstrated that innate immunity can also play important roles in the initiation and/or progression of autoimmune disease. This Research Topic provides discussions of how innate immunity influences autoimmune diseases.

INNATE-LIKE B CELLS AND AUTOIMMUNITY

The role of B-lymphocytes was initially believed to be limited to immunoglobulin secretion. With further study, it became evident that B-cells also engage in the innate branch of the immune system and can modulate the activity of other cell populations. As reviewed in this Research Topic, it is possible that targeting certain innate-like B cell subsets could represent a novel therapeutic approach for inducing resolution of inflammation of autoimmune and inflammatory responses Tsay and Zouali.

IMMUNE CELL-DERIVED EXTRACELLULAR VESICLES

Virtually all cell types release nano- to micro-scale membrane-enclosed vesicles, termed extracellular vesicles (EVs). Their potential to mediate intercellular communications is triggering intense research in a variety of disciplines. In this Research Topic, immune cell-derived EVs are shown to efficiently shuttle a TLR3 ligand to synovial fibroblasts and to potentially activate proinflammatory responses, suggesting their involvement in the pathogenicity of rheumatoid arthritis (RA) Frank-Bertoncelj et al. Interestingly, investigations into an experimental model of primary progressive multiple sclerosis support their potential therapeutic usefulness (1).

OPEN ACCESS

Edited and reviewed by:
Francesca Granucci,
University of Milano-Bicocca, Italy

***Correspondence:**
Moncef Zouali
moncef.zouali@wanadoo.fr

Specialty section:
This article was submitted to Molecular Innate Immunity, a section of the journal Frontiers in Immunology

Received: *11 April 2019*
Accepted: *16 May 2019*
Published: *04 June 2019*

Citation:
Zouali M and La Cava A (2019) Editorial: Innate Immunity Pathways in Autoimmune Diseases. Front. Immunol. 10:1245. doi: 10.3389/fimmu.2019.01245

OVERCOMING PLASMACYTOID DENDRITIC CELL IMMUNE TOLERANCE

Plasmacytoid dendritic cells (pDCs) are key actors in antiviral and antitumor immunity. This highly specialized cell subset plays a central role at the interface of innate and adaptive immunity through secretion of type I interferons (IFNs) and expression of TLRs, but also receptors involved in preventing abnormal immune responses. Crosslinking of these regulatory receptors could therefore efficiently suppress abnormal cytokine production. Accordingly, studies reported in this Research Topic indicate that pharmacological targeting of MEK1/2-ERK signaling could be a strategy to overcome immune tolerance of pDCs and re-establish their immunogenic activity Janovec et al. However, as discussed in this Research Topic, the increased expression of type I IFNs-regulated genes (the so-called "type I IFN signature") in RA patients could be heterogeneous and dependent on the clinical stage of the disease Rodriguez-Carrio et al. This observation suggests that clinical and therapeutic considerations have to be tailored according to the autoimmune patient's characteristics rather than to the disease itself.

MODULATING FUNCTIONAL PROPERTIES OF TLR FOR THERAPEUTIC PURPOSES

Homo- or hetero-dimerization of TLRs can be induced by agonist binding, which can lead to lateral translocation in the membrane until the recruitment of downstream adaptors. As discussed in this Research Topic, identification of TLR micro-domains that participate in membrane association and orientation of individual domains could be targeted using novel activators or inhibitors to modulate TLR functional properties and reach the desired therapeutic effects Patra et al.

CHRONOTHERAPEUTIC TARGETING OF TLRS IN AUTOIMMUNITY

In responses to drugs, genome-wide association studies are used to map and characterize genes that contribute to inter-individual variability. While, our understanding of how particular genes determine the dynamics of drug effects remains incomplete, chronotherapy aims to design schedules of drug intake based on circadian biorhythms, cyclic production of factors, and receptor expression on target cells (2). This Research Topic presents information that could be useful to design clinical studies aiming to achieve chronotherapeutic HCQ effects and to reduce the pathological consequence of TLR9 activation Martinez-Garcia et al.

EPIGENETIC INSUFFICIENCY IN AN AUTO-INFLAMMATORY MILIEU

In autoimmune diseases, gene expression based solely on DNA sequence alterations and/or mutations is not sufficient to explain the variety of clinical manifestations observed, indicating that epigenetic deregulation contributes to the severity of these disorders. For example, there is an altered expression of Dicer1 (an endoribonuclease involved in the maturation of small non-coding RNAs such as microRNAs) in experimental mice (3), and β-cell specific disruption of Dicer1 leads to progressive impairment of insulin secretion and development of diabetes mellitus (4). As discussed in this Research Topic, reduced Dicer1 expression could contribute to a vicious cycle during which inflammation, together with inappropriate innate immunity responses, would create appropriate conditions for the initiation and/or progression of autoinflammatory diseases De Cauwer et al.

ENDOGENOUS REGULATORS OF THE INFLAMMATORY RESPONSE

Semaphorins comprise secreted and membrane-bound proteins endowed with immunomodulatory functions. Their potential relevance to autoimmune diseases comes from animal studies. For example, Semaphorin-3A (Sema3A) has beneficial therapeutic effects in a mouse model of RA. As discussed in this Research Topic, Sema3A was also efficient in both treating and preventing glomerular damage in a lupus mouse model Bejar et al. At present, its potential therapeutic usefulness remains uncertain because it can also induce autoimmune disease when overexpressed (5).

Other regulators of inflammatory responses are the calcium-dependent peptidyl-arginine deiminases (PADs) that citrullinate extracellular proteins during inflammation. In this Research Topic, active extracellular PADs are shown to play an important role in RA, a disease where affected joints have high levels of protein citrullination and autoantibodies against citrullinated proteins are important for its diagnosis Zhou et al.

Cytokines, such as IL-15, could represent new targets of innate immune response regulation, considering that its over-expression is shown in this Research Topic to reduce complement-dependent cytotoxicity and astrocyte loss in a mouse model of neuromyelitis optica Li et al.

CONCLUSIONS

Mounting evidence has convincingly demonstrated that innate immune responses play a critical role in the initiation, progression, and maintenance of autoimmune disease. This Research Topic provides multiple examples of how different innate immunity components can contribute to the inflammatory processes that precede, underlie, and accompany the clinical manifestations of autoimmune disease. Further investigations have the potential to unveil new targets of therapeutic intervention that might ultimately lead to improved diagnosis, management, and outcomes in autoimmune disease patients.

AUTHOR CONTRIBUTIONS

All authors listed have made a substantial, direct and intellectual contribution to the work, and approved it for publication.

FUNDING

MZ is supported by a Senior Jade Mountain Award (Ministry of Education, Taiwan).

ACKNOWLEDGMENTS

We would like to thank all authors for their contributions to this Research Topic.

REFERENCES

1. Laso-Garcia F, Ramos-Cejudo J, Carrillo-Salinas FJ, Otero-Ortega L, Feliu A, Gomez-de Frutos M, et al. Therapeutic potential of extracellular vesicles derived from human mesenchymal stem cells in a model of progressive multiple sclerosis. *PLoS ONE.* (2018) 13:e0202590. doi: 10.1371/journal.pone.0202590
2. Wei K, Wang Q, Gan J, Zhang S, Ye M, Gragnoli C, et al. Mapping genes for drug chronotherapy. *Drug Discov Today.* (2018) 23:1883–8. doi: 10.1016/j.drudis.2018.06.011
3. Divekar AA, Dubey S, Gangalum PR, Singh RR. Dicer insufficiency and microRNA-155 overexpression in lupus regulatory T cells: an apparent paradox in the setting of an inflammatory milieu. *J Immunol.* (2011) 186:924–30. doi: 10.4049/jimmunol.1002218
4. Kalis M, Bolmeson C, Esguerra JL, Gupta S, Edlund A, Tormo-Badia N, et al. Beta-cell specific deletion of Dicer1 leads todefective insulin secretion and diabetes mellitus. *PLoS ONE.* (2011) 6:e29166. doi: 10.1371/journal.pone.0029166
5. Liu LN, Li XM, Ye DQ, Pan HF. Emerging role of semaphorin-3A in autoimmune diseases. *Inflammopharmacology.* (2018) 26:655–65. doi: 10.1007/s10787-018-0484-y

Conflict of Interest Statement: The authors declare that the research was conducted in the absence of any commercial or financial relationships that could be construed as a potential conflict of interest.

frontiers in Immunology

ORIGINAL RESEARCH
published: 25 September 2017
doi: 10.3389/fimmu.2017.01200

Spontaneous Secretion of the Citrullination Enzyme PAD2 and Cell Surface Exposure of PAD4 by Neutrophils

*Yebin Zhou[1†], Bo Chen[1†], Nanette Mittereder[1], Raghothama Chaerkady[2], Martin Strain[3], Ling-Ling An[1], Saifur Rahman[1], Wenting Ma[1], Choon Pei Low[3], Denice Chan[3], Frances Neal[3], Clifton O. Bingham III[4], Kevon Sampson[4], Erika Darrah[4], Richard M. Siegel[5], Sarfaraz Hasni[6], Felipe Andrade[4], Katherine A. Vousden[3], Tomas Mustelin[1] and Gary P. Sims[1]**

[1] Department of Respiratory, Inflammation, and Autoimmunity, MedImmune LLC, Gaithersburg, MD, United States, [2] Antibody Discovery and Protein Engineering, MedImmune LLC., Gaithersburg, MD, United States, [3] Antibody Discovery and Protein Engineering, MedImmune LTD., Cambridge, United Kingdom, [4] Division of Rheumatology, Department of Medicine, School of Medicine, Johns Hopkins University, Baltimore, MD, United States, [5] Immunoregulation Section, Autoimmunity Branch, National Institute of Arthritis and Musculoskeletal and Skin Diseases (NIAMS), NIH, Bethesda, MD, United States, [6] Office of the Clinical Director, National Institute of Arthritis and Musculoskeletal and Skin Diseases (NIAMS), NIH, Bethesda, MD, United States

Autoantibodies directed against citrullinated epitopes of proteins are highly diagnostic of rheumatoid arthritis (RA), and elevated levels of protein citrullination can be found in the joints of patients with RA. Calcium-dependent peptidyl-arginine deiminases (PAD) are the enzymes responsible for citrullination. PAD2 and PAD4 are enriched in neutrophils and likely drive citrullination under inflammatory conditions. PADs may be released during NETosis or cell death, but the mechanisms responsible for PAD activity under physiological conditions have not been fully elucidated. To understand how PADs citrullinate extracellular proteins, we investigated the cellular localization and activity of PAD2 and PAD4, and we report that viable neutrophils from healthy donors have active PAD4 exposed on their surface and spontaneously secrete PAD2. Neutrophil activation by some stimulatory agents increased the levels of immunoreactive PAD4 on the cell surface, and some stimuli reduced PAD2 secretion. Our data indicate that live neutrophils have the inherent capacity to express active extracellular PADs. These novel pathways are distinguished from intracellular PAD activation during NETosis and calcium influx-mediated hypercitrullination. Our study implies that extracellular PADs may have a physiological role under non-pathogenic conditions as well as a pathological role in RA.

Keywords: neutrophil, citrullination, PAD2, PAD4, rheumatoid arthritis

OPEN ACCESS

Edited by:
Antonio La Cava, University of California, Los Angeles, United States

Reviewed by:
Elmar Pieterse, Radboud University Nijmegen Medical Center, Netherlands
Indira Neeli, University of Tennessee Health Science Center, United States

***Correspondence:**
Gary P. Sims
simsg@medimmune.com

†These authors have contributed equally to this work.

Specialty section:
This article was submitted to Molecular Innate Immunity, a section of the journal Frontiers in Immunology

Received: *28 July 2017*
Accepted: *11 September 2017*
Published: *25 September 2017*

Citation:
Zhou Y, Chen B, Mittereder N, Chaerkady R, Strain M, An L-L, Rahman S, Ma W, Low CP, Chan D, Neal F, Bingham CO III, Sampson K, Darrah E, Siegel RM, Hasni S, Andrade F, Vousden KA, Mustelin T and Sims GP (2017) Spontaneous Secretion of the Citrullination Enzyme PAD2 and Cell Surface Exposure of PAD4 by Neutrophils. Front. Immunol. 8:1200. doi: 10.3389/fimmu.2017.01200

INTRODUCTION

Protein citrullination is the process by which the basic amino acid residue arginine is converted into the neutral residue citrulline. This reaction is catalyzed by the calcium-dependent enzyme peptidyl-arginine deiminase (PAD), of which there are five isozymes (PAD1-4 and PAD6) encoded by distinct genes in the human genome (1). These enzymes are involved in various physiological

processes, including skin cornification, myelin sheath maintenance, and gene expression regulation (2, 3). Abnormal protein citrullination has been implicated in the pathogenesis of multiple sclerosis (4, 5), psoriasis (6), Alzheimer's disease (7), and cancer (8–10), but it has been examined predominately in the context of rheumatoid arthritis (RA).

Autoantibodies targeting citrullinated proteins are found in approximately 70% of RA patients, and their presence is highly diagnostic for the disease (11–13). PAD activity has been detected in the synovial fluid (14), and citrullinated proteins are also prominent in the synovium of some RA patients (15–19). The roles of PADs and their enzymatic activity in RA is supported by genetic evidence which has shown that PAD2 and PAD4 SNPs are associated with RA susceptibility (20–22), and the RA-associated HLA-DRB1 susceptibility alleles have been shown to present citrullinated antigens more efficiently (23). Neutrophils express high levels of PAD2 and PAD4 (24, 25) and are likely to be important in protein citrullination in the joints of patients with RA where they are abundant (26).

The process by which proteins become citrullinated in RA remains unclear. The profile of citrullinated proteins in the joint suggests that citrullination takes place both intracellularly and extracellularly. In excess of 100 citrullinated proteins have been identified in the synovial fluid which includes several neutrophil-associated intracellular proteins, as well as extracellular matrix proteins and serum proteins such as immunoglobulin, fibrinogen, complement, and albumin (16, 19).

Intracellular citrullination may occur as part of the physiological function of PADs and has been best studied for PAD4. PAD4 is the only member of the PAD enzyme family with a nuclear localization sequence, and its enzymatic activity is believed to impact gene expression by directly citrullinating transcription factors (27, 28) or by regulating histones (29, 30). Histone citrullination mediated by PAD4 has also been implicated in the formation of neutrophil extracellular traps (NETs) under some conditions (31–34), a process important in protection against infection but dysregulated in several autoimmune diseases (35–37). A recent study further identified that PAD inhibition could impact neutrophil cytokine production by regulating NF-κB p65 nuclear translocation (38). How citrullination is initiated intracellularly under physiological conditions remains uncertain as all PADs require millimolar calcium levels to be active. Such high levels of calcium are not found intracellularly unless the cell membrane is compromised. For example, a massive influx of calcium into cells can be triggered by the membrane attack complex of complement, perforin, bacteria toxins, or calcium ionophores (24, 39, 40), leading to the citrullination of numerous intracellular proteins in a process referred to as "leukotoxic hypercitrullination" (41). Evidence of leukotoxic hypercitrullination has been detected in synovial fluid from some patients with RA (24), but is unlikely to occur under normal physiological conditions.

The source of PAD responsible for the citrullination of extracellular proteins also remains unclear. In this case, serum, and to a lesser extent synovial fluid, contain levels of free calcium ions sufficient for PAD activity (14). However, since PADs lack transmembrane regions or secretory signal sequences, PAD expression and function was predicted to be intracellularly restricted (1). PADs may be released from neutrophils undergoing NETosis or from damaged or dying cells (42).

We aim to identify the source and circumstances necessary for PAD activity, which may help to understand the processes leading to the excessive protein citrullination and generation of neoepitopes in RA, and may provide further insight into the normal physiological roles of PAD enzymes. In this study, we investigated the cellular localization and activity of PADs in viable neutrophils in culture with and without stimuli associated with autoimmune conditions. Interestingly, we demonstrate that catalytically active PAD4 is expressed on the cell surface of viable human neutrophils, and active PAD2 is released into the culture media from neutrophils of healthy donors without stimulation. These findings identify novel mechanisms of extracellular protein citrullination that occur in the absence of neutrophil apoptosis, necrosis, or NETosis. These mechanisms are distinct from the hypercitrullination reaction triggered by massive calcium influx into neutrophils. Furthermore, our findings provide a new avenue for studies to clarify the role of citrullination in normal neutrophil physiology and disease pathogenesis.

RESULTS

Immunofluorescence Microscopy Analysis Reveals Granular Staining Patterns of PAD2/4 Expression within Neutrophils

Previous studies identified nuclear localization of PAD4 in neutrophils (43). We used a slightly different fixation and permeabilization method to stain neutrophils from healthy donors with four different anti-PAD4 antibodies, followed by immunofluorescence microscopy. All anti-PAD4 antibodies resulted in a similar mainly cytosolic, granular staining (**Figure 1A**). Some staining appeared to be associated with the plasma membrane, and some had a perinuclear distribution. Under our staining conditions, less nuclear PAD4 staining was evident than previously reported (43).

Antibodies against PAD2 produced a similar granular staining of neutrophils (**Figure 1B**), but no PAD2 was detected within the nucleus. The specificity of the antibodies was confirmed by preincubation with recombinant PADs prior to staining. These findings suggest that PAD2 and PAD4 are not freely soluble cytosolic proteins, but are largely associated with internal structures in the neutrophils.

Detection of PAD4 but Not PAD2 on the Surface of Neutrophils

Since some of the cytosolic PAD2 and PAD4 staining appeared very close to the plasma membrane, we tested whether these proteins could be detected on the neutrophil surface in the absence of permeabilization. Indeed, a punctate signal was observed for PAD4 (**Figure 2A**) but not for PAD2 (data not shown). Some of the staining appeared to be intracellular, suggesting that surface-exposed PAD4 may be internalized during incubation.

We further confirmed the apparent surface exposure of a fraction of cellular PAD4 in flow cytometric analyses of unfixed human neutrophils isolated from fresh blood samples obtained from

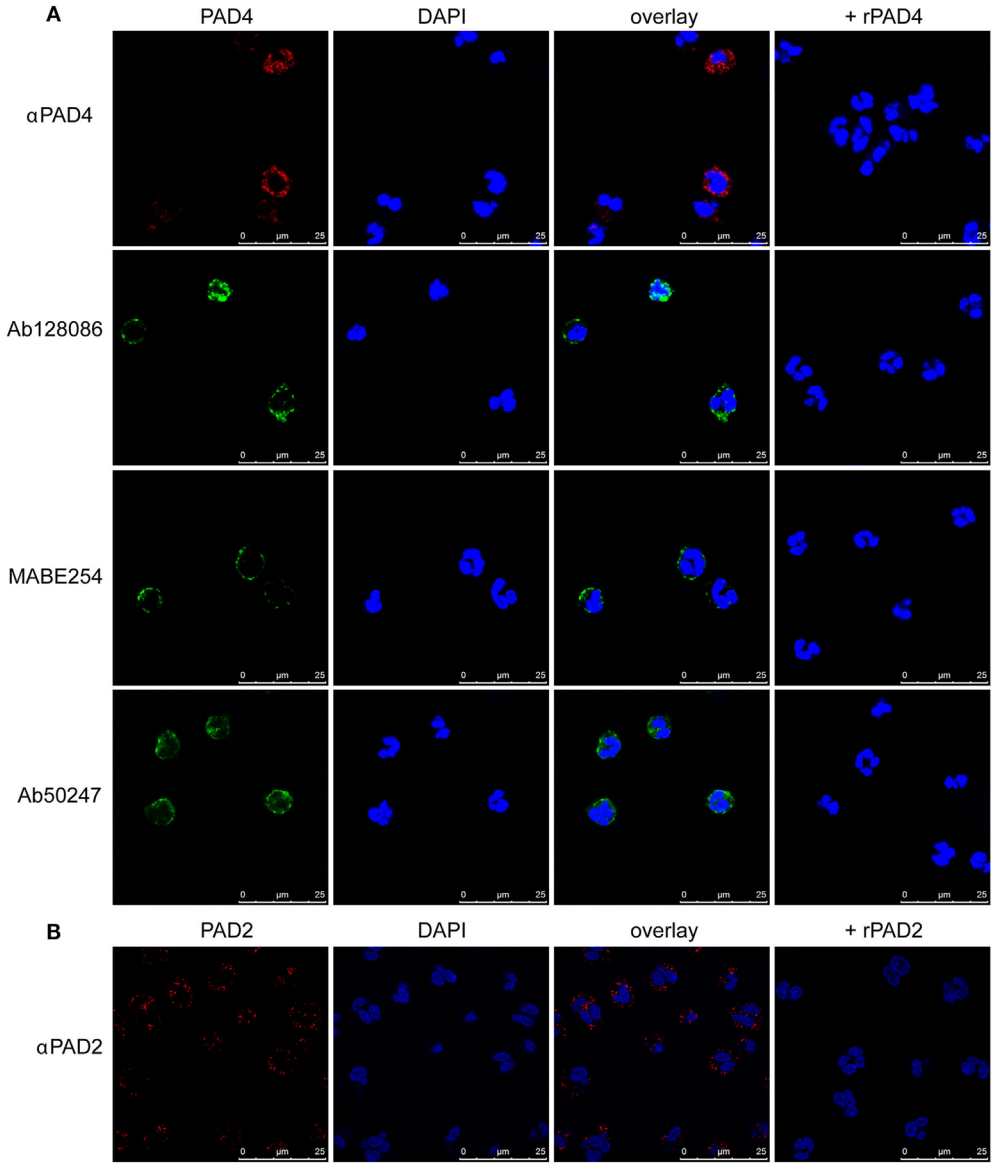

FIGURE 1 | Immunofluorescence staining of PAD4 and PAD2 in resting neutrophils. Staining of permeabilized neutrophils with four different anti-PAD4 antibodies as indicated in panel **(A)** or PAD2 antibody in panel **(B)**. DAPI staining was used to identify nuclear DNA. In parallel samples, recombinant PAD2 or PAD4 were preincubated with antibodies prior to cell staining. Results are representative of three different healthy donors.

healthy volunteers. Analysis was gated on live intact neutrophils with DAPI exclusion to avoid any detection of intracellular PAD in dead or broken cells (negative annexin V gating showed similar results). Clear surface staining was seen with the anti-PAD4 antibody, which was unaffected by preincubation with recombinant PAD2 but abolished by preincubation with recombinant PAD4 (**Figures 2B,C**). These findings were confirmed in cells from five different donors, although there was some variation in surface PAD4 levels between donors. In contrast, negligible staining with anti-PAD2 antibodies (**Figures 2D,E**) was seen in cells from the same donors. Surface expression of PAD4 on neutrophils was also verified using ImageStream, which captures fluorescence images of individual cells during flow cytometry (Figures S1A,B in Supplementary Material). Confocal imaging of CD16 and PAD4 co-staining further confirmed the cell membrane location of PAD4 (Figure S2 in Supplementary Material).

To evaluate whether soluble PAD4 (e.g., released from dying cells) could bind to the surface of live neutrophils, we incubated neutrophils with 100 μg/ml of recombinant human PAD4, washed the cells several times, and stained them for PAD4. Analysis of these cells by flow cytometry did not reveal any increase in staining compared with cells treated with medium alone (data not shown), indicating that neutrophils do not bind soluble PAD4. Neutrophils could potentially be damaged or activated during the isolation process. To further rule out exposure of the antibody to intracellular PAD4 and test if PAD4 was expressed in other

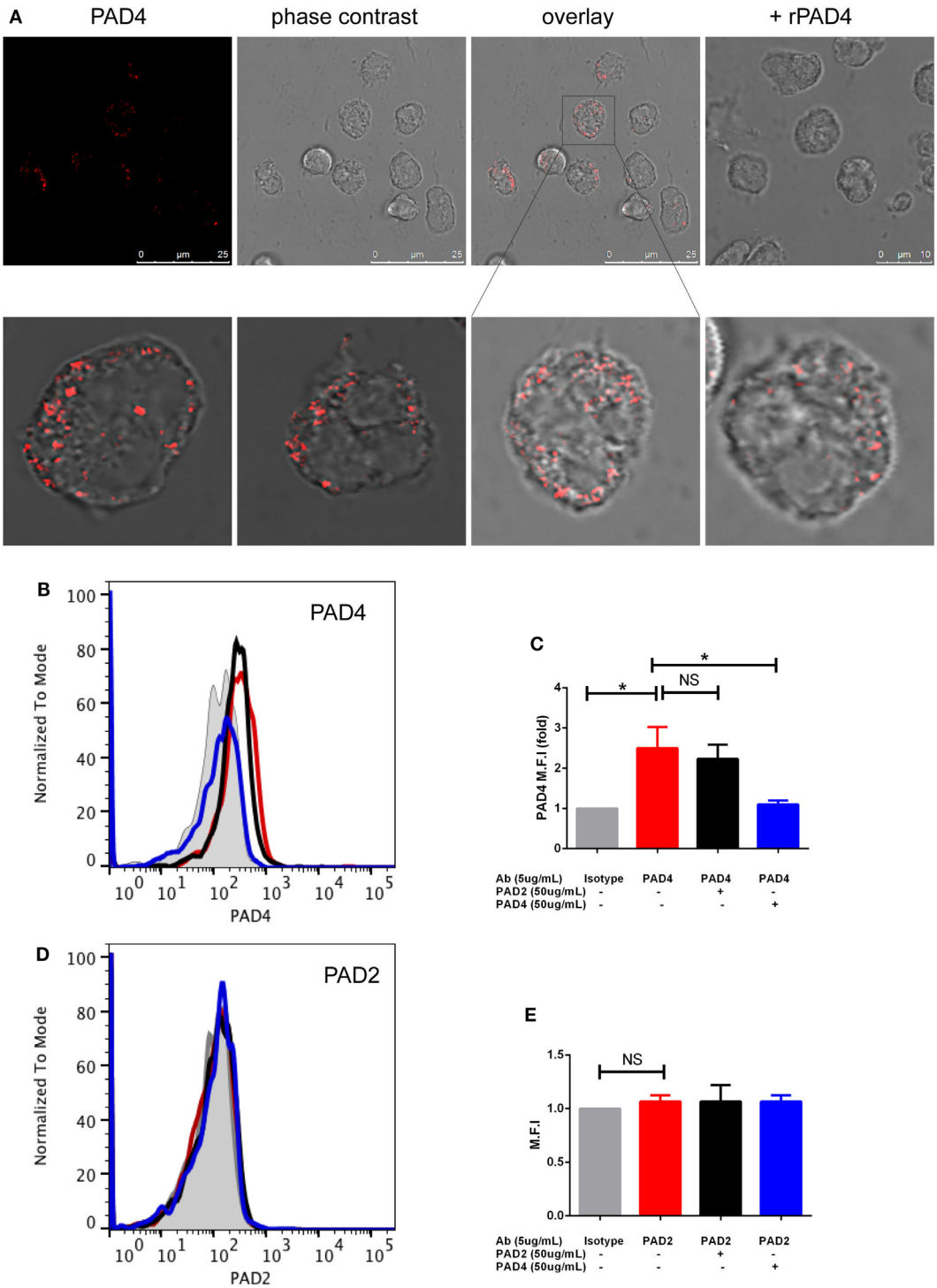

FIGURE 2 | Immunofluorescence and flow cytometric analysis of PAD4 and PAD2 in non-permeabilized neutrophils. **(A)** (Upper panels) Panel 1: staining of non-permeabilized neutrophils with an anti-PAD4 antibody; panel 2: phase-contrast image of panel 1; panel 3: overlay of anti-PAD4 staining and the phase-contrast image; panel 4: a parallel sample stained with anti-PAD4 incubated with recombinant PAD4 prior to cell staining. (Lower panels) Panels 1, 2, and 4: several different fields of anti-PAD4 staining overlaid with phase-contrast images; panel 3: magnified portion of the image above. **(B)** Flow cytometry of non-permeabilized neutrophils using an isotype-matched control antibody (gray shading), anti-PAD4 (red line), anti-PAD4 preincubated with recombinant PAD2 (black line), or anti-PAD4 preincubated with recombinant PAD4 (blue line). **(C)** Quantification of the mean fluorescence intensity (MFI) from the analysis of five separate donors analyzed as described in panel **(B)**. **(D)** Similar experiment conducted with anti-PAD2 antibodies. **(E)** Quantification of the MFI from the analysis of five separate donors analyzed as described in **(D)**. Data were analyzed by paired *t*-test (*$p < 0.05$, $^{ns}p > 0.05$).

leukocytes, we directly stained whole blood, which circumvents the need to isolate neutrophils. It is noteworthy that the relative increase in mean fluorescence intensity (MFI) with PAD4 staining was similar whether the staining was performed with whole blood or isolated neutrophils from the same donor. By gating on other leukocyte populations within the whole blood stained samples, we observed some PAD4 reactivity on monocytes, but not on NK cells, B cells, T cells, or platelets (Figure S1C in Supplementary Material). Surface staining of PAD2 was not detected on any cells of the leukocyte lineage.

Taken together, these results suggest that PAD4 but not PAD2 was expressed on the surface of viable resting neutrophils and monocytes.

Regulation of Surface PAD4 Expression during Neutrophil Activation

To simulate conditions that occur during inflammation, infection, and autoimmune conditions, we stimulated neutrophils and looked for changes in the cell surface expression of PAD4. Neutrophils were stimulated for 15 min, and live cells were gated on the basis of DAPI exclusion. PAD4 expression was determined with fluorescently labeled antibodies. Treatment of neutrophils with ribonucleoprotein immune complexes (RNP-IC) resulted in a dose-dependent induction of PAD4 expression on the surface of neutrophils from three different donors (**Figure 3A**), with a maximum induction associated with an eightfold increase in MFI. Similarly, stimulation with TNF-α induced a significant elevation in surface PAD4 expression (**Figure 3B**), as did stimulation with PMA (**Figure 3C**), the TLR5 agonist flagellin (**Figure 3D**), and the TLR6/2 agonist FSL-1 (**Figure 3E**). In contrast, IL-8 did not cause any change in surface PAD4 levels (**Figure 3F**). Additional stimuli, such as heat-killed *Listeria monocytogenes* (a TLR2 agonist), the TLR7 agonist imiquimod, the TLR8 agonist ss40RNA, immune complexes (IC) without nucleic acids, and GM-CSF, also induced upregulation of surface PAD4 levels, whereas formylpeptide, PAM3 (TLR1/2 agonist), and lipopolysaccharide (LPS) (TLR4 agonist) caused small increases that were not statistically significant (data not shown). Stimulation with IL-6 did not cause any changes in PAD4 expression on the surface of neutrophils from any of the three donors (data not shown). To rule out the possibility that surface expression of PAD4 only increased as a consequence of the induction of NETosis, the NETosis inhibitor DPI was used in conjunction with various stimuli. DPI had no effect on the upregulation of PAD4 surface expression induced by RNP-IC, PMA, or TNF-α (Figure S3 in Supplementary Material). We conclude that a number of physiologically relevant activators of neutrophils caused a significant increase in surface PAD4 levels on human neutrophils, whereas others did not.

PAD4 Surface Expression on Neutrophils from RA and SLE Patients

Since several surface PAD4-increasing stimuli are elevated in the serum of patients with RA or SLE (e.g., TNF-α, GM-CSF, IC), we hypothesize that surface PAD4 could be upregulated in those patients. Thus, we examined the surface expression of PAD4 on neutrophils and monocytes in fresh whole blood samples from patients with RA, patients with SLE, and healthy donors. Surface PAD4 expression was detected on neutrophils and monocytes from RA patients at levels very similar to those of the healthy donors (**Figures 4A,B**). Surface PAD4 was also detected on neutrophils in patients with SLE, but, similar to patients with RA, there was no difference compared with the levels detected from healthy donors (**Figure 4C**). These results suggested that surface PAD4 expression were similar in peripheral blood leukocytes between patients with RA or SLE and healthy donors.

Extracellular Fibrinogen Citrullination by Neutrophils from Healthy Donors

To determine whether the PAD4 detected on the surface of intact neutrophils was catalytically active, we incubated freshly isolated neutrophils with a well-known substrate for citrullination, fibrinogen, and used an anti-citrullinated fibrinogen monoclonal antibody (mAb) to detect its citrullination. The anti-citrullinated fibrinogen mAb did not react with native fibrinogen, whereas a brief incubation of fibrinogen with active recombinant human PAD2 or PAD4 resulted in a strong recognition of fibrinogen β-chain citrullination (**Figure 5A**, lane 9). Fibrinogen citrullination by recombinant PAD4 was also confirmed by mass spectrometry analysis (Table S1 in Supplementary Material).

When freshly isolated neutrophils were incubated with fibrinogen, this protein became reactive with the anti-citrullinated fibrinogen mAbs (**Figure 5A**). Citrullination was time-dependent, detectable within 1 h, and increased through at least 4 h. Fibrinogen citrullination had an absolute requirement for extracellular calcium and was blocked by chelation with either EDTA or EGTA (**Figure 5A**, lane 11), thus providing further evidence of extracellular fibrinogen citrullination. Neutrophil-conditioned media was also able to citrullinate fibrinogen (**Figure 5A**, lane 10). Equal loading of fibrinogen was confirmed by Coomassie staining (**Figure 5A**, lower panel). Citrullination of the fibrinogen β-chain and additional citrullination sites in the α- and γ-chains in the presence of live neutrophils was also confirmed by mass spectrometry analysis (Table S2 in Supplementary Material).

To exclude the possibility that a few dead or broken neutrophils could be the source of PAD activity, we evaluated levels of the intracellular protein GAPDH in the neutrophil-conditioned media by western blotting. Although GAPDH was not detected up to 4 h after initiation of the culture, disruption of neutrophils by treatment with 0.005% Triton X-100 resulted in some GAPDH release at 4 h (**Figure 5B**). Furthermore, necrotic or apoptotic cells were not detected by DAPI staining until four or more hours after Triton X-100 treatment, suggesting good neutrophil viability and integrity under our experimental conditions.

Citrullination of Extracellular Histone H3 by PAD4 Expressed on the Surface of Neutrophils

To confirm the activity of PAD4 on the surface of neutrophils, we developed an alternative PAD activity assay using histone H3 as a substrate. As histones are readily citrullinated by PAD4 both *in vitro* and *in vivo* (25), we incubated freshly isolated human neutrophils with recombinant histone H3 and detected

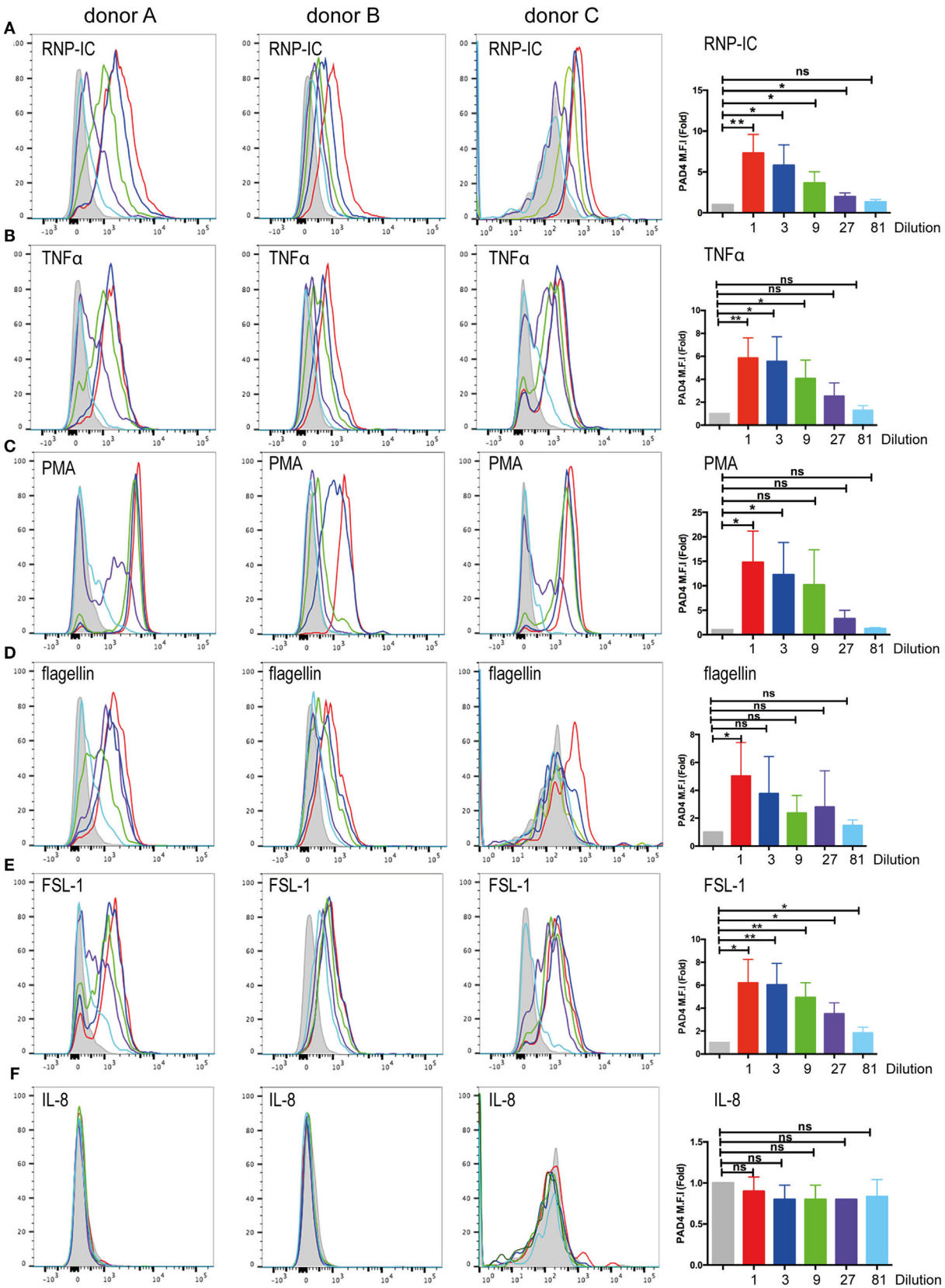

FIGURE 3 | Continued

FIGURE 3 | Continued
Flow cytometric analysis of surface PAD4 expression by stimulated neutrophils obtained from healthy donors. Flow cytometric analysis of surface PAD4 expression on non-permeabilized neutrophils from three healthy donors following treatment with various stimuli; medium alone (gray shaded) was used as a control. **(A)** Immune complexes (IC) (50 ng RNP plus 2% anti-RNP containing SLE serum) (red line) and the same IC diluted 1/3 (blue line), 1/9 (green line), 1/27 (purple line), and 1/81 (light blue line); **(B)** TNF-α, **(C)** PMA, **(D)** flagellin, **(E)** FSL-1, **(F)** IL-8. Concentrations of stimuli used in panels **(B–F)** were 10 ng/ml (red line), 3 ng/ml (blue line), and 1 ng/ml (green line), 0.3 ng/ml (purple line), and 0.1 ng/ml (light blue line). Bar graphs on the right shows the average mean fluorescence intensity (MFI) from the analysis of the three donors by paired *t*-test (*$p < 0.05$, **$p < 0.01$, $^{ns}p > 0.05$).

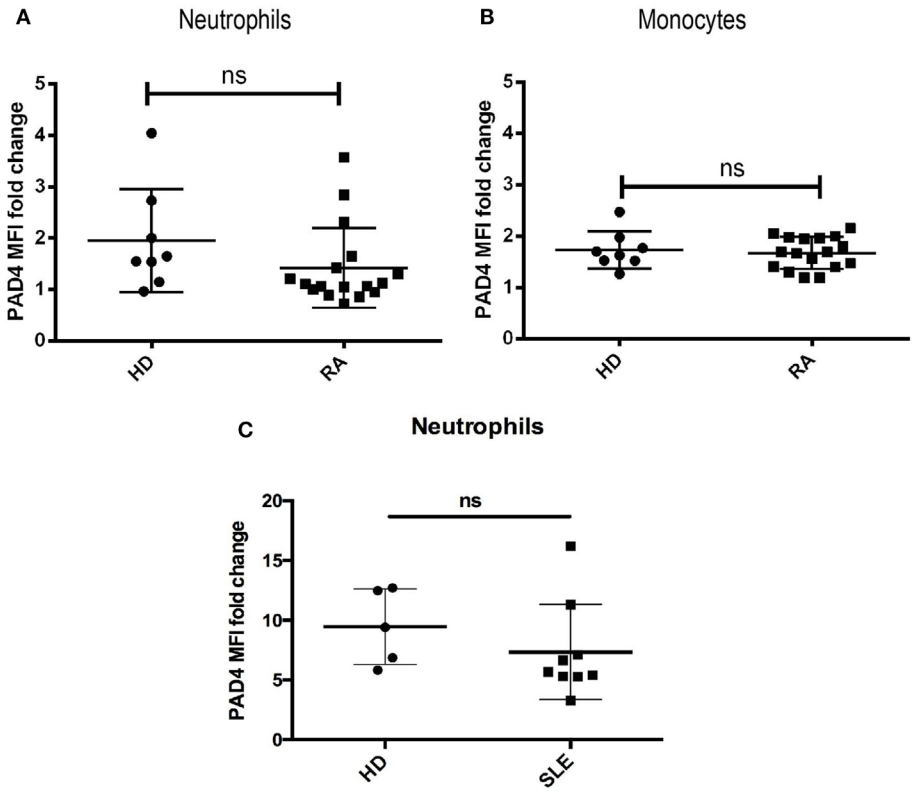

FIGURE 4 | Flow cytometric analysis of surface PAD4 levels in whole blood samples. Summary of mean fluorescence intensity (MFI) of PAD4 staining of different cells types from healthy donors, patients with rheumatoid arthritis (RA), and patients with SLE. **(A)** Neutrophils from healthy donors ($n = 8$) and patients from RA ($n = 18$). The difference between the two groups is not statistically significant by unpaired *t*-test. **(B)** Monocytes from the same donors in panel **(A)**. **(C)** neutrophils from healthy donors ($n = 5$) and patients from SLE ($n = 9$), $^{ns}p > 0.05$.

histone citrullination with a mAb specific for histone H3 citrullinated on Arg-2. As seen in **Figure 5C**, histone H3 became citrullinated within minutes of incubation with freshly isolated human neutrophils (**Figure 5C**, lanes 1–6). As with fibrinogen citrullination, extracellular calcium was required for histone H3 citrullination (**Figure 5C**, lane 11). Citrullinated histones were not detected when neutrophils were incubated without histone H3 (**Figure 5C**, lane 7), indicating that endogenous histones were not released under our experimental conditions. Similar to fibrinogen citrullination, neutrophil-conditioned media was able to citrullinate histone H3 (**Figure 5C**, lane 10). We also noted the appearance of a lower molecular weight band that increased in density with the duration of incubation of samples with live neutrophils. The density of this band was reduced by the inclusion of protease inhibitors, but not the MMP inhibitor, GM-6001, indicating that this band represents a proteolytically processed histone H3 (**Figure 5D**).

To rule out the possibility that histone toxicity was responsible for cell death and the release of PADs, we followed live neutrophils cultured in the presence of 1 mg/ml histone H3 (the same concentration that was used in our H3 citrullination assay) and DAPI (to stain dying cells) (Movie S1 in Supplementary Material). The rate of cell death remained negligible for at least 45 min with >90% viability, and all cells maintained an intact morphology. However, histone H3 citrullination was detectable at 5 min and peaked between 30 and 45 min, demonstrating that the citrullination was indeed mediated by viable neutrophils.

Taken together, the results of both fibrinogen and histone H3 citrullination assays indicated that neutrophil surface PAD4

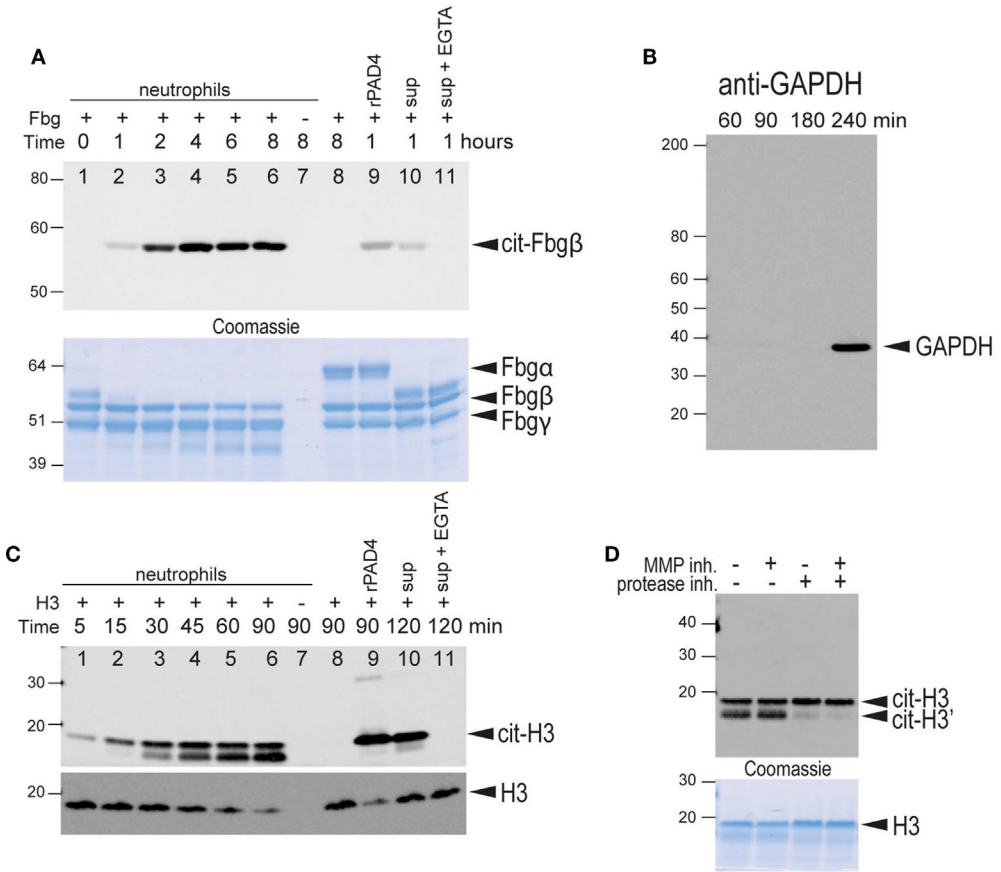

FIGURE 5 | Citrullination of extracellular substrates by intact neutrophils or neutrophil-conditioned media. **(A)** Upper panel, anti-citrullinated fibrinogen immunoblot of the supernatant from the incubation of fibrinogen for the indicated times in the presence of human neutrophils (lanes 1–7). Lane 7, fibrinogen was omitted. Lane 8 only contained fibrinogen. Lane 9, fibrinogen and recombinant PAD4. Lane 10, neutrophil-conditioned media. Lane 11, neutrophil with 2 mM EGTA. Lower panel, Coomassie Brilliant blue staining as a loading control. The bands corresponding to the α, β, and γ chains of fibrinogen are indicated. Note that α-fibrinogen is rapidly degraded by neutrophil-associated proteases. **(B)** Control immunoblot with anti-GAPDH, an intracellular protein, to demonstrate that significant lysis of neutrophils occurs only after 4 h of incubation with Triton X at 37°C under the experimental conditions. **(C)** Upper panel, anti-citrullinated histone H3 immunoblot of the supernatant from the incubation of histone H3 for the indicated time periods in the presence of human neutrophils (lanes 1–7). Lane 7, histone was omitted. Lane 8 only contained histone H3. Lane 9 contained histone H3 and recombinant PAD4. Lane 10, neutrophil-conditioned media. Lane 11, neutrophil with 2 mM EGTA. Note that citrullinated histone H3 is also cleaved by neutrophil-associated protease(s) to generate a slightly smaller protein. Lower panel, anti-histone H3 immunoblot as a loading control. This antibody does not recognize the proteolytically cleaved H3. **(D)** A similar experiment performed in the presence of an MMP inhibitor, a protease inhibitor cocktail, or both, as indicated. Lower panel, Coomassie Brilliant blue staining as a loading control. All data are representative of five independent experiments with different donors.

is enzymatically active. Notably, neutrophils were also able to secrete active PAD into the surrounding environment.

Identification of PAD2 As Predominantly Secreted PAD

Since neutrophil-conditioned media was capable of citrullinating fibrinogen (**Figure 5A**, lane 10) or histone H3 (**Figure 5B**, lane 10), we sought to determine whether the soluble PAD activity was mediated by PAD4 released from the cell surface. We performed western blot analysis of concentrated culture supernatants from healthy donor neutrophils using antibodies for the detection of PAD4 and PAD2. Surprisingly, PAD2 was clearly observed in all four samples (**Figure 6A**), whereas PAD4 was barely detectable even after longer exposures (**Figure 6B**). Nano-LC-MS/MS mass spectrometry confirmed the presence of PAD2 in the supernatants with 43 to 58 peptide-spectrum matches (between the four donors) covering an average of 38.8% of the protein. PAD4 was also detected but with far fewer peptide-spectrum matches (Figure S4 in Supplementary Material). These results indicate that the PAD activity in the neutrophil-conditioned media in the absence of stimulation is predominantly due to PAD2.

Analysis of the Contribution of PAD2 versus PAD4 to Protein Citrullination Using Inhibitory Antibodies

To evaluate the relative contributions of PAD2 and PAD4 in extracellular protein citrullination, we developed monoclonal

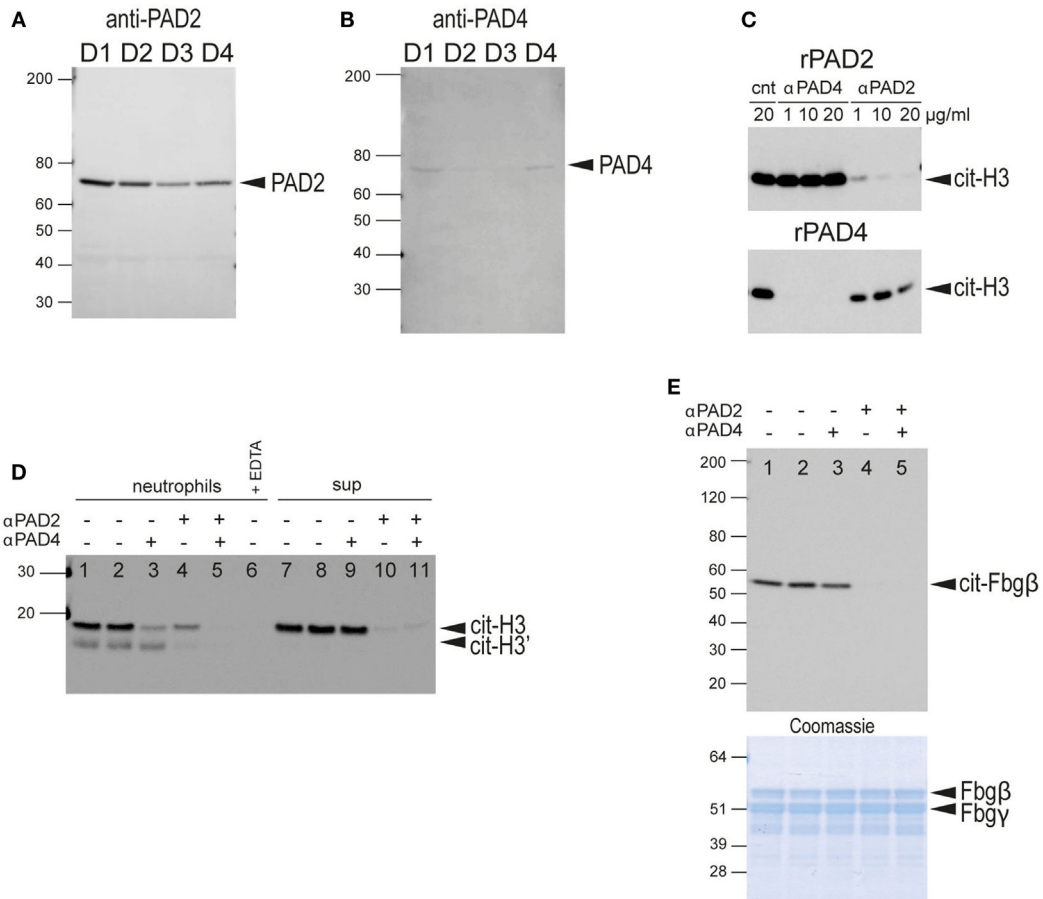

FIGURE 6 | Western blot analysis of secreted PADs in neutrophil-conditioned media and determination of neutrophil PAD2/PAD4 extracellular activity. **(A)** Anti-PAD2 immunoblot of concentrated neutrophil-conditioned media from four different healthy donors (D1–D4). **(B)** Anti-PAD4 immunoblot of same samples with longer exposure time. **(C)** Characterization of the blocking anti-PAD2 and anti-PAD4 antibodies. Upper panel, anti-citrullinated histone H3 immunoblot of a reaction with recombinant PAD2 in the presence of control NIP228 IgG antibody (lane 1), blocking anti-PAD4 antibody (lanes 2–4), or a blocking anti-PAD2 antibody (lanes 5–7) at the indicated concentrations. Lower panel, similar reaction with recombinant PAD4 in the presence of the same antibodies. **(D)** Anti-citrullinated histone H3 immunoblot of the culture supernatant of human neutrophils incubated with histone H3 plus blocking anti-PAD2 or anti-PAD4 antibodies as indicated (lane 1–5); 2 mM EDTA was added to demonstrate the calcium-dependence of the reaction (lane 6); neutrophil-conditioned media, plus blocking antibodies as indicated (lanes 7–11). No antibodies were added in lanes 1 and 7, whereas control IgG NIP228 was added in lanes 2 and 8. **(E)** Anti-citrullinated fibrinogen immunoblot of the supernatant from the incubation of fibrinogen with neutrophils plus blocking antibodies. No antibodies were added in lane 1, whereas control IgG NIP228 was added in lane 2. Lower panel, Coomassie Brilliant blue staining as a loading control. All data are representative of five independent experiments with different donors.

antibodies for PAD2 and PAD4 capable of specifically inhibiting the catalytic activity of their respective PAD targets. The specificity of each antibody was demonstrated with recombinant PAD2 and PAD4 using histone H3 as substrate (**Figure 6C**).

When these antibodies were used in histone H3 citrullination assays with intact healthy neutrophils, both antibodies reduced PAD activity, but the anti-PAD4 antibody had a greater effect (**Figure 6D**, lanes 3 and 4). The combination of both antibodies completely blocked citrullination of histone H3 (**Figure 6D**, lane 5). In contrast, when these antibodies were added to histone H3 citrullination assays with neutrophil-conditioned media, the anti-PAD2 antibody had a substantial inhibitory effect, whereas the anti-PAD4 antibody had a minimal effect (**Figure 6D**, lanes 9 and 10). These data are consistent with the notion that PAD activity secreted by neutrophils is predominantly mediated by PAD2, whereas PAD activity associated with intact neutrophils is largely mediated by cell-bound PAD4, with some contribution from newly secreted PAD2.

In contrast to the histone H3 assay, fibrinogen citrullination of intact neutrophils was inhibited with the anti-PAD2 antibody, and the anti-PAD4 antibody had no effect (**Figure 6E**). Western blot analysis using an anti-modified citrulline antibody (more broadly citrulline reactive) showed a similar pattern (data not shown). Thus, it appears that extracellular fibrinogen was preferably citrullinated by secreted PAD2 rather than cell surface-exposed PAD4. This result may also explain the slower kinetics of fibrinogen citrullination compared to histone H3 citrullination by live neutrophils.

Kinetics and Quantitation of Secreted PAD Activity

Secretion of PAD2 could provide means for neutrophils to modify extracellular matrix proteins or even cytokines without physically interacting with those substrates. To further characterize the pattern of PAD secretion, we developed quantitative ELISA-based fibrinogen and histone H3 citrullination assays to measure PAD activity. The assay was first validated with recombinant human PAD2 and PAD4, which both produced dose-dependent increases in citrullination (fibrinogen shown in **Figure 7A**, histone H3 not shown). The kinetics of PAD secretion was investigated by analysis of neutrophil-conditioned media. Neutrophils secreted measurable PAD activity within minutes of initiation of the assay, with the highest activity detected at approximately 1 h (**Figure 7B**). Similar kinetics was observed in assays of both histone and fibrinogen substrates.

To examine the respective contributions of PAD2 and PAD4 to citrullination in this ELISA assay format, conditioned media were incubated with blocking antibodies prior to the assay. These experiments demonstrated that most of the activity was mediated by PAD2 with a minor or negligible contribution by PAD4 (**Figures 7C,D**). This result is consistent with the detection of PAD2 in neutrophil supernatants by mass spectrometry and western blotting, and the inhibition of PAD activity observed in western blot assays. Taken together, these data confirm that PAD2 is secreted spontaneously by neutrophils and is predominately responsible for the PAD activity found in the neutrophil-conditioned media.

Regulation of PAD2 Secretion during Neutrophil Activation

Surface PAD4 levels were found to change in response to neutrophil activators, thus we evaluated the impact of these stimuli on PAD2 secretion. Interestingly, PAD2 secretion from neutrophils was significantly reduced by stimulation with PMA or ICs (**Figure 8**). LPS also reduced PAD2 secretion, but to a lesser extent (**Figure 8**). IL-6 reduced PAD2 secretion in some but not all donors. Other stimuli (IL-8, GM-CSF, TNF-α, fMLP, flagellin, FSL-1, PAM3, heat-killed *L. monocytogenes*, imiquimod, and ss40RNA) had no detectable effects on PAD2 secretion (data not shown). This result demonstrated that PAD2 secretion was reduced by some inflammatory stimuli, and it was regulated differently from PAD4 surface expression.

DISCUSSION

Citrullination is a posttranslational protein modification involved in various physiological processes including gene expression

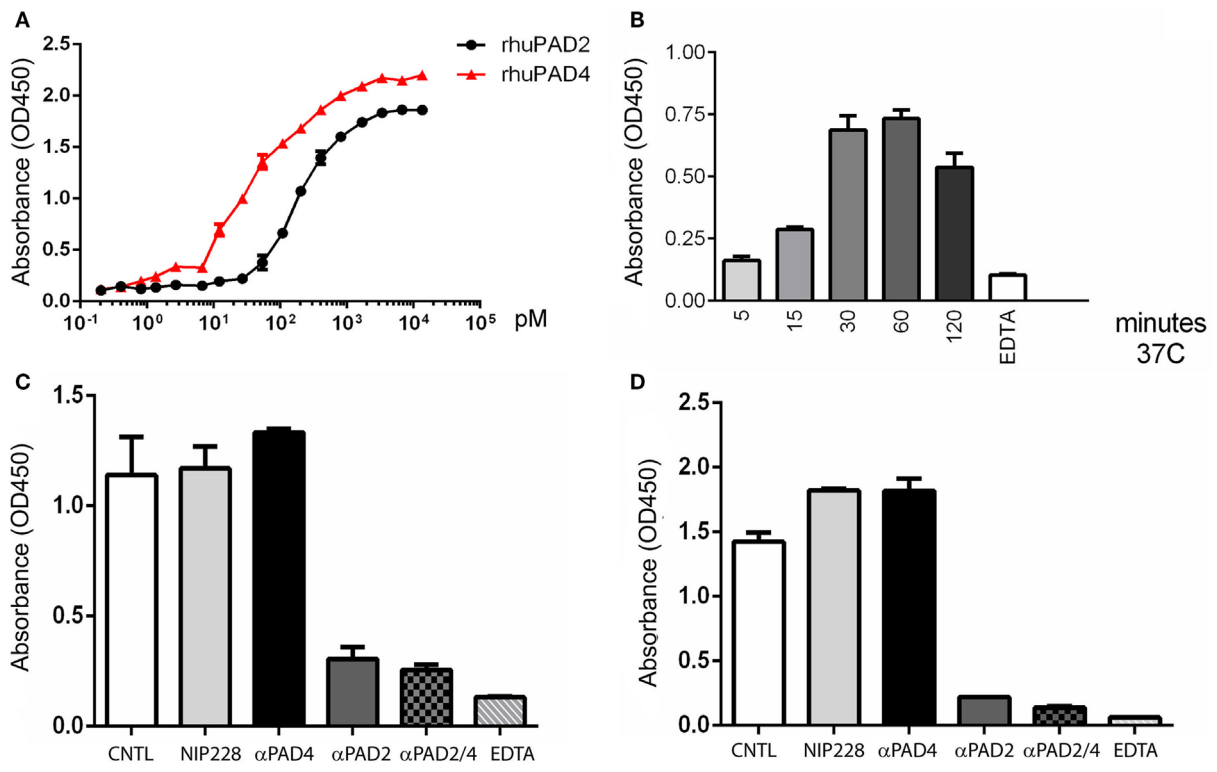

FIGURE 7 | ELISA-based protein citrullination analysis of kinetics and activity of PADs released from neutrophils. **(A)** Dose–response curves of fibrinogen citrullination mediated by recombinant human PAD2 and PAD4. **(B)** Kinetics of fibrinogen citrullination by neutrophil-conditioned media. **(C)** Citrullination of fibrinogen and **(D)** histone H3 by neutrophil-conditioned media can be blocked by the anti-PAD2 inhibitory antibody but not the anti-PAD4 antibody. All data are representative of four independent experiments with different donors.

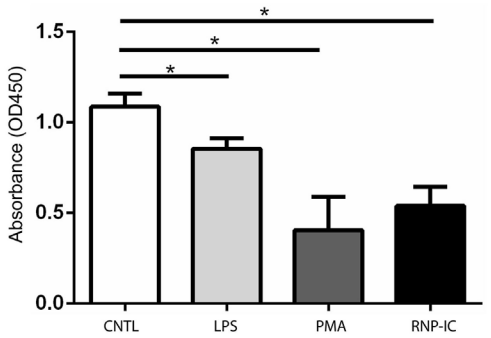

FIGURE 8 | ELISA-based histone H3 citrullination analysis of regulation of PAD2 secretion by neutrophil activators. Quantification of PAD2 activity in conditioned media from neutrophils stimulated with 50 ng RNP plus 2% anti-RNP containing SLE serum, 10 ng/ml PMA and 10 ng/ml lipopolysaccharide (LPS). Data represent the mean OD reading ± SD of four donors with statistical analysis by paired *t*-test (*$p < 0.05$).

regulation, skin cornification, and hair follicle development (2, 38). Dysregulation of PAD expression or citrullination has been implicated in MS, cancer, and SLE (1), and autoimmune responses against citrullinated proteins are strongly associated with RA (12). Neutrophils are considered the main source of PAD enzymes responsible for citrullination in autoimmune diseases, including RA and SLE (44, 45). How the citrullination process is initiated under disease conditions and, even more fundamentally, what are the normal physiological functions of PADs in neutrophils are questions that remain unclear. This study provides the first evidence that resting neutrophils express PAD4 on the surface and secrete PAD2 into the surrounding environment. These extracellular PADs are enzymatically active, and their expression levels were regulated by several inflammatory factors. These findings identify new mechanisms by which PADs can citrullinate extracellular proteins and suggest that extracellular PADs could have a normal physiological role.

Extracellular PADs have been mostly examined in the context of patients with RA, where PAD expression and citrullination were increased in synovial fluid (14). Those PADs were thought to be the consequence of PAD molecules "hitch-hiking" on the extruded DNA NETs or being released from dying neutrophils (42). Our data suggest two alternative routes for externalization of PADs, namely, expression of PAD4 on the surface of neutrophils and spontaneous secretion of PAD2, even in the absence of any inflammatory stimuli. These two processes are independent of NETosis or other forms of cell death and can contribute to extracellular protein citrullination. We demonstrated that extracellular fibrinogen and histone H3 can be citrullinated by neutrophil extracellular PADs. Those two substrates are also citrullinated in synovial fluid from patients with RA and are common autoantigens in patients (17, 18, 46). The new mechanism for extracellular citrullination which we propose here could contribute to the generation of citrullinated neoepitopes important in RA. Intriguingly, while histone H3 was citrullinated by both extracellular PADs, fibrinogen was predominantly citrullinated by PAD2 secreted by neutrophils. This is consistent with a previous study that highlighted substrate preference by different PADs (25), and also indicates that endogenous PADs could have stricter substrate selection than recombinant enzymes.

We observed that secreted PAD2 and surface expressed PAD4 were differentially regulated following neutrophil activation by several inflammatory factors. This could imply that these extracellular PADs may have important functions in an inflammatory environment. Our understanding of PAD4 in inflammation has been largely limited to its role in the initiation of NETosis through chromatin decondensation by histone citrullination (32, 33). However, our data suggest that upregulation of surface PAD4 is associated with multiple inflammatory stimuli. These stimuli include IC and phorbol ester, which can induce NETosis (47, 48), as well as stimulants such as TNF-α which do not trigger NETosis (35). Notably, the cell surface PAD4 upregulation with immune stimuli was rapid, occurring well before any evidence of NETosis was apparent and was not affected by the NETosis inhibitor. These results all point to a broader and earlier involvement for PAD4 in the inflammatory process. The level of surface PAD4 was not increased on circulating neutrophils from RA and SLE patients compared to controls; however, it remains plausible that PAD4 expression is increased on neutrophils in the joints and other sites of inflammation, where there are increased levels of IC deposition and TNF-α (49, 50). Interestingly, anti-PAD3/PAD4 autoantibodies are found in RA patients (51). These autoantibodies could potentially bind to surface PADs and promote Fc- or complement-mediated effector functions. Indeed, anti-PAD3/PAD4 antibodies were associated with a more aggressive disease course, including radiographic progression and interstitial lung disease (51, 52). We observed that stimuli increasing the upregulation of cell surface PAD4 tended to reduce extracellular PAD2 activity, including PMA, a stimulus which induces NETosis. This implies that these enzymes are differentially regulated and may have alternative functions. At present, the mechanism by which PAD2 and PAD4 traffic from an intracellular location to the exterior of the neutrophil remains unclear. We did not observe PAD2 expression on the cell surface of leukocytes, although we cannot rule out the possibility that alternative antibodies with other epitope specificity may detect surface bound PAD2.

The presence of catalytically active PAD4 on the external surface of viable normal neutrophils, as well as the spontaneous secretion of PAD2, suggest that these enzymes have physiological roles under healthy conditions. All PADs require millimolar levels of calcium to be active, which are normal in serum but do not exist intracellularly unless cells are severely comprised (24, 39, 40). Indeed, small quantities of citrullinated proteins (53) and soluble PAD2 protein have been detected in healthy human subjects (54).

The exact physiological functions for surface PAD4 and secreted PAD2 remain open questions. They could indeed be involved in many functions depending on different substrates. Histone citrullination in neutrophils has been mainly linked to NETosis and antibacterial innate immunity (32–34). It is worth noting that antibacterial properties of histones are reduced upon citrullination, as its toxicity depends on positively charged arginine and lysine (55). Circulating extracellular histones can also be detected in non-infectious diseases, particularly in those

that involve tissue injury, such as acute respiratory distress syndrome and sepsis (56–59). In addition, endogenous histones have been reported to enhance sterile inflammation by increasing cytokine production through Toll-like receptor signaling or NLRP3 inflammasome activation (60–62). One could envision that neutrophils may use surface-exposed PAD4 and/or secreted PAD2 to diminish the extraordinarily potent pro-inflammatory and toxic properties of extracellular histones at a site of tissue injury or infection. A similar effect of citrullination on reducing toxicity on the bactericidal protein LL37 has also been reported (63). Finally, a number of chemokines and other inflammatory mediators have been reported to be citrullinated, resulting in changed properties, such as altered receptor binding leading to reduced inflammatory properties (64, 65). Given the range of substrates, cell surface expressed PAD4 and secreted PAD2 could provide a new dimension of immune regulation under physiological conditions, most likely functioning as a "brake" to potentially inactivate these substrates.

Extracellular PADs identified in our study could also modulate neutrophil function through regulating cell adhesion and migration. We demonstrated that extracellular fibrinogen could be readily citrullinated by neutrophil-secreted PAD2. Previous studies suggested that citrullination of R35 and R44, on fibrinogen alpha and beta chains, respectively, will destroy thrombin recognition sites and inhibit thrombosis (66, 67). Thus, neutrophils may engage in regulating fibrin polymerization during their migration through tissues under conditions that result in fibrin polymerization and deposition. Fibrin deposits are notable in synovial tissue from RA patients, and abundant citrullination can be detected both in fibrin deposits and on fibrinogen (68, 69). This tempering effect of citrullination on fibrinogen polymerization could be physiologically relevant in resolving tissue injury or in the migration of neutrophils through damaged tissue. Another potential mechanism by which extracellular PADs may affect neutrophil adhesion and migration would be by citrullinating adhesion molecules (e.g., integrins at their RGD motif) and inhibiting integrin-mediated adhesion (70, 71).

In conclusion, we provide the first evidence that resting neutrophils from healthy donors express enzymatically active PAD4 on their cell surfaces and secrete active PAD2. Surface expression of PAD4 and secretion of PAD2 are also regulated by neutrophil stimulation. Their extracellular location provides a new mechanism by which extracellular proteins may be citrullinated under normal conditions. Potential functions of extracellular PADs could even extend beyond neutrophils as we observed that monocytes also expressed PAD4 on the surface. This promises to be an interesting area of research as it remains uncertain what the exact roles of extracellular PADs are under physiological conditions, and what levels of PAD2 and PAD4 activity are necessary to trigger clinical manifestations.

MATERIALS AND METHODS

Neutrophil Isolation from Patients and Healthy Donors

Blood from healthy volunteers was obtained with informed consent under MedImmune, LLC's blood donation program, and studies using human cells were performed in accordance with the Institutional Review Board guidelines. Neutrophils were isolated from heparin anti-coagulated blood on a discontinuous Ficoll gradient as previously described (72).

Blood samples from patients with RA and systemic lupus erythematosus were collected from Johns Hopkins University Hospital Arthritis Center (Baltimore, MD, USA) and the National Institutes of Health (Bethesda, MD, USA) lupus clinic, respectively, with informed consent and IRB approval. All patients met the American College of Rheumatology classification criteria (73, 74).

Antibodies and Reagents

Antibodies for detection of PAD4 (Ab128086 and Ab50247), PAD2 (Ab16478), citrullinated histone H3 (R2 citrullination, Ab176843), and total histone H3 (Ab24834) were from Abcam (Cambridge, MA, USA). Antibodies for detection of PAD4 (MABE254) and modified citrulline were from EMD Millipore (Billerica, MA, USA). Antibodies for flow cytometric analyses (FITC-CD45, PE-CD15, BV421-CD3, APC-CY7-CD56, and PE-CY7-CD14) and CD16 (clone 3G8) were from BioLegend (San Diego, CA, USA) and BUV395-CD19 was from BD Bioscience (San Jose, CA, USA).

Recombinant human PAD2, recombinant human PAD4, and human IgG1 clone NIP228 were made in house. Alexa-647-labeled PAD2 and PAD4 staining antibodies and PAD2 and PAD4 blocking antibodies were generated in house and were human IgG1isotype. Control antibodies, PAD blocking antibodies, and Alexa-647 fluorochrome-labeled anti-PAD monoclonal antibodies were engineered with mutant Fc regions to subvert complement and Fcγ receptor binding (75) to minimize non-specific interactions with neutrophils. Recombinant human histone H3, human fibrinogen, and the anti-citrullinated fibrinogen western blot antibody (clone 10E9.2) were from Cayman Chemicals (Ann Arbor, MI, USA). Anti-GAPDH (D16H11) was from Cell Signaling (Danvers, MA, USA). The anti-citrullinated fibrinogen ELISA antibody (clone 20B2) was from Modiquest (Molenstraat, Netherlands).

DPI, TNF-α, fMLP, PMA, HRP-, or FITC-labeled anti-mouse IgG and anti-rabbit IgG secondary antibodies were from Invitrogen (Carlsbad, CA, USA). Recombinant GM-CSF, IL-6, and IL-8 were from R&D system (Minneapolis, MN, USA). The human TLR1-9 agonist kit was from InvivoGen (San Diego, CA, USA). The MMP inhibitor GM-6001 was from Enzo Life Sciences (Farmingdale, NY, USA). The protease inhibitor cocktail was from Thermo Fisher (Waltham, MA, USA).

Immunofluorescence Microscopy

Fresh isolated neutrophils were resuspended in Hanks' balanced salt solution (HBSS) without calcium and magnesium (Invitrogen) with 2% heat-inactivated human AB serum (Sigma-Aldrich, St. Louis, MO, USA) at a density of 500,000 cells/ml and seeded for adherence on L-lysine-coated glass coverslips. Subsequently, cells were fixed with 4% paraformaldehyde for 15 min at room temperature. For permeabilization, fixed cells were treated with 1% Triton X-100 for 1 min and blocked in 1% BSA in PBS for 1 h at 37°C. All primary antibodies (Alexa-647-labeled anti-PAD4

staining antibody, Ab128086, MABE254 and Ab50247 for PAD4; Alexa-647-labeled anti-PAD2 staining antibody for PAD2, Alexa-488-labeled CD16) were used at a concentration of 10 μg/ml in PBS with 1% BSA. Cells were incubated with antibodies for 1 h at 37°C. For recombinant PAD competition, the primary antibody was first incubated with 100 μg/ml recombinant human PAD2 or PAD4 for 15 min at room temperature. A FITC-conjugated secondary antibody (Invitrogen) was used at 1:5,000 dilutions for detection of unlabeled primary antibodies. DAPI was used as a counterstain in permeabilized cells. Images were acquired using a TCS SP2 Leica laser-scanning confocal microscope with 63× objective.

Flow Cytometry and ImageStream Analysis

Isolated neutrophils were resuspended in HBSS without calcium and magnesium at a density of 2×10^6 cells/ml. The Alexa-647 fluorochrome-labeled anti-PAD2 staining antibody and anti-PAD4 staining antibody were added at 5 μg/ml. For recombinant PAD competition, antibodies were preincubated with 50 μg/ml recombinant human PAD2 or PAD4 for 15 min at room temperature. Cells were incubated with antibodies on ice for 30 min. Flow cytometry was performed using LSRII and ImageStream X. The results were analyzed using the FlowJo software package (Tree Star) or ImageStream analysis software (EMD Millipore). Neutrophils were gated based on forward and side scatter patterns.

Whole Blood Assay

Fresh blood was obtained from healthy donors, RA patients, and lupus patients. Aliquots of 50 μl blood were stained on ice for 30 min with an Ab cocktail (FITC-CD45, PE-CD15, BV421-CD3, APC-CY7-CD56, PE-CY7-CD14, BUV395-CD19, and Medi-PAD2/PAD4 staining antibody, all at 5 μg/ml). Flow cytometry was performed using an LSRII Instrument. After acquisition, the flow cytometry data were analyzed using the FlowJo software package (Tree Star). The following populations were gated for analysis: neutrophils (CD45+ CD15+), monocytes (CD45+ CD14+), T cells (CD45+ CD3+), B cells (CD45+ CD19+), and NK cells (CD45+ CD56+).

Neutrophil Citrullination Assay

Neutrophils were resuspended in HBSS at a density of 10^7 cells/ml. For surface PAD activity assays, one million neutrophils were incubated with 100 μg human fibrinogen or recombinant human histone H3 for various durations at 37°C in HBSS with 1 mM DTT and 2 mM $CaCl_2$. After incubation, cells were removed by 10-min 300 *g* centrifugation, and the supernatant was collected for western blot analysis. Supernatants from neutrophils alone, naïve fibrinogen or histone H3, and fibrinogen histone H3 citrullinated by recombinant human PAD4 were used as controls.

For secreted PAD activity assays, one million neutrophils were incubated in HBSS buffer for 1 h at 37°C. Subsequently, cells were removed by 10-min 300 *g* centrifugation, and supernatants were collected, which were then incubated for 1 h at 37°C with 100 μg fibrinogen or histone H3 in HBSS with 1 mM DTT and 2 mM $CaCl_2$. Western blot analysis was performed afterward to detect citrullinated substrates.

Concentration of Neutrophil-Conditioned Media

Freshly isolated neutrophils were resuspended in HBSS at a density of 2×10^7 cells/ml and incubated at 37°C for 1 h. Cells were removed by 10-min 300 *g* centrifugation, and supernatants were concentrated by filtering through an Amicon ultra-0.5 ml 30 kDa protein concentration column (EMD Millipore). Concentrated neutrophil-conditioned media was analyzed by western blotting and mass spectrometry.

PAD Activity Inhibition

Recombinant human PAD2 or PAD4 (5 ng) was preincubated with a NIP228 control antibody, PAD2 blocking antibody, and PAD4 blocking antibody for 10 min at room temperature. Histone H3 (5 μg) was then added with 2 mM calcium and incubated for another hour at 37°C.

Neutrophils or neutrophil-conditioned media were preincubated with the NIP228 control antibody, PAD2 blocking antibody and PAD4 blocking antibody for 15 min at room temperature. For fibrinogen citrullination, all antibodies were used at 1 μg/ml final concentration. For histone H3 citrullination, the antibody as used at a final concentration of 5 μg/ml. Fibrinogen and histone H3 were added after preincubation. Fibrinogen was incubated for an additional 4 h at 37°C. Histone H3 was incubated for 30 min. Western blot analysis was performed afterward to determine substrate citrullination level.

Neutrophil-Secreted PAD ELISA Assay

96-well ELISA plates were coated with either 1 μg/ml human fibrinogen or histone H3 overnight at 4°C. Freshly isolated neutrophils were resuspended in HBSS at a density of 10^7 cells/ml and incubated at 37°C from 5 min to 2 h. Cells were removed by 10-min 300 *g* centrifugation, and supernatants were diluted 1:10 in Tris–HCl buffer with 1 mM DTT and 5 mM calcium.

Diluted supernatants were either added directly to coated plates or preincubated with blocking antibodies at a concentration of 10 μg/ml for 15 min before adding to plates.

Citrullination assays were performed at 37°C for 90 min. The reaction was stopped by washing the plates with PBS + 0.05% tween20. Anti-citrullinated fibrinogen (20B2) and anti-citrullinated histone H3 (Ab176843) antibodies were used for detection. The OD450 was measured.

Neutrophil Activation

10× RNP-IC was prepared by incubating equal volumes of 20 μg/ml RNP and 40% lupus serum containing a high titer of anti-RNP IgG for 1 h at room temperature. 10× Ig-IC was prepared by incubating equal volumes of 1 mg/ml biotinylated R347 IgG and 3 μM streptavidin for 1 h at room temperature. TNF-α, fMLP, PMA, GM-CSF, IL-6, IL-8, and a human TLR1–9 agonist kit were used according to the manufacturers' protocols. For NETosis inhibition, cells were incubated with 10 μM DPI for 10 min at room temperature prior to adding stimuli.

Isolated neutrophils were resuspended in HBSS at a density of 2×10^6 cells/ml. All stimuli were used with a 1:3:9:27:81 dilution series. Activation was performed at 37°C for 15 min. Cells were washed and resuspended after stimulation before FACS analysis.

Isolated neutrophils were treated separately with the highest dose of the stimuli in HBSS for 30 min. Cells were then removed by 10-min 300 *g* centrifugation, and supernatants were collected for ELISA analysis.

Mass Spectrometry Analysis

Concentrated neutrophil-conditioned media samples were processed using the filter-aided sample preparation method (76). Resulting peptides were analyzed using nanoflow LC-MS/MS (Dionex RSLCnano interfaced with Orbitrap Fusion Tribrid mass spectrometer). Mass spectrometry data were analyzed using the Mascot search engine with Proteome Discoverer software (Thermo Fisher) and quantified using Scaffold software. The normalized total spectra counts for PAD4 and PAD2 were compared to estimate the expression levels of PAD4 and PAD2.

Recombinant PAD4 or neutrophil-citrullinated fibrinogen samples (5 μg) were reduced and alkylated prior to automated on-column trypsin digestion using a Perfinity™ workstation. Peptide samples from each experiment were analyzed using a nanoflow LC-MS/MS system. Mass spectrometry data were searched using Mascot software, with the following search parameters: nine missed trypsin cleavages, oxidation of methionine, and deamidation of N and Q residues. Arginine citrullination was confirmed using the Mascot (v2.5.1) search engine by including neutral loss of 43.006 Da in addition to 0.984-Da mass shift for deamidation.

Western Blot Analysis

Equivalent amounts of proteins were separated by SDS-polyacrylamide gel electrophoresis (4–12% gel) and then transferred to a nitrocellulose membrane. Membranes were then probed using anti-citrullinated fibrinogen (clone 10E9.2), anti-citrullinated histone H3 (Ab176843), anti-total histone H3 (Ab24834), anti-GAPDH (clone D16H11), anti-PAD2 (Ab16478), and anti-PAD4 (MABE254) antibodies using the iBind (Invitrogen) system. An HRP-conjugated anti-mouse IgG and anti-rabbit IgG were used as the secondary detection antibodies before visualization of immunoreactive bands with an ECL reagent (Thermo Fisher).

Statistical Analysis

Data analysis was performed with GraphPad Prism (GraphPad, La Jolla, CA, USA). Unpaired *t*-test was used in PAD4 expression comparison between patients with RA or SLE and healthy donors. Paired *t*-test was used in other statistical analysis.

ETHICS STATEMENT

Blood from healthy volunteers was obtained with informed consent under MedImmune, LLC's blood donation program, and studies using human cells were performed in accordance with the Institutional Review Board guidelines. Blood samples from patients with RA and systemic lupus erythematosus were collected from Johns Hopkins University Hospital Arthritis Center (Baltimore, MD, USA) and the National Institutes of Health (NIH; Bethesda, MD, USA) lupus clinic, respectively, with informed consent and IRB approval.

AUTHOR CONTRIBUTIONS

TM, GPS, and YZ generated ideas for this study and wrote the manuscript. YZ, BC, NM, SR, and WM performed experiment and analyzed data. MS, CL, DC, FN, and KAV generated recombinant proteins and antibodies. RC generated and analyzed mass spec data. CB, KS, ED, and FA provided RA samples. RS and SH provided lupus samples. All authors reviewed the manuscript for content, provided suggestions, and approved the final manuscript.

ACKNOWLEDGMENTS

The authors thank Caroline Colley, Lisa Vinall for antibody screening and Michelle K. Jones for clinical research support. CB, KS, ED, and FA are supported by National Institute of Arthritis and Musculoskeletal and Skin Diseases (NIAMS)/National Institutes of Health (NIH) grant P30-AR053503. The content is solely the responsibility of the authors and does not necessarily represent the official views of NIAMS or the NIH.

SUPPLEMENTARY MATERIAL

The Supplementary Material for this article can be found online at http://journal.frontiersin.org/article/10.3389/fimmu.2017.01200/full#supplementary-material.

FIGURE S1 | PAD4 surface expression on isolated neutrophils and blood cell population. **(A)** Representative fluorescent image of isotype control antibody staining of isolated neutrophils obtained with ImageStream. **(B)** Representative fluorescent image of PAD4 staining of isolated neutrophils obtained with ImageStream. **(C)** Representative flow cytometry data obtained from analysis of healthy donor-derived neutrophils, monocytes, B cells, T cells, NK cells, and platelets stained with a control antibody (gray shade) of anti-PAD4 (red line). Note that only neutrophils and monocytes are positively stained. All images are representatives of three different donors.

FIGURE S2 | PAD4 and CD16 co-staining on isolated neutrophils. Representative fluorescent image of PAD4 and CD16 staining of neutrophils, PAD4 channel (left panel), CD16 channel (middle panel), and overlay (right panel).

FIGURE S3 | PAD4 upregulation by ribonucleoprotein immune complexes (RNP-IC), PMA, and TNFα was not affected by NETosis inhibitor DPI. Representative fluorescent image of PAD4 staining of isolated neutrophils stimulated with RNP-IC (left panel), PMA (middle panel), and TNFα (right panel) with or without NETosis inhibitor DPI.

FIGURE S4 | PAD2 is the dominant secreted PADs in neutrophil-conditioned media detected by mass spectrometry. Total spectral counts of PAD2/4 analyzed by LC-MS are shown in the figure. PAD2 and PAD4 theoretically produce similar number of tryptic peptides hence data show higher level of PAD2.

MOVIE S1 | Incubation of neutrophils with histone H3. Neutrophils isolated from healthy donors were incubated with 1 mg/ml human recombinant histone H3 in Hanks' balanced salt solution (HBSS) buffer. DAPI was added to indicate cell death.

REFERENCES

1. Bicker KL, Thompson PR. The protein arginine deiminases: structure, function, inhibition, and disease. *Biopolymers* (2013) 99:155–63. doi:10.1002/bip.22127
2. Vossenaar ER, Zendman AJ, van Venrooij WJ, Pruijn GJ. PAD, a growing family of citrullinating enzymes: genes, features and involvement in disease. *Bioessays* (2003) 25:1106–18. doi:10.1002/bies.10357
3. Anzilotti C, Pratesi F, Tommasi C, Migliorini P. Peptidylarginine deiminase 4 and citrullination in health and disease. *Autoimmun Rev* (2010) 9:158–60. doi:10.1016/j.autrev.2009.06.002
4. Moscarello MA, Mastronardi FG, Wood DD. The role of citrullinated proteins suggests a novel mechanism in the pathogenesis of multiple sclerosis. *Neurochem Res* (2007) 32:251–6. doi:10.1007/s11064-006-9144-5
5. Harauz G, Musse AA. A tale of two citrullines – structural and functional aspects of myelin basic protein deimination in health and disease. *Neurochem Res* (2007) 32:137–58. doi:10.1007/s11064-006-9108-9
6. Ishida-Yamamoto A, Senshu T, Takahashi H, Akiyama K, Nomura K, Iizuka H. Decreased deiminated keratin K1 in psoriatic hyperproliferative epidermis. *J Invest Dermatol* (2000) 114:701–5. doi:10.1046/j.1523-1747.2000.00936.x
7. Ishigami A, Masutomi H, Handa S, Nakamura M, Nakaya S, Uchida Y, et al. Mass spectrometric identification of citrullination sites and immunohistochemical detection of citrullinated glial fibrillary acidic protein in Alzheimer's disease brains. *J Neurosci Res* (2015) 93:1664–74. doi:10.1002/jnr.23620
8. Wang H, Xu B, Zhang X, Zheng Y, Zhao Y, Chang X. PADI2 gene confers susceptibility to breast cancer and plays tumorigenic role via ACSL4, BINC3 and CA9 signaling. *Cancer Cell Int* (2016) 16:61. doi:10.1186/s12935-016-0335-0
9. McNee G, Eales KL, Wei W, Williams DS, Barkhuizen A, Bartlett DB, et al. Citrullination of histone H3 drives IL-6 production by bone marrow mesenchymal stem cells in MGUS and multiple myeloma. *Leukemia* (2017) 31:373–81. doi:10.1038/leu.2016.187
10. Durrant LG, Metheringham RL, Brentville VA. Autophagy, citrullination and cancer. *Autophagy* (2016) 12:1055–6. doi:10.1080/15548627.2016.1166326
11. Schellekens GA, de Jong BA, van den Hoogen FH, van de Putte LB, van Venrooij WJ. Citrulline is an essential constituent of antigenic determinants recognized by rheumatoid arthritis-specific autoantibodies. *J Clin Invest* (1998) 101:273–81. doi:10.1172/JCI1316
12. Klareskog L, Ronnelid J, Lundberg K, Padyukov L, Alfredsson L. Immunity to citrullinated proteins in rheumatoid arthritis. *Annu Rev Immunol* (2008) 26:651–75. doi:10.1146/annurev.immunol.26.021607.090244
13. Ally MM, Hodkinson B, Meyer PW, Musenge E, Tintinger GR, Tikly M, et al. Circulating anti-citrullinated peptide antibodies, cytokines and genotype as biomarkers of response to disease-modifying antirheumatic drug therapy in early rheumatoid arthritis. *BMC Musculoskelet Disord* (2015) 16:130. doi:10.1186/s12891-015-0587-1
14. Damgaard D, Senolt L, Nielsen MF, Pruijn GJ, Nielsen CH. Demonstration of extracellular peptidylarginine deiminase (PAD) activity in synovial fluid of patients with rheumatoid arthritis using a novel assay for citrullination of fibrinogen. *Arthritis Res Ther* (2014) 16:498. doi:10.1186/s13075-014-0498-9
15. Kinloch A, Lundberg K, Wait R, Wegner N, Lim NH, Zendman AJ, et al. Synovial fluid is a site of citrullination of autoantigens in inflammatory arthritis. *Arthritis Rheum* (2008) 58:2287–95. doi:10.1002/art.23618
16. Tutturen AE, Fleckenstein B, de Souza GA. Assessing the citrullinome in rheumatoid arthritis synovial fluid with and without enrichment of citrullinated peptides. *J Proteome Res* (2014) 13:2867–73. doi:10.1021/pr500030x
17. Chang X, Zhao Y, Wang Y, Chen Y, Yan X. Screening citrullinated proteins in synovial tissues of rheumatoid arthritis using 2-dimensional western blotting. *J Rheumatol* (2013) 40:219–27. doi:10.3899/jrheum.120751
18. van Beers JJ, Schwarte CM, Stammen-Vogelzangs J, Oosterink E, Božič B, Pruijn GJ. The rheumatoid arthritis synovial fluid citrullinome reveals novel citrullinated epitopes in apolipoprotein E, myeloid nuclear differentiation antigen, and beta-actin. *Arthritis Rheum* (2013) 65:69–80. doi:10.1002/art.37720
19. Wang F, Chen FF, Gao WB, Wang HY, Zhao NW, Xu M, et al. Identification of citrullinated peptides in the synovial fluid of patients with rheumatoid arthritis using LC-MALDI-TOF/TOF. *Clin Rheumatol* (2016) 35:2185–94. doi:10.1007/s10067-016-3247-4
20. Suzuki A, Yamada R, Chang X, Tokuhiro S, Sawada T, Suzuki M, et al. Functional haplotypes of PADI4, encoding citrullinating enzyme peptidylarginine deiminase 4, are associated with rheumatoid arthritis. *Nat Genet* (2003) 34:395–402. doi:10.1038/ng1206
21. Chang X, Xia Y, Pan J, Meng Q, Zhao Y, Yan X. PADI2 is significantly associated with rheumatoid arthritis. *PLoS One* (2013) 8:e81259. doi:10.1371/journal.pone.0081259
22. Stahl EA, Raychaudhuri S, Remmers EF, Xie G, Eyre S, Thomson BP, et al. Genome-wide association study meta-analysis identifies seven new rheumatoid arthritis risk loci. *Nat Genet* (2010) 42:508–14. doi:10.1038/ng.582
23. Scally SW, Petersen J, Law SC, Dudek NL, Nel HJ, Loh KL, et al. A molecular basis for the association of the HLA-DRB1 locus, citrullination, and rheumatoid arthritis. *J Exp Med* (2013) 210:2569–82. doi:10.1084/jem.20131241
24. Romero V, Fert-Bober J, Nigrovic PA, Darrah E, Haque UJ, Lee DM, et al. Immune-mediated pore-forming pathways induce cellular hypercitrullination and generate citrullinated autoantigens in rheumatoid arthritis. *Sci Transl Med* (2013) 5:209ra150. doi:10.1126/scitranslmed.3006869
25. Darrah E, Rosen A, Giles JT, Andrade F. Peptidylarginine deiminase 2, 3 and 4 have distinct specificities against cellular substrates: novel insights into autoantigen selection in rheumatoid arthritis. *Ann Rheum Dis* (2012) 71:92–8. doi:10.1136/ard.2011.151712
26. Hollingsworth JW, Siegel ER, Creasey WA. Granulocyte survival in synovial exudate of patients with rheumatoid arthritis and other inflammatory joint diseases. *Yale J Biol Med* (1967) 39:289–96.
27. Li P, Yao H, Zhang Z, Li M, Luo Y, Thompson PR, et al. Regulation of p53 target gene expression by peptidylarginine deiminase 4. *Mol Cell Biol* (2008) 28:4745–58. doi:10.1128/MCB.01747-07
28. Zhang X, Gamble MJ, Stadler S, Cherrington BD, Causey CP, Thompson PR, et al. Genome-wide analysis reveals PADI4 cooperates with Elk-1 to activate c-Fos expression in breast cancer cells. *PLoS Genet* (2011) 7:e1002112. doi:10.1371/journal.pgen.1002112
29. Christophorou MA, Castelo-Branco G, Halley-Stott RP, Oliveira CS, Loos R, Radzisheuskaya A, et al. Citrullination regulates pluripotency and histone H1 binding to chromatin. *Nature* (2014) 507:104–8. doi:10.1038/nature12942
30. Cuthbert GL, Daujat S, Snowden AW, Erdjument-Bromage H, Hagiwara T, Yamada M, et al. Histone deimination antagonizes arginine methylation. *Cell* (2004) 118:545–53. doi:10.1016/j.cell.2004.08.020
31. Neeli I, Khan SN, Radic M. Histone deimination as a response to inflammatory stimuli in neutrophils. *J Immunol* (2008) 180:1895–902. doi:10.4049/jimmunol.180.3.1895
32. Neeli I, Dwivedi N, Khan S, Radic M. Regulation of extracellular chromatin release from neutrophils. *J Innate Immun* (2009) 1:194–201. doi:10.1159/000206974
33. Wang Y, Li M, Stadler S, Correll S, Li P, Wang D, et al. Histone hypercitrullination mediates chromatin decondensation and neutrophil extracellular trap formation. *J Cell Biol* (2009) 184:205–13. doi:10.1083/jcb.200806072
34. Rohrbach AS, Slade DJ, Thompson PR, Mowen KA. Activation of PAD4 in NET formation. *Front Immunol* (2012) 3:360. doi:10.3389/fimmu.2012.00360
35. Kessenbrock K, Krumbholz M, Schönermarck U, Back W, Gross WL, Werb Z, et al. Netting neutrophils in autoimmune small-vessel vasculitis. *Nat Med* (2009) 15:623–5. doi:10.1038/nm.1959
36. Hakkim A, Fürnrohr BG, Amann K, Laube B, Abed UA, Brinkmann V, et al. Impairment of neutrophil extracellular trap degradation is associated with lupus nephritis. *Proc Natl Acad Sci U S A* (2010) 107:9813–8. doi:10.1073/pnas.0909927107
37. Radic M, Marion TN. Neutrophil extracellular chromatin traps connect innate immune response to autoimmunity. *Semin Immunopathol* (2013) 35:465–80. doi:10.1007/s00281-013-0376-6
38. Sun B, Dwivedi N, Bechtel TJ, Paulsen JL, Muth A, Bawadekar M, et al. Citrullination of NF-κB p65 promotes its nuclear localization and TLR-induced expression of IL-1β and TNFα. *Sci Immunol* (2017) 2:eaal3062. doi:10.1126/sciimmunol.aal3062
39. Zhou Y, Di Pucchio T, Sims GP, Mittereder N, Mustelin T. Characterization of the hypercitrullination reaction in human neutrophils and other leukocytes. *Mediators Inflamm* (2015) 2015:236451. doi:10.1155/2015/236451
40. Konig MF, Abusleme L, Reinholdt J, Palmer RJ, Teles RP, Sampson K, et al. *Aggregatibacter actinomycetemcomitans*-induced hypercitrullination links

periodontal infection to autoimmunity in rheumatoid arthritis. *Sci Transl Med* (2016) 8:369ra176. doi:10.1126/scitranslmed.aaj1921
41. Konig MF, Andrade F. A critical reappraisal of neutrophil extracellular traps and NETosis mimics based on differential requirements for protein citrullination. *Front Immunol* (2016) 7:461. doi:10.3389/fimmu.2016.00461
42. Spengler J, Lugonja B, Ytterberg AJ, Zubarev RA, Creese AJ, Pearson MJ, et al. Release of active peptidyl arginine deiminases by neutrophils can explain production of extracellular citrullinated autoantigens in rheumatoid arthritis synovial fluid. *Arthritis Rheumatol* (2015) 67:3135–45. doi:10.1002/art.39313
43. Nakashima K, Hagiwara T, Yamada M. Nuclear localization of peptidylarginine deiminase V and histone deimination in granulocytes. *J Biol Chem* (2002) 277:49562–8. doi:10.1074/jbc.M208795200
44. Sorensen OE, Borregaard N. Neutrophil extracellular traps – the dark side of neutrophils. *J Clin Invest* (2016) 126:1612–20. doi:10.1172/JCI84538
45. Thieblemont N, Wright HL, Edwards SW, Witko-Sarsat V. Human neutrophils in auto-immunity. *Semin Immunol* (2016) 28:159–73. doi:10.1016/j.smim.2016.03.004
46. Corsiero E, Pratesi F, Prediletto E, Bombardieri M, Migliorini P. NETosis as source of autoantigens in rheumatoid arthritis. *Front Immunol* (2016) 7:485. doi:10.3389/fimmu.2016.00485
47. Brinkmann V, Reichard U, Goosmann C, Fauler B, Uhlemann Y, Weiss DS, et al. Neutrophil extracellular traps kill bacteria. *Science* (2004) 303:1532–5. doi:10.1126/science.1092385
48. Lood C, Blanco LP, Purmalek MM, Carmona-Rivera C, De Ravin SS, Smith CK, et al. Neutrophil extracellular traps enriched in oxidized mitochondrial DNA are interferogenic and contribute to lupus-like disease. *Nat Med* (2016) 22:146–53. doi:10.1038/nm.4027
49. Moelants EA, Mortier A, Van Damme J, Proost P. Regulation of TNF-alpha with a focus on rheumatoid arthritis. *Immunol Cell Biol* (2013) 91:393–401. doi:10.1038/icb.2013.15
50. Firestein GS. Evolving concepts of rheumatoid arthritis. *Nature* (2003) 423:356–61. doi:10.1038/nature01661
51. Darrah E, Giles JT, Ols ML, Bull HG, Andrade F, Rosen A. Erosive rheumatoid arthritis is associated with antibodies that activate PAD4 by increasing calcium sensitivity. *Sci Transl Med* (2013) 5:186ra165. doi:10.1126/scitranslmed.3005370
52. Giles JT, Darrah E, Danoff S, Johnson C, Andrade F, Rosen A, et al. Association of cross-reactive antibodies targeting peptidyl-arginine deiminase 3 and 4 with rheumatoid arthritis-associated interstitial lung disease. *PLoS One* (2014) 9:e98794. doi:10.1371/journal.pone.0098794
53. Makrygiannakis D, af Klint E, Lundberg IE, Löfberg R, Ulfgren AK, Klareskog L, et al. Citrullination is an inflammation-dependent process. *Ann Rheum Dis* (2006) 65:1219–22. doi:10.1136/ard.2005.049403
54. Damgaard D, Palarasah Y, Skjødt K, Catrina AI, Hensen SM, Pruijn GJ, et al. Generation of monoclonal antibodies against peptidylarginine deiminase 2 (PAD2) and development of a PAD2-specific enzyme-linked immunosorbent assay. *J Immunol Methods* (2014) 405:15–22. doi:10.1016/j.jim.2013.12.008
55. Li P, Li M, Lindberg MR, Kennett MJ, Xiong N, Wang Y. PAD4 is essential for antibacterial innate immunity mediated by neutrophil extracellular traps. *J Exp Med* (2010) 207:1853–62. doi:10.1084/jem.20100239
56. Abrams ST, Zhang N, Manson J, Liu T, Dart C, Baluwa F, et al. Circulating histones are mediators of trauma-associated lung injury. *Am J Respir Crit Care Med* (2013) 187:160–9. doi:10.1164/rccm.201206-1037OC
57. Xu J, Zhang X, Pelayo R, Monestier M, Ammollo CT, Semeraro F, et al. Extracellular histones are major mediators of death in sepsis. *Nat Med* (2009) 15:1318–21. doi:10.1038/nm.2053
58. Ekaney ML, Otto GP, Sossdorf M, Sponholz C, Boehringer M, Loesche W, et al. Impact of plasma histones in human sepsis and their contribution to cellular injury and inflammation. *Crit Care* (2014) 18:543. doi:10.1186/s13054-014-0543-8
59. Zhang Y, Wen Z, Guan L, Jiang P, Gu T, Zhao J, et al. Extracellular histones play an inflammatory role in acid aspiration-induced acute respiratory distress syndrome. *Anesthesiology* (2015) 122:127–39. doi:10.1097/ALN.0000000000000429
60. Xu J, Zhang X, Monestier M, Esmon NL, Esmon CT. Extracellular histones are mediators of death through TLR2 and TLR4 in mouse fatal liver injury. *J Immunol* (2011) 187:2626–31. doi:10.4049/jimmunol.1003930
61. Huang H, Evankovich J, Yan W, Nace G, Zhang L, Ross M, et al. Endogenous histones function as alarmins in sterile inflammatory liver injury through toll-like receptor 9 in mice. *Hepatology* (2011) 54:999–1008. doi:10.1002/hep.24501
62. Allam R, Darisipudi MN, Tschopp J, Anders HJ. Histones trigger sterile inflammation by activating the NLRP3 inflammasome. *Eur J Immunol* (2013) 43:3336–42. doi:10.1002/eji.201243224
63. Koziel J, Bryzek D, Sroka A, Maresz K, Glowczyk I, Bielecka E, et al. Citrullination alters immunomodulatory function of LL-37 essential for prevention of endotoxin-induced sepsis. *J Immunol* (2014) 192:5363–72. doi:10.4049/jimmunol.1303062
64. Mortier A, Loos T, Gouwy M, Ronsse I, Van Damme J, Proost P. Posttranslational modification of the NH2-terminal region of CXCL5 by proteases or peptidylarginine deiminases (PAD) differently affects its biological activity. *J Biol Chem* (2010) 285:29750–9. doi:10.1074/jbc.M110.119388
65. Loos T, Mortier A, Gouwy M, Ronsse I, Put W, Lenaerts JP, et al. Citrullination of CXCL10 and CXCL11 by peptidylarginine deiminase: a naturally occurring posttranslational modification of chemokines and new dimension of immunoregulation. *Blood* (2008) 112:2648–56. doi:10.1182/blood-2008-04-149039
66. Nakayama-Hamada M, Suzuki A, Furukawa H, Yamada R, Yamamoto K. Citrullinated fibrinogen inhibits thrombin-catalysed fibrin polymerization. *J Biochem* (2008) 144:393–8. doi:10.1093/jb/mvn079
67. Okumura N, Haneishi A, Terasawa F. Citrullinated fibrinogen shows defects in FPA and FPB release and fibrin polymerization catalyzed by thrombin. *Clin Chim Acta* (2009) 401:119–23. doi:10.1016/j.cca.2008.12.002
68. Chang X, Yamada R, Suzuki A, Sawada T, Yoshino S, Tokuhiro S, et al. Localization of peptidylarginine deiminase 4 (PADI4) and citrullinated protein in synovial tissue of rheumatoid arthritis. *Rheumatology* (2005) 44:40–50. doi:10.1093/rheumatology/keh414
69. Masson-Bessière C, Sebbag M, Girbal-Neuhauser E, Nogueira L, Vincent C, Senshu T, et al. The major synovial targets of the rheumatoid arthritis-specific antifilaggrin autoantibodies are deiminated forms of the alpha- and beta-chains of fibrin. *J Immunol* (2001) 166:4177–84. doi:10.4049/jimmunol.166.6.4177
70. Sipilä K, Haag S, Denessiouk K, Käpylä J, Peters EC, Denesyuk A, et al. Citrullination of collagen II affects integrin-mediated cell adhesion in a receptor-specific manner. *FASEB J* (2014) 28:3758–68. doi:10.1096/fj.13-247767
71. Shelef MA, Bennin DA, Mosher DF, Huttenlocher A. Citrullination of fibronectin modulates synovial fibroblast behavior. *Arthritis Res Ther* (2012) 14:R240. doi:10.1186/ar4083
72. Zhou Y, Wu J, Kucik DF, White NB, Redden DT, Szalai AJ, et al. Multiple lupus-associated ITGAM variants alter Mac-1 functions on neutrophils. *Arthritis Rheum* (2013) 65:2907–16. doi:10.1002/art.38117
73. Aletaha D, Neogi T, Silman AJ, Funovits J, Felson DT, Bingham CO III, et al. 2010 rheumatoid arthritis classification criteria: an American College of Rheumatology/European league against rheumatism collaborative initiative. *Ann Rheum Dis* (2010) 69:1580–8. doi:10.1136/ard.2010.138461
74. Hochberg MC. Updating the American College of rheumatology revised criteria for the classification of systemic lupus erythematosus. *Arthritis Rheum* (1997) 40:1725. doi:10.1002/art.1780400928
75. Oganesyan V, Gao C, Shirinian L, Wu H, Dall'Acqua WF. Structural characterization of a human Fc fragment engineered for lack of effector functions. *Acta Crystallogr D Biol Crystallogr* (2008) 64:700–4. doi:10.1107/S0907444908007877
76. Wisniewski JR, Zougman A, Nagaraj N, Mann M. Universal sample preparation method for proteome analysis. *Nat Methods* (2009) 6:359–62. doi:10.1038/nmeth.1322

Conflict of Interest Statement: YZ, BC, NM, RC, MS, SR, WM, CL, DC, KV, GS, and TM are full-time employees of MedImmune, a member of the AstraZeneca group. FA is supported by a research grant from MedImmune and serves as a consultant for Bristol-Myers Squibb Company.

frontiers in Immunology

ORIGINAL RESEARCH
published: 16 January 2018
doi: 10.3389/fimmu.2017.02007

Heterogeneity of the Type I Interferon Signature in Rheumatoid Arthritis: A Potential Limitation for Its Use As a Clinical Biomarker

Javier Rodríguez-Carrio[1,2], Mercedes Alperi-López[2,3], Patricia López[1,2], Francisco J. Ballina-García[2,3] and Ana Suárez[1,2]*

[1] Area of Immunology, Department of Functional Biology, Faculty of Medicine, University of Oviedo, Oviedo, Spain, [2] Instituto de Investigación Sanitaria del Principado de Asturias (ISPA), Oviedo, Spain, [3] Department of Rheumatology, Hospital Universitario Central de Asturias, Oviedo, Spain

Introduction: An increased expression of interferon (IFN)-responding genes (IRGs), the so-called IFN signature, has been reported in rheumatoid arthritis (RA). However, some controversy exists concerning its clinical relevance. The main aim of this study is to evaluate whether quantitative and qualitative differences in the activation of the IFN pathway may account for these findings.

Methods: The expression of IFN-induced protein 44 (IFI44), IFN-induced protein 44 like (IFI44L), IFN alpha inducible protein 6, and MX dynamin-like GTPase 1 (MX1) was determined in peripheral blood in 98 RA patients (IFI6) and 28 controls. RA patients were classified into groups according to their clinical stage and treatments received: very early RA (VERA), biological disease-modifying antirheumatic drug (bDMARD) naive, and bDMARD. An additional group of 13 RA patients candidates for tumor necrosis factor alpha (TNFα) blockade was also recruited. The associations among IRGs were evaluated by network and principal component analyses.

Results: The expression of all IRGs was increased in RA to different levels. The IFN score was increased in all RA groups (VERA, bDMARD-naïve, and bDMARD), but important differences in their degree of activation and in the relationships among IRGs were observed. The IFN score correlated with the accumulated disease activity score 28-joints, and it was found to be a predictor of clinical outcome in VERA. No differences in the IFN score were observed between the bDMARD-naive and bDMARD groups, but opposite associations with the clinical parameters were noted. Interestingly, the correlations among IRGs delineate different pictures between these two groups. The IFN score at baseline predicted poor clinical outcome upon TNFα blockade. Although no absolute changes in the IFN score were found, TNFα-blockade shifted the associations among IRGs.

Conclusion: A certain heterogeneity within the IFN signature can be recognized in RA, depending on the clinical stage. The structure of the IFN signature may be a potential explanation for the controversy in this field and must be considered to decipher its clinical relevancein RA.

Keywords: arthritis, interferon, IFN signature, biomarker, autoimmunity

OPEN ACCESS

Edited by:
Antonio La Cava, University of California, Los Angeles, United States

Reviewed by:
Gunnar Houen, State Serum Institute (SSI), Denmark
Kichul Ko, University of Chicago Medical Center, United States

****Correspondence:***
Javier Rodríguez-Carrio
rodriguezcjavier@uniovi.es

Specialty section:
This article was submitted to Molecular Innate Immunity, a section of the journal Frontiers in Immunology

Received: *23 November 2017*
Accepted: *27 December 2017*
Published: *16 January 2018*

Citation:
Rodríguez-Carrio J, Alperi-López M, López P, Ballina-García FJ and Suárez A (2018) Heterogeneity of the Type I Interferon Signature in Rheumatoid Arthritis: A Potential Limitation for Its Use As a Clinical Biomarker. Front. Immunol. 8:2007. doi: 10.3389/fimmu.2017.02007

INTRODUCTION

Rheumatoid arthritis (RA) is a chronic systemic autoimmune condition hallmarked by joint inflammation and destruction. A number of immune mediators have been linked to RA pathogenesis, including adaptive and innate components. A growing body of evidence supports an emerging role for type I interferons (IFNs) (1). Due to their immunomodulatory effects (2), the type I IFNs are thought to prompt the breakdown of tolerance and the subsequent perpetuation of autoimmune phenomena (3, 4). Actually, several IFN-related genes have been identified as risk loci for RA (3), and development of arthritis after treatment with IFNα has been extensively documented (5, 6).

Signaling through the type I IFN pathway leads to an increased expression of several IFN-responding genes (IRGs). This global expression profile, referred to as the "IFN signature," has been found in peripheral blood in a subset of RA patients [from 25 to 65% (7–10)]. Moreover, increased serum levels of IFNα have been demonstrated in RA (11). Elevated IFNα serum levels in the synovial fluid and IFN signature in the synovial membrane have also been reported (8, 12).

Although the potential role of the type I IFN as biomarkers has been investigated with enormous interest, the findings reported until date are contradictory and the current evidence is limited. On the one hand, inconclusive results of the association between the IFN score and clinical features have been reported (9, 10, 13, 14). On the other hand, longitudinal changes of the IFN score have been described, partly attributed to the use of different immunomodulatory drugs (15–17). In addition, the majority of the studies were focused on patients with established disease, whereas a major knowledge gap exists for the role of the IFN signature in (very) early RA. Finally, a physiological diversification of the type I IFN response in different autoimmune diseases has been described, hence suggesting that different pathogenic roles for the type I IFNs may be expected in different clinical contexts (18). However, whether this can be applied to a single disease remains unknown.

Therefore, it is tempting to speculate that not only the degree of activation but also the composition of the IFN response could be relevant for its role as a biomarker. Taken all these ideas into account, we hypothesized that certain heterogeneity within the type I IFN signature in RA may impair its applicability as a biomarker, hence explaining the controversy reported in previous works. Thus, in this study, we aimed to analyze the potential associations between the IFN score and clinical features in RA patients depending on their clinical stage [from very early RA (VERA) to established disease], with a focus on the relationships among IRGs.

Abbreviations: ACPA, anticitrullinated peptide antibodies; bDMARDs, biological DMARDs; CRP, C-reactive protein; csDMARDs, conventional synthetic DMARDs; DAS28, disease activity score 28-joints; DMARDs, disease-modifying antirheumatic drugs; EULAR, European league against rheumatism; ESR, erythrocyte sedimentation rate; HAQ, health assessment questionnaire; HC, healthy control; IFI6, interferon alpha inducible protein 6; IFI44, interferon-induced protein 44; IFI44L, interferon-induced protein 44 like; IFN, interferon; IRG, interferon-responding gene; MHC, major histocompatibility factor; MX1, MX dynamin-like GTPase 1; NSAIDs, non-steroidal anti-inflammatory drugs; RA, rheumatoid arthritis; RF, rheumatoid factor; TNF, tumor necrosis factor alpha.

MATERIALS AND METHODS

Ethical Approval

The study was approved by the Institutional Review Board (Comité de Ética de Investigación Clínica del Principado de Asturias) in compliance with the Declaration of Helsinki. All study subjects gave written informed consent.

Patients and Controls

Our study involved 98 RA patients [2010 ACR/European league against rheumatism (EULAR) classification criteria] recruited from the Department of Rheumatology at Hospital Universitario Central de Asturias. A complete clinical examination, including disease activity score 28-joints (DAS28) and health assessment questionnaire (HAQ) calculations, was performed on all patients during the clinical appointment. Patients recruited at onset and not being previously exposed to any treatment were considered as VERA. These patients were prospectively followed up for 1 year, and clinical outcomes were registered at 6 and 12 months. DAS28 score accumulated over 1 year was calculated (19). Clinical management was performed according to EULAR recommendations (20). In addition, a group of 13 biologicals-naive RA patients [12 women; median age, 43 (range, 30–65), DAS28 5.08 (1.93), 38.5% RF+, 46.1% ACPA+], candidates for tumor necrosis factor alpha (TNFα)-blockers was prospectively followed up for 3 months. A blood sample was obtained before and 3 months after the initiation of the TNFα blockade therapy. The clinical response was evaluated by EULAR criteria (21). Patients exhibiting a good response were compared to those with moderate or no response.

Simultaneously, 28 gender- and age-matched healthy controls (HCs) were recruited from the same population. A blood sample was collected from all individuals by venipuncture.

RNA Isolation and RT-PCR

Blood samples were immediately processed after extraction. Whole blood was stabilized with RNA Stabilization Reagent for Blood/Bone Marrow (Roche, Germany) according to the manufacturer's instructions and stored at −20°C. Then samples were thawed at room temperature, and mRNA was isolated using the mRNA Isolation Kit for Blood/Bone Marrow (Roche), according to the protocol provided by the manufacturer. Reverse transcription was carried out using Transcription First Strand cDNA Synthesis Kit (Roche).

Real-time PCR

Gene expression was evaluated with TaqMan pre-designed assays for the following genes: IFN-induced protein 44 (IFI44; ref. Hs00197427_m1), IFN-induced protein 44 like (IFI44L; ref. Hs00915292_m1), MX dynamin-like GTPase 1 (MX1; ref. Hs00895608_m1), and IFN alpha inducible protein 6 (IFI6; ref. Hs00242571_m1). Reactions were performed in TaqMan® Gene Expression Master Mix. Real-time quantitative PCR was performed in an ABI Prism HT7900 (Applied Biosystems, Germany)

instrument, and Ct values were analyzed with the software SDS 2.3. All samples were assayed by triplicate, and the average was used. Expression levels were evaluated by the $2^{-\Delta Ct}$ method, using the GAPDH gene expression as the housekeeping to normalize Ct values. The expression levels were log transformed.

Statistical Analyses

Continuous variables were summarized as median (interquartile range) or mean ± SD, whereas *n* (%) was used for categorical ones. Differences between groups were analyzed by Mann–Whitney *U*-test, Kruskal–Wallis (with Dunn–Bonferroni correction for multiple comparisons), or χ^2 tests, as appropriate. Wilcoxon test was used for paired samples. The size effect of the differences was evaluated by Hedges'g statistic (22). Correlations were assessed by Spearman ranks test. The associations of continuous variables adjusted for confounders were analyzed by multiple regression models, and B coefficients (B) with 95% confidence intervals (CIs) were calculated. The discriminative capacity was studied using receiving operator characteristics analyses, and the area under the curve (AUC) was computed. *Z*-scores were calculated for each IRG from the distribution found in the whole population. Principal component analyses (correlation method) were performed with the individual IRGs, and biplots were generated to visualize the associations among IRG in the different groups of patients. Since strong correlations among IRGs were observed, an IFN score was calculated by averaging all IRGs per sample. $P < 0.050$ was considered as statistically significant. Statistical analyses were performed using SPSS 22.0, R 3.3.1 and GraphPad Prism 5.0 for Windows.

TABLE 1 | Characteristics of the subjects recruited in this study.

	HC (*n* = 28)	RA (*n* = 98)	*P* value
Demographical features			
Age (years); median (range)	49.38 (35.17–60.17)	52.93 (22.00–65.10)	0.174
Gender (f/m)	20/8	79/19	0.334
Disease features			
Disease duration (years)		4.00 (7.08)	
Age at diagnosis (years); median (range)		47.37 (19.00–65.00)	
Disease activity (DAS28)		4.01 (2.10)	
Tender joint count		3.00 (7.00)	
Swollen joint count		2.00 (5.00)	
Patient global assessment (0–100)		50.00 (35.00)	
Erythrocyte sedimentation rate (mm/h)		18.00 (29.00)	
C-reactive protein (mg/l)		2.30 (4.50)	
Health assessment questionnaire (0–3)		1.00 (1.16)	
RF (+), *n* (%)		58 (59.1)	
ACPA (+), *n* (%)		61 (62.2)	
Erosive disease, *n* (%)		41 (41.8)	
Treatments, *n* (%)			
None		18 (18.3)	
Glucocorticoids		56 (57.1)	
Methotrexate		65 (66.3)	
Tumor necrosis factor alpha blockers		36 (36.7)	

Variables were summarized as median (interquartile range) or n (%), as appropriate, unless otherwise stated. Differences in demographic parameters were assessed by Mann–Whitney U-tests or χ^2 tests, according to the distribution of the variables.

RESULTS

IRG Genes and IFN Score: Quantitative and Qualitative Approaches

To gain insight into the type I IFN signature in RA, the expression of IRGs, either independently or as a whole in a composite IFN score, was quantified in 98 RA patients and 28 HC (**Table 1**). All IRGs were upregulated in RA (**Figure 1A**), although a less-pronounced difference was observed in IFI44. A composite IFN score was computed as previously described, and a higher value was found in RA (**Figure 1A**).

Importantly, certain heterogeneity among RA patients was observed. Therefore, we aimed to analyze whether the IFN score may differ according to the clinical stage of RA. Then patients were classified into three groups: VERA (patients recruited at onset, not being exposed to any treatment), biological disease-modifying antirheumatic drug (bDMARD)-naive [patients on conventional synthetic DMARDs (csDMARD) treatment alone or in combination—glucocorticoids and/or methotrexate—not being previously exposed to any bDMARD], and bDMARD (patients on bDMARD therapy—all under TNFi treatment—with previous no response to csDMARD) (Table S1 in Supplementary Material). Although the IFN score was increased in all groups, quantitative differences were observed between VERA patients and their established counterparts (**Figure 1B**), hence indicating that the level of IRGs expression differed according to the disease course. No differences were found with the use of bDMARDs. Leukocyte populations did not exhibit notable differences among the groups analyzed (Table S2 in Supplementary Material). Only a slight increase in neutrophil count was observed in VERA patients. To exclude a potential confounding effect of the leukocyte composition, the IFN score was corrected by the neutrophil-to-lymphocyte ratio, and the differences among groups remained unchanged. Similarly, the IFN score did not correlate with any of the leukocyte populations nor in the whole RA population neither in the different clinical stages. Overall, a major effect of leukocyte composition on the IFN score can be ruled out.

Apart from quantitative differences, we aimed to evaluate whether qualitative differences, that is, distinct associations among IRGs, can be also found. To this aim, a PCA approach was conducted, and biplots were produced to visualize the potential associations among IRGs. First, a global PCA including all RA patients and HC was performed. Although a significant overlap was detected, differences were noted among groups (**Figure 2A**). The biggest differences were observed between HC and RA patients. The ellipse from VERA patients lie between those of HC and established RA groups. Again, IFI44 showed an outlier position in the graph compared to the rest of IRGs. However, certain dispersion was noted. It is important to note that differences observed in the IRGs expression and the distinct sample sizes could also limit a proper appraisal of the qualitative differences among groups. Therefore, additional analyses to gain insight into these differences were warranted.

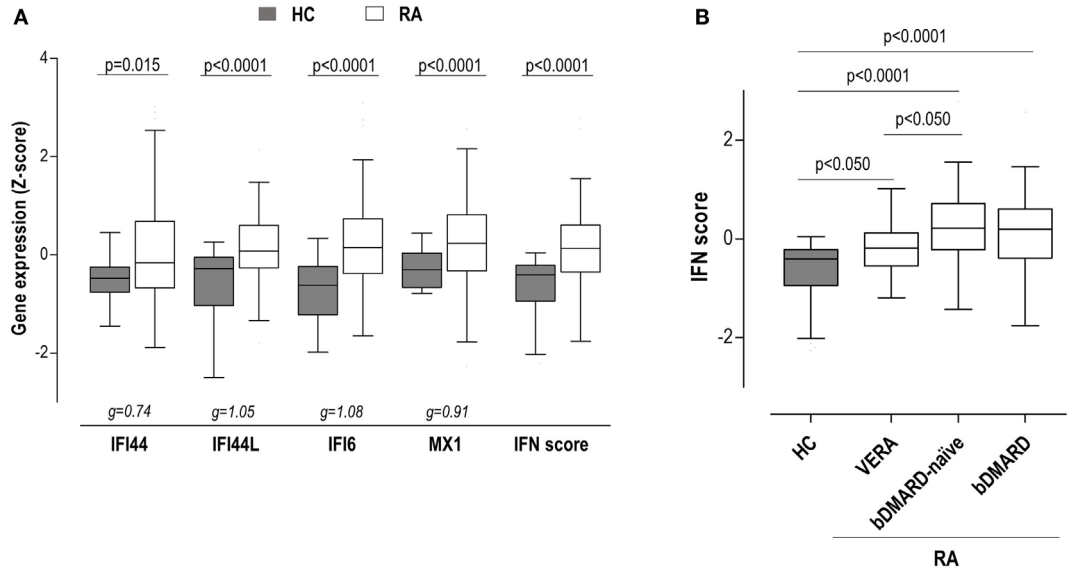

FIGURE 1 | Interferon (IFN)-responding gene (IRG) expression and IFN score in rheumatoid arthritis (RA) patients. **(A)** The expression of the individual IRGs [IFN-induced protein 44 (IFI44), IFN-induced protein 44 like (IFI44L), IFN alpha inducible protein 6 (IFI6), and MX dynamin-like GTPase 1 (MX1)] and the levels of the IFN score were compared between healthy control (HC) (gray boxes) and RA patients (white boxes). **(B)** The levels of the IFN score were compared between HC and RA patients according to the different clinical stages. Boxes represent 25th and 75th percentiles, whereas whiskers represent minimum and maximum values. Statistical analyses were performed by Kruskal–Wallis with Dunn–Bonferroni tests for multiple comparisons. *P* values correspond to those obtained in the multiple comparisons tests. For the analysis of individual IRGs, Hedges'g statistics (at the bottom of the graph) was included to account for the differential size effects observed across IRGs.

Then independent biplots were generated for each group (**Figure 2B**). Based on the angles between the vectors of the IRGs, these analyses revealed that distinct pictures hallmarked the clinical stages analyzed. First, remarkable differences were observed between HC and RA patients. Next, a distinct picture was found in the VERA group compared to both the bDMARD-naive and bDMARD groups, depending on the relative position of the IRGs. A shortening of the angles between IFI6 and MX1 as well as between IFI44 and IFI44L was seen in the established groups, especially in the bDMARD group. Furthermore, the associations among IRGs were plotted in correlation graphs (**Figure 3A**). This approach revealed that the associations among IRG were not homogeneous in the groups analyzed and, more importantly, IRGs exhibited a higher overall degree of correlation in patients with established RA, especially in the bDMARD group. Finally, network graphs were generated to visualize the interactions among independent genes (**Figure 3B**). Notably, the structure of the network differed among the groups analyzed, IRGs describing different grouping patterns. Networks seem to show a progressive change from HC, where a weaker network (that is, with subtle links among IRGs) is observed, toward a strengthening of these links along the clinical stages, with an enhanced overall degree of correlation being found in bDMARD patients, hence confirming our previous observations.

Overall, these results confirm quantitative and qualitative changes in the activation of the type I IFN pathway in RA. Differential profiles of correlations among IRGs can be observed according to disease status, hence pointing to certain heterogeneity within the IFN signature.

IFN Signature As Predictor of Clinical Response in VERA

Next, we studied the clinical relevance of the IFN signature in the distinct groups. First, the potential role of the IFN signature as predictor of the clinical outcome in untreated, VERA patients was assessed. Therefore, patients were prospectively followed up for 1 year and disease activity and response to csDMARD treatment (glucocorticoids and methotrexate in combination) were registered at 6 (T6) and 12 months (T12).

Although the IFN score at baseline (BL) was observed to be increased already in this very early stage (**Figure 1B**), when IRGs were analyzed, only differences in IFI44L and IFI6 were observed (**Figure 4A**). Regarding clinical features, a positive correlation between IFN score and anticitrullinated peptide antibody (ACPA) titer was found ($r = 0.532$, $P = 0.034$).

Interestingly, our analyses did not retrieve an association between the IFN score and the DAS28 at sampling ($r = -0.055$, $P = 0.835$), but with DAS28 at T6 ($r = 0.620$, $P = 0.008$) and T12 ($r = 0.552$, $P = 0.041$). Consequently, the IFN score at BL was positively associated with the accumulated DAS28 over 1 year (AUC DAS28: $r = 0.593$, $P = 0.025$). A multivariate analysis including IFN score, ACPA, rheumatoid factor (RF), and gender revealed that IFN score at BL may be the only independent predictor of accumulated DAS28 [B (95% CI): 12.883 (−0.381 to 26.147), $P = 0.051$], although statistical significance was not reached. Then patients were grouped according to their clinical response at T6 [responders (R), $n = 8$] and T12 (R, $n = 10$). A higher IFN score at diagnosis was observed in patients who exhibited a poor clinical response at T6 (**Figure 4B**), compared to

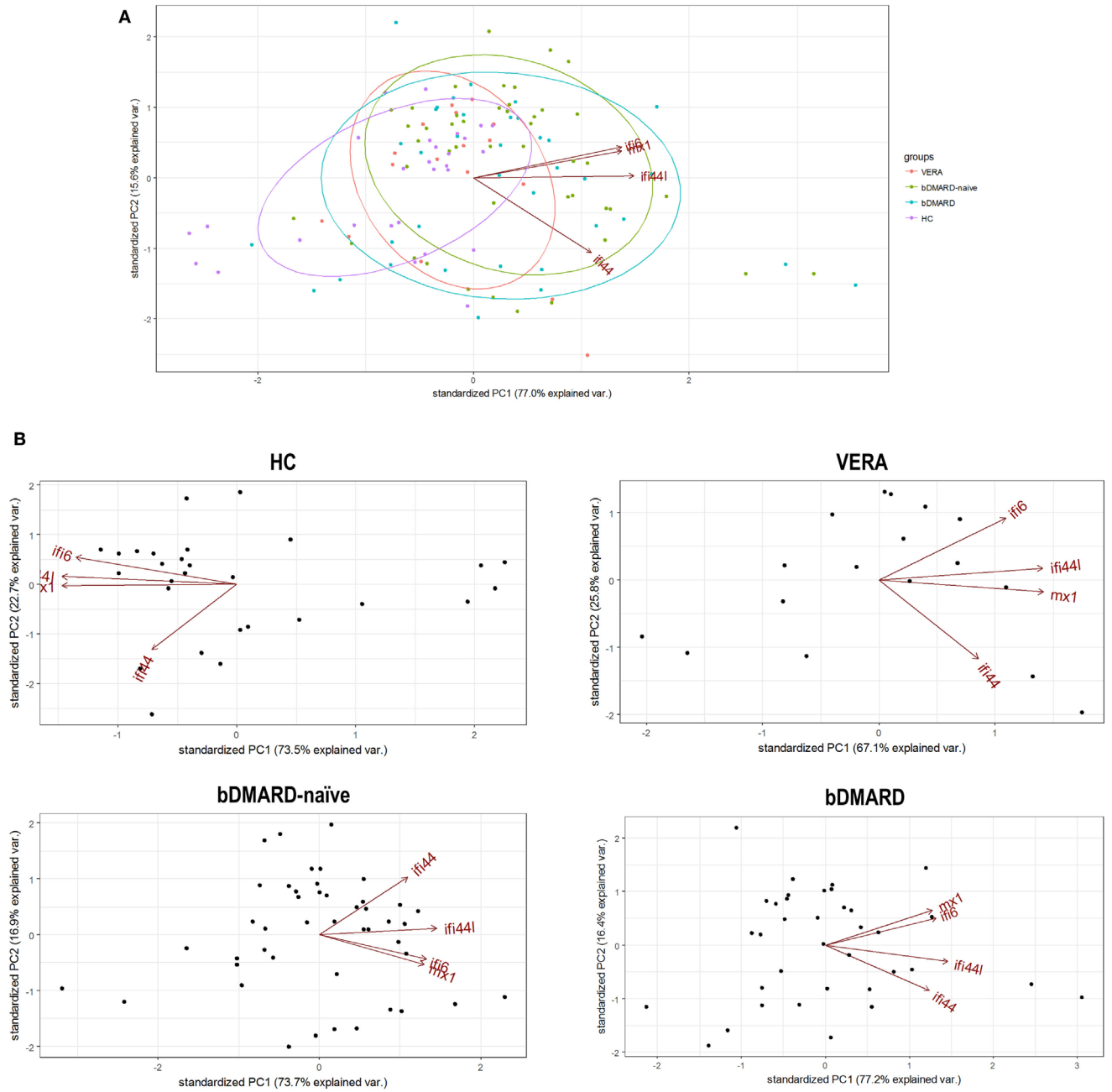

FIGURE 2 | Analysis of the associations among interferon (IFN)-responding genes (IRGs) by PCA. **(A)** Biplot from the PCA (correlation method) conducted on all the groups analyzed [healthy control (HC), purple; VERA, red; biological disease-modifying antirheumatic drug (bDMARD)-naive, green; and bDMARD, blue]. Arrows represent the original variables. The angles between the arrows represent their correlation. Ellipses are drawn for each group (probability set as 0.68, by default). KMO = 0.705, Bartlett sphericity test $P = 4 \times 10^{-8}$, determinant = 0.032. **(B)** PCA conducted individually for each group of individuals included in the study: HC [KMO = 0.695, Bartlett sphericity test $P = 1.5 \times 10^{-25}$, determinant = 0.012], VERA [KMO = 0.734, Bartlett sphericity $P = 2 \times 10^{-7}$, determinant = 0.051], bDMARD-naive [KMO = 0.700, Bartlett sphericity test $P = 1 \times 10^{-23}$, determinant = 0.053], and bDMARD [KMO = 0.642, Bartlett sphericity test $P = 2 \times 10^{-25}$, determinant = 0.020].

either good responders or HC. Equivalent results were observed at 12 months [non-responder (NR) vs R: 0.17 (0.82) vs −0.44 (0.77), $P = 0.039$; vs HC: −0.40 (72), $P = 0.003$]. This association with the clinical outcome was observed when IRGs were analyzed individually except for IFI44 (Figure S1 in Supplementary Material), both at T6 and T12. Interestingly, even in the case of MX1, despite not being increased compared to HC, increased levels were observed in NR. Next, the ability of the IFN score to discriminate between responders and non-responders was evaluated by COR curves. Accordingly, IFN score showed a good

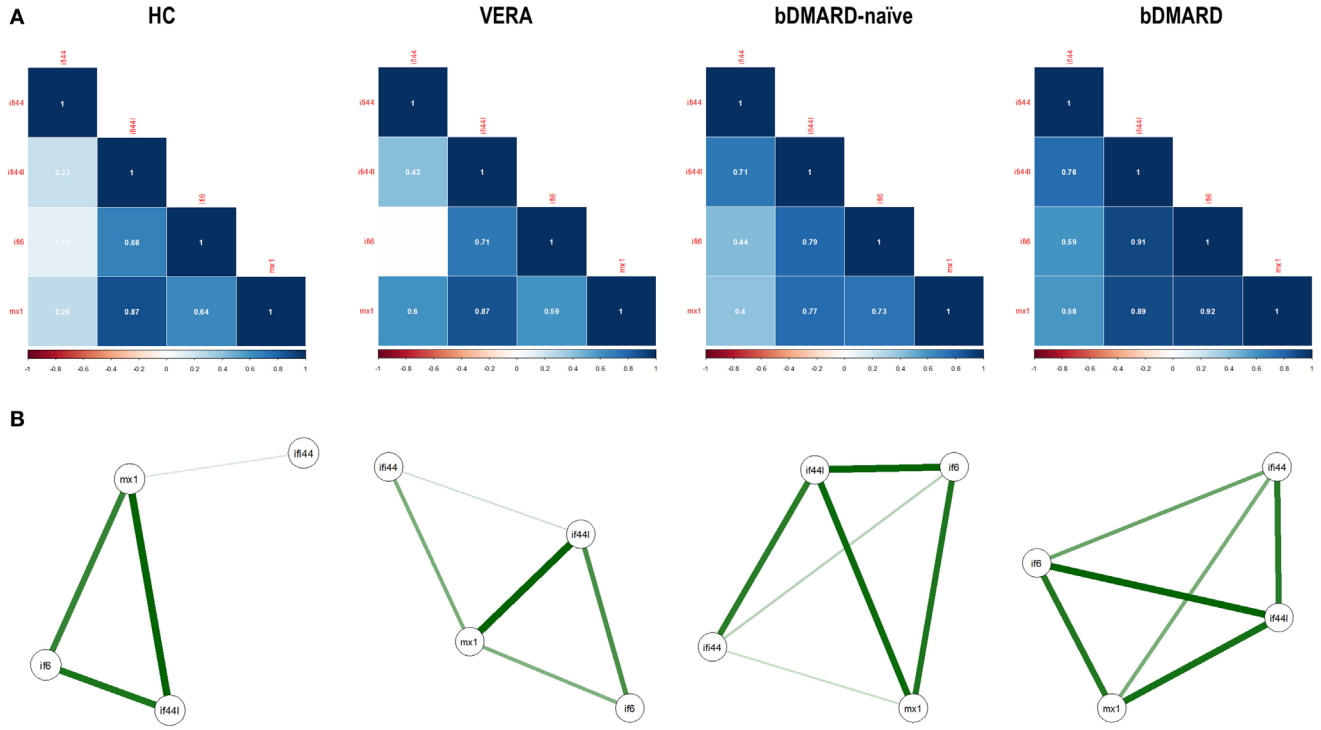

	HC	VERA	bDMARD-naïve	bDMARD
Branches, n	4	5	6	6
Branches, % out of maximum	66.6	83.3	100	100
Accumulated correlation scores, sum	2.79	3.19	3.84	4.65
Upregulated IRGs, n		2	4	4
Hedges' g statistic (IFN score)		0.78	1.24	1.14

FIGURE 3 | Analysis of the correlations and structure of the interferon (IFN)-responding genes (IRGs) networks. **(A)** Analyses of the correlations among IRG in the different groups studied. Correlation matrices were plotted in 2 × 2 correlograms. Correlation coefficients were depicted in white. Color of the tiles is proportional to the strength of the correlation (color scale is represented at the bottom of each grap). **(B)** Network analyses of the IRGs in the groups studied. Each node corresponds to an IRG, and the lines illustrate the strength (width) and sign (green, positive; red, negative) of the correlations between each pair of variables. The interferon (IFN) network in healthy control (HC) is characterized by a group of three IRGs closely correlated [IFN-induced protein 44 like (IFI44L), MX dynamin-like GTPase 1, and IFN alpha inducible protein 6 (IFI6)], almost not related to IFI44L. Stronger correlations were observed in very early rheumatoid arthritis (VERA) and rheumatoid arthritis (RA) established groups compared to HC, and a more complex, intricate network was observed in biological disease-modifying antirheumatic drug (bDMARD) patients, with a closer location of all IRGs and a strong correlation between IFN-induced protein 44 (IFI44) and IFI44L. Similarly, a correlation between IFI6 and IFI44 is differentially expressed in established RA, compared to VERA or HC. Additional information on the network structure and its overall activation was summarized in the table at the bottom of the figure.

discriminative capacity. Exclusion of the IFI44 expression [IFN score (3 genes)] from the composite score did not substantially change the results. Similarly, a lower but still good discriminative capacity was found when only IFI6 and IFI44L were retained in the IFN score (**Figure 4C**).

In sum, a high IFN score at diagnosis in untreated RA patients is linked to a poor clinical outcome, thus shedding some light into their potential clinical implications as a biomarker.

IFN Signature in Established RA

Next, an analysis of the potential associations between the IFN score and clinical features in patients with established RA was performed.

The IFN score was not correlated with DAS28, disease duration, or RF/ACPA positivity in the bDMARD-naive group. In addition, no associations with GC or MTX treatment were found. The clinical response of these patients to csDMARD therapy was monitored during 1 year, and five patients were switched to a bDMARD treatment due to clinical inefficacy of csDMARD treatment. The analysis of these patients revealed that IFN score at study entry did not differ compared to those who continued on csDMARDs [−0.13 (0.89) vs 0.27 (0.89), $P = 0.140$].

Then the associations between the IFN score and clinical features were analyzed in patients undergoing bDMARD treatment (all anti-TNFα agents). Surprisingly, a negative correlation between IFN score and DAS28 was observed ($r = -0.358$,

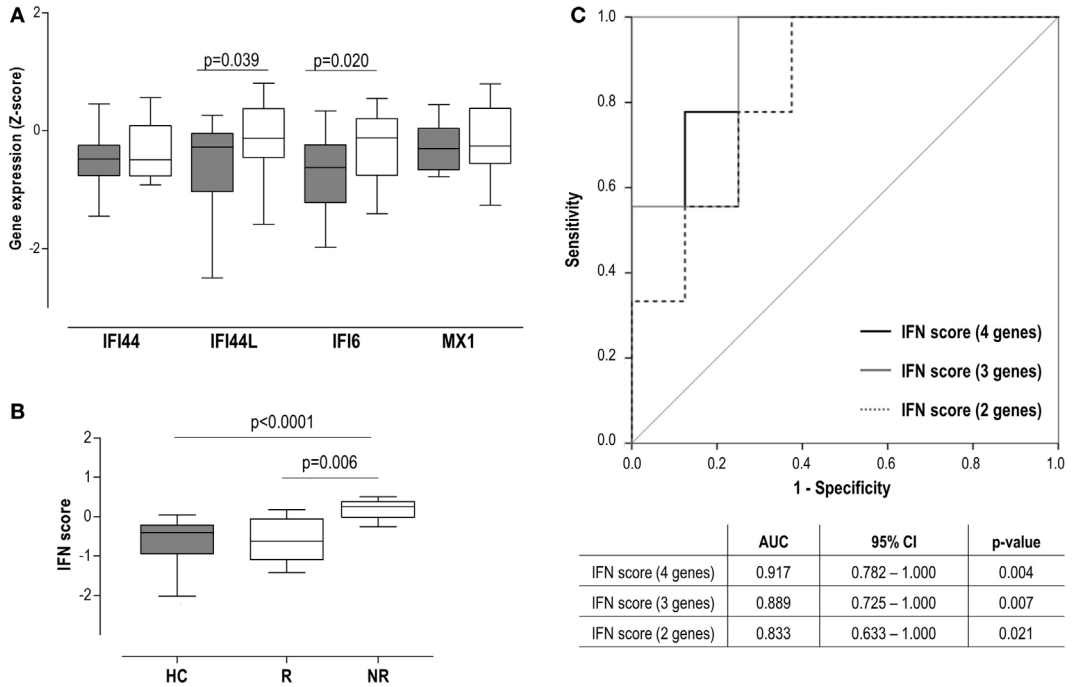

	AUC	95% CI	p-value
IFN score (4 genes)	0.917	0.782 – 1.000	0.004
IFN score (3 genes)	0.889	0.725 – 1.000	0.007
IFN score (2 genes)	0.833	0.633 – 1.000	0.021

FIGURE 4 | Interferon (IFN) signature as a biomarker of clinical outcome in very early rheumatoid arthritis (VERA) patients. **(A)** Analysis of the individual IFN-responding genes expression in VERA patients (white boxes) compared to healthy control (HC) (gray boxes). **(B)** Differences in the IFN score among HC and rheumatoid arthritis patients classified as responders (R) or non-responders (NRs) according to European league against rheumatism criteria after 6 months. Boxes represent 25th and 75th percentiles, whereas whiskers represent minimum and maximum values. Statistical analyses were performed by Kruskal–Wallis with Dunn–Bonferroni tests for multiple comparisons. *P* values correspond to those obtained in the multiple comparisons tests. **(C)** Area under the curve (AUC) receiving operator characteristic analysis of the IFN score to predict response at 12 months. AUCs, 95% confidence intervals (CIs), and *P* values are shown in the table for the IFN score: four genes [IFN-induced protein 44 (IFI44), IFN-induced protein 44 like (IFI44L), IFN alpha inducible protein 6 (IFI6), and MX dynamin-like GTPase 1 (MX1)], three genes (IFI44L, IFI6, and MX1), and two genes (IFI44L and IFI6).

$P = 0.032$), but no associations were found with disease duration or HAQ. When individual genes were analyzed, MX1 showed a stronger correlation with DAS28 ($r = -0.459$, $P = 0.005$) compared to the other IRGs (IFI44: $r = -0.104$, $P = 0.546$; IFI44L: $r = -0.384$, $P = 0.021$ and IFI6: $r = -0.394$, $P = 0.017$). In addition, negative associations with RF titer ($r = -0.565$, $P < 0.001$) and trend with ACPA levels ($r = -0.302$, $P = 0.087$) were found for the IFN score. Importantly, no effect of GC or MTX co-treatment was observed.

As a conclusion, the IFN score was not associated with the clinical response to csDMARD in established RA. Surprisingly, opposed associations with clinical features were noted between bDMARD naive and bDMARD patients, a negative correlation with disease activity being found in the latter. Whether bDMARD-induced qualitative changes on the IFN signature underlie these contrary results remains to be elucidated.

Changes in the IFN Score upon TNFα Blockade

Although a similar IFN score between bDMARD-naive and their bDMARD-treated counterparts was found, its clinical relevance was notably different between them. Then we hypothesized that qualitative changes within the IFN score composition occurring upon TNFα blockade may underlie these findings. To further explore this idea, the IFN score was prospectively analyzed in a group of 13 biological-naive RA patients at BL and after 3 months upon TNFα blockade [post-treatment (PT)].

On the one hand, neither the IFN score nor individual IRGs changed upon TNFα blockade (**Figure 5A**). No changes in leukocytes, neutrophils, lymphocytes, or monocytes were observed (all $P > 0.050$). No association between IFN score and DAS28 at sampling was found in none of the time points analyzed. However, IFN score at BL was an independent predictor of DAS28 after treatment [B (95% CI): 0.577 (0.052–1.102), $P = 0.035$] after adjusting for gender, RF, and ACPA positivity. However, when patients were grouped according to their clinical outcome, no differences in the IRGs expression levels were observed (**Figure 4A**) (Table S3 in Supplementary Material).

Next, we evaluated the associations among IRGs upon TNFα blockade. First, a PCA conducted with IRGs from RA patients before and after TNFα blockade (**Figure 5B**) revealed that independent groups could not be identified, which is in line with the lack of absolute differences observed. Actually a notable overlap was found, similar to that of bDMARD-naive and bDMARD groups in **Figure 2A**. Nevertheless, BL and PT showed different distributions, which may be attributed to distinct genes

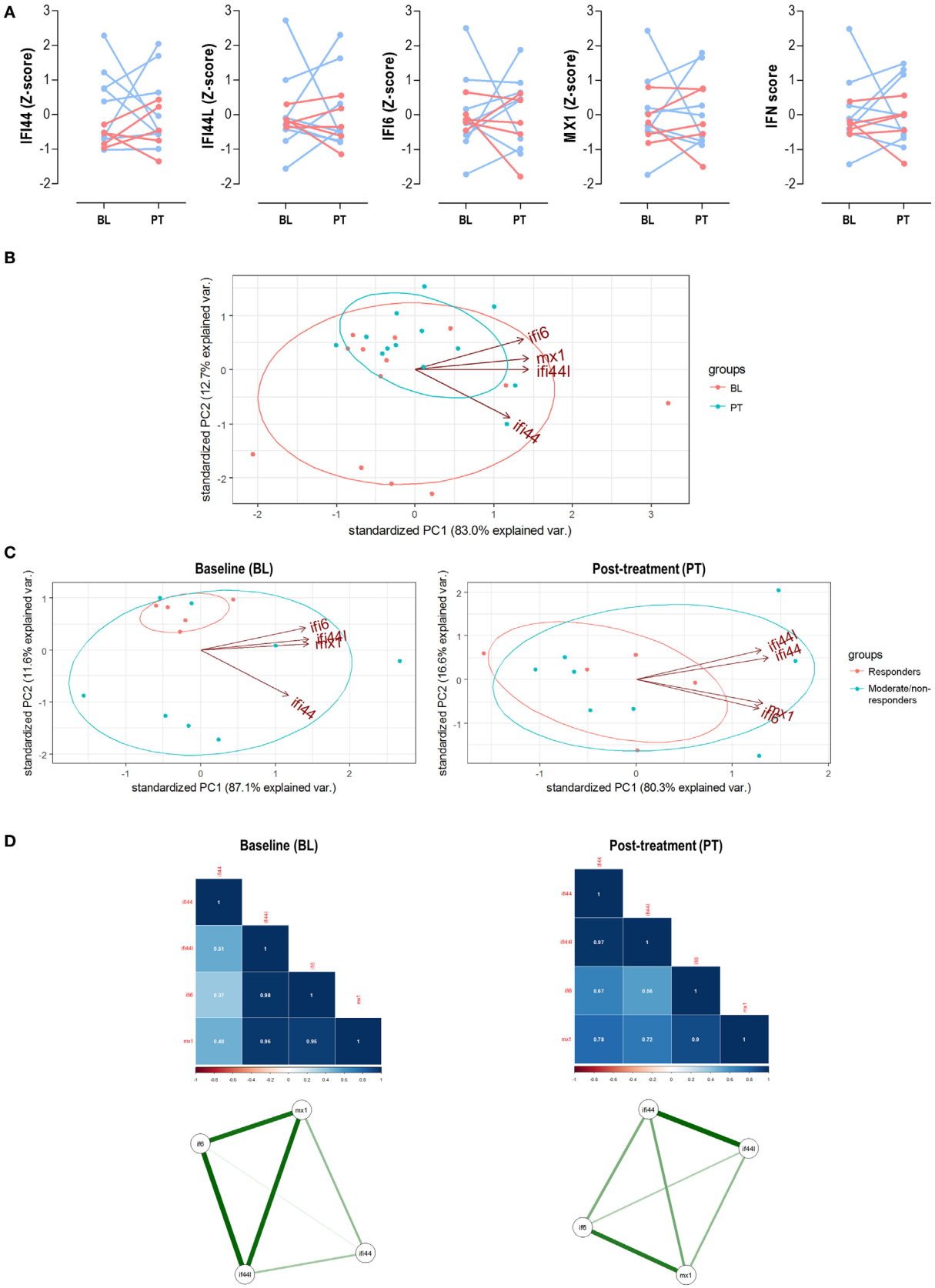

FIGURE 5 | Continued

FIGURE 5 | Analysis of the interferon (IFN) signature upon tumor necrosis factor alpha (TNFα) blockade. **(A)** Paired analyses of the expression of the individual IFN-responding genes (IRGs) and IFN score at baseline (BL) and posttreatment (PT) with anti-tumor necrosis factor alpha (TNFα) in 13 patients prospectively followed up. Patients were represented in red (responders) and blue (moderate/non-responders). Statistical analyses were performed by Wilcoxon test. **(B)** Biplot from the PCA (correlation method) conducted on the—BL, red; PT, blue—samples from rheumatoid arthritis patients. Ellipses are drawn for each group (probability set as 0.68, by default). **(C)** PCA independently conducted for BL and PT samples to evaluate changes in the IRG occurring upon TNFα blockade. **(D)** Correlation matrices and network analyses of the IRGs in the BL and PT samples. Stronger associations among IFN-induced protein 44 like (IFI44L), IFN alpha inducible protein 6 (IFI6), and MX dynamin-like GTPase 1 (MX1) were found in the BL samples, with a farther location for IFN-induced protein 44 (IFI44). However, a more uniform pattern among IRGs was found after TNFα blockade (PT), pointing toward two IRG clusters (IFI44 + IFI44L and IFI6 + MX1). These results confirmed those obtained in the PCA and are in line with the findings from the cross-sectional analysis (**Figure 2**).

hallmarking each group. In fact, when the associations among individual IRGs were compared between BL and PT samples, different IRGs profiles were detected (**Figure 5C**). The correlation graphs and the network analyses (**Figure 5D**) supported changes in the correlation profiles among the IRGs and confirmed different structural organization of the IFN signature before and after TNFα blockade. Interestingly, these observations also paralleled those obtained in our cross-sectional analysis (**Figure 3**).

Taken together, these results confirm that TNFα blockade lead to profound qualitative changes within the coordinate expression of IRGs rather than absolute changes in the gene expression levels. These qualitative changes may underlie the different associations observed with clinical features.

DISCUSSION

Although a compelling body of evidence highlights a potential role for type I IFNs in RA, its clinical relevance remains poorly understood. This study sheds new light on the type I IFN activation in RA. Our findings revealed that the IFN signature is present already in the very early stage of the disease, and quantitative and qualitative changes occur along the disease course. Although the type I IFN score at onset can be proposed as a biomarker of clinical outcome, a different picture is observed in patients with established disease, especially in patients undergoing bDMARD treatment. Distinct associations among IRGs paralleled these observations. Overall, our results add some complexity to this field and suggest that the IFN signature(s) are less uniform and simple than currently considered.

An important finding from our study is the characterization of the type I IFN signature during the earliest phase of RA. Although several studies have focused on the type I IFN signature in patients with established disease (9, 10, 13, 14), this is the first study where IRGs are quantitatively and qualitatively analyzed in a group of untreated, VERA patients, and its clinical relevance is prospectively assessed. A potential role for type I IFNs during the early stage of the disease can be expected. These findings are in line with previous evidence linking arthritis development to the use of IFNα as a therapeutic agent (5, 6). In addition, it has been reported that activation of the type I IFN program in arthralgia patients is associated with the progression of arthritis (23, 24). In this sense, our results not only found an activation of the type I IFN signature but also go further by pointing to a clinical relevance for the IFN score at disease onset as a biomarker of clinical response. Equivalent results were recently reported by Cooles et al. in relation to the clinical response to initial therapy with csDMARDs (25). However, patients undergoing glucocorticoid treatment were excluded from the analysis to avoid a potential confounding effect. Then, our findings expand the previous evidence, since glucocorticoid treatment did not interfere with the prognostic capacity of the IFN score in VERA patients. Further studies are warranted to elucidate the clinical significance of the IFN signature in the long term.

Another remarkable finding from our study is the complexity observed within the IFN signature along the disease course. The associations among individual IRGs were not homogeneous in RA, but differed according to the disease course. Then, it seems that the type I IFN signature is not the mere result of a global overactivation, but specific expression programs may be detected. The identification of the main genes hallmarking the IFN signature and, more importantly, the distinct associations found among them will be a key to understand the relevance of the IFN signature. Although most of the previous studies have focused on the first point, less attention has been paid to the latter. Interestingly, it has been reported that the overall state of correlation and co-regulation phenomena are crucial to the type I IFN signature (26). Similarly, Somers et al. found prominent differences among IRGs in lupus when analyzed on the basis of a PCA, with three clusters being defined by five IRGs (27). However, whether a similar picture could be found in RA remained unknown. Our approach led us to propose that the IFN signature exhibited quantitative and qualitative changes among the different clinical stages in RA. Different profiles within the IFN signature were observed, suggesting that distinct IRGs (or IRGs clusters) were responsible for the IFN signature in each clinical stage. This picture may be related to the existence of co-regulation and co-expression mechanisms within gene expression profiles. In this sense, a proper analysis of the associations among genes can help to delineate functional biological programs with clinical relevance (26, 28), such as the response to a therapy or the disease aggravation, hence supporting the need of capturing such heterogeneity.

Therefore, it seems plausible that heterogeneity of the IFN signature may impair its clinical applicability. This notion was proposed in a recent article, where the IFN signature was observed to be affected by some csDMARDs, with the exception of MTX (14). This is in line, at least in part, with the results herein reported. However, our results add to the current knowledge by studying the associations among IRGs. Overall, these findings may explain why the type I IFN signature was associated with clinical features in very early, untreated RA patients, but not in those on csDMARD treatment. Similar conclusions have been recently published by other authors (25). Overall, it is feasible that the distinct profiles of the IFN response observed may be a

source of controversy in relation to previous studies. Although some confounders, which can alter the IFN response have been reported (14, 25, 29, 30), they were restricted to the degree of activation. However, this is the first time that a qualitative insight is addressed.

An equivalent scenario is depicted in the comparison between biological-naive patients and their biological-treated counterparts. Despite not differing in their absolute IFN score, divergent associations with clinical parameters were registered in the cross-sectional analysis. Similar results were observed in the prospective subgroup. Interestingly, a poor outcome upon TNFα blockade had been linked to the activation of the IFN pathway in RA (15), although no differences were observed upon treatment, which is in line with our findings. In that article, a large interindividual variation was observed (15), being attributed to the result of different regulatory mechanisms. However, this heterogeneity was not approached. On the other hand, distinct profiles among IRG were found before and after the exposure to this therapy. Importantly, the IFN score was negatively associated with different clinical features in bDMARD-treated patients, thus suggesting a potential regulatory or suppressive impact of the IFN score in these patients. Among the individual genes analyzed, stronger associations were observed for MX1, hence pointing to this gene as a potential driver of this effect. Interestingly, MX1 is known to be a gene target gene of IFNβ (31, 32). Consequently, it may be conceivable that bDMARD treatment could be related to an IFNβ-related, rather than a IFNα-related signature. Actually, both IFNs have been described to contribute to the IFN signature in RA (33, 34) and the IFNβ/α ratio has been reported to be a predictor of good therapeutic response in anti-TNF-treated patients (33). Recently, de Jong et al. have revealed a notable diversification of the IFN signature among patients with immune-mediated diseases with regards to the ratio between IFNα- and IFNβ-specific response programs (18). Interestingly, RA patients exhibited an intermediate position between SLE patients (mostly IFNα specific) and IFNβ-treated multiple sclerosis patients (mostly IFNβ specific). Importantly, MX1 was identified as one of the IFNβ-related genes. However, the clinical relevance of this IFNα/β ratio was not analyzed. Overall, all these findings reinforce the idea that not only the degree of activation of the type I IFN but also its composition are key to unveil its potential role as biomarker in RA.

In conclusion, our results revealed that the IFN signature was not quantitatively and qualitatively homogeneous in RA, but certain heterogeneity can be recognized. Both the disease course and therapies are associated with changes in the levels of expression and the structure of the IRGs response in RA, hence limiting its clinical relevance. To the best of our knowledge, this is the first study where the peripheral blood type I IFN signature, together with its clinical relevance, was quantitatively and qualitatively analyzed in VERA. Although this work represents a proof-of-concept study of the type I IFN signature in RA and its clinical relevance, it paves the ground for future, larger studies involving a higher number of IRG and long-term clinical outcomes. This will allow the identification of the best panel of IRGs and the best approach to be implemented in the context of personalized medicine.

ETHICS STATEMENT

The study was approved by the Institutional Review Board (Comité de Ética de Investigación Clínica del Principado de Asturias) in compliance with the Declaration of Helsinki. All study subjects gave written informed consent.

AUTHOR CONTRIBUTIONS

JR-C performed most of the experimental procedures, carried out the statistical analyses and drafted and edited the manuscript. PL performed some experimental procedures. MA-L and FB-G were in charge of patients' recruitment and clinical data collection and management. AS conceived the study, designed the protocols and drafted and edited the manuscript. All authors read and approved the final version of the manuscript.

FUNDING

This work was supported by European Union FEDER funds and "Fondo de Investigación Sanitaria" (FIS, PI12/00523 and PI16/00113; ISCIII, Spain), and SER/FER funds (Sociedad Española de Reumatología, FER043/2016). JR-C is supported by a postdoctoral contract from the "Juan de la Cierva" program (FJCI-2015-23849; MINECO, Spain).

SUPPLEMENTARY MATERIAL

The Supplementary Material for this article can be found online at http://www.frontiersin.org/articles/10.3389/fimmu.2017.02007/full#supplementary-material.

REFERENCES

1. Rodríguez-Carrio J, López P, Suárez A. Type I IFNs as biomarkers in rheumatoid arthritis: towards disease profiling and personalized medicine. *Clin Sci* (2015) 128(8):449–64. doi:10.1042/CS20140554
2. Kalliolias GD, Ivashkiv LB. Overview of the biology of type I interferons. *Arthritis Res Ther* (2010) 12(Suppl 1):S1. doi:10.1186/ar2881
3. Rönnblom L, Alm GV, Eloranta ML. The type I interferon system in the development of lupus. *Semin Immunol* (2011) 23(2):113–21. doi:10.1016/j.smim.2011.01.009
4. Rönnblom L, Eloranta M-L. The interferon signature in autoimmune diseases. *Curr Opin Rheumatol* (2013) 25(2):248–53. doi:10.1097/BOR.0b013e32835c7e32
5. Cacopardo B, Benanti F, Pinzone M, Nunnari G. Rheumatoid arthritis following PEG-interferon-alfa-2a plus ribavirin treatment for chronic hepatitis C: a case report and review of the literature. *BMC Res Notes* (2013) 6(1):437. doi:10.1186/1756-0500-6-437
6. De Souza EP, Segundo PTE, Jose FF. Case report rheumatoid arthritis induced by a-interferon therapy. *J Rheumatol* (2001) 20:297–9. doi:10.1007/PL00011206

7. Fu Q, Chen X, Cui H, Guo Y, Chen J, Shen N, et al. Association of elevated transcript levels of interferon-inducible chemokines with disease activity and organ damage in systemic lupus erythematosus patients. *Arthritis Res Ther* (2008) 10(5):R112. doi:10.1186/ar2510
8. Higgs BW, Liu Z, White B, Zhu W, White WI, Morehouse C, et al. Patients with systemic lupus erythematosus, myositis, rheumatoid arthritis and scleroderma share activation of a common type I interferon pathway. *Ann Rheum Dis* (2011) 70(11):2029–36. doi:10.1136/ard.2011.150326
9. van der Pouw Kraan TCTM, Wijbrandts CA, van Baarsen LGM, Voskuyl AE, Rustenburg F, Baggen JM, et al. Rheumatoid arthritis subtypes identified by genomic profiling of peripheral blood cells: assignment of a type I interferon signature in a subpopulation of patients. *Ann Rheum Dis* (2007) 66(8):1008–14. doi:10.1136/ard.2006.063412
10. van der Pouw Kraan TCTM, van Baarsen LGM, Wijbrandts CA, Voskuyl AE, Rustenburg F, Baggen JM, et al. Expression of a pathogen-response program in peripheral blood cells defines a subgroup of rheumatoid arthritis patients. *Genes Immun* (2008) 9(1):16–22. doi:10.1038/sj.gene.6364438
11. Rodríguez-Carrio J, De Paz B, López P, Prado C, Alperi-López M, Javier Ballina-García F, et al. IFNα serum levels are associated with endothelial progenitor cells imbalance and disease features in rheumatoid arthritis patients. *PLoS One* (2014) 9(1):e86069. doi:10.1371/journal.pone.0086069
12. Hopkins SJ, Meager A. Cytokines in synovial fluid: II. The presence of tumour necrosis factor and interferon. *Clin Exp Immunol* (1988) 73(1):88–92.
13. Cantaert T, Van Baarsen LG, Wijbrandts CA, Thurlings RM, De Sande V, Bos C, et al. Corrigendum to type I interferons have no major influence on humoral autoimmunity in rheumatoid arthritis [Rheumatology (2010) 49:156–166] 10.1093/rheumatology/kep345. *Rheumatology* (2014) 53(4):770. doi:10.1093/rheumatology/keu139
14. De Jong TD, Blits M, De Ridder S, Vosslamber S, Wolbink G, Nurmohamed MT, et al. Type I interferon response gene expression in established rheumatoid arthritis is not associated with clinical parameters. *Arthritis Res Ther* (2016) 18:290. doi:10.1186/s13075-016-1191-y
15. van Baarsen LG, Wijbrandts CA, Rustenburg F, Cantaert T, van der Pouw Kraan TC, Baeten DL, et al. Regulation of IFN response gene activity during infliximab treatment in rheumatoid arthritis is associated with clinical response to treatment. *Arthritis Res Ther* (2010) 12(1):R11. doi:10.1186/ar2912
16. Vosslamber S, Raterman HG, van der Pouw Kraan TCTM, Schreurs MWJ, von Blomberg BME, Nurmohamed MT, et al. Pharmacological induction of interferon type I activity following treatment with rituximab determines clinical response in rheumatoid arthritis. *Ann Rheum Dis* (2011) 70(6):1153–9. doi:10.1136/ard.2010.147199
17. van Baarsen LGM, Wijbrandts CA, Gerlag DM, Rustenburg F, van der Pouw Kraan TCTM, Dijkmans BAC, et al. Pharmacogenomics of infliximab treatment using peripheral blood cells of patients with rheumatoid arthritis. *Genes Immun* (2010) 11(8):622–9. doi:10.1038/gene.2010.34
18. de Jong TD, Vosslamber S, Mantel E, de Ridder S, Wesseling JG, van der Pouw Kraan TCTM, et al. Physiological evidence for diversification of IFNα- and IFNβ-mediated response programs in different autoimmune diseases. *Arthritis Res Ther* (2016) 18(1):49. doi:10.1186/s13075-016-0946-9
19. Matthews JN, Altman DG, Campbell MJ, Royston P. Analysis of serial measurements in medical research. *BMJ* (1990) 300(6719):230–5. doi:10.1136/bmj.300.6725.680-a
20. Smolen JS, Landewé R, Bijlsma J, Burmester G, Chatzidionysiou K, Dougados M, et al. EULAR recommendations for the management of rheumatoid arthritis with synthetic and biological disease-modifying antirheumatic drugs: 2016 update. *Ann Rheum Dis* (2017) 76(6):960–77. doi:10.1136/annrheumdis-2016-210715
21. Van Gestel AM, Anderson JJ, Van Riel PLCM, Boers M, Haagsma CJ, Rich B, et al. ACR and EULAR improvement criteria have comparable validity in rheumatoid arthritis trials. *J Rheumatol* (1999) 26(3):705–11.
22. Nakagawa S, Cuthill IC. Effect size, confidence interval and statistical significance: a practical guide for biologists. *Biol Rev Camb Philos Soc* (2007) 82(4):591–605. doi:10.1111/j.1469-185X.2007.00027.x
23. Van Baarsen LGM, Bos WH, Rustenburg F, Van Der Pouw Kraan TCTM, Wolbink GJJ, Dijkmans BAC, et al. Gene expression profiling in autoantibody-positive patients with arthralgia predicts development of arthritis. *Arthritis Rheum* (2010) 62(3):694–704. doi:10.1002/art.27294
24. Lübbers J, Brink M, van de Stadt LA, Vosslamber S, Wesseling JG, van Schaardenburg D, et al. The type I IFN signature as a biomarker of preclinical rheumatoid arthritis. *Ann Rheum Dis* (2013) 72(5):776–80. doi:10.1136/annrheumdis-2012-202753
25. Cooles FAH, Anderson AE, Lendrem DW, Norris J, Pratt AG, Hilkens CMU, et al. The interferon gene signature is increased in patients with early treatment-naive rheumatoid arthritis and predicts a poorer response to initial therapy. *J Allergy Clin Immunol* (2017). Available from: http://linkinghub.elsevier.com/retrieve/pii/S0091674917315683
26. Reynier F, Petit F, Paye M, Turrel-Davin F, Imbert PE, Hot A, et al. Importance of correlation between gene expression levels: application to the type I interferon signature in rheumatoid arthritis. *PLoS One* (2011) 6(10):e24828. doi:10.1371/journal.pone.0024828
27. Somers EC, Zhao W, Lewis EE, Wang L, Wing JJ, Sundaram B, et al. Type I interferons are associated with subclinical markers of cardiovascular disease in a cohort of systemic lupus erythematosus patients. *PLoS One* (2012) 7(5):e37000. doi:10.1371/journal.pone.0037000
28. Chou JW, Zhou T, Kaufmann WK, Paules RS, Bushel PR. Extracting gene expression patterns and identifying co-expressed genes from microarray data reveals biologically responsive processes. *BMC Bioinformatics* (2007) 8:427. doi:10.1186/1471-2105-8-427
29. de Jong TD, Sellam J, Agca R, Vosslamber S, Witte BI, Tsang-A-Sjoe M, et al. A multi-parameter response prediction model for rituximab in rheumatoid arthritis. *Joint Bone Spine* (2017) (in press). doi:10.1016/j.jbspin.2017.02.015
30. de Jong TD, Vosslamber S, Blits M, Wolbink G, Nurmohamed MT, van der Laken CJ, et al. Effect of prednisone on type I interferon signature in rheumatoid arthritis: consequences for response prediction to rituximab. *Arthritis Res Ther* (2015) 17:78. doi:10.1186/s13075-015-0564-y
31. Sheikh F, Dickensheets H, Gamero AM, Vogel SN, Donnelly RP. An essential role for IFN-β in the induction of IFN-stimulated gene expression by LPS in macrophages. *J Leukoc Biol* (2014) 96(4):591–600. doi:10.1189/jlb.2A0414-191R
32. Petry H, Cashion L, Szymanski P, Ast O, Orme A, Gross C, et al. Mx1 and IP-10: biomarkers to measure IFN-beta activity in mice following gene-based delivery. *J Interferon Cytokine Res* (2006) 26(10):699–705. doi:10.1089/jir.2006.26.699
33. Mavragani CP, La DT, Stohl W, Crow MK. Association of the response to tumor necrosis factor antagonists with plasma type I interferon activity and interferon-β/α ratios in rheumatoid arthritis patients: a post hoc analysis of a predominantly hispanic cohort. *Arthritis Rheum* (2010) 62(2):392–401. doi:10.1002/art.27226
34. Gordon RA, Grigoriev G, Lee A, Kalliolias GD, Ivashkiv LB. The interferon signature and STAT1 expression in rheumatoid arthritis synovial fluid macrophages are induced by tumor necrosis factor α and counter-regulated by the synovial fluid microenvironment. *Arthritis Rheum* (2012) 64(10):3119–28. doi:10.1002/art.34544

Conflict of Interest Statement: The authors declare no conflicts of interest. Funding bodies had no role in study conception, design, experimental procedures, analysis, or decision to publish.

frontiers in Immunology

ORIGINAL RESEARCH
published: 29 January 2018
doi: 10.3389/fimmu.2018.00028

TLR3 Ligand Poly(I:C) Exerts Distinct Actions in Synovial Fibroblasts When Delivered by Extracellular Vesicles

Mojca Frank-Bertoncelj[1], David S. Pisetsky[2,3], Christoph Kolling[4], Beat A. Michel[1], Renate E. Gay[1], Astrid Jüngel[1] and Steffen Gay[1]*

[1] Center of Experimental Rheumatology, Department of Rheumatology, University Hospital Zurich, Schlieren, Switzerland, [2] Department of Medicine, Duke University Medical Center, Durham, NC, United States, [3] Medical Research Service, Durham VA Medical Center (VHA), Durham, NC, United States, [4] Schulthess Clinic, Zurich, Switzerland

Extracellular vesicles (EV) can modulate the responses of cells to toll-like receptor (TLR) ligation; conversely, TLR ligands such as double-stranded RNA (dsRNA) can enhance the release of EV and influence of the composition and functions of EV cargos. Inflamed synovial joints in rheumatoid arthritis (RA) are rich in EV and extracellular RNA; besides, RNA released from necrotic synovial fluid cells can activate the TLR3 signaling in synovial fibroblasts (SFs) from patients with RA. Since EV occur prominently in synovial joints in RA and may contribute to the pathogenesis, we questioned whether EV can interact with dsRNA, a TLR3 ligand, and modify its actions in arthritis. We have used as model the effects on RA SFs, of EV released from monocyte U937 cells and peripheral blood mononuclear cells upon stimulation with Poly(I:C), a synthetic analog of dsRNA. We show that EV released from unstimulated cells and Poly(I:C)-stimulated U937 cells [Poly(I:C) EV] differ in size but bind similar amounts of Annexin V and express comparable levels of MAC-1, the receptor for dsRNA, on the vesicular membranes. Specifically, Poly(I:C) EV contain or associate with Poly(I:C) and at least partially protect Poly(I:C) from RNAse III degradation. Poly(I:C) EV shuttle Poly(I:C) to SFs and reproduce the proinflammatory and antiviral gene responses of SFs to direct stimulation with Poly(I:C). Poly(I:C) EV, however, halt the death receptor-induced apoptosis in SFs, thereby inverting the proapoptotic nature of Poly(I:C). These prosurvival effects sharply contrast with the high toxicity of cationic liposome-delivered Poly(I:C) and may reflect the route of Poly(I:C) delivery *via* EV or the fine-tuning of Poly(I:C) actions by molecular cargo in EV. The demonstration that EV may safeguard extracellular dsRNA and allow dsRNA to exert antiapoptotic effects on SFs highlights the potential of EV to amplify the pathogenicity of dsRNA in arthritis beyond inflammation (by concurrently enhancing the expansion of the invasive synovial stroma).

Keywords: double-stranded RNA, extracellular vesicles, Poly(I:C), synovial fibroblasts, inflammation, apoptosis, innate immunity

OPEN ACCESS

Edited by:
Moncef Zouali, Institut National de la Santé et de la Recherche Médicale, France

Reviewed by:
Philippe Georgel, Université de Strasbourg, France
Fanlei Hu, Peking University People's Hospital, China

****Correspondence:***
Mojca Frank-Bertoncelj
mojca.frank@usz.ch

Specialty section:
This article was submitted to Molecular Innate Immunity, a section of the journal Frontiers in Immunology

Received: *21 August 2017*
Accepted: *04 January 2018*
Published: *29 January 2018*

Citation:
Frank-Bertoncelj M, Pisetsky DS, Kolling C, Michel BA, Gay RE, Jüngel A and Gay S (2018) TLR3 Ligand Poly(I:C) Exerts Distinct Actions in Synovial Fibroblasts When Delivered by Extracellular Vesicles. Front. Immunol. 9:28. doi: 10.3389/fimmu.2018.00028

INTRODUCTION

Extracellular vesicles (EV) are a heterogeneous group of vesicles that are secreted from cells to enter the extracellular space where they can exhibit a variety of immunological properties. EV vary in size, mechanisms of biogenesis, and molecular composition of vesicular membranes and intravesicular cargos, including a variety of lipids, proteins, and nucleic acids (1). The structure of EV can stabilize of vesicular cargos and thereby allows EV to act in intercellular communication and the transfer of

informational molecules *in vivo* over varying distances (2). EV control fundamental cellular functions such as cellular migration, invasion, and immune responses (2, 3) and have a prominent role in human diseases, functioning as drivers of disease, disease biomarkers, or potential therapeutics (2, 3).

EV are increasingly recognized for their potentially important roles in the pathogenesis of autoimmune diseases, including rheumatoid arthritis [RA] (3, 4). Synovial fluid from patients with RA contains increased amounts of EV derived from platelets, monocytes, lymphocytes and neutrophils (5–8). These EV can promote the matrix-degrading and/or proinflammatory properties in synovial fibroblasts (SFs) and/or neutrophils (5, 6, 9, 10), thereby aggravating the arthritis; EV, however, can have also chondroprotective (7) and proresolving (11) functions, which could be exploited therapeutically (4). EV contain or can associate with proinflammatory cytokines (5), damage-associated molecular patterns (DAMPs) (11), or citrullinated autoantigens (6, 12) and can modulate their proinflammatory actions (6, 13) in inflammatory arthritis.

Signaling *via* toll-like receptors (TLRs) is central to the innate immune responses and the pathogenesis of autoimmune diseases, including RA (14). TLR ligands such as polyinosinic-polycytidylic acid [Poly(I:C)] can enhance the release of EV from a diversity of cell types that populate the synovium in RA (9) and can specify the composition and function of EV cargos (15). Conversely, EV can influence the responses of cells to TLR ligation (16). Poly(I:C) is a synthetic analog of double-stranded RNA (dsRNA) that activates the signaling *via* TLR3 and cytoplasmic dsRNA sensors such as melanocyte differentiation-associated 5 (MDA5, also known as IFIH1) (17, 18). Poly(I:C) is used to model the actions of extracellular dsRNA. Extracellular dsRNA is released *in vivo* from injured tissues and dying cells and can aggravate tissue damage *via* TLR3-dependent mechanisms (19). Synovial tissues from patients with RA contain increased amounts of extracellular RNA (20) and are rich in the expression of TLR3 (21). RNA released from necrotic synovial fluid cells activates the proinflammatory signaling *via* TLR3 in SFs, the key effector cells in joint inflammation and destruction in RA (22). Besides, stimulation of SFs with Poly(I:C) recapitulates the cytokine composition of synovial fluid in RA (23).

Since EV and extracellular RNA share the common extracellular space in inflamed synovial joints of patients with RA, they may interact to influence the functions of each other, thereby contributing distinctly to the activation of SFs and the pathogenesis of inflammatory arthritis. Here, we show that EV released from monocyte U937 cells stimulated with Poly(I:C) incorporate Poly(I:C) into their structure, at least partially protect Poly(I:C) from RNAse degradation and shuttle Poly(I:C) to SFs from patients with RA. While Poly(I:C)-containing EV could recapitulate the antiviral and proinflammatory effects of Poly(I:C) in RA SFs, these EV inverted the proapoptotic actions of Poly(I:C), thereby protecting SFs from death receptor-induced apoptosis. In sum, these findings suggest that the EV-rich milieu of inflamed synovial joints in RA fosters the pathogenicity of dsRNA by guarding the integrity of dsRNA and diversifying its actions beyond the effects of free dsRNA.

MATERIALS AND METHODS

Cell Culture

Human U937 cells (Leibniz Institute DSMZ-German Collection of Microorganisms and Cell Cultures) were maintained in RPMI 1640 cell culture medium (Gibco by Life Technologies) supplemented with 10% fetal calf serum (FCS). U937 cells of passages 8–40 were used in the experiments. Human SFs were derived from synovial tissues of RA patients obtained during joint replacement surgery at the Schulthess Clinic, Zurich, Switzerland. All patients fulfilled the American College of Rheumatology 1987 criteria for RA (24). SFs were cultured in Dulbecco's modified Eagle's medium (DMEM, Gibco by Life Technologies) supplemented with 10% FCS and SFs of passages 4–8 were used in the experiments. For preparation of the cell culture media, FCS was heat inactivated at 56°C and was sterile filtered (0.22 µm). Cell cultures were negative for mycoplasma contamination as assessed by MycoAlert mycoplasma detection kit (Lonza).

Peripheral blood mononuclear cells (PBMCs) were isolated from peripheral blood of healthy donors ($n = 3$) by density gradient centrifugation using Ficoll-Paque™ according to manufacturer's recommendations (Milteny Biotec). PBMCs were maintained in RPMI 1640 supplemented with 10% FCS in the presence or absence of Poly(I:C) for 16 h. For flow cytometry measurements of MAC-1 expression PBMCs were isolated from healthy donors using also the Ficoll-Percoll method as described in previous studies (25, 26).

Treatment of U937 Cells and PBMCs and Preparation of EV

U937 cells and PBMCs were stimulated with 20 µg/ml high-molecular-weight Poly(I:C) [Poly(I:C) HMW, InvivoGen] for 16 h or were left untreated. EV were isolated from the conditioned media of 15 million U937 cells using differential centrifugation protocol. Cells were pelleted at 360 *g*, 6 min, RT, and the supernatants were centrifuged at 1,400 *g*, 10 min, RT to remove cell debris. Cell- and cell debris-free supernatants (~8 ml) were then centrifuged at 20,000 *g*, 4°C, 20 min to obtain EV pellets. EV pellets were washed in two subsequent centrifugation steps (20,000 *g*, 4°C, 20 min) with Dulbecco's phosphate-buffered saline (DPBS, Gibco by Life Technologies) and finally resuspended in DMEM supplemented with 0.5% FCS. The supernatant from the last washing step of EV pellets (control Sup) served as a negative control for a potential carryover of residual soluble Poly(I:C) or soluble U937 cell-derived mediators *via* EV suspensions. Additionally, sterile filtered (220 nm filter) RPMI 1640 medium containing 10% FCS was incubated with 20 µg/mL Poly(I:C) for 16 h under the same conditions as cells. This medium was differentially centrifuged as described above to pellet potential residual FCS-derived EV (remaining after sterile filtering the cell culture media through 0.22 µm filters, a standard step during cell culture media preparation in our laboratory). FCS EV control samples were used in stimulation experiments to determine whether potential residual FCS-derived EV are responsible for the observed effects of Poly(I:C) EV. In a subset of experiments

15 million U937 cells were incubated with 100 ng/ml LPS from Escherichia coli J5 (List Biological Laboratories, # 301) or 10 ng/ml of recombinant human TNF alpha (R&D Systems, # 210-TA) and LPS EV or TNF EV, respectively, were isolated according to the protocol described above. The control Sup obtained from the last washing step of LPS EV pellets increased the expression of *IL-6* mRNA in SFs, pointing toward the potential LPS contamination in control Sup and LPS EV. Thus, we used only TNF EV in further analyses.

Characterization of EV

Size distribution and number of EV were determined by nanoparticle tracking analysis (NTA) using NanoSight LM10 Instrument (NanoSight Ltd., number of tracks 322–772, temperature 28.8–28.9°C, viscosity 0.82 cP, 30 frames/s, time 60 s). NTA enables automatic tracking and sizing of particles based on their Brownian motion and diffusion coefficient, thereby measuring an absolute concentration of particles and the frequency distribution of particle sizes. For NTA, EV pellets derived from 15×10^6 U937 cells ($n = 2$ per condition) were resuspended in sterile filtered DPBS and diluted 1:10. Undiluted FCS EV samples showed minimal contamination with particles, accounting for ~1% of all particles in media conditioned with cells.

In addition to NTA, EV were analyzed on FACSCanto II or FACSCalibur flow cytometers (BD Biosciences) using BD FACSDIVA or FlowJo V10, respectively. The settings for EV analysis were established with the Megamix fluorescent beads (Biocytex) according to the manufacturer's protocol. EV were labeled with PE Mouse Anti-Human CD11b/Mac-1 (BD Pharmingen, #555388, 2.5 μg/ml), PE Mouse IgG1 κ Isotype control (BD Pharmingen, #555749, 2.5 μg/ml) or FITC-Annexin V (5 μl per sample, BD Pharmingen, 556419) for 15 min at RT in the dark, thoroughly washed and analyzed by flow cytometry.

The total amount of protein in EV pellets derived from 15 million U937 cells (lysed in 50 μl RIPA buffer) was determined spectrophotometrically using the Pierce™ BCA Protein Assay Kit (Thermo Fisher Scientific) according to the manufacturer's instructions.

Treatment of SFs

During coculture experiments with EV, SFs were maintained in DMEM supplemented with 0.5% FCS. 100,000 SFs were stimulated with EV derived from 3×10^6 untreated or Poly(I:C)-stimulated U937 cells for 24 h. A set of negative control experiments included treatment of SFs with control Sup and FCS EV controls. SFs were directly stimulated with HMW Poly(I:C) (20 pg/ml to 20 μg/ml, InvivoGen, # tlrl-pic-5) or were transfected with HMW Poly(I:C) (0.02–1 μg/ml, InvivoGen, # tlrl-pic-5) using Lipofectamine 2000 (Invitrogen) according to manufacturer's instructions. Apoptosis was induced in SFs with 200 ng/ml of recombinant human TNF-related apoptosis-inducing ligand (TRAIL) (R&D Systems, #375-TEC) or with 100 ng/ml human recombinant Fas ligand (FasL) (R&D Systems, #126-FL) in the absence or presence of Poly(:C) EV, Con EV, TNF EV or Sup controls. SFs were treated with TRAIL and directly stimulated with HMW Poly(I:C) (20pg/ml-20μg/ml, InvivoGen, # tlrl-pic-5) or transfected with HMW Poly(I:C) (0.02–1 μg/ml, InvivoGen, # tlrl-pic-5). To inhibit the NF-kB signaling, sc-514 (50 μM, EMD Millipore) was diluted in DMSO (Sigma) and added to the cell culture medium 1 h before treatment of SFs with EV in the presence or absence of TRAIL. DMSO, containing no sc-514 was used as a control. The efficacy of sc-514 (50 μM, EMD Millipore) in inhibiting the NF-kB signaling was tested in SFs, stimulated with 10 ng/ml TNF alpha (R&D Systems, # 210-TA) for 24 h.

ReporterGene Assay

To measure NF-κB activity, SFs were transfected with 1.2 μg of pRL_GAPDH plus 1.8 μg of pGL4.32[*luc2P*/NF-κB-RE/Hygro] vector (Promega) or pGL4.27[luc2P/minP/Hygro] vector (Promega), using Nucleofector technology (Amaxa/Lonza). At 24 h after transfection, SFs were stimulated with EV in the presence or absence of 200 ng/mL TRAIL for 6 h, detached with trypsin and lysed in 1× Passive Lysis Buffer (Promega). Firefly luciferase activity was measured with a Dual Luciferase Reporter Assay System (Promega) and normalized to the activity of *Renilla* luciferase.

Quantitative Real-time Polymerase Chain Reaction

Total RNA was isolated from SFs and U937 cells using miRNeasy Mini Kit (Qiagen) including on-column DNase I (Qiagen) digestion. 300 ng of total RNA was reverse transcribed using Random Hexamers and MultiScribe Reverse Transcriptase (Applied Biosystems/Thermo Fisher Scientific). The expression of proinflammatory genes (*IL-6, IL-8*) and antiviral genes [*MDA5*, retinoic acid-inducible gene 1 (*RIG-I*), *TLR3*, interferon beta (*IFNB*)] was measured by SYBR Green or TaqMan qPCR (7500 or 7900HT real-time PCR systems, Life Technologies) with normalization to *18S rRNA*, glyceraldehyde 3-phosphate dehydrogenase (*GAPDH)* or hypoxantine-guanine phosphoribosyltransferase (*HPRT1*) as indicated in respective figure legends. No template control samples, dissociation curves and samples containing the untranscribed RNA were measured in parallel. The primer sequences are given in Table S1 in Supplementary Material; except primers for *18S rRNA* and *IFNB* (Applied Biosystems). The expression of target mRNAs was determined using the comparative threshold cycle method as described in Ref. (27).

Enzyme-Linked Immunosorbent Assay

The secretion of IL-6 and IL-8 into supernatants of SFs was measured with the human IL-6 and IL-8 ELISA sets (BD Biosciences), according to the manufacturer's instructions.

The Association of Poly(I:C) with U937 Cells and U937 Cell-Derived EV

To study the surface binding and internalization of Poly(I:C) into U937 cells and their cognate EV, 750,000 U937 cells were stimulated with 5 μg/ml Poly(I:C) HMW Fluorescein (InvivoGen, # tlrl-picf) or 5 μg/ml Poly(I:C) HMW Rhodamine (InvivoGen, # tlrl-picr) for 16 h. U937 cells and EV pellets were thoroughly washed and the presence of fluorescently labeled Poly(I:C) was measured by FACSCalibur flow cytometer (BD Biosciences). To

assess whether Poly(I:C) can directly interact with EV, conditioned medium from unstimulated U937 cells was centrifuged to remove cells and cellular debris. Cell-free medium, containing Con EV was then incubated with 5 μg/ml Poly(I:C) HMW Rhodamine (InvivoGen, # tlrl-picr) for 120 min, 37°C, 5% CO_2 followed by the isolation of EV and detection of Rhodamine Poly(I:C) by FACSCalibur flow cytometer (BD Biosciences).

To determine whether "vesicular" Poly(I:C) can be degraded by RNase, U937 cell-derived Fluorescein Poly(I:C) EV and Con EV, preincubated with Rhodamine Poly(I:C), were digested with RNase III (*E. coli*, Applied Biosystems/Ambion) for 2 h at 37°C according to the manufacturer's protocol. Additionally, Poly(I:C), Rhodamine Poly(I:C) and Fluorescein Poly(I:C) were digested in tube with RNase III (*E. coli*, Applied Biosystems/Ambion) for 2 h at 37°C according to the manufacturer's protocol. The efficiency of digestion of "vesicular" and "soluble" Poly(I:C) was assessed by flow cytometry (FACSCalibur, BD Biosciences) and agarose gel electrophoresis (using 1kB GeneRuler DNA ladder, Thermo Fisher Scientific). For flow cytometry analysis, 10 μg/ml of HMW Fluorescein Poly(I:C) was digested by 0.2 U/μl RNAse III.

Transfer of Poly(I:C) to SFs *via* EV

To study the transfer of Poly(I:C) to SFs *via* EV, SFs were treated for 24 h with EV released from U937 cells upon stimulation with 5 μg/ml Poly(I:C) HMW Rhodamine or Poly(I:C) HMW Fluorescein. SFs were treated also with the Sup from the last washing of EV pellets or were stimulated with 5 μg/ml Rhodamine Poly(I:C) or 10 μg/ml Fluorescein Poly(I:C) for 24 h.

The presence of fluorescently-labeled Poly(I:C) in SFs was determined by flow cytometry and confocal microscopy. For flow cytometry, SFs were detached using the accutase, thoroughly washed with DPBS and immediately analyzed by FACSCalibur flow cytometer (BD Biosciences).

For confocal microscopy SFs, cultured in chamber slides (Lab-Tek; Nunc), were thoroughly washed with DPBS and fixed with 4% paraformaldehyde for 20 min RT. The slides were blocked with 1% bovine serum albumin/5% human serum for 40 min and incubated with FITC Mouse Anti-Human CD90 (BD Pharmingen, # 555595, 10 μg/ml, CD90 is a fibroblast surface marker) or FITC Mouse IgG1 κ isotype control antibodies (BD Pharmingen, # 555748, 10 μg/ml) for 1 h at RT. The nuclei were stained with DAPI (Sigma-Aldrich). Slides were covered with fluorescence mounting medium (Dako Cytomation). The images were taken by confocal laser scanning microscope Leica SP5 (Leica Microsystems) using the LAS AF software (Leica Microsystems).

Flow Cytometry Analysis of U937 and PBMCs

U937 cells and PBMCs were analyzed on FACSCalibur flow cytometer (BD Biosciences). Fc receptors were preblocked with 10% FCS-containing DPBS for 30 min, 4°C. Cells were labeled with PE Mouse Anti-Human CD11b/Mac-1 (BD Pharmingen, #555388, 10 μg/ml), PE Mouse Anti-Human CD14 (BD Pharmingen, # 555398, 10 μg/ml) or PE Mouse IgG1 κ Isotype control (BD Pharmingen, #555749, 10 μg/ml) for 45 min, 4°C in the dark, thoroughly washed and analyzed.

Western Blot

Cells were lysed in ice cold RIPA buffer and the insoluble material was removed by centrifugation at 12,000 *g*, 10 min. Whole cell lysates were separated on 10% SDS-polyacrylamide gels and electroblotted onto nitrocellulose membranes (Amersham Protran, GE Healthcare). Membranes were blocked in 5% (weight/volume) nonfat milk in TBS-T (20 mM Tris base, 137 mM sodium chloride, 0.1% Tween 20, pH 7.6) for 1 h. Western blots were performed using rabbit anti Caspase 3 antibodies (Cell Signaling, #9662, 1:1,000), which detect both cleaved and uncleaved forms of caspase 3, and mouse anti α-tubulin antibodies (Abcam, #ab7291, 1:10,000). Secondary antibodies conjugated with horseradish peroxidase were from Jackson ImmunoResearch (#111-036-047 and #115-036-062, 1:10,000). Protein bands were visualized using the enhanced chemiluminescence Western blot detection reagent (GE Healthcare) and the Fusion Fx Imager/Fusion software (Vilber Lourmat). Densitometry analysis of protein bands was carried out using the Bio-ID software (Vilber Lourmat). For quantification of Western blots, the levels of cleaved caspase 3 were normalized to the levels of uncleaved caspase 3.

Annexin V Apoptosis Assay

U937 and SFs were washed with DPBS and 1×10^6 cells/ml were resuspended in Annexin V binding buffer (BD Biosciences). Cells were labeled with FITC Annexin V (5 μl, BD Pharmingen, #556419) and propidium iodide (PI, Sigma-Aldrich) in the dark for 15 min, RT and analyzed by flow cytometry (FACSCalibur; BD Biosciences). Cells stained with Annexin V alone, PI alone and unstained cells were used to set up flow cytometry settings.

Statistical Analysis

Data were analyzed with GraphPad Prism version 7.0. The distribution of data was tested with Kolmogorov–Smirnov and D'Agostino and Pearson omnibus normality tests for small and large samples, respectively. Multiple group comparisons were performed by one-way ANOVA with Tukey's, Dunnett's, or Sidak's multiple comparisons tests (normal distribution) with or without Geisser–Greenberg correction for unequal sphericity or Friedmann test with Dunn's multiple comparisons test (distribution not normal). Paired samples were compared with two-tailed paired *t*-test (normally distributed data) or Wilcoxon signed rank test (distribution not normal). *P*-value <0.05 was considered statistically significant. Heatmaps of experimental data (details provided in respective figure legends) were produced with Shiny by R Studio, developed by Functional Genomics Center Zurich, University of Zurich and ETH Zurich, Switzerland, using row scaling transformation of data.

RESULTS

Characterization of U937 Cell-Derived EV

We analyzed the size distribution and the amount of EV released from U937 cells using the NTA. NTA efficiently detects particles with diameters up to 1 μm, whereas Brownian motion of larger

particles such as apoptotic bodies is slower and they are less readily detected (28). Our differential centrifugation protocol should predominantly isolate EV in the size range of microvesicles (0.1–1 μm) (29) while lacking exosomes (50–100 nm) that sediment at high centrifugation forces. Our protocol should also deplete apoptotic bodies (1–5 μm) (29) through a precentrifugation step at 1,600 *g* (30, 31). Accordingly, particles with sizes of microvesicles predominated in the EV preparations from unstimulated U937 cells (Con EV) [**Figure 1A**, median (10th, 90th percentile): 218 nm (114, 371 nm) and 227 (131, 368 nm), $n = 2$] and Poly(I:C)-stimulated U937 cells [Poly(I:C) EV] [**Figure 1B**, 346 nm (217, 504 nm) and 287 (187, 413 nm), $n = 2$]. A prominent peak of smaller particles was present in Con EV pellets (**Figure 1A**). In all, these results suggested that Con EV and Poly(I:C) EV might differ in composition or origin.

As measured by NTA, Poly(I:C) EV pellets contained smaller amounts of particles (5.20×10^9/ml, 4.26×10^9/ml, $n = 2$) compared with Con EV pellets (6.73×10^9/ml, 5.98×10^9/ml, $n = 2$). In contrast, the total protein content did not differ between Poly(I:C) EV and Con EV pellets (**Figure 1C**). Stimulation with Poly(I:C) increases the release of EV from different cell types as measured by flow cytometry (32, 33). Poly(I:C) enhances apoptosis in a variety of cell types (34, 35) including U937 cells (Figure S1A in Supplementary Material), thereby enriching cell supernatants for apoptotic vesicles, including apoptotic bodies. A depletion of apoptotic bodies by our protocol and their better visibility on flow cytometer could contribute to detecting the smaller amounts of particles in Poly(I:C) EV pellets by NTA compared with flow cytometry (32, 33). Alternatively, enhanced aggregation of particles in Poly(I:C) EV pellets might diminish the particle numbers and increase the particle size, while the total protein content would not change.

The International Society for Extracellular Vesicles set the guidelines on minimal experimental requirements for identifying EV, including the detection of phosphatidylserine and cell surface markers on vesicular membranes (36). As detected by flow cytometry, U937 cell-derived Con EV and Poly(I:C) EV bound similar amounts of Annexin V (**Figure 1D**) and expressed similar levels of the U937 cell surface molecule MAC-1 (**Figure 1E**), also known as integrin subunit alpha M (ITGAM) or CD11B, which is a cell surface receptor for extracellular dsRNA (37). Untreated and Poly(I:C)-treated U937 cells expressed similar levels of MAC-1 on their surface (Figure S1B in Supplementary Material).

Altogether, these measurements showed that Poly(I:C) EV and Con EV differ in size while exhibiting similar Annexin V binding and MAC-1 expression on the surface.

Poly(I:C) EV Mimic the Proinflammatory and Antiviral Responses Induced by Poly(I:C)

Previous studies have shown that immune cell-derived EV, including EV from U937 cells, released *ex vivo* upon stimulation with proinflammatory mediators, enhance the matrix-destructive and proinflammatory properties of SFs (9). Besides, a transfer of cellular RNA *via* EV was shown sufficient for inducing the NF-kB signaling in recipient human embryonic kidney 293T cells (38). Here, we demonstrate that SFs, cocultured with U937 cell-derived Poly(I:C) EV activated signaling through the NF-kB pathway (**Figure 2A**), which coincided with the increased expression of proinflammatory genes (Figures S2A,B in Supplementary Material) and the enhanced secretion of IL-6 (**Figure 2B**; Figure S2A in Supplementary Material) and IL-8 (**Figure 2C**; Figure S2B in Supplementary Material) proteins into cell culture media. By using a set of negative controls in our experiments, including Sup controls (**Figures 2B,C**), FCS EV controls (Figure S2C in Supplementary Material), and Con EV (**Figures 2B,C**), we ruled out the carryover of soluble Poly(I:C) and U937-derived mediators *via* EV pellets, concluding thereby that the observed proinflammatory effects are specifically attributed to Poly(I:C) EV.

Polymyxin B strongly inhibited the LPS-induced secretion of IL-6 from SFs (Figure S2D in Supplementary Material), but had a limited effect on the IL-6 secretion induced with Poly(I:C) EV (**Figure 2B**). This argued against the presence of contaminating LPS in Poly(I:C) EV pellets and rather suggested a possible mild negative effect of Polymyxin B on the integrity of vesicular membrane (39). SFs cocultured with either Poly(I:C) EV or Poly(I:C) EV plus Polymyxin B clustered together based on the magnitude of their proinflammatory responses (**Figures 2D,E**), but clearly diverged from SFs treated with negative controls, which clustered together with untreated SFs (**Figures 2D,E**).

In addition to enhancing the proinflammatory responses, Poly(I:C) EV increased the expression of antiviral genes in SFs. The expression of genes such as *IFNB*, *MDA5*, and *RIG-I* was upregulated, while *TLR3* mRNA expression remained rather unchanged as shown by the clustering of transcriptional responses in SFs upon Poly(I:C) EV coculture (**Figure 2F**) as well as gene expression measurements in a larger set of SFs (**Figure 2G**).

Collectively, these results demonstrated that gene expression changes in the presence of Poly(I:C) EV were largely reminiscent of the transcriptional activation of SFs with Poly(I:C) (23, 40, 41). These effects of Poly(I:C) EV on SFs could reflect the transfer of Poly(I:C)-induced molecules from U937 cells to SFs *via* EV as shown for ovarian carcinoma (HEY) cell-derived Poly(I:C)-induced exosomes (15). Yet, we did not detect *IL-6* mRNA in U937 cells under our qPCR conditions and the levels of *IL-8*, *MDA5*, and *RIG-I* mRNAs in U937 cells did not alter upon Poly(I:C) stimulation (Figure S2E in Supplementary Material), indicating that both Con EV and Poly(IC) EV could shuttle these transcripts to SFs. The exclusive activation of SFs by Poly(I:C) EV thus suggested that Poly(I:C) EV might capture and transfer Poly(I:C) to SFs, thereby activating the dsRNA signaling pathways.

U937 Cell-Derived EV Capture Poly(I:C)

Extracellular nucleic acids, such as dsDNA, readily associate with EV (42), and EV contain a diversity of small and long intracellular RNA species (with lengths up to 4,000 bases) (30). Vesicular RNA can be transferred to recipient cells in cocultures and tissue microenvironments altering thereby recipient cell functions (38, 43, 44). Based on these studies, we speculated that EV could capture at least some of the HMW Poly(I:C) molecules (1.5–8 kb) and transfer them to SFs. To study the capturing of Poly(I:C) in vesicles, we stimulated U937 cells with Rhodamine Poly(I:C) or

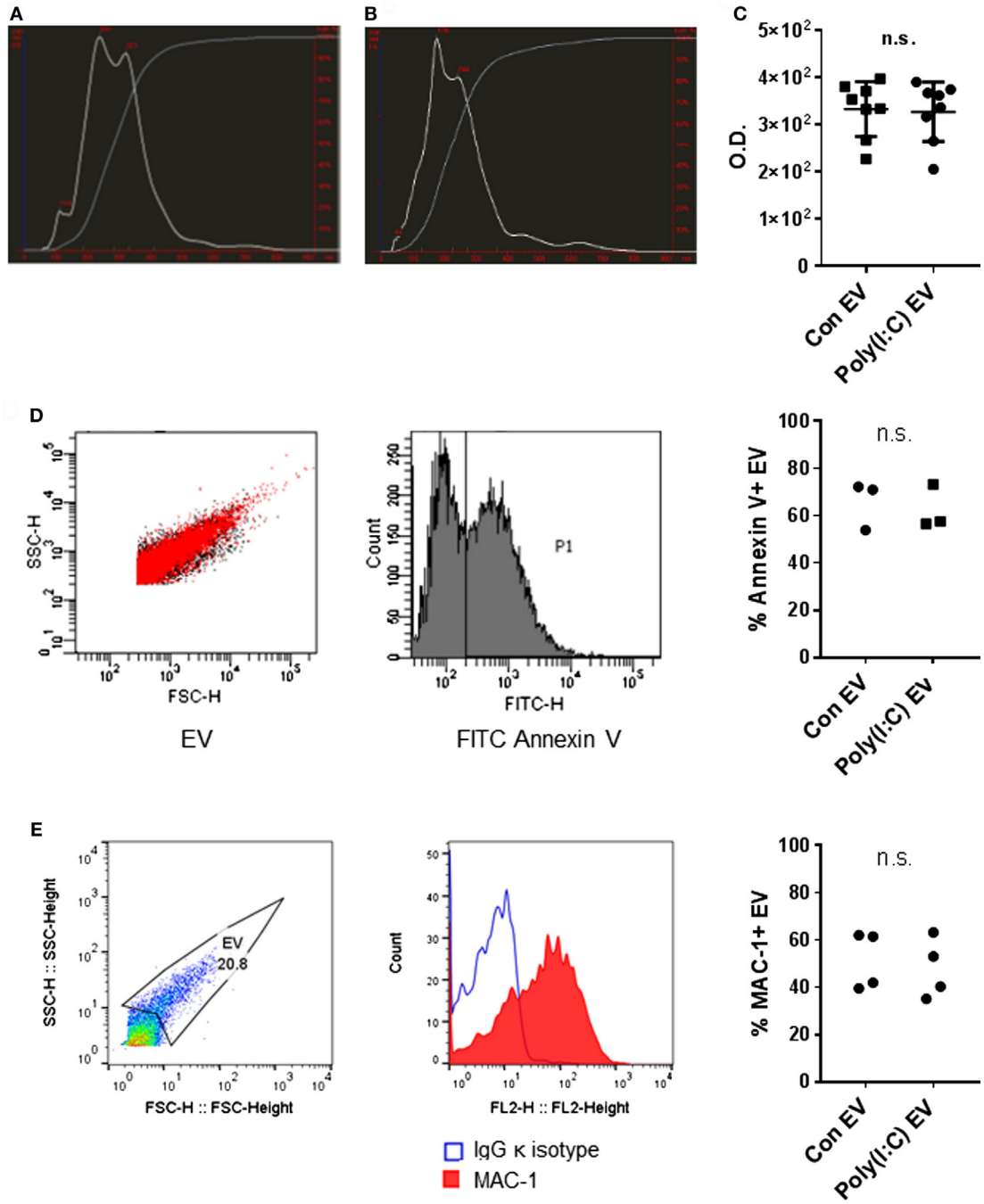

FIGURE 1 | Characterization of U937 cell-derived extracellular vesicles (EV). Size distribution of particles (white line) and cumulative percentage of particles under given size (gray line) in EV preparations from **(A)** untreated U937 cells and **(B)** Poly(I:C)-stimulated U937 cells as detected by nanoparticle tracking analysis, shown is one of $n = 2$ biological replicates per condition. **(C)** Total protein amount in EV from untreated U937 cells (Con EV) and Poly(I:C)-stimulated U937 cells [Poly(I:C) EV] as measured by BCA Protein Assay, $n = 8$ biological replicates, mean ± SD. **(D)** Binding of FITC Annexin V to the surface of Con EV and Poly(I:C) EV with SSC-H/FSC-H profile of EV and histogram of FITC-labeled Annexin V binding, shown is one sample of $n = 3$ biological replicates per condition. Percentage of Annexin V-positive EV as measured by flow cytometry. **(E)** The expression of MAC-1 on the surface of Poly(I:C) EV with SSC-H/FSC-H profile of EV and FL2 histogram of MAC-1 positivity, as measured by flow cytometry. Shown is one sample of $n = 4$ biological replicates per condition. Percentage of MAC-1-positive EV as measured by flow cytometry. Statistics: **(C–E)** two-tailed paired *t*-test, ns, not significant.

Fluorescein Poly(I:C); we digested Poly(I:C) EV with RNAse III in a subset of experiments. We showed that fluorescently labeled Poly(I:C) was present in U937 cells (Figure S3A in Supplementary Material) and their cognate EV (**Figure 3A**; Figures S3B,C in Supplementary Material), and variable proportions of EV, as detected by flow cytometry, contained Poly(I:C) (**Figure 3A**;

Figures S3B,C in Supplementary Material). This finding is consistent with recent studies showing the capture of Poly(I:C) as well as other TLR ligands in exosomes from dendritic cells that were exposed to Poly(I:C) or other TLR ligands (45, 46). We also analyzed soluble HMW Fluorescein Poly(I:C) by flow cytometry. This analysis demonstrated that vesicular and soluble fluorescent

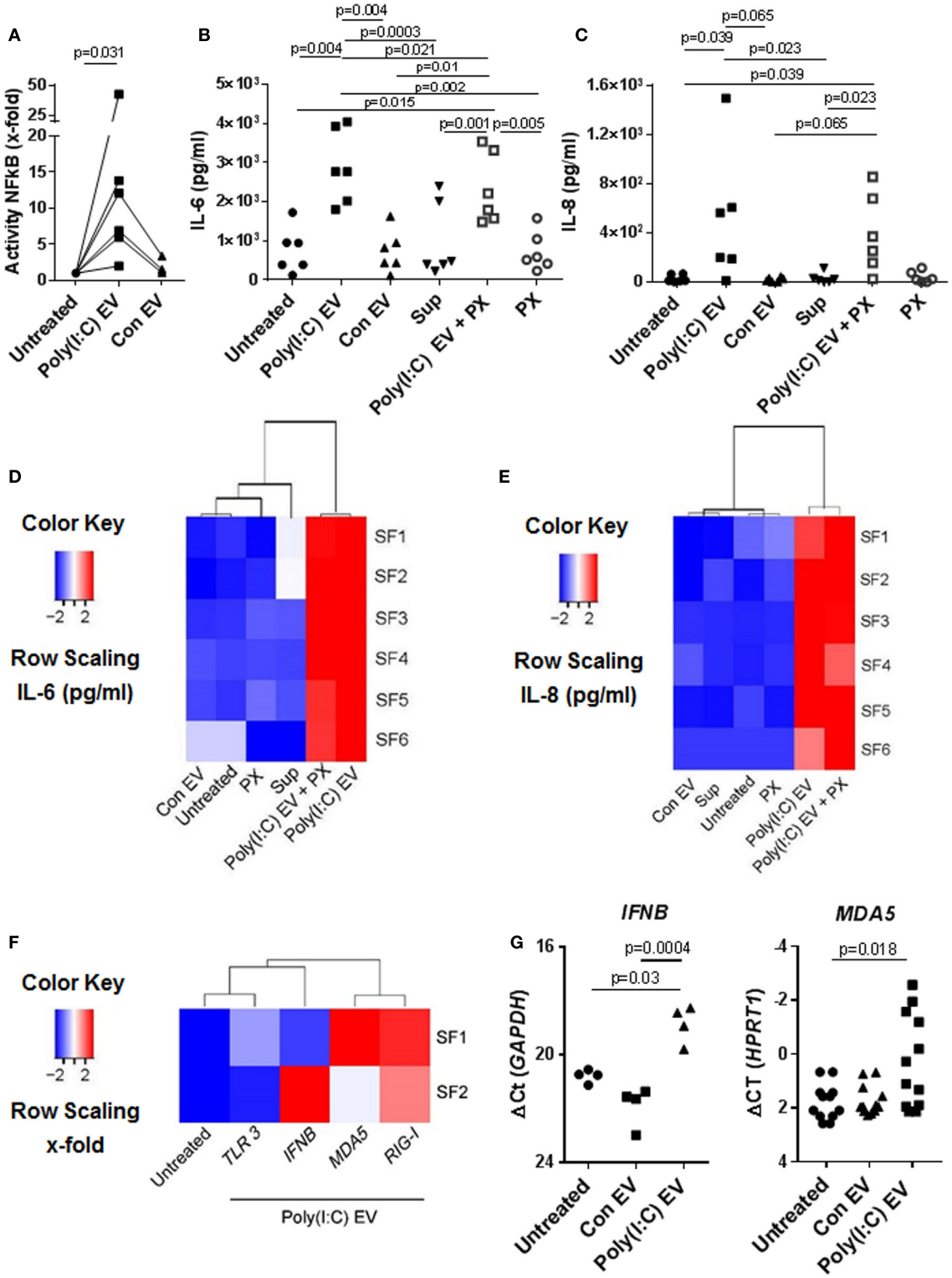

FIGURE 2 | Continued

FIGURE 2 | Extracellular vesicles (EV) derived from Poly(I:C)-stimulated U937 induce proinflammatory and antiviral responses in synovial fibroblasts (SFs). **(A)** The activity of NF-κB in synovial fibroblasts cocultured with EV derived from unstimulated U937 cells (Con EV) or Poly(I:C)-stimulated U937 cells [Poly(I:C) EV], as measured by a Dual Luciferase Reporter Assay System and expressed as x-fold induction compared to untreated cells, shown are biological replicates. Secretion of **(B)** IL-6 and **(C)** IL-8 proteins (pg/ml) into supernatants of synovial fibroblasts as measured by ELISA (biological replicates). Polymyxin B (PX) was used to control for LPS contamination. Supernatants from the last washing step of Poly(I:C) EV pellets (supernatants) were used to control for the carryover of soluble Poly(I:C) or U937-derived mediators. **(D,E)** Heatmaps show clustering of proinflammatory responses in synovial fibroblasts under different experimental conditions based on the IL-6 and IL-8 ELISA [see **(B,C)**]. **(F)** Heatmap demonstrates the clustering of antiviral gene responses in synovial fibroblasts cocultured with Poly(I:C) EV (qPCR, x-fold induction as compared with unstimulated cells, screening experiment with $n = 2$ biological replicates). **(G)** The expression of *MDA5* and *IFNB* in synovial fibroblasts cocultured with Con EV or Poly(I:C) EV, qPCR data expressed as ΔCt with normalization to *GAPDH* and *HPRT1*, respectively, shown are biological replicates. In the screening experiment, *MDA5* and *IFNB* showed variable induction upon coculture of synovial fibroblasts with Poly(I:C) EV and were thus measured in a larger cohort of synovial fibroblasts. Statistics: **(A)** Wilcoxon signed rank test, **(B)** one-way ANOVA with Tukey's multiple comparison test and Geisser-Greenhouse correction for unequal sphericity, **(C)** Friedmann test with Dunn's multiple comparisons test, **(G)** one-way ANOVA with Tukey's multiple comparisons test (*IFNB*), Friedmann test with Dunn's multiple comparisons test (*MDA5*).

Poly(I:C) have comparable median florescence intensities, but distinct forward/side scatter characteristics, which enables their discrimination by flow cytometry (**Figure 3B**). Specifically, soluble Fluorescein Poly(I:C) was detected largely within cytometer noise and only few fluorescent events spilled into the EV flow cytometry window.

Extracellular RNA, present in EV, bound to cell surface molecules, or complexed with Argonaut proteins, can be protected from RNAse degradation (47–49). To investigate RNAse sensitivity of the EV-contained Poly(I:C) we used flow cytometry and showed that EV-contained Poly(I:C) is at least partially resistant to degradation with RNAse III (**Figure 3B**). In contrast, this nuclease could efficiently degrade soluble fluorescent Poly(I:C) (Figures S3D,E in Supplementary Material). RNAse-digested soluble Fluorescein Poly(I:C) spilled to a greater extent into the EV flow cytometry window compared with nondigested soluble Fluorescein Poly(I:C) and was characterized with a large (more than 15-fold) increase in median fluorescence intensity (MFI) compared to nondigested soluble Fluorescein Poly(I:C) (**Figure 3B**). In contrast, MFIs of vesicular Fluorescein Poly(I:C) increased only moderately and non-significantly in the presence of increasing concentrations of RNase III (**Figure 3B**). This indicated that RNAse III-treated Fluorescein Poly(I:C) EV contained a limited amount of degraded Fluorescein Poly(I:C) and that EV at least partially protected Poly(I:C) from degradation with RNAse III. Additionally, we removed cells and cell debris from the cell culture media of unstimulated U937 cells *via* centrifugation and incubated the resulting cell-free media with fluorescently-labeled Poly(I:C). These experiments showed that Poly(I:C) readily associated with Con EV in the cell-free media from unstimulated U937 cells (**Figure 3C**). MFI of vesicular Rhodamine Poly(I:C) did not increase significantly in the presence of RNAse III (**Figure 3C**). This further demonstrated that in a complex with EV, Poly(I:C) was rather protected from RNAse III degradation (**Figure 3C**).

Collectively, these results demonstrated that Poly(I:C) can associate with EV, either trapped intravesicularly or bound to the vesicular surface in a manner that makes it rather resistant to RNase III degradation.

How cells sense and internalize extracellular dsRNA to signal through the intracellularly located dsRNA sensors is not completely understood (50). The cell surface receptor CD11b/CD18 (Mac-1) is one of the sensors for extracellular Poly(I:C) and participates in Poly(I:C) internalization into mouse macrophages (37). We showed that MAC-1 was present on the surface of U937 cells (Figure S1B in Supplementary Material) and U937-cell derived EV (**Figure 1E**). Similar amounts of MAC-1 were detected in unstimulated and Poly(I:C)-stimulated U937 cells (Figure S1B in Supplementary Material) as well as their cognate EV (**Figure 1E**). The presence of MAC-1 on U937 cells and EV suggested that MAC-1 may be one of the receptors contributing to the surface binding as well as trapping of Poly(I:C) within U937 cells and their EV.

Poly(I:C) EV Transfer Poly(I:C) to SFs

Extracellular vesicles can transfer RNA between cells and thereby influence the recipient cell's functions (43, 51). To explore whether EV can shuttle Poly(I:C) to SFs, we cocultured SFs with EV isolated from U937 that were stimulated with fluorescently labeled Poly(I:C). Additionally, SFs were directly treated with fluorescently-labeled Poly(I:C). As demonstrated by flow cytometry (**Figure 4A**) and fluorescence confocal microscopy (**Figure 4B**; Figure S4A in Supplementary Material), Poly(I:C) EV transferred Poly(I:C) to SFs. The distribution of Rhodamine Poly(I:C) differed in SFs stimulated with Poly(I:C) as compared with Poly(I:C) EV (**Figure 4B**; Figure S4A in Supplementary Material). The precise 3D localization (intra/extracellular) of vesicular Poly(I:C) was difficult to determine because of the flat fibroblast morphology (Figure S4A in Supplementary Material). Nevertheless, the recapitulation of Poly(I:C) responses by Poly(I:C) EV (**Figure 2**; Figure S2 in Supplementary Material) clearly showed that vesicular Poly(I:C) can efficiently induce Poly(I:C) responses in SFs. In these experiments, fluorescently labeled Poly(I:C) was not detected in SFs treated with Sup from the last washing step of Poly(I:C) EV (**Figure 4A**), thereby excluding potential carryover of soluble Poly(I:C) *via* EV pellets. Additionally, Fluorescein Poly(I:C) EV were readily detectable in the Sup of SFs at 24 h after starting the cocultures (Figure S4B in Supplementary Material), demonstrating the stability of vesicular Poly(I:C) in the extracellular space over time.

In summary, these results suggested that, in microenvironments that contain extracellular dsRNA (e.g., endogenous dsRNA released from damaged tissues), monocyte-derived EV could play a prominent role in the intercellular shuttling of dsRNA and cellular responses to extracellular dsRNA.

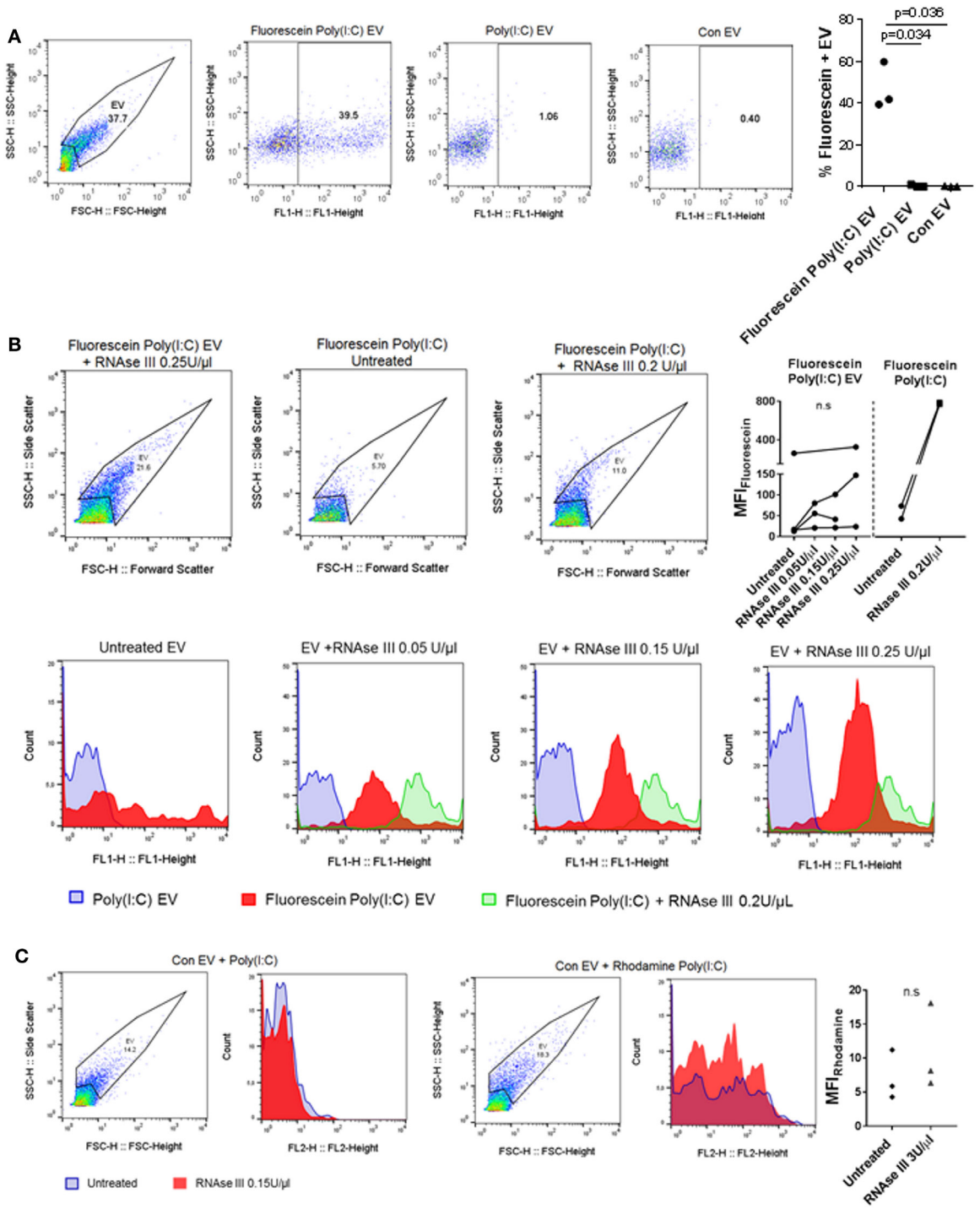

FIGURE 3 | U937 cell-derived extracellular vesicles (EV) incorporate Poly(I:C) and may protect Poly(I:C) from degradation with RNase III. **(A)** The presence of Fluorescein Poly(I:C) in U937-derived EV. SSC-H/FSC-H and SSC-H/FL1 profiles of EV with percentage of gated events, as measured by flow cytometry. Shown are a representative sample of $n = 3$ biological replicates and quantification of flow cytometry data as percentage of Fluorescein Poly(I:C)-positive EV. Control EV (Con EV)-derived from untreated U937 cells. **(B)** Detection of soluble and vesicular Fluorescein Poly(I:C) digested or not with RNAse III. SSC-H/FSC-H profiles and FL1 histograms of EV and Poly(I:C), as measured by flow cytometry. Shown is one of $n = 3$–4 biological replicates for EV and one of $n = 2$ replicates for soluble Fluorescein Poly(I:C). Quantification of changes in median fluorescence intensities (MFI) of vesicular and soluble Fluorescein Poly(I:C) in the presence and absence of RNAse III. **(C)** Association of control EV (Con EV) with Poly(I:C) or Rhodamine Poly(I:C) in the presence or absence of RNase III, as measured by flow cytometry, shown is one from $n = 3$ biological replicates. Quantification of MFI changes in Rhodamine Poly(I:C) EV in the presence of RNAse III. Statistics: **(A,B)** one-way ANOVA with Tukey's multiple comparisons test, **(C)** two-tailed paired *t*-test, ns, not significant.

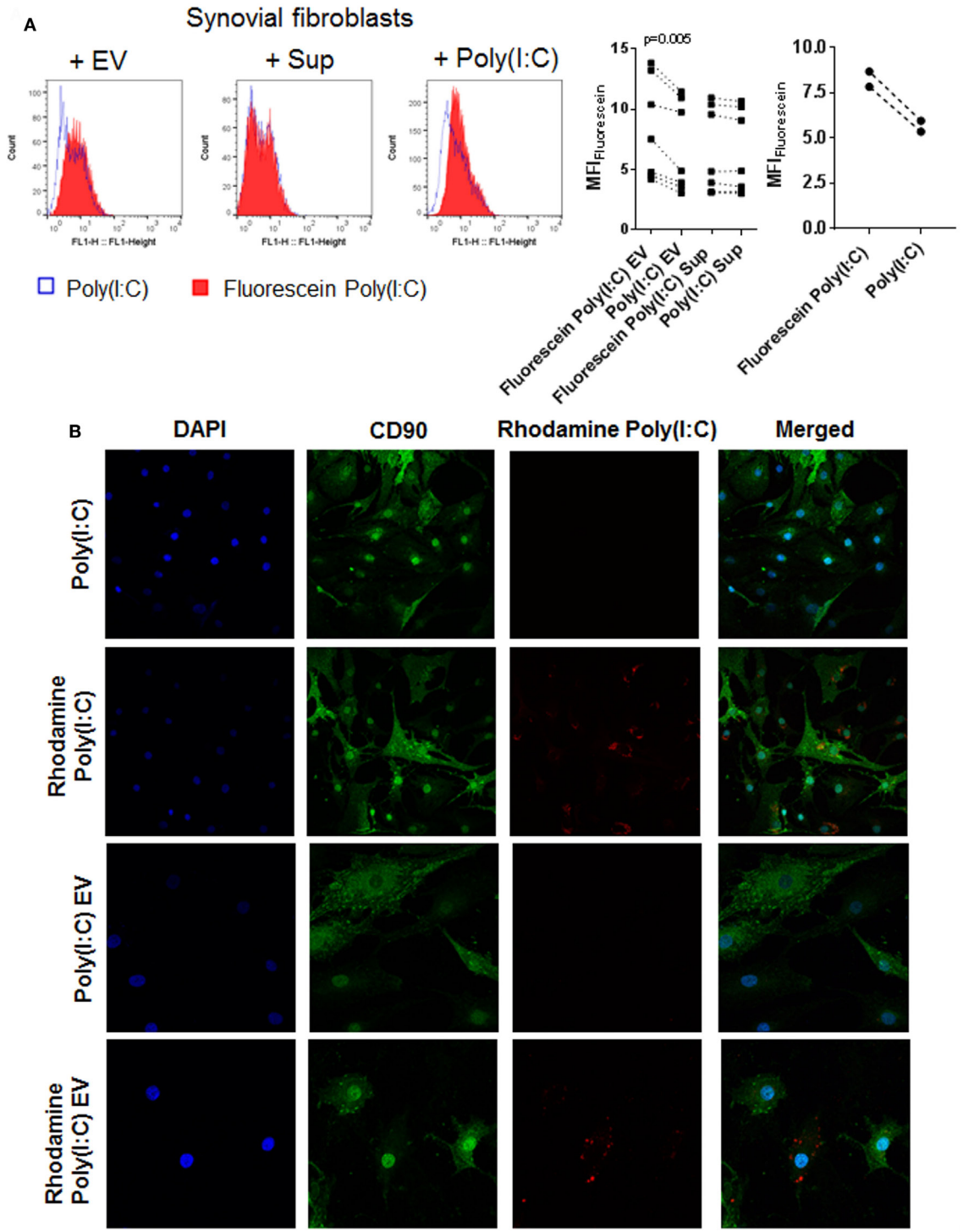

FIGURE 4 | U937 cell derived extracellular vesicles (EV) shuttle Poly(I:C) to synovial fibroblasts. **(A)** The presence of Fluorescein Poly(I:C) in synovial fibroblasts either cocultured with U937 cell-derived Fluorescein Poly(I:C) EV or Poly(I:C) EV, or treated with supernatants from the last washing step of the respective EV pellets or stimulated with Poly(I:C)/Fluorescein Poly(I:C). Sup were used to control for the contamination with soluble Poly(I:C). Shown are FL1 histogram of fluorescein fluorescence in a representative sample and quantification of changes in median fluorescence intensities (MFI) of synovial fibroblasts upon different treatments. **(B)** Confocal microscopy on synovial fibroblasts treated with Poly(I:C) or Rhodamine Poly(I:C) or cocultured with U937 cell-derived Poly(I:C) EV or Rhodamine Poly(I:C) EV for 24 h. Nuclei-DAPI (blue), FITC Mouse Anti-Human CD90 (green, fibroblast marker), Rhodamine Poly(I:C) (red). Magnification: 20× [Poly(I:C), Rhodamine Poly(I:C)] and 40× [Poly(I:C) EV, Rhodamine Poly(I:C) EV]. Statistics: **(A)** one way ANOVA with Sidak's multiple comparison test and Geisser-Greenhouse correction for unequal sphericity.

Poly(I:C) EV Deliver a Prosurvival Signal during Death Receptor Induced-Apoptosis

Poly(I:C) increases apoptosis of a variety of cell types (34, 35) including SFs (Figure S5A in Supplementary Material, in doses > 5 μg/ml). Intracellular delivery of very small amounts of Poly(I:C) by transfection with Lipofectamine 2000 was highly toxic for SFs (Figure S5B in Supplementary Material). In contrast, Poly(I:C) EV did not activate proapoptotic pathways in SFs (**Figure 5A**; Figure S5C in Supplementary Material). As estimated from the magnitude of *MDA5* and *IL-6* transcriptional responses of SF to direct stimulation with Poly(I:C) (Figures S5D,E in Supplementary Material), Poly(I:C) EV most likely transferred only a small amount of Poly(I:C) to SFs. Although these amounts were sufficient to induce the proinflammatory and antiviral responses, they might be too small to convey the proapoptotic effects of Poly(I:C).

Decreased cell death of SFs from RA joints in response to proapoptotic stimuli such as TRAIL could contribute to synovial hyperplasia and the formation of the invasive synovial tissue that destroys articular cartilage (52). To further explore the effects of Poly(I:C) EV on the apoptotic pathways in SFs, we treated SFs with the death receptor ligands TRAIL and FasL. Poly(I:C) EV decreased the TRAIL-induced apoptosis (**Figures 5B,C**; Figure S6A in Supplementary Material) and FasL-induced apoptosis of SFs (Figure S6B in Supplementary Material) as detected by Annexin V/PI apoptosis assay and Western blot measurement of cleaved caspase 3. Additionally, we performed a set of negative control experiments with Con EV and control Sup (**Figures 5B,C**; Figure S6A in Supplementary Material) as well as positive control experiments with Poly(I:C) transfection (Figure S5B in Supplementary Material), direct stimulation with Poly(I:C) (Figure S6C in Supplementary Material) or TNF EV (Figure S6D in Supplementary Material). Using these sets of experiments, we could exclude the possibility of antiapoptotic actions of contaminating soluble Poly(I:C) or U937-derived mediators and proposed that the observed prosurvival effects on death receptor-induced apoptosis are a specific action of Poly(I:C) EV. Therefore, the amount as well as the route of Poly(I:C) delivery to a cell (as part of a complex EV cargo) could be crucial in regulating the balance between prosurvival and proapoptotic actions of Poly(I:C).

All in all, these results showed that Poly(I:C) EV mimic the proinflammatory and antiviral responses of SFs induced by direct stimulation with Poly(I:C), yet, have unique prosurvival effects on death receptor-induced apoptosis which is in contrast to the high toxicity of transfected Poly(I:C).

Poly(I:C) EV from PBMCs Reproduce the Prosurvival Actions of U937-Cell Derived Poly(I:C) EV

The interactions between monocytes or monocyte-derived EV and SFs can modulate synovial disease pathways in inflammatory arthritis (9, 52). U937 cells stimulated with TLR ligands are a relevant model for studying the effects of monocyte-derived EV in SFs (9); nevertheless, the analysis of these effects in primary human cells is desirable. To investigate the properties of EV from primary cells, we characterized the activity of EV from PBMCs cultured *ex vivo* in the presence or absence of Poly(I:C). We showed that PBMC-derived Poly(I:C) EV, but not Con EV or Sup controls, efficiently decreased TRAIL-induced apoptosis in SFs (**Figure 5D**; Figure S7A in Supplementary Material), displaying the antiapoptotic actions of U937 cell-derived Poly(I:C) EV. This finding showed that Poly(I:C) EV, derived from myeloid and/or lymphoid cells induced similar antiapoptotic responses in SFs, suggesting a general mechanism of EV, derived from these cells, in modulation of responses to dsRNA. Within the PBMC population, monocytes expressed high amounts of MAC-1, whereas lymphocytes expressed medium amounts of MAC-1 on their surface (Figure S7B in Supplementary Material). Accordingly, the MAC-1 high peak was not present in monocyte-depleted PBMCs (Figure S7B in Supplementary Material). This suggested that both monocyte- and lymphocyte-derived EV in the EV pellets from PBMCs could trap or interact with Poly(I:C).

Activation of the NF-kB Pathway Confers Prosurvival Actions to Poly(I:C) EV

Inhibition of NF-kB signaling can sensitize a variety of cell types to apoptosis induced by TRAIL (53, 54). Here we showed that Poly(I:C) EV efficiently activated NF-kB signaling in SFs in the absence or presence of TRAIL (**Figures 2A** and **5E,F**). Accordingly, SFs cocultured with Poly(I:C) EV ± TRAIL clustered together based on the magnitude of NF-kB signaling (**Figure 5E**), while diverging from SFs treated with Con EV and/or TRAIL that clustered with untreated cells (**Figure 5E**). Next, we inhibited the NF-kB activity with sc-514, an inhibitor of the inhibitor of nuclear factor kappa B kinase subunit beta (IKBKB, also known as IKK-2). Pretreatment of SFs with sc-514 impaired the prosurvival effects of Poly(I:C) EV during TRAIL-induced apoptosis (**Figure 5G**; Figure S8A in Supplementary Material), thus substantiating the role for NF-kB activation in the prosurvival actions of Poly(I:C) EV. A strong repression of the TNF-driven production of IL-6 in SFs (Figure S8B in Supplementary Material) confirmed the efficiency of sc-514 in repressing NF-kB signaling in SF.

In contrast to Poly(I:C) EV, transfected Poly(I:C) (Figure S5B in Supplementary Material) or direct stimulation with Poly(I:C) (Figure S6C in Supplementary Material) had no effect on TRAIL-induced apoptosis of SFs. Transfected Poly(I:C) was highly toxic with more than 90% cell death in SFs (Figure S5B in Supplementary Material). Meanwhile, direct stimulation of SFs with Poly(I:C) can activate the NF-kB signaling (23), however, it also enhanced apoptosis of SFs (Figure S5A in Supplementary Material). Increased apoptosis of SFs in the presence of high dose Poly(I:C) could mask the NF-kB-dependent reduction in TRAIL-induced apoptosis. In turn, small doses of Poly(I:C) might not be sufficient to activate SFs (Figures S5D,E in Supplementary Material) unless delivered to cells *via* EV (**Figures 2B,C**; Figures S5D,E in Supplementary Material).

Collectively, this indicates that Poly(I:C) EV efficiently deliver small amounts of Poly(I:C), which can selectively activate antiviral and proinflammatory responses in SFs, the latter contributing to the prosurvival effects of Poly(I:C) EV during TRAIL-induced apoptosis.

DISCUSSION

Extracellular vesicles are increasingly recognized as key players in the immune responses to TLR activation (11, 15, 16, 45, 46). Here we show that EV derived from monocyte U937 cells efficiently shuttle the TLR3 ligand Poly(I:C) to SFs and activate Poly(I:C)-induced signaling with enhanced proinflammatory and antiviral gene responses. Our experimental approach highlights the key importance of experimental controls that track the potential transfer of a stimulus [Poly(I:C)] *via* EV when studying the

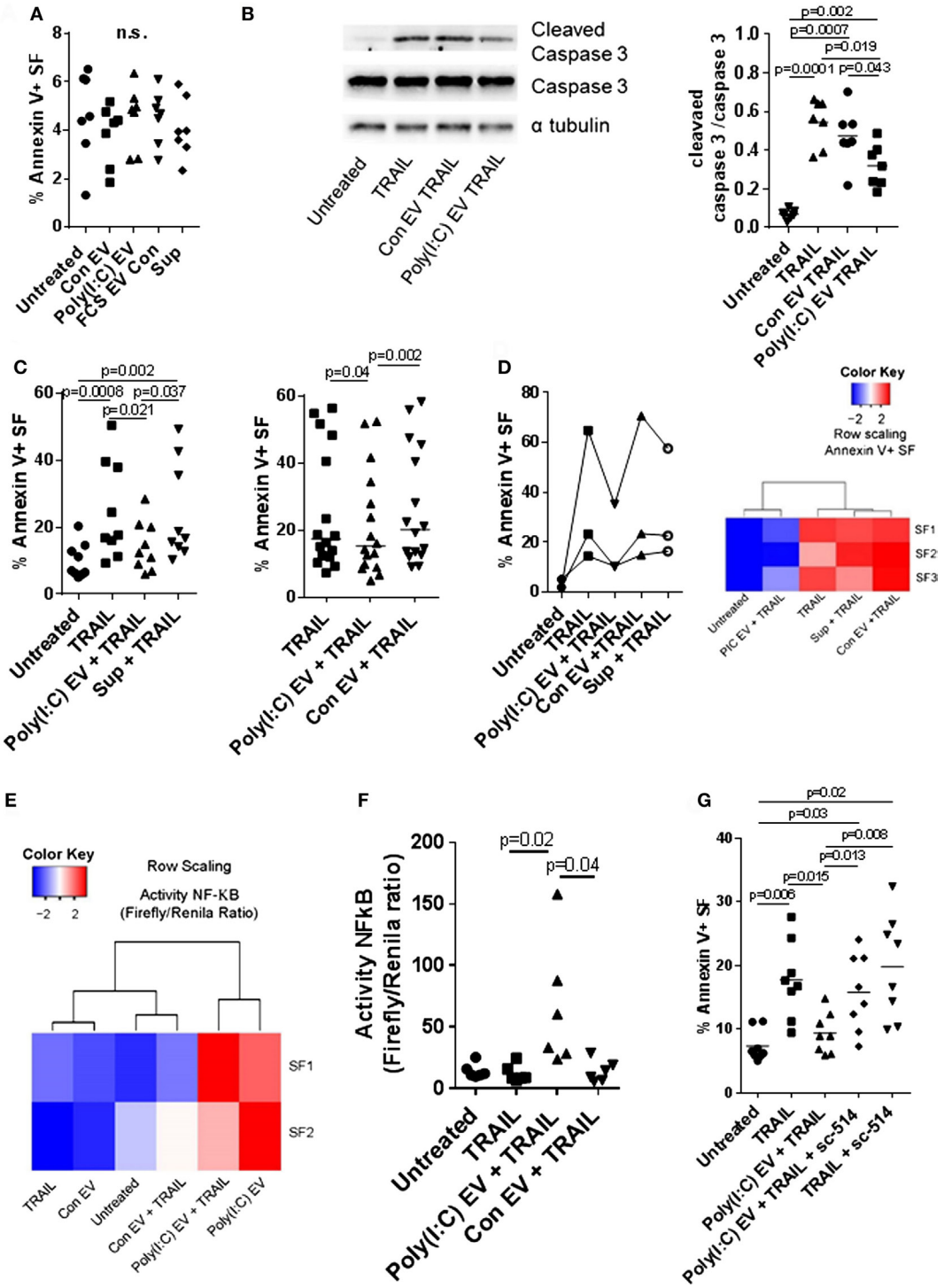

FIGURE 5 | Continued

FIGURE 5 | Extracellular vesicles (EV) derived from Poly(I:C)-stimulated U937 cells have antiapoptotic effects in synovial fibroblasts. **(A)** Percentage of apoptotic Annexin V-positive synovial fibroblasts upon treatment with U937 cell-derived EV, as measured by flow cytometry (representative flow cytometry charts are provided as Figure S5C in Supplementary Material). Supernatants from the last washing step of Poly(I:C) EV pellets and fetal calf serum EV control (FCS EV) were used to control for Poly(I:C) carryover and the effects of potential residual FCS-derived EV, respectively. **(B)** The cleavage of caspase 3 in synovial fibroblasts treated for 24 h with TRAIL ± U937 cell-derived EV. Shown is Western blot for caspase 3 and cleaved caspase 3 from one of $n = 7$ biological replicates with α tubulin as loading control. The nitrocellulose membrane from the same gel was used for detection of caspase3, cleaved caspase 3 and α tubulin with different exposure times for detection of each protein. Provided is merged image and the original gel images are provided as Figure S9 in Supplementary Material. Densitometry analysis of the cleaved caspase 3 bands was normalized to uncleaved caspase 3 bands. **(C)** Percentage of apoptotic Annexin V-positive synovial fibroblasts upon treatment with TRAIL ± U937 cell-derived EV or supernatants from the last washing step of Poly(I:C) EV pellets (supernatants), as measured by flow cytometry (representative flow cytometry charts are provided as Figure S6A in Supplementary Material). Shown are two different experimental setups with $n = 9$ and $n = 16$ biological replicates. **(D)** Percentage of apoptotic Annexin V-positive synovial fibroblasts, as measured by flow cytometry, upon treatment with TRAIL ± peripheral blood mononuclear cell (PBMC)-derived EV or supernatants from the last washing step of Poly(I:C) EV pellets (supernatants). Representative flow cytometry charts are provided as Figure S7A in Supplementary Material. PBMCs from healthy donors were cultured *ex vivo* in the presence or absence of Poly(I:C) for 16 h. Heatmap (row scaling) shows the clustering of TRAIL-induced apoptotic responses of synovial fibroblasts (SFs) under different experimental conditions based on the flow cytometry measurements of Annexin V binding. **(E,F)** The activity of NF-κB in synovial fibroblasts cocultured with U937 cell-derived EV ± TRAIL for 6 h, as measured by a Dual Luciferase Reporter Assay System. Data are expressed as the ratio of the activity of Firefly to Renilla luciferase in cells transfected with pRL_GAPDH plus pGL4.32[*luc2P*/NF-κB-RE/Hygro] or pGL4.27[luc2P/minP/Hygro] vectors for 30 h. Shown are two different experimental setups: **(E)** a screening experiment with $n = 2$ biological replicates and **(F)** a confirmatory experiment with $n = 6$ biological replicates. **(G)** Percentage of apoptotic Annexin V-positive synovial fibroblasts, as measured by flow cytometry, upon treatment with TRAIL ± Poly(I:C) EV and/or sc-514 (50 μM), the inhibitor of IKK-2, shown are biological replicates. Representative flow cytometry charts are provided as Figure S8A in Supplementary Material. Statistics: **(A)** one-way ANOVA with Dunnett's multiple comparisons test and Geisser–Greenberg correction for unequal variances **(B,C,F)** Friedmann ANOVA with Dunn's multiple comparisons test **(G)** one-way ANOVA with Tukey's multiple comparisons test and Geisser–Greenberg correction for unequal variances. ns, not significant.

effects of stimulus-induced EV. We demonstrate that Poly(I:C) is present in EV released from Poly(I:C)-stimulated U937 cells but can also directly associate with EV in cell culture media from unstimulated U937 cells. These observations suggest that, in microenvironments (e.g., RA synovial joints) that are rich in extracellular RNA (20, 22) and monocyte-derived EV (55), extracellular RNA may directly interact with EV to become a bound constituent. Additionally, EV might shuttle the extracellular dsRNA from the sites of generation to distant sites, thereby inducing proinflammatory and antiviral responses in recipient cells at remote locations.

The capacity of extracellular dsRNA to transcriptionally activate target genes relies on its extracellular stability and efficient intracellular delivery. Our experiments demonstrate that, similar to RNA in circulating EV, Poly(I:C) in vesicle form is stable over time and is rather protected from RNAse III degradation; this stability contrasts with the susceptibility of free Poly(I:C) to enzyme degradation. This finding suggests that the association of dsRNA with monocyte-derived EV within the proinflammatory milieu of RA joints could potentially protect extracellular dsRNA from RNase degradation. Indeed, large amounts of extracellular RNA are present in the RA synovium despite increased activity of RNases in synovial fluid from RA joints (20, 56). In turn, OA joints exhibit increased RNAse activity but small amounts of extracellular RNA (20).

The entry of Poly(I:C) into cells and the responses of cells to Poly(I:C) can vary with a cell type and the molecular weight of Poly(I:C) (57). A number of cell surface receptors such as MAC-1 and class A scavenger receptors can participate in the extracellular recognition and/or cellular uptake of Poly(I:C) (37, 50), clathrin-dependent endocytosis (58), and raftlin (17, 57) can also have essential roles in cellular internalization of Poly(I:C). We and others (46) provide evidence that EV can play an important role in the cellular entry and intercellular transfer of dsRNA. This ability of EV for transferring RNA has important implications for understanding the biology of extracellular dsRNA and developing new therapy, for example in the design of exosome-based antitumor vaccines (45, 46, 59). dsRNA and EV seem to utilize similar mechanisms of cellular uptake. Clathrin and MAC-1 are present on neutrophil-derived EV and are involved in the internalization of neutrophil-derived EV into platelets (60). Blocking the clathrin- or MAC-1-dependent uptake of neutrophil-derived EV by using chlorpromazine and MAC-1 antibodies, respectively, significantly decreases the production of TxA_2 in platelets (60). We demonstrated that, similar to neutrophil-derived EV, U937 cell-derived EV express MAC-1 on their surface, suggesting that MAC-1 might participate in EV loading and intercellular shuttling of Poly(I:C).

We showed that the proinflammatory and antiviral responses of SFs in cocultures with Poly(I:C) EV largely recapitulate the transcriptional activation of SFs directly stimulated with Poly(I:C) although *TLR3* mRNA expression does not increase. The induction of *MDA5* and *RIG-I* mRNAs upon direct stimulation of SFs with Poly(I:C) is much stronger compared with the induction of *TLR3* mRNA (41). This reduced response might explain the lack of transcriptional activation of the *TLR3* gene in SFs cocultured with Poly(I:C) EV, which shuttle rather a limited amount of Poly(I:C). In addition, EV are expected to transfer the U937-derived molecular cargo to SFs, including DNA, RNA, protein and lipids as shown for a variety of other target cell–EV interactions (10, 61, 62). U937 cell-derived molecules might directly configure fibroblast responses and might also fine-tune the actions of EV-delivered Poly(I:C), for example, by shuttling the myeloid cell-derived miR-223(63), which is predicted to target *TLR3* mRNA (64). EV released from hepatitis B virus-infected HepG2 hepatocyte cells transfer virus-induced microRNA, which inhibit the induction of IL12p40 upon stimulation of THP-1 macrophages with Poly(I:C) and CL097 (65). Additionally, Poly(I:C) EV might shuttle a distinct molecular cargo compared with Con EV, which might contribute to or independently activate SFs.

On the basis of our experiments, we argue that the antiviral and proinflammatory effects of Poly(I:C) EV which we describe

here are primarily caused by the transcriptional activation of SFs with EV-delivered Poly(I:C). Autologous exosomes released from ovarian carcinoma (HEY) cells upon Poly(I:C) stimulation transfer the Poly(I:C)-induced transcripts to Poly(I:C) naive HEY cells, thereby recapitulating Poly(I:C)-driven cell activation (15). In contrast, we used U937 cells, a myeloid cell type, for EV production, but studied the effects of EV in SFs, a non-myeloid cell type. Myeloid and non-myeloid cells distinctly respond to Poly(I:C) of different molecular weights (57). Whereas RAW264.7 cells, THP-1 cells and human PBMCs are preferentially activated by low-molecular-weight (LMW) Poly(I:C) (~1–1.5 kb), HMW Poly(I:C) (>5 kb) elicits strong antiviral and cytokine responses in fibroblasts (57). Whether EV inherit cell-type specific preference for the size of Poly(I:C) molecules and can thereby invoke distinct responses in myeloid and non-myeloid cells remains to be uncovered. Our experiments show that, while HMW Poly(I:C) increases the apoptosis of U937 cells and SFs, only SFs upregulate the expression of antiviral and cytokine genes. This finding strongly suggests that the transfer of vesicular Poly(I:C) is the main factor in recapitulating Poly(I:C) responses in SFs cocultured with Poly(I:C) EV. Similarly, dendritic cell-derived exosomes can cross-present TLR ligands, thereby activating the bystander dendritic cells (46). Furthermore, EV from virus-infected cells shuttle viral RNA and elicit antiviral responses in recipient dendritic cells (66).

Extracellular vesicles share the extracellular space with soluble mediators and can modulate the effects of soluble molecules in proinflammatory microenvironments. EV derived from the acute lymphoblastic leukemia (CCRF) cells modify the actions of the proinflammatory cytokine TNF in U937 cells, resulting in antagonistic, additive or synergistic effects (13). Here we demonstrate that U937 cell-derived Poly(I:C) EV exhibit unique antiapoptotic actions in SFs during death receptor-induced apoptosis; this action depends on the Poly(I:C) EV-driven activation of NF-kB. These effects cannot be induced by Con EV, TNF EV or Poly(I:C) alone, but can be reproduced by PBMC-derived Poly(I:C) EV. This suggests that the presence of Poly(I:C) in the complex with EV rather than a specificity of a cell type determines the antiapoptotic actions of Poly(I:C) EV. Thus, in addition to altering the cellular responses to cytokines (13), EV modify also the actions of extracellular dsRNA. Poly(I:C) EV have a unique capacity to simultaneously promote the proinflammatory and antiapoptotic responses in SFs. The antiapoptotic effects sharply contrast the high toxicity of transfected Poly(I:C) and might be attributed to the route of delivery of Poly(I:C) (*via* EV), the complexing of Poly(I:C) with EV or the fine-tuning of Poly(I:C) actions by molecular cargo from U937 cells.

By their ability to transfer pathogen-associated molecular patterns (PAMP)-induced or DAMP-induced transcripts as well as PAMPs or DAMPs themselves, EV have properties consistent with an important role as messengers of an ongoing infection or tissue damage, communicating a danger signal to the host. Our work shows that, by shuttling dsRNA *via* EV, the cells of origin can reduce the need for an active production of danger signaling molecules such as proinflammatory cytokines and antiviral molecules. EV containing dsRNA can reproduce the antiviral and proinflammatory actions of dsRNA, nevertheless, these structures allow dsRNA to exert antiapoptotic effects on SFs. This unexpected inversion in the nature of dsRNA actions by EV might potentiate the pathogenicity of dsRNA *in vivo* by enhancing the expansion of the invasive synovial tissue in RA. As such, blocking the EV-dsRNA interactions could have therapeutic effects in arthritis. Future studies will define the contribution of EV to RA pathogenesis and effects of EV containing RNA in terms of proinflammatory and antiapoptotic actions.

ETHICS STATEMENT

This study was approved by the local ethic committee of the University Hospital Zurich, Switzerland and was carried out in accordance with the recommendations of the local ethic committee of the University Hospital Zurich, Switzerland. All subjects gave written informed consent in accordance with the Declaration of Helsinki.

AUTHOR CONTRIBUTIONS

MF-B designed and performed the experiments, acquired and analyzed the data, and wrote the manuscript. DP participated in critical discussion of the data and drafting the manuscript. CK communicated with patients, obtained informed consents and synovial tissues, and drafted the manuscript. BM and RG were involved in the coordination of the study and drafting the manuscript. AJ set the basis of the project and participated in discussions. SG participated in project discussion, coordinated the project and drafted the manuscript. All authors have seen and approved the manuscript and its contents and are aware of the responsibilities connected to authorship.

ACKNOWLEDGMENTS

We thank Peter Künzler and Benvinda Campos Henriques (University Hospital Zurich) for technical assistance, Selene Glück (EPFL) for critical suggestions, Michelle Trenkmann (Nature Communications) for manuscript editing and critical suggestions, Salima Sadallah (Unversity of Basel) for NanoSight analysis, and Agnieszka Pajak (University Hospital Zurich) for isolation of PBMCs using Ficoll-Percol.

FUNDING

This work was funded by Articulum Fellowship 2011, IMI-BTCure (grant 115142) and the Institute of Rheumatology Research (IRR).

SUPPLEMENTARY MATERIAL

The Supplementary Material for this article can be found online http://www.frontiersin.org/articles/10.3389/fimmu.2018.00028/full#supplementary-material.

REFERENCES

1. Kalra H, Simpson RJ, Ji H, Aikawa E, Altevogt P, Askenase P, et al. Vesiclepedia: a compendium for extracellular vesicles with continuous community annotation. *PLoS Biol* (2012) 10(12):e1001450. doi:10.1371/journal.pbio.1001450
2. Maas SL, Breakefield XO, Weaver AM. Extracellular vesicles: unique intercellular delivery vehicles. *Trends Cell Biol* (2017) 27(3):172–88. doi:10.1016/j.tcb.2016.11.003
3. Buzas EI, Gyorgy B, Nagy G, Falus A, Gay S. Emerging role of extracellular vesicles in inflammatory diseases. *Nat Rev Rheumatol* (2014) 10(6):356–64. doi:10.1038/nrrheum.2014.19
4. Malda J, Boere J, van de Lest CH, van Weeren P, Wauben MH. Extracellular vesicles – new tool for joint repair and regeneration. *Nat Rev Rheumatol* (2016) 12(4):243–9. doi:10.1038/nrrheum.2015.170
5. Boilard E, Nigrovic PA, Larabee K, Watts GF, Coblyn JS, Weinblatt ME, et al. Platelets amplify inflammation in arthritis via collagen-dependent microparticle production. *Science* (2010) 327(5965):580–3. doi:10.1126/science.1181928
6. Cloutier N, Tan S, Boudreau LH, Cramb C, Subbaiah R, Lahey L, et al. The exposure of autoantigens by microparticles underlies the formation of potent inflammatory components: the microparticle-associated immune complexes. *EMBO Mol Med* (2013) 5(2):235–49. doi:10.1002/emmm.201201846
7. Headland SE, Jones HR, Norling LV, Kim A, Souza PR, Corsiero E, et al. Neutrophil-derived microvesicles enter cartilage and protect the joint in inflammatory arthritis. *Sci Transl Med* (2015) 7(315):315ra190. doi:10.1126/scitranslmed.aac5608
8. Gyorgy B, Szabo TG, Turiak L, Wright M, Herczeg P, Ledeczi Z, et al. Improved flow cytometric assessment reveals distinct microvesicle (cell-derived microparticle) signatures in joint diseases. *PLoS One* (2012) 7(11):e49726. doi:10.1371/journal.pone.0049726
9. Distler JH, Jungel A, Huber LC, Seemayer CA, Reich CF III, Gay RE, et al. The induction of matrix metalloproteinase and cytokine expression in synovial fibroblasts stimulated with immune cell microparticles. *Proc Natl Acad Sci U S A* (2005) 102(8):2892–7. doi:10.1073/pnas.0409781102
10. Jungel A, Distler O, Schulze-Horsel U, Huber LC, Ha HR, Simmen B, et al. Microparticles stimulate the synthesis of prostaglandin E(2) via induction of cyclooxygenase 2 and microsomal prostaglandin E synthase 1. *Arthritis Rheum* (2007) 56(11):3564–74. doi:10.1002/art.22980
11. Mancek-Keber M, Frank-Bertoncelj M, Hafner-Bratkovic I, Smole A, Zorko M, Pirher N, et al. Toll-like receptor 4 senses oxidative stress mediated by the oxidation of phospholipids in extracellular vesicles. *Sci Signal* (2015) 8(381):ra60. doi:10.1126/scisignal.2005860
12. Skriner K, Adolph K, Jungblut PR, Burmester GR. Association of citrullinated proteins with synovial exosomes. *Arthritis Rheum* (2006) 54(12):3809–14. doi:10.1002/art.22276
13. Szabo GT, Tarr B, Paloczi K, Eder K, Lajko E, Kittel A, et al. Critical role of extracellular vesicles in modulating the cellular effects of cytokines. *Cell Mol Life Sci* (2014) 71(20):4055–67. doi:10.1007/s00018-014-1618-z
14. Joosten LA, Abdollahi-Roodsaz S, Dinarello CA, O'Neill L, Netea MG. Toll-like receptors and chronic inflammation in rheumatic diseases: new developments. *Nat Rev Rheumatol* (2016) 12(6):344–57. doi:10.1038/nrrheum.2016.61
15. Srinivasan S, Su M, Ravishankar S, Moore J, Head P, Dixon JB, et al. TLR-exosomes exhibit distinct kinetics and effector function. *Sci Rep* (2017) 7:41623. doi:10.1038/srep41623
16. Keyel PA, Tkacheva OA, Larregina AT, Salter RD. Coordinate stimulation of macrophages by microparticles and TLR ligands induces foam cell formation. *J Immunol* (2012) 189(9):4621–9. doi:10.4049/jimmunol.1200828
17. Watanabe A, Tatematsu M, Saeki K, Shibata S, Shime H, Yoshimura A, et al. Raftlin is involved in the nucleocapture complex to induce poly(I:C)-mediated TLR3 activation. *J Biol Chem* (2011) 286(12):10702–11. doi:10.1074/jbc.M110.185793
18. Kato H, Takeuchi O, Sato S, Yoneyama M, Yamamoto M, Matsui K, et al. Differential roles of MDA5 and RIG-I helicases in the recognition of RNA viruses. *Nature* (2006) 441(7089):101–5. doi:10.1038/nature04734
19. Takemura N, Kawasaki T, Kunisawa J, Sato S, Lamichhane A, Kobiyama K, et al. Blockade of TLR3 protects mice from lethal radiation-induced gastrointestinal syndrome. *Nat Commun* (2014) 5:3492. doi:10.1038/ncomms4492
20. Zimmermann-Geller B, Koppert S, Fischer S, Cabrera-Fuentes HA, Lefevre S, Rickert M, et al. Influence of extracellular RNAs, released by rheumatoid arthritis synovial fibroblasts, on their adhesive and invasive properties. *J Immunol* (2016) 197(7):2589–97. doi:10.4049/jimmunol.1501580
21. Ospelt C, Brentano F, Rengel Y, Stanczyk J, Kolling C, Tak PP, et al. Overexpression of toll-like receptors 3 and 4 in synovial tissue from patients with early rheumatoid arthritis: toll-like receptor expression in early and longstanding arthritis. *Arthritis Rheum* (2008) 58(12):3684–92. doi:10.1002/art.24140
22. Brentano F, Schorr O, Gay RE, Gay S, Kyburz D. RNA released from necrotic synovial fluid cells activates rheumatoid arthritis synovial fibroblasts via toll-like receptor 3. *Arthritis Rheum* (2005) 52(9):2656–65. doi:10.1002/art.21273
23. Jones DS, Jenney AP, Swantek JL, Burke JM, Lauffenburger DA, Sorger PK. Profiling drugs for rheumatoid arthritis that inhibit synovial fibroblast activation. *Nat Chem Biol* (2017) 13(1):38–45. doi:10.1038/nchembio.2211
24. Silman AJ. The 1987 revised American Rheumatism Association criteria for rheumatoid arthritis. *Br J Rheumatol* (1988) 27(5):341–3. doi:10.1093/rheumatology/27.5.341
25. Repnik U, Knezevic M, Jeras M. Simple and cost-effective isolation of monocytes from buffy coats. *J Immunol Methods* (2003) 278(1–2):283–92. doi:10.1016/S0022-1759(03)00231-X
26. Arts RJ, Carvalho A, La Rocca C, Palma C, Rodrigues F, Silvestre R, et al. Immunometabolic pathways in BCG-induced trained immunity. *Cell Rep* (2016) 17(10):2562–71. doi:10.1016/j.celrep.2016.11.011
27. Schmittgen TD, Livak KJ. Analyzing real-time PCR data by the comparative C(T) method. *Nat Protoc* (2008) 3(6):1101–8. doi:10.1038/nprot.2008.73
28. Dragovic RA, Gardiner C, Brooks AS, Tannetta DS, Ferguson DJ, Hole P, et al. Sizing and phenotyping of cellular vesicles using nanoparticle tracking analysis. *Nanomedicine* (2011) 7(6):780–8. doi:10.1016/j.nano.2011.04.003
29. Gyorgy B, Szabo TG, Pasztoi M, Pal Z, Misjak P, Aradi B, et al. Membrane vesicles, current state-of-the-art: emerging role of extracellular vesicles. *Cell Mol Life Sci* (2011) 68(16):2667–88. doi:10.1007/s00018-011-0689-3
30. Crescitelli R, Lasser C, Szabo TG, Kittel A, Eldh M, Dianzani I, et al. Distinct RNA profiles in subpopulations of extracellular vesicles: apoptotic bodies, microvesicles and exosomes. *J Extracell Vesicles* (2013) 2:10. doi:10.3402/jev.v2i0.20677
31. Atkin-Smith GK, Paone S, Zanker DJ, Duan M, Phan TK, Chen W, et al. Isolation of cell type-specific apoptotic bodies by fluorescence-activated cell sorting. *Sci Rep* (2017) 7:39846. doi:10.1038/srep39846
32. Spencer DM, Gauley J, Pisetsky DS. The properties of microparticles from RAW 264.7 macrophage cells undergoing in vitro activation or apoptosis. *Innate Immun* (2014) 20(3):239–48. doi:10.1177/1753425913492552
33. Gauley J, Pisetsky DS. The release of microparticles by RAW 264.7 macrophage cells stimulated with TLR ligands. *J Leukoc Biol* (2010) 87(6):1115–23. doi:10.1189/jlb.0709465
34. Hsu WM, Huang CC, Lee HY, Wu PY, Wu MT, Chuang HC, et al. MDA5 complements TLR3 in suppression of neuroblastoma. *Oncotarget* (2015) 6(28):24935–46. doi:10.18632/oncotarget.4511
35. Palchetti S, Starace D, De Cesaris P, Filippini A, Ziparo E, Riccioli A. Transfected poly(I:C) activates different dsRNA receptors, leading to apoptosis or immunoadjuvant response in androgen-independent prostate cancer cells. *J Biol Chem* (2015) 290(9):5470–83. doi:10.1074/jbc.M114.601625
36. Lotvall J, Hill AF, Hochberg F, Buzas EI, Di Vizio D, Gardiner C, et al. Minimal experimental requirements for definition of extracellular vesicles and their functions: a position statement from the International Society for Extracellular Vesicles. *J Extracell Vesicles* (2014) 3:26913. doi:10.3402/jev.v3.26913
37. Zhou H, Liao J, Aloor J, Nie H, Wilson BC, Fessler MB, et al. CD11b/CD18 (Mac-1) is a novel surface receptor for extracellular double-stranded RNA to mediate cellular inflammatory responses. *J Immunol* (2013) 190(1):115–25. doi:10.4049/jimmunol.1202136
38. Lai CP, Kim EY, Badr CE, Weissleder R, Mempel TR, Tannous BA, et al. Visualization and tracking of tumour extracellular vesicle delivery and RNA translation using multiplexed reporters. *Nat Commun* (2015) 6:7029. doi:10.1038/ncomms8029
39. Hanna SL, Huang JL, Swinton AJ, Caputo GA, Vaden TD. Synergistic effects of polymyxin and ionic liquids on lipid vesicle membrane stability and aggregation. *Biophys Chem* (2017) 227:1–7. doi:10.1016/j.bpc.2017.05.002

40. Carrion M, Juarranz Y, Perez-Garcia S, Jimeno R, Pablos JL, Gomariz RP, et al. RNA sensors in human osteoarthritis and rheumatoid arthritis synovial fibroblasts: immune regulation by vasoactive intestinal peptide. *Arthritis Rheum* (2011) 63(6):1626–36. doi:10.1002/art.30294
41. Karpus ON, Heutinck KM, Wijnker PJ, Tak PP, Hamann J. Triggering of the dsRNA sensors TLR3, MDA5, and RIG-I induces CD55 expression in synovial fibroblasts. *PLoS One* (2012) 7(5):e35606. doi:10.1371/journal.pone.0035606
42. Pisetsky DS, Gauley J, Ullal AJ. Microparticles as a source of extracellular DNA. *Immunol Res* (2011) 49(1–3):227–34. doi:10.1007/s12026-010-8184-8
43. van der Vos KE, Abels ER, Zhang X, Lai C, Carrizosa E, Oakley D, et al. Directly visualized glioblastoma-derived extracellular vesicles transfer RNA to microglia/macrophages in the brain. *Neuro Oncol* (2016) 18(1):58–69. doi:10.1093/neuonc/nov244
44. Zomer A, Maynard C, Verweij FJ, Kamermans A, Schafer R, Beerling E, et al. In vivo imaging reveals extracellular vesicle-mediated phenocopying of metastatic behavior. *Cell* (2015) 161(5):1046–57. doi:10.1016/j.cell.2015.04.042
45. Damo M, Wilson DS, Simeoni E, Hubbell JA. TLR-3 stimulation improves anti-tumor immunity elicited by dendritic cell exosome-based vaccines in a murine model of melanoma. *Sci Rep* (2015) 5:17622. doi:10.1038/srep17622
46. Sobo-Vujanovic A, Munich S, Vujanovic NL. Dendritic-cell exosomes cross-present toll-like receptor-ligands and activate bystander dendritic cells. *Cell Immunol* (2014) 289(1–2):119–27. doi:10.1016/j.cellimm.2014.03.016
47. Nakazawa F, Kannemeier C, Shibamiya A, Song Y, Tzima E, Schubert U, et al. Extracellular RNA is a natural cofactor for the (auto-)activation of factor VII-activating protease (FSAP). *Biochem J* (2005) 385(Pt 3):831–8. doi:10.1042/BJ20041021
48. Winter J, Diederichs S. Argonaute proteins regulate microRNA stability: increased microRNA abundance by argonaute proteins is due to microRNA stabilization. *RNA Biol* (2011) 8(6):1149–57. doi:10.4161/rna.8.6.17665
49. Zhou H, Xu W, Qian H, Yin Q, Zhu W, Yan Y. Circulating RNA as a novel tumor marker: an in vitro study of the origins and characteristics of extracellular RNA. *Cancer Lett* (2008) 259(1):50–60. doi:10.1016/j.canlet.2007.09.016
50. Nellimarla S, Mossman KL. Extracellular dsRNA: its function and mechanism of cellular uptake. *J Interferon Cytokine Res* (2014) 34(6):419–26. doi:10.1089/jir.2014.0002
51. Skog J, Wurdinger T, van Rijn S, Meijer DH, Gainche L, Sena-Esteves M, et al. Glioblastoma microvesicles transport RNA and proteins that promote tumour growth and provide diagnostic biomarkers. *Nat Cell Biol* (2008) 10(12):1470–6. doi:10.1038/ncb1800
52. Neumann E, Lefevre S, Zimmermann B, Gay S, Muller-Ladner U. Rheumatoid arthritis progression mediated by activated synovial fibroblasts. *Trends Mol Med* (2010) 16(10):458–68. doi:10.1016/j.molmed.2010.07.004
53. Ravi R, Bedi GC, Engstrom LW, Zeng Q, Mookerjee B, Gelinas C, et al. Regulation of death receptor expression and TRAIL/Apo2L-induced apoptosis by NF-kappaB. *Nat Cell Biol* (2001) 3(4):409–16. doi:10.1038/35070096
54. Karacay B, Sanlioglu S, Griffith TS, Sandler A, Bonthius DJ. Inhibition of the NF-kappaB pathway enhances TRAIL-mediated apoptosis in neuroblastoma cells. *Cancer Gene Ther* (2004) 11(10):681–90. doi:10.1038/sj.cgt.7700749
55. Berckmans RJ, Nieuwland R, Kraan MC, Schaap MC, Pots D, Smeets TJ, et al. Synovial microparticles from arthritic patients modulate chemokine and cytokine release by synoviocytes. *Arthritis Res Ther* (2005) 7(3):R536–44. doi:10.1186/ar1706
56. Liote F, Champy R, Moenner M, Boval-Boizard B, Badet J. Elevated angiogenin levels in synovial fluid from patients with inflammatory arthritis and secretion of angiogenin by cultured synovial fibroblasts. *Clin Exp Immunol* (2003) 132(1):163–8. doi:10.1046/j.1365-2249.2003.02117.x
57. Mian MF, Ahmed AN, Rad M, Babaian A, Bowdish D, Ashkar AA. Length of dsRNA (poly I:C) drives distinct innate immune responses, depending on the cell type. *J Leukoc Biol* (2013) 94(5):1025–36. doi:10.1189/jlb.0312125
58. Itoh K, Watanabe A, Funami K, Seya T, Matsumoto M. The clathrin-mediated endocytic pathway participates in dsRNA-induced IFN-beta production. *J Immunol* (2008) 181(8):5522–9. doi:10.4049/jimmunol.181.8.5522
59. Lener T, Gimona M, Aigner L, Borger V, Buzas E, Camussi G, et al. Applying extracellular vesicles based therapeutics in clinical trials – an ISEV position paper. *J Extracell Vesicles* (2015) 4:30087. doi:10.3402/jev.v4.30087
60. Rossaint J, Kuhne K, Skupski J, Van Aken H, Looney MR, Hidalgo A, et al. Directed transport of neutrophil-derived extracellular vesicles enables platelet-mediated innate immune response. *Nat Commun* (2016) 7:13464. doi:10.1038/ncomms13464
61. Al-Nedawi K, Meehan B, Micallef J, Lhotak V, May L, Guha A, et al. Intercellular transfer of the oncogenic receptor EGFRvIII by microvesicles derived from tumour cells. *Nat Cell Biol* (2008) 10(5):619–24. doi:10.1038/ncb1725
62. Nager AR, Goldstein JS, Herranz-Perez V, Portran D, Ye F, Garcia-Verdugo JM, et al. An actin network dispatches ciliary GPCRs into extracellular vesicles to modulate signaling. *Cell* (2017) 168(1–2):252–63.e14. doi:10.1016/j.cell.2016.11.036
63. Ismail N, Wang Y, Dakhlallah D, Moldovan L, Agarwal K, Batte K, et al. Macrophage microvesicles induce macrophage differentiation and miR-223 transfer. *Blood* (2013) 121(6):984–95. doi:10.1182/blood-2011-08-374793
64. Heikham R, Shankar R. Flanking region sequence information to refine microRNA target predictions. *J Biosci* (2010) 35(1):105–18. doi:10.1007/s12038-010-0013-7
65. Kouwaki T, Fukushima Y, Daito T, Sanada T, Yamamoto N, Mifsud EJ, et al. Extracellular vesicles including exosomes regulate innate immune responses to hepatitis B virus infection. *Front Immunol* (2016) 7:335. doi:10.3389/fimmu.2016.00335
66. Dreux M, Garaigorta U, Boyd B, Decembre E, Chung J, Whitten-Bauer C, et al. Short-range exosomal transfer of viral RNA from infected cells to plasmacytoid dendritic cells triggers innate immunity. *Cell Host Microbe* (2012) 12(4):558–70. doi:10.1016/j.chom.2012.08.010

Conflict of Interest Statement: The authors declare that the research was conducted in the absence of any commercial or financial relationships that could be construed as a potential conflict of interest.

frontiers in Immunology

ORIGINAL RESEARCH
published: 26 February 2018
doi: 10.3389/fimmu.2018.00364

The MEK1/2-ERK Pathway Inhibits Type I IFN Production in Plasmacytoid Dendritic Cells

Vaclav Janovec[1,2,3‡], Besma Aouar[4‡], Albert Font-Haro[1,2,3‡], Tomas Hofman[2], Katerina Trejbalova[1], Jan Weber[3], Laurence Chaperot[5], Joel Plumas[6], Daniel Olive[4], Patrice Dubreuil[4], Jacques A. Nunès[4], Ruzena Stranska[4†§] and Ivan Hirsch[1,2,3,4*§]*

[1] Institute of Molecular Genetics of the Czech Academy of Sciences, Prague, Czechia, [2] Department of Genetics and Microbiology, Faculty of Sciences, Biocev, Charles University, Prague, Czechia, [3] Institute of Organic Chemistry and Biochemistry of the Czech Academy of Sciences, Gilead Sciences & IOCB Research Centre (GSRC), Prague, Czechia, [4] Cancer Research Center of Marseille, CNRS UMR7258, INSERM U1068, Institut Paoli-Calmettes, Aix-Marseille Université UM105, Marseille, France, [5] Etablissement Français du Sang Rhône-Alpes, Grenoble, France, [6] INSERM U 1209, CNRS UMR 5309, Institute for Advanced Biosciences, Université Grenoble Alpes, Grenoble, France

Recent studies have reported that the crosslinking of regulatory receptors (RRs), such as blood dendritic cell antigen 2 (BDCA-2) (CD303) or ILT7 (CD85g), of plasmacytoid dendritic cells (pDCs) efficiently suppresses the production of type I interferons (IFN-I, α/β/ω) and other cytokines in response to toll-like receptor 7 and 9 (TLR7/9) ligands. The exact mechanism of how this B cell receptor (BCR)-like signaling blocks TLR7/9-mediated IFN-I production is unknown. Here, we stimulated BCR-like signaling by ligation of RRs with BDCA-2 and ILT7 mAbs, hepatitis C virus particles, or BST2 expressing cells. We compared BCR-like signaling in proliferating pDC cell line GEN2.2 and in primary pDCs from healthy donors, and addressed the question of whether pharmacological targeting of BCR-like signaling can antagonize RR-induced pDC inhibition. To this end, we tested the TLR9-mediated production of IFN-I and proinflammatory cytokines in pDCs exposed to a panel of inhibitors of signaling molecules involved in BCR-like, MAPK, NF-κB, and calcium signaling pathways. We found that MEK1/2 inhibitors, PD0325901 and U0126 potentiated TLR9-mediated production of IFN-I in GEN2.2 cells. More importantly, MEK1/2 inhibitors significantly increased the TLR9-mediated IFN-I production blocked in both GEN2.2 cells and primary pDCs upon stimulation of BCR-like or phorbol 12-myristate 13-acetate-induced protein kinase C (PKC) signaling. Triggering of BCR-like and PKC signaling in pDCs resulted in an upregulation of the expression and phoshorylation of c-FOS, a downstream gene product of the MEK1/2-ERK pathway. We found that the total level of c-FOS was higher in proliferating GEN2.2 cells than in the resting primary pDCs. The PD0325901-facilitated restoration of the TLR9-mediated IFN-I production correlated with the abrogation of MEK1/2-ERK-c-FOS signaling. These results indicate that the MEK1/2-ERK pathway inhibits TLR9-mediated type I IFN production in pDCs and that pharmacological targeting of MEK1/2-ERK signaling could be a strategy to overcome immunotolerance of pDCs and re-establish their immunogenic activity.

Keywords: plasmacytoid dendritic cells, toll-like receptors 7 and 9 (TLR7/9), B cell-like receptor signaling, regulatory receptors, blood dendritic cell antigen 2, MEK1/2, c-FOS, type I interferon

OPEN ACCESS

Edited by:
Moncef Zouali, INSERM U1132, Paris Diderot University, France

Reviewed by:
Junji Xing, Houston Methodist Research Institute, United States
Nadine Varin-Blank, INSERM U978, France

****Correspondence:***
Ruzena Stranska
ruzena.stranska@kuleuven.be;
Ivan Hirsch
ivan.hirsch@inserm.fr,
ivan.hirsch@natur.cuni.cz

†Present address:
Ruzena Stranska, Rega Institute, Laboratory of Virology and Chemotherapy, KU Leuven, Leuven, Belgium

‡These authors have contributed equally to this work.

§Jointly directed this study.

Specialty section:
This article was submitted to Molecular Innate Immunity, a section of the journal Frontiers in Immunology

Received: *20 November 2017*
Accepted: *09 February 2018*
Published: *26 February 2018*

Citation:
Janovec V, Aouar B, Font-Haro A, Hofman T, Trejbalova K, Weber J, Chaperot L, Plumas J, Olive D, Dubreuil P, Nunès JA, Stranska R and Hirsch I (2018) The MEK1/2-ERK Pathway Inhibits Type I IFN Production in Plasmacytoid Dendritic Cells. Front. Immunol. 9:364. doi: 10.3389/fimmu.2018.00364

INTRODUCTION

Plasmacytoid dendritic cells (pDCs) are a highly specialized subset of dendritic cells that play a central role at the interface of innate and adaptive immunity. They are important actors in antiviral and antitumor immunity, but also potent inducers of autoimmune diseases (1–6). They sense viruses by endosomal toll-like receptors 7 and 9 (TLR7/9), recognizing ssRNA or CpG containing DNA. TLR signaling leads to the secretion of proinflammatory cytokines and chemokines, such as interleukin 1, tumor necrosis factor α (TNF-α), IL-6, IL-8, and most importantly type I IFNs (IFN-I, α/β/ω) (7–10).

In addition to TLR7/9, pDCs express multiple specific receptors that facilitate antigen capture and presentation and, moreover, regulate pDC function, preventing thus abnormal immune responses. These regulatory receptors (RRs), include Fc receptors and lectin-like receptors (11, 12), which signal through the B cell receptor (BCR)-like pathway involving spleen tyrosine kinase (SYK) associated with the immunoreceptor tyrosine-based activation motif-containing adapter of RR, Bruton's tyrosine kinase, B-cell linker protein, phospholipase Cγ 2, MEK1/2-ERK, and induction of intracellular Ca2+ mobilization (8, 9, 12). Among these RRs, blood dendritic cell antigen 2 (BDCA-2, CD303, CLEC4C) is an lectin-like receptor (13), while immunoglobulin-like transcript (ILT7, CD85g) binds to and can be activated by bone marrow stromal cell antigen 2 (BST2, CD317, tetherin, HM1.24) protein, the expression of which is found on cells pre-exposed to IFN-I or on the surface of human cancer cells (14). Signaling *via* pDC RRs attenuates TLR-induced production of IFN-I and proinflammatory cytokines by an unknown mechanism (8–13, 15, 16). This physiological feedback mechanism of IFN control is hijacked in the pathogenesis of several chronic viral infections and cancers, leading to immune tolerance (10, 17–19). We have recently shown that hepatitis C virus (HCV) particles inhibit the production of IFN-α *via* the binding of E2 glycoprotein to RRs BDCA-2 and DCIR (dendritic cell immunoreceptor) and induce a rapid phosphorylation of AKT and ERK, in a manner similar to the cross-linking of BDCA-2 or DCIR (10, 17, 19).

Here, we addressed the question of whether specific pharmacological targeting of BCR-like signaling can restore functionality to pDCs abrogated by ligation of RRs, and what the underlying mechanism of this abrogation is. In our previous work, we demonstrated that a highly specific inhibitor of SYK blocks both BCR-like and TLR7/9 signaling and, therefore, it is not compatible with restoration of pDC function (15). In this study, we have tested the effects of inhibitors of c-Jun N-terminal kinase (JNK), MEK1/2 kinase, p38 kinase, and calcium-dependent phosphatase calcineurin, acting through a BCR-like signaling pathway, and of NF-κB activating TANK binding kinase 1 (TBK1) on the IFN-I production in pDCs exposed to a TLR9 agonist. Surprisingly, we found that inhibitors of MEK1/2 potentiated IFN-I and IL-6 production in pDC cell line GEN2.2, but not in primary pDCs stimulated by the TLR9 agonist. More importantly, inhibitors of MEK1/2 significantly increased TLR9-mediated production of IFN-I that had been blocked in both GEN2.2 cells and primary pDCs by ligation of RRs with BDCA-2 and ILT7 mAbs, or HCV particles, or with BST2 expressing cells. Moreover, the restauration of IFN-I production by MEK1/2 inhibitor was observed when TLR9 signaling had been blocked by phorbol 12-myristate 13-acetate (PMA), an agonist of protein kinase C (PKC), which stimulates MEK1/2-ERK signaling.

Furthermore, our results show that BCR-like and PKC signaling induced in pDCs the expression and phoshorylation of c-FOS, a downstream gene product of the MEK1/2-ERK pathway. c-FOS is known to associate with c-JUN to form activator protein 1 (AP-1) transcription factor and to exert within the cell a pleiotropic effect, including cell differentiation, proliferation, apoptosis, and the immune response (20–23). While a previous study reported that the c-FOS induced by tumor progression locus 2 (TPL-2) inhibits TLR9-mediated production of IFN-I in mouse macrophages and myeloid DCs, but not in pDCs (24), we show that MEK1/2-ERK-induced c-FOS was involved in the inhibition of TLR9-mediated production of IFN-I in human pDCs. Our results suggest that the MEK1/2-ERK-dependent expression and phosphorylation of c-FOS exerts an intrinsic block of TLR9-mediated production of type I IFN. Pharmacological targeting of MEK1/2-ERK signaling could be a strategy to overcome immunotolerance of pDCs and re-establish their immunogenic activity.

RESULTS

MEK1/2 Inhibitor Potentiates CpG-A-Induced Production of IFN-α in pDC Cell Line GEN2.2

In order to restore TLR7/9-mediated production of IFN-I blocked by ligation of RRs, we first searched for an inhibitor of BCR signaling that does not inhibit signaling triggered by TLR7/9 agonists. To this end, we selected a panel of kinase inhibitors involved in BCR-like, MAPK, NF-κB, and calcium signaling, and control inhibitors of TLR7/9 signaling, and tested their effect on the production of IFN-α in a pDC cell line GEN2.2 exposed to TLR9 agonist CpG-A (**Figures 1A,B**; Figure S1 in Supplementary Material). To facilitate biochemical analyses of cell signaling, which is still difficult to perform in rare and *in vitro* short living human primary pDCs, we performed our studies in human pDC line GEN2.2, which shares the key features of human primary pDCs (15, 25–30).

While inhibitors of JNK (SP600125), TBK1 (BX795), NF-κB (Bay11-7082), p38 MAPK (SB253080), and calcineurin (FK506) inhibited dramatically IFN-α production, MEK1/2 inhibitor PD032590 significantly increased IFN-α production ($p = 0.0022$, **Figure 1B**). In repeated independent experiments ($N = 34$), production of IFN-α in CpG-A-stimulated GEN2.2 cells increased 2.55 ± 0.63 times (mean ± SEM, $p < 0.0001$),

Abbreviations: AP-1, activator protein 1; BLNK, B-cell linker protein; BCR, B cell receptor; BDCA-2, blood dendritic cell antigen 2; BST2, bone marrow stromal cell antigen 2; BTK, Bruton's tyrosine kinase; FcRs, Fc receptors; geq, genome equivalent; HCV, hepatitis C virus; ITAM, immunoreceptor tyrosine-based activation motif; IL-1, interleukin 1; IFN-I α/β/ω, type I interferons; PMA, phorbol myristoyl acetate; PLCγ2, phospholipase Cγ 2; PKC, protein kinase C; RRs, regulatory receptors; SRE, serum response element; SYK, spleen tyrosine kinase; TNF-α, tumor necrosis factor α; TPL-2, tumor progression locus 2; TBK1, TANK binding kinase 1.

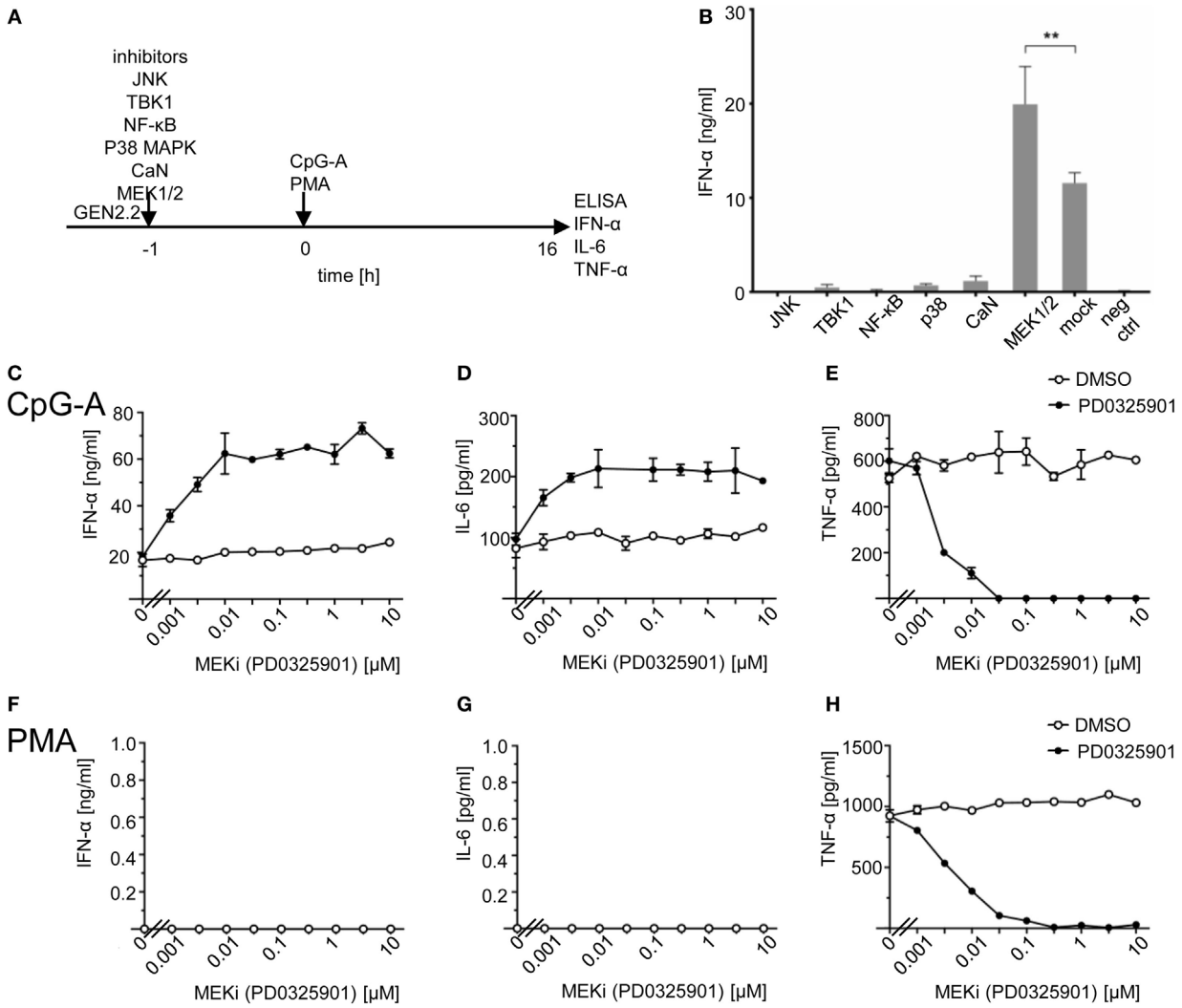

FIGURE 1 | Effect of MEK1/2 inhibitor PD0325901 on cytokine production in CpG-A and phorbol myristoyl acetate (PMA)-stimulated GEN2.2 cells. **(A)** Experimental outline. GEN2.2 cells separated from MS-5 feeder cells were exposed or not to inhibitors of Jun N-terminal kinase (JNK), TANK binding kinase 1 (TBK1), NF-κB, p38 MAPK, calcineurin, or MEK1/2 for 1 h and then stimulated with CpG-A at 4 μg/ml. The concentration of IFN-α, IL-6, and tumor necrosis factor α (TNF-α) in the cell-free supernatant was determined by ELISA after a 16 h treatment. **(B)** The production of IFN-α by GEN2.2 cells stimulated with CpG-A in the presence of JNK (SP600125, 10 μM), TBK1 (BX795, 1 μM), NF-κB (Bay11-7082, 1 μM), p38 MAPK (SB253080, 1 μM), calcineurin (FK506, 0.1 μM), or MEK1/2 (PD0325901, 1 μM) inhibitors. The PD0325901 concentration-dependent production of IFN-α **(C,F)**, IL-6 **(D,G)**, and TNF-α **(E,H)** in CpG-A-induced **(C–E)** or PMA-induced **(F–H)** GEN2.2 cells. The data show mean and SEM of two independent experiments in biological triplicates **(B–H)**. **, $p < 0.01$; two-tailed Mann–Whitney test.

from 18.4 ± 1.4 ng/ml in the absence of MEK1/2 inhibitor to 44.2 ± 2.7 ng/ml in the culture pretreated with 1 μM PD0325901 (Figure S2 in Supplementary Material). In spite of the variability of IFN-α production in CpG-A-stimulated GEN2.2 cells, the ratio of IFN-α production in GEN2.2 cells cultured in the presence and in the absence of PD0325901 was highly reproducible. The same results were obtained with MEK1/2 inhibitor U0126 (data not shown). We found that in addition to IFN-α also IL-6 production in CpG-A-stimulated GEN2.2 cells was synergized by MEK1/2 inhibitor PD0325901 (**Figures 1C,D**), whereas production of TNF-α was inhibited (**Figure 1E**), suggesting that the MEK1/2-ERK pathway positively regulates TNF-α expression or secretion (31). The strongest synergistic effects on IFN-α production (synergistic index >3) were observed for combinations of ≥0.01 μM PD0325901 and 4 μg/ml CpG-A. Synergistic effects of these combinations were also demonstrated for the production of IL-6 (synergistic index >2). In contrast to the synergistic effect observed with ≥0.01 μM PD0325901, the combination of 0.001 μM PD0325901 with 4 μg/ml CpG-A had only an additive effect on the production of IL-6 (**Figure 1D**). In the control experiment, PMA-induced the production of TNF-α (but not that of IFN-α and IL-6), which was strongly inhibited by

PD0325901 (**Figures 1F–H**). Collectively, these results show that the CpG-A-induced TLR9-mediated production of IFN-α and IL-6 are potentiated by MEK1/2 inhibitor PD0325901.

MEK1/2 Inhibitor Potentiates Herpesvirus- and CpG-B-Induced Production of IFN-α in pDC Cell Line GEN2.2

CpG-A is a synthetic mimic of an unmethylated CpG-rich dsDNA of bacteria and viruses. Therefore, we tested whether production of IFN-α in GEN2.2 cells stimulated with natural TLR9 agonists, herpes simplex virus type 1 (HSV-1), and human cytomegalovirus (HCMV) could be potentiated with PD0325901 (**Figures 2A,B**). Our results show that PD0325901 significantly potentiated production of IFN-α in GEN2.2 cells exposed to HSV-1 (2.14-fold, $N = 3$, $p = 0.0022$), or HCMV (1.98-fold, $N = 3$, $p = 0.0022$).

While aggregating CpG-A is transported to the interferon-regulatory factor 7 endosomes, where activates production of IFN-I, monomeric CpG-B is transferred to the NF-κB endosomes, which leads to maturation of pDCs, formation of pro-inflammatory cytokines and only a limited production of IFN-α (7–10). PD0325901 significantly potentiated production of IFN-α in CpG-B-stimulated GEN2.2 cells (1.43-fold, $N = 7$, $p = 0.007$), although less strongly than in CpG-A-stimulated cells (**Figure 2C**). Taken together, MEK1/2 inhibitor PD0325901 potentiated production of IFN-α in pDC cell line GEN2.2 stimulated with synthetic TLR9 agonists CpG-A and CpG-B, and natural agonists HSV-1 and HCMV.

MEK1/2 Inhibitors Partially Restore TLR9-Mediated IFN-α Production Blocked by Ligation of RRs with BDCA-2 and ILT7 mAbs

Subsequently, with respect to the ability of PD0325901 to synergize TLR7/9-mediated IFN-α production, we investigated the capacity of PD0325901 to reverse the inhibitory effect of the ligation of RRs on TLR9-mediated IFN-α production. We exposed PD0325901-pretreated GEN2.2 cells and primary pDCs to 5 μg/ml of BDCA-2 mAb and subsequently to TLR9 agonist CpG-A (**Figure 3A**). In the absence of the MEK1/2 inhibitor, the production of IFN-α induced in GEN2.2 cells by CpG-A was suppressed by BDCA-2 mAb to 13% ($p = 0.0006$, **Figure 3B**). As already shown in **Figure 1C**, PD0325901 significantly potentiated CpG-A-induced production of IFN-α in GEN2.2 cells (3.8-fold, $N = 6$, $p = 0.0022$, **Figures 3B,C**). As expected, PD0325901 potentiated the production of IFN-α inhibited in GEN2.2 cells by BDCA-2 mAb. This partial restoration of IFN-α production in GEN2.2 cells was highlighted after standardization to the quantity of IFN-α produced in the absence of PD0325901 (7.3-fold, $p = 0.0022$, **Figure 3C**).

As in GEN2.2 cells, exposure of primary pDCs from healthy donors to BDCA-2 mAb suppressed the production of IFN-α induced by CpG-A to 11.5% ($N = 9$, $p = 0.0039$, **Figure 3D**). The major difference observed in primary pDCs compared to GEN2.2 cells consisted in the lack of the potentiation of CpG-A-induced production of IFN-α by PD0325901 in the absence of BDCA-2 mAb (**Figures 3B–E**). In contrast, a similar restoration effect to the one in GEN2.2 was observed in primary pDCs

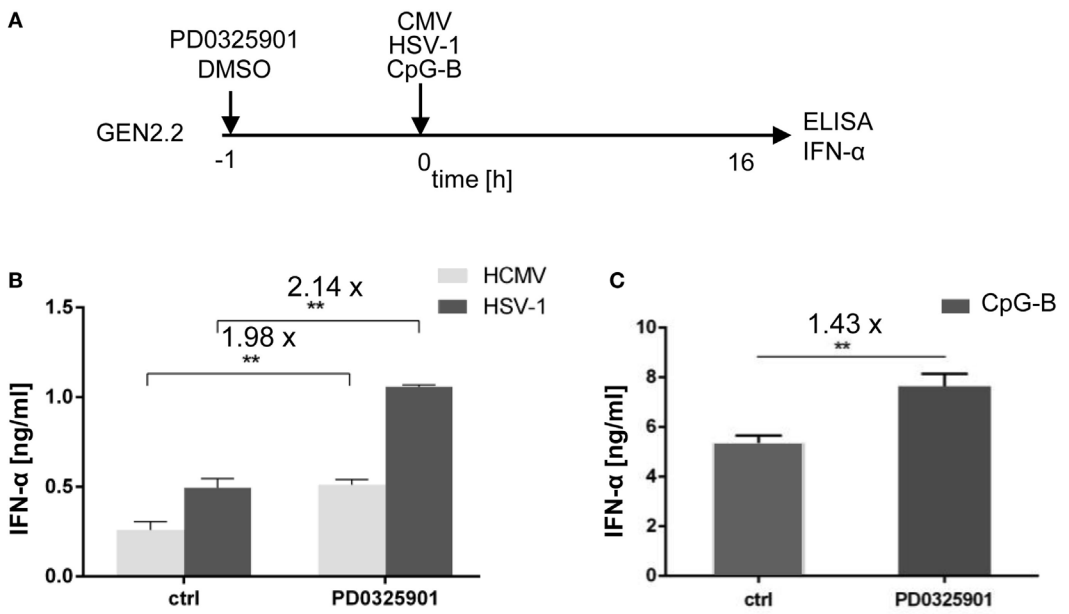

FIGURE 2 | Effect of MEK1/2 inhibitor PD0325901 on the potentiation of IFN-α production stimulated with HSV-1, human cytomegalovirus (HCMV), or CpG-B. **(A)** Experimental outline. GEN2.2 cells separated from MS-5 feeder cells were incubated with the MEK1/2 inhibitor PD0325901 (1 μM) for 1 h before stimulation with HSV-1 or HCMV at the MOI of 10 $TCID_{50}$ per cell, or with 4 μg/ml CpG-B. After a 16 h culture, the IFN-α production was determined in the cell-free supernatants by ELISA. $N = 3$, **, $p < 0.01$; two-tailed Student's *t*-test. **(B)** The production of IFN-α by GEN2.2 cells stimulated with HSV-1 or HCMV in the presence or absence of PD0325901. **(C)** The production of IFN-α by GEN2.2 cells stimulated with CpG-B in the presence or absence of PD0325901. The data show mean and SEM of three independent experiments. $N = 7$, **, $p < 0.01$; two-tailed Mann–Whitney test.

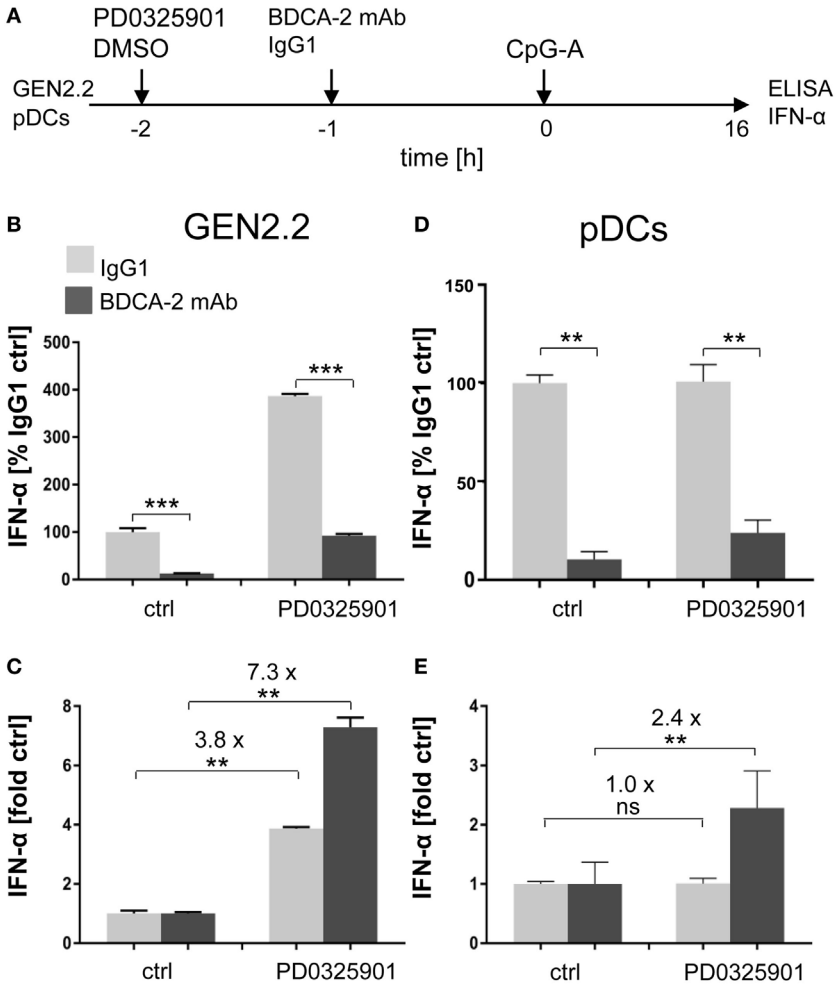

FIGURE 3 | Effect of MEK1/2 inhibitor PD0325901 on the blockade of IFN-α production by ligation of regulatory receptors of GEN2.2 cells or primary plasmacytoid dendritic cells (pDCs) with blood dendritic cell antigen 2 (BDCA-2) mAb. **(A)** Experimental outline. GEN2.2 cells separated from MS-5 feeder cells or primary pDCs were incubated with the MEK1/2 inhibitor for 1 h before stimulation with BDCA-2 mAb and CpG-A. After a 16 h culture, the IFN-α production was determined in the cell-free supernatants by ELISA. **(B,D)** The IFN-α production was normalized to the level induced by CpG-A in the presence of IgG1 and in the absence of the MEK1/2 inhibitor. **(C,E)** The same data showing the IFN-α production in panels **(B–D)** were normalized to the level induced by CpG-A in the absence of the MEK1/2 inhibitor. The data show mean ± SEM of **(B,C)** six independent experiments with GEN2.2 cells, **, $p < 0.01$; ***, $p < 0.001$; two-tailed Mann–Whitney test, and **(D,E)** nine independent experiments with primary pDCs from different healthy donors, **, $p < 0.01$; two-tailed paired Wilcoxon test.

exposed to PD0325901 prior to BDCA-2 mAb (**Figures 3D,E**). PD0325901 significantly restored the production of IFN-α inhibited by BDCA-2 mAb (2.4-fold, $p = 0.0039$, **Figure 3E**). A similar restoration effect was observed with PD0325901 at 10 nM concentration (Figure S3 in Supplementary Material) and with MEK1/2 inhibitor U0126 using ILT7 mAb for crosslinking RR (Figure S4 in Supplementary Material). In conclusion, these results show that MEK1/2 inhibitors significantly increased the TLR9-mediated IFN-I production blocked by ligation of RRs.

MEK1/2 Inhibitor Restores TLR7/9-Mediated IFN-α Production Blocked by HCV Virions

We and others reported that some viruses, such as HCV (19, 32), HBV (18), or HIV (17), interact *via* their envelope glycoproteins with RR BDCA-2 expressed on pDCs, and activate the BCR-like pathway leading to the inhibition of IFN-α production. We tested whether MEK1/2 inhibitor PD0325901 restores IFN-α production in pDC cell line GEN2.2 (**Figures 4A,B**) and in primary pDCs (**Figures 4A,C**) stimulated with CpG-A, and in parallel exposed to HCV particles (10 HCV geq/cell). We confirmed that in the absence of MEK1/2 inhibitor, HCV virions inhibited IFN-α production in both cell types, to 35% in GEN2.2 cells (**Figure 4B**) and to 34% in primary pDCs (**Figure 4C**) (19, 33). We observed that the treatment with PD0325901 significantly restored CpG-A-stimulated production of IFN-α inhibited by HCV virions in GEN2.2 cells (4.2-fold, $p = 0.025$, **Figure 4B**) and in primary pDCs (3.2-fold, $p = 0.0059$, **Figure 4C**), in a more robust way than that observed with BDCA-2 mAb (**Figure 3**). Collectively, pharmacological targeting of MEK1/2-ERK abrogates the HCV suppression of IFN-α production.

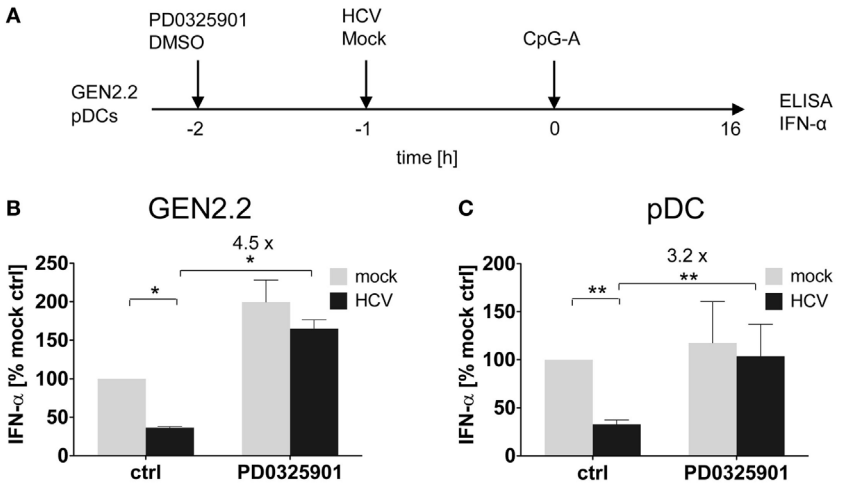

FIGURE 4 | Effect of MEK1/2 inhibition on the hepatitis C virus (HCV) blockade of IFN-α in GEN2.2 cells or primary plasmacytoid dendritic cells (pDCs). **(A)** Experimental outline. GEN2.2 cells separated from MS-5 feeder cells **(B)**, or primary pDCs **(C)**, were incubated with 1 μM MEK1/2 inhibitor PD0325901 for 1 h and then treated with HCV virions at MOI = 10 geq/cell for 1 h before CpG-A stimulation. After a 16 h culture, the IFN-α production was determined in the cell-free supernatants by ELISA. **(B,C)** The IFN-α production was normalized to the level induced by CpG-A in the presence of a mock-infected control and in the absence of PD0325901. The data show mean ± SEM of **(B)** two independent experiments with GEN2.2 cells, *, $p < 0.05$; unpaired, two-tailed *t*-test and **(C)** ten independent experiments with primary pDCs from different healthy donors, **, $p < 0.01$; two-tailed paired Wilcoxon test.

MEK1/2 Inhibitor Restores TLR9-Mediated IFN-α Production Blocked by Ligation of RRs with BST2 Expressing HEK293T Cells

ILT7 is another pDC-specific receptor with a regulatory function that signals through the BCR-like pathway and inhibits TLR-mediated IFN-α production (11). In order to evaluate the restoration effect of MEK1/2 inhibitors, we exposed GEN2.2 cells to a HEK293T cell line which expressed BST2, a natural ligand of ILT7 (11), in approximately 95% of cells (**Figure 5A**; Figure S5 in Supplementary Material). In the absence of MEK1/2 inhibitor, the co-culture of GEN2.2 cells with the BST2 expressing HEK293T inhibited IFN-α production induced by CpG-A to 47.4% ($p = 0.001$, **Figure 5B**). When the GEN2.2 cells were exposed to 1 μM PD0325901 prior to co-culture with BST2 expressing HEK293T cells and CpG-A simulation, the IFN-α production significantly increased (4.7-fold, $p = 0.001$, **Figure 5B**). In conclusion, the MEK1/2 inhibitor restored TLR9-mediated IFN-α production blocked by ligation of RR ILT7 with BST2.

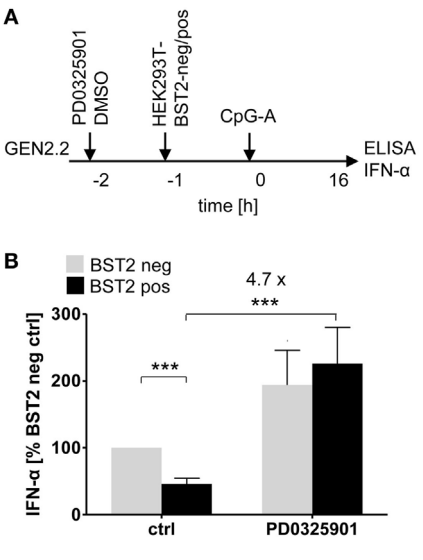

FIGURE 5 | Effect of MEK1/2 inhibition on the blockade of IFN-α by co-culture of GEN2.2 cells with BST2-expressing HEK293T cells. **(A)** Experimental outline. In total 10^5 GEN2.2 cells pretreated with 1 μM PD0325901 were added to a monolayer of 10^5 control HEK293T cells or to the same amount of BST2-expressing HEK293T cells in a volume of 200 μl. The proportion of BST2-expressing cells in the lentivirus-transduced HEK293T cells was determined by flow cytometry using the anti-BST2-PE antibody (Figure S4 in Supplementary Material). The co-cultures of GEN2.2 and HEK293T cells were kept for 1 h at 37°C before adding CpG-A. After a 16 h culture, the IFN-α production was determined in the cell-free supernatants by ELISA. **(B)** The IFN-α production was normalized to the IFN-α level induced in GEN2.2 cells by CpG-A in co-culture with the mock-transduced BST2-negative HEK293T cells and in the absence of PD0325901. The data show mean ± SEM of five independent co-culture experiments of GEN2.2 cells with BST2-negative or BST2-positive HEK293 cells, *, $p < 0.05$; ***, $p < 0.001$; two-tailed Mann–Whitney test.

MEK1/2 Inhibitor Restores TLR9-Mediated IFN-α Production Blocked by PMA

A recent study showed that treatment of pDCs with PMA, an agonist of PKC activating MEK1/2-ERK signaling pathway, has led to a dose-dependent reduction of IFN-α secretion (34). We investigated the capacity of PD0325901 to reverse the inhibitory effect of PMA on TLR9-mediated IFN-α production (**Figure 6A**). In the absence of the MEK1/2 inhibitor, the production of IFN-α induced in GEN2.2 cells by CpG-A was suppressed by PMA to 25% ($N = 6$, $p = 0.0022$, **Figure 6B**). PD0325901 significantly potentiated CpG-A-induced production of IFN-α in GEN2.2 cells (1.56-fold, $N = 6$, $p = 0.0022$, **Figure 6B**). PD0325901 completely restored the production of IFN-α inhibited in GEN2.2 cells by

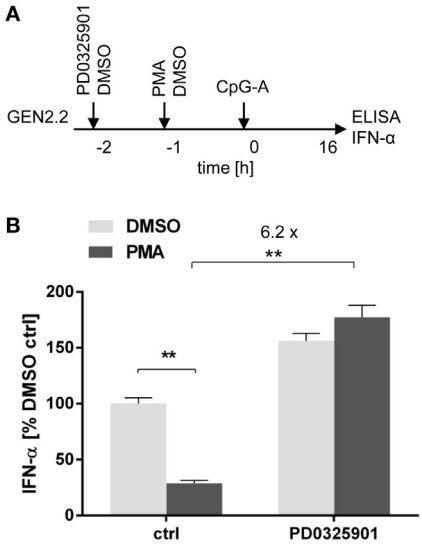

FIGURE 6 | Effect of MEK1/2 inhibitor PD0325901 on the blockade of IFN-α production in phorbol myristoyl acetate (PMA)-stimulated GEN2.2 cells. **(A)** Experimental outline. GEN2.2 cells separated from MS-5 feeder cells were incubated with the MEK1/2 inhibitor for 1 h before stimulation with PMA. After a 16 h culture, the IFN-α production was determined in the cell-free supernatants by ELISA. **(B)** The IFN-α production was normalized to the level induced by CpG-A in the presence of DMSO and in the absence of the MEK1/2 inhibitor. The data show mean ± SEM of six independent experiments with GEN2.2 cells. **, $p < 0.01$; two-tailed Mann–Whitney test.

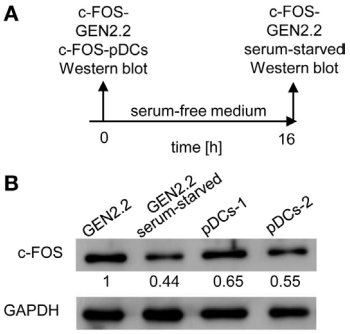

FIGURE 7 | c-FOS in proliferating GEN2.2 cells, GEN2.2 cells starved in the serum-free medium and in primary plasmacytoid dendritic cells (pDCs). **(A)** Experimental outline. Total cell extracts were prepared from GEN2.2 cells immediately after their separation from MS-5 feeder cells (GEN2.2), GEN2.2 cells separated from MS-5 feeder cells and starved overnight in the serum-free medium (GEN2.2 serum-starved), and from primary pDCs isolated from two healthy donors by magnetic-bead purification without any further culture (pDCs-1, pDCs-2). **(B)** c-FOS levels were determined in the total cell extract by Western blotting by rabbit polyclonal Ab c-FOS (sc-52). The values shown below each band represent relative quantity of c-FOS determined by densitometry normalized to proliferating GEN2.2 cells. GAPDH was used as a loading control.

PMA (6.18-fold, $p = 0.0022$, **Figure 6B**). In conclusion, activation of MEK1/2-ERK pathway by PMA inhibited the TLR9-mediated IFN-α production and this effect was abrogated by PD0325901.

c-FOS Levels in pDC Cell Line GEN2.2 Are Higher Than Those in Primary pDCs

The implication of MEK1/2 in the crosstalk of BCR-like and TLR7/9 signaling led us to investigate the role of c-FOS, a downstream immediate early response gene (20), in the regulation of TLR7/9 response. To this end, we compared the levels of c-FOS protein in the GEN2.2 cell line with those in primary pDCs (**Figures 7A,B**). We found that the quantity of c-FOS in GEN2.2 cells cultured in complete medium was approximately double that of primary pDCs (**Figure 7B**). Among numerous transcription factor binding sites in the upstream promoter region of *c-FOS*, the serum response element plays a central regulatory role in responding to external stimuli by growth factors and mitogens (20). To assess the basal level of c-FOS in GEN2.2 cells, we determined c-FOS levels in GEN2.2 starved for 16 h in serum-free medium. The starvation reduced the quantity of c-FOS in GEN2.2 cells to the level present in primary pDCs (**Figure 7B**).

Expression of c-FOS Induced by BDCA-2 Crosslinking Precedes and Exceeds That Induced by CpG-A

We determined the effect of CpG-A and BDCA-2 mAb on the kinetics of expression of the *c-FOS* gene in the serum-starved GEN2.2 cells pretreated or not with PD0325901 (**Figure 8A**). The peak of *c-FOS* transcription occurred 60 min after stimulation with CpG-A (**Figure 8B**), while crosslinking of BDCA-2 induced an earlier (30 min) and a stronger transcription of *c-FOS* (**Figure 8C**). Pretreatment with PD0325901 blocked the induction of *c-FOS* transcription by both CpG-A and BDCA-2 mAb (**Figures 8B,C**). In addition to the quantification of *c-FOS* mRNA by qRT-PCR, we determined the c-FOS protein levels in the serum-starved GEN2.2 cells exposed to CpG-A or BDCA-2 mAb by western blot (**Figures 8D,E**). While stimulation of GEN2.2 cells with CpG-A decreased the level of c-FOS protein (0.82-fold), crosslinking of BDCA-2 increased the production of c-FOS (1.46-fold).

PD0325901 Inhibits G1/S Phase Transition of GEN2.2 Cell Cycle

While pDC line GEN2.2 shares many features with primary pDCs (15, 25–30), GEN2.2 cells principally differ from primary pDCs by their capacity to proliferate. To further analyze this difference, we tested whether the higher basal level of c-FOS in proliferating GEN2.2 cells relative to primary pDCs is related to the MEK1/2-ERK-mediated c-FOS induction and G1/S phase transition of the cell cycle (21) (**Figures 9A,B**). Proliferating GEN2.2 cells were treated with PD0325901, corresponding concentration of DMSO, CpG-A, and BDCA-2 mAb, or starved in serum-free medium, and the impact on their cell cycle was analyzed 16 h later. Cell cycle of a control culture of GEN2.2 cells was analyzed immediately after separation from MS-5 cells. We found that the MEK1/2-ERK pathway inhibitor PD0325901 blocked the cell cycle in proliferating GEN2.2 cells. The cell cycle was also strongly inhibited in the serum-starved GEN2.2 cells, although the impairment of the cell cycle in this cell culture did not permit to calculate residual S phase and G2/M phase cells according to mathematical model used in our analyses. As expected, BDCA-2 crosslinking did not block,

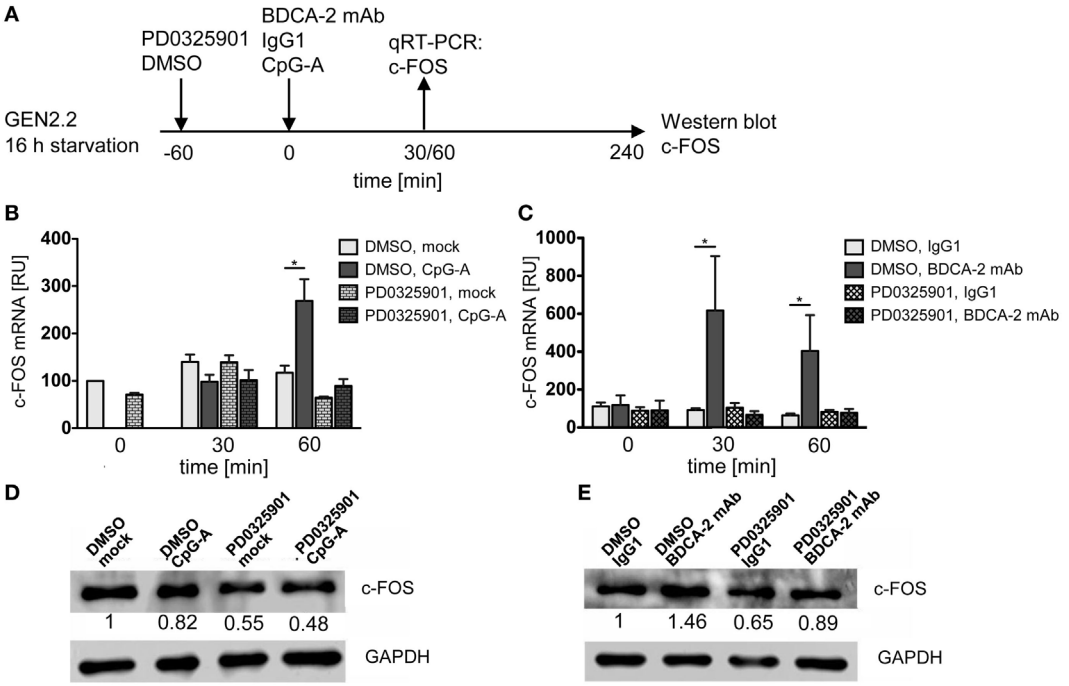

FIGURE 8 | *c-FOS* mRNA and protein expression in GEN2.2 stimulated with TLR9 or RR agonists. **(A)** Experimental outline. GEN2.2 cells separated from MS-5 feeder cells and starved in a serum-free medium for 16 h were pretreated or not with MEK1/2 inhibitor PD0325901 for 1 h and then exposed to CpG-A **(B,D)** or blood dendritic cell antigen 2 (BDCA-2) mAb **(C,E)**. **(B,C)** The expression of human *c-FOS* mRNA was quantified after 30 or 60-min exposure to CpG-A **(B)** or BDCA-2 mAb **(C)** by TaqMan qRT-PCR in the total cellular RNA. The data normalized to time zero show mean ± SEM of three independent experiments; *, $p < 0.05$; two-tailed Mann–Whitney test. **(D,E)** c-FOS protein levels were determined after 240 min exposure to CpG-A **(D)** or BDCA-2 mAb **(E)** in the total cell extract by Western blotting by rabbit polyclonal Ab c-FOS (sc-52). Relative quantity of c-FOS protein normalized to mock-treated GEN2.2 cells determined by densitometry is shown below each band. GAPDH was used as a loading control (representative result of three independent experiments).

but stimulated G1/S phase transition, consistently with increase of c-FOS level in BDCA-2-crosslinked cells (**Figure 8E**). CpG-A stimulation had only slight effect on G1/S phase transition. Cell cycle arrest in the GEN2.2 cells pretreated with PD0325901 or starved for serum (**Figure 9B**) correlated with the decline in the c-FOS level (**Figures 7** and **8D,E**) and with the potentiation of CpG-A-induced production of IFN-α (**Figure 1C**).

BDCA-2 Crosslinking Induces Phosphorylation of c-FOS

It was reported that ERK1/2-mediated post-translational phosphorylation enhances c-FOS stability and transcriptional activity (20, 22, 23). We assessed the phosphorylation of ERK1/2 at T202/Y204 and c-FOS at T325 in serum-starved GEN2.2 cells treated with RR agonist BDCA-2 mAb, TLR9 agonist CpG-A, and PKC agonist PMA (**Figure 10A**). c-FOS phosphorylation was analyzed using Western blotting with the P(T325)-c-FOS antibody. In the control experiment, 15 or 60 min exposure of GEN2.2 cells to PMA-induced strong phosphorylation of ERK1/2 at T202/Y204 and the c-FOS at T325, which was efficiently inhibited by PD0325901 (**Figure 10B**). The levels of total c-FOS and ERK1/2 remained unchanged in GEN2.2 cells stimulated with PMA for 15 or 60 min (Figure S6 in Supplementary Material). Stimulation with BDCA-2 mAb induced strong phosphorylation of ERK1/2 at T202/Y204 and the c-FOS phosphorylation at T325, which was abrogated by pretreatment with MEK1/2 inhibitor PD0325901 (**Figure 10C**; Figure S7 in Supplementary Material). In contrast to BDCA-2 mAb or PMA, CpG-A-induced ERK-1/2 T202/Y204 phosphorylation without inducing the phosphorylation of c-FOS T325 (**Figure 10D**). In conclusion, all three agonists induced phosphorylation of ERK-1/2, which was inhibited by 1 μM PD0325901. BDCA-2 mAb and PMA induced phosphorylation of c-FOS while CpG-A did not. The phosphorylation of c-FOS was inhibited by PD0325901, which is consistent with the regulation of c-FOS by MEK1/2-ERK signaling.

BDCA2 Crosslinking in GEN2.2 Cells and Primary pDCs Induces Upregulation of c-FOS

A recent study reported that BDCA-2 crosslinking and internalization result in up to 16 hr-lasting resistance of pDCs to TLR7/9-mediated stimulation suggesting a stability of the IFN-I inhibitory signal (35). Although c-FOS expression is usually rapid and transient, c-FOS stability is enhanced by phosphorylation (20, 22, 23). These observations led us to investigate the stability of c-FOS levels after stimulation of the BCR-like or TLR9 pathways. We analysed the quantity of c-FOS in the GEN2.2 cell line 16 h after stimulation with the control PMA, BDCA-2 mAb, and CpG-A by flow cytometry in the presence or absence of PD0325901 (**Figure 11A**). The results show that stimulation with PMA and

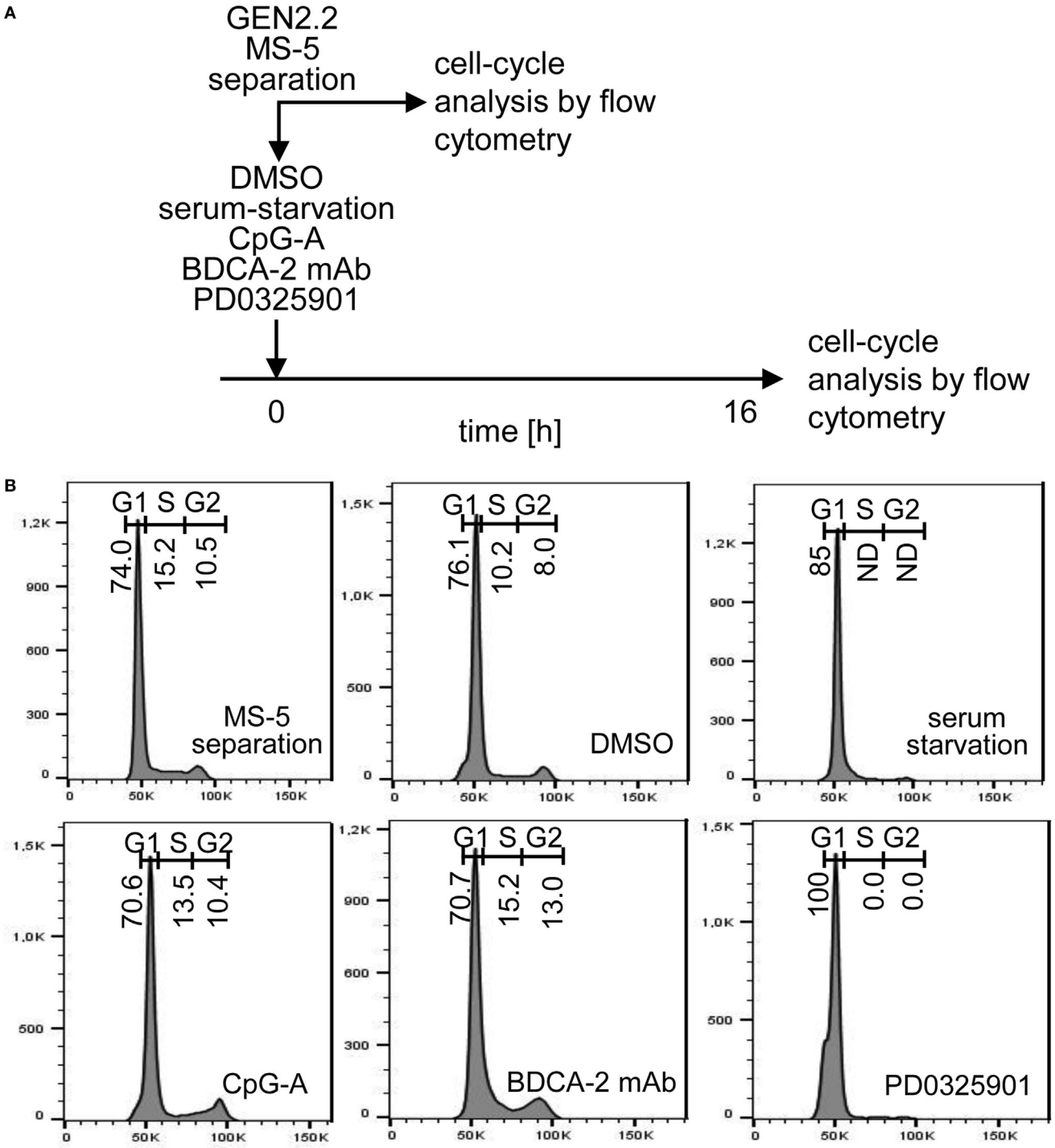

FIGURE 9 | Cell cycle analysis of GEN2.2 cells cultured in the presence of PD0325901, CpG-A, blood dendritic cell antigen 2 (BDCA-2) mAb, or in serum-free medium. **(A)** Experimental outline. GEN2.2 cells separated from MS-5 feeder cells were exposed for 16 hr to 1 μM PD0325901, 4 μg/ml CpG-A, 0.25 μg/ml BDCA-2 mAb, or DMSO (mock-treated control), or analyzed immediately after separation from MS-5 cells. **(B)** Cell cycle analysis using Hoechst 33342 stain. Histograms of live GEN2.2 cells (representative result of three independent experiments) stained with Hoechst 33342 dye showing DNA content distribution. Live/Dead cell discrimination was performed by Zombie Green™ Fixable Viability Kit. ND, not determined.

BDCA-2 mAb induced a sustained increase in c-FOS levels, while stimulation with CpG-A did not (**Figure 11B**). The increase in c-FOS levels in the PMA and BDCA-2 stimulated GEN2.2 cells was inhibited by PD0325901. MFI of c-FOS significantly increased after BDCA-2 crosslinking and PMA stimulation of GEN2.2 cells but not after stimulation with CpG-A ($N = 3$, **Figure 11C**). While

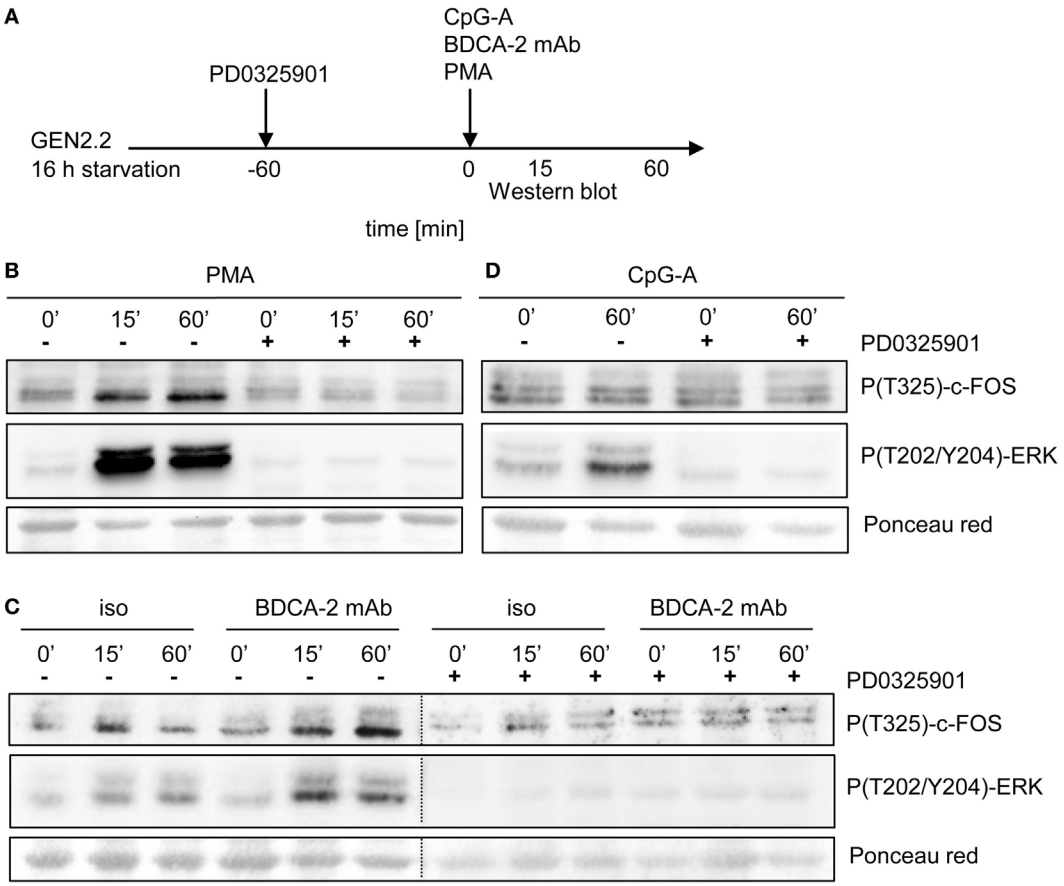

FIGURE 10 | Activation of c-FOS and ERK in GEN2.2 cells stimulated with phorbol myristoyl acetate (PMA), blood dendritic cell antigen 2 (BDCA-2) mAb and CpG-A. **(A)** Experimental outline. GEN2.2 cells separated from MS-5 feeder cells and starved in a serum-free medium for 16 h were pretreated or not with MEK1/2 inhibitor PD0325901 for 1 h and then stimulated with PMA **(B)**, BDCA-2 mAb **(C)**, or CpG-A **(D)**. The activation of c-FOS was evaluated by analysis of c-FOS phosphorylation using Western blotting with the P(T325)-c-FOS antibody. The phosphorylation of ERK-1 was determined by P(T202/Y204) ERK-1. Ponceau red was used as a loading control. Figure **(C)** is composed of two images of two different gels with samples from the same experiment. The two images are separated by a dotted line. Full scans of the original gels are shown in Figure S7 in Supplementary Material.

PD0325901 almost completely inhibited c-FOS production in GEN2.2 cells stimulated by PMA, it exerted only partial inhibition in BDCA-2 mAb-crosslinked cells.

To assess whether stimulation of BDCA-2 in primary pDCs also upregulates the expression of c-FOS, we exposed PBMCs from three healthy donors to BDCA-2 mAb and determined the level of c-FOS in a rapidly dying population of primary pDCs 4 hr later. Because the low proportion of pDCs in PBMCs makes their biochemical analyses difficult, we used flow cytometry for this purpose (**Figures 11A, D–F**). The MFI of c-FOS induced by BDCA-2 mAb increased 2.19 ± 0.85 times compared to isotypic IgG1 control in pDCs (**Figure 11E**). These results show that the stimulation of RRs of pDCs results in a sustained increase of the c-FOS level not only in the GEN2.2 cell line but also in primary pDCs.

DISCUSSION

Our results demonstrate the important role of MEK1/2-ERK signaling in the RR-mediated inhibition of IFN-α and IL-6 production in pDCs. We showed that MEK1/2 inhibitors PD0325901 and U0126 were the only constituents of the panel of inhibitors of BCR-like signaling that not only did not abrogate, but even stimulated TLR9 signaling in GEN2.2 cells. Pharmacological targeting of MEK1/2 in GEN2.2 cells or primary pDCs significantly abrogated inhibition of the TLR9-mediated production of IFN-I induced by BCR-like or PKC signaling. Both BCR-like and PKC signaling activated MEK1/2-ERK pathway.

The molecular mechanism by which the ligation of the RRs antagonizes TLR7/9 signaling in pDCs remains elusive despite years of intense research in many laboratories (8–10, 12–14, 16, 35). We show here that MEK1/2-ERK signaling upregulated the production and phosphorylation of c-FOS. Thus, the potentiation of IFN-I by PD0325901 treatment of GEN2.2 cells could be consequence of a natural role of c-FOS in cell proliferation. The role of c-FOS in the activation of the G1/S cell cycle transition and in the inhibition of IFN-α and IL-6 production in GEN2.2 cells should be further investigated. A higher level of c-FOS in proliferating GEN2.2 cells in comparison with resting primary

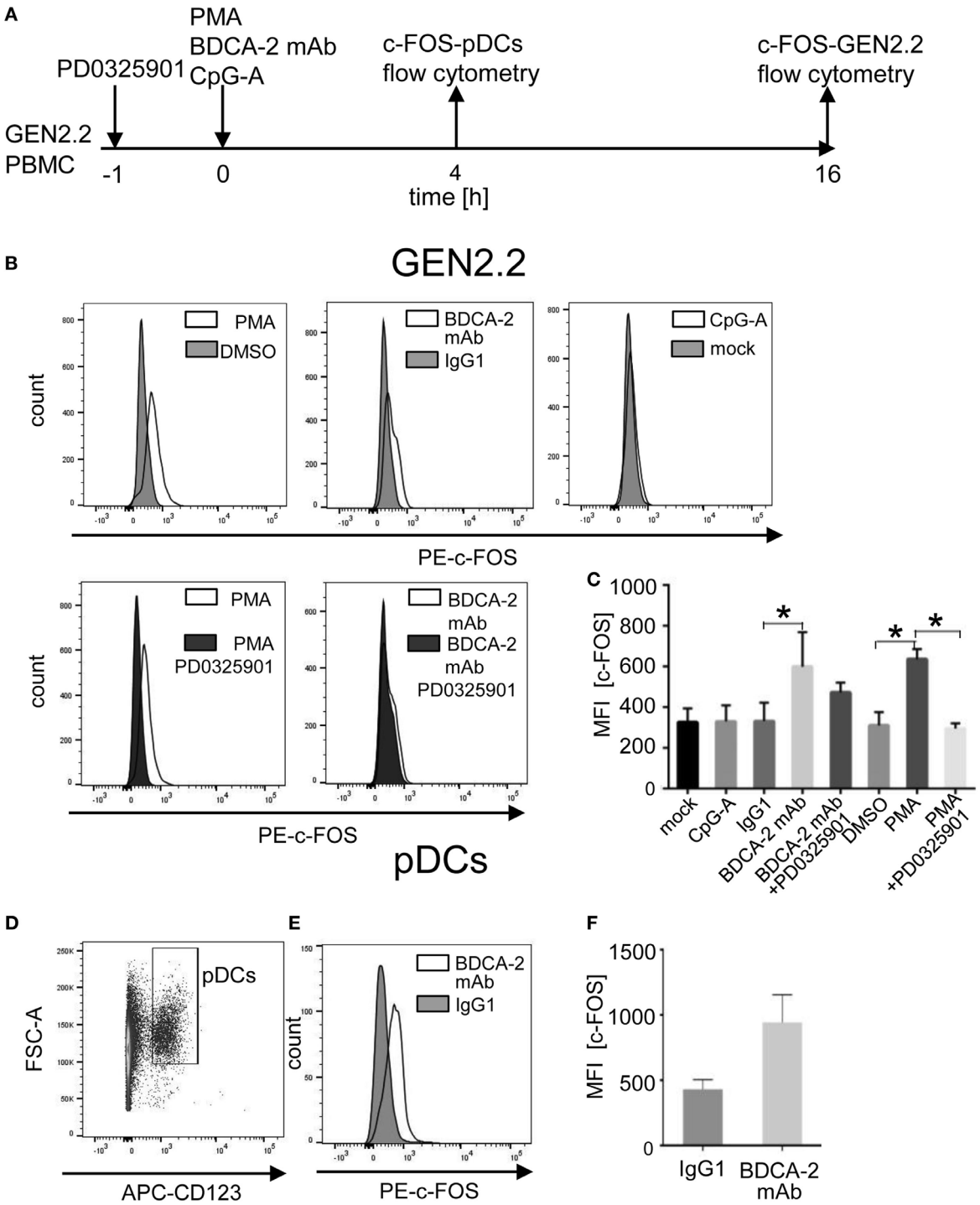

FIGURE 11 | Induction of total c-FOS in GEN2.2 cells and primary plasmacytoid dendritic cells (pDCs). **(A)** Experimental outline. GEN2.2 cells separated from MS-5 feeder cells exposed or not to PD0325901 were stimulated with phorbol myristoyl acetate (PMA), blood dendritic cell antigen 2 (BDCA-2) mAb, or CpG-A for 16 h. Peripheral blood mononuclear cells (PBMCs) of healthy donors were exposed to BDCA-2 mAb or IgG1 isotype Ab and quantity of the total c-FOS in pDCs gated from PBMCs was determined 4 h later. **(B)** Fluorescence intensity of the total c-FOS in GEN2.2 cells. Viable GEN2.2 cells were gated according to Live/Dead Zombie Green kit, semipermeabilized and stained with PE-conjugated c-FOS (9F6) rabbit mAb. Control light shaded areas show c-FOS in unstimulated PD0325901 mock-treated GEN2.2 cells. Dark shaded areas show c-FOS in PD0325901-treated GEN2.2 cells. Representative result of three independent experiments. **(C)** The data show mean MFI ± SEM of the total c-FOS in GEN2.2 cells determined in three independent experiments. *, $p < 0.05$; unpaired, two-tailed *t*-test. **(D)** Primary pDCs in PBMCs were gated negatively for Zombie green- (living cells) and FITC-Lin$^-$ and positively for APC-CD123+. **(E)** c-FOS in semipermeabilized primary pDCs gated from PBMCs stimulated with BDCA-2 mAb or IgG1 isotype for 4 h was stained with PE-c-FOS (9F6) rabbit mAb. Representative result of three independent experiments with PBMCs from different healthy donors. **(F)** The data show mean MFI ± SEM of the total c-FOS in primary pDCs gated from BDCA-2-stimulated or unstimulated PBMCs determined in three independent experiments in PBMCs of different donors.

pDCs represents a major difference between these cell types and is consistent with the different outcome of MEK1/2-ERK inhibition. The demonstration of the synergistic effect of MEK1/2 inhibitors on the CpG-A-induced production of IFN-α suggests that under steady-state conditions a natural intrinsic block regulated by MEK1/2 controls the IFN-α level in GEN2.2 cells to a higher level than that in primary pDCs. Release of this block could be a part of the restoration mechanism of IFN-α by MEK1/2 inhibitors in pDCs exposed to RR agonists.

The levels of inhibition of IFN-I production by crosslinking of RR and their restoration by MEK1/2-ERK inhibitors varied depending on the RR ligand. This could be related to differences in the cell-surface distribution of targeted receptors (BDCA-2, ILT7, DCIR) and avidity of tested ligands (BDCA-2 and ILT7 mAbs, HCV particles, or BST2 expressing cells). Among them, BDCA-2 mAb was the most potent inhibitor of IFN-I production. Surprisingly the relative levels of inhibition and restoration of IFN-I production were similar in GEN2.2 cell line and primary pDCs. In addition to differences in receptor/ligand interactions, the levels of inhibition and restoration of IFN-I production were dependent on the mechanism of stimulation of MEK1/2-ERK pathway by BCR-like or PKC signaling. While pretreatment with PD0325901 led to almost complete inhibition of c-FOS expression induced by PMA, c-FOS expression induced by BDCA-2 mAb was only partially inhibited. This suggests that expression of c-FOS induced by BDCA-2 crosslinking and internalization could be partially MEK1/2-ERK independent.

MEK1/2 inhibitor PD0325901 potentiated production of IFN-α in pDC cell line GEN2.2 stimulated by both synthetic (CpG-A and CpG-B) and natural (HSV-1 and HCMV) agonists. In the absence of PD0325901, exposure of pDCs to HSV-1 and HCMV results in a non-permissive infection and TLR9-mediated production of IFN-α (36, 37). Interestingly, the quantity of IFN-α produced by murine pDCs exposed to murine CMV (MCMV) is down-modulated by MCMV-induced stimulation of DAP12, an adaptor molecule of murine RR (38). Recent study demonstrated that EBV and double-stranded DNA viruses induce TRIM29 leading to suppression of IFN-α production (39). The potential role of TRIM29 in HSV-1 and HCVM-mediated inhibition of IFN-α production in pDCs needs to be clarified.

A previous report implicated c-FOS induced by MAP3-kinase TPL-2 in the negative regulation of TLR9-mediated production of IFN-β in mouse macrophages and myeloid (mDCs), but not in mouse pDCs (24). In contrast, we show here that c-FOS induced by MEK1/2-ERK signaling is involved in the regulation of TLR9 signaling in human pDCs. It is possible that TPL-2 and MEK1/2-ERK signaling are interpreted differently in mouse and human pDCs compared with macrophages and mDCs as a consequence of an interaction of ERK activation with other signaling pathways triggered by TLR9 (18). Several cell type-specific studies have shown that the interaction of TLR7/9 with BCR-like signaling may be regulated in a different way in human pDCs (7, 12, 14, 16, 35, 40).

Activation of Ras/MEK1/2/ERK downregulates expression of IFN-I also in human epithelial cancer cells (41). Together with our experiments, these results suggest that MEK1/2-ERK signaling can play a general role in regulation of IFN-I. Another recent study demonstrated that MEK1/2-ERK-mediated phosphorylation of c-FOS in HCV-infected hepatocytes induced miR-21, which targeted MyD88 and IRAK1 and contributed to the suppression of IFN-I production (42). We did not detect a significant increase of miR-21 level in GEN2.2 cells exposed to BDCA-2 mAb or CpG-A (not shown).

We have demonstrated that inhibitors of MEK1/2 restore the production of IFN-I inhibited by ligation of RRs with HCV particles or with BST2 expressing cancer cells. These results suggest that pharmacological targeting of MEK1/2-ERK signaling could be a strategy to overcome immunotolerance of pDCs and re-establish their immunogenic activity. This finding complements our previous results showing that an inhibitor of SYK, a protein kinase involved in both TLR7/9 and BCR-like pathways, could be a useful tool to suppress the overproduction of IFN-I and to re-establish tolerogenic homeostatic functions of pDCs (15). The role of IFN-I in the pathogenesis of chronic viral infections and cancer is unclear and ambivalent. IFN-I responses are critical in the early phases of immune response to infections, but the chronic and systemic activation of pDCs can paradoxically lead to deleterious consequences for the immune system (43, 44). It is likely that an intense signaling occurs in the mucosa, involving a local accumulation of pDCs producing IFN-I early during HIV-1 infection, which is associated with the chronic activation of the immune system (45, 46). While in this era of great success of direct-acting antivirals against HIV and HCV the stimulation of IFN response might represent an adjuvant therapy, important namely in the case of virus escape, the induction of IFN-I in combination with existing antivirals may cure HBV infection (47–49). IFN-I also plays an important role in antitumor immunity (3, 50). The addition of exogenous IFN-α reverts the immunotolerance of tumor-associated pDCs in breast and ovarian carcinoma (4, 51). Pharmacological targeting of MEK1/2 signaling may constitute an attractive new approach to study mechanisms of modulation of pDC activation in pathophysiological conditions such as chronic viral infections and cancer.

MATERIALS AND METHODS

Isolation and Culture of Primary pDCs

Peripheral blood mononuclear cells (PBMCs) from healthy anonymous donors were obtained from the national blood services (Etablissement Francais du Sang, Marseille, France). Blood samples were obtained after written consent following the approval of the EFS, Marseille, France, and the Center de Recherche en Cancérologie de Marseille (CRCM) in accordance to the convention signed the 20th May 2014. pDCs purified from PBMCs as described previously were 75–95% pure, with a contamination of less than 5% mDCs (32, 33, 52, 53). Isolated pDCs were cultured in RPMI 1640 supplemented with 10% fetal calf serum (FCS). To optimize viability in overnight experiments, recombinant IL-3 (R&D Systems Europe, Ltd., Abingdon, UK) was added to a final concentration of 10 ng/mL.

pDC Line GEN2.2

Human pDC line GEN2.2 (25) was grown in a RMPI 1640 medium supplemented with L-glutamine, 10% FCS, 1% sodium pyruvate,

and 1% MEM nonessential amino acids, on a monolayer of the murine stromal feeder cell line MS-5 grown in RPMI 1640 supplemented with L-glutamine, 10% FCS, and 1% sodium pyruvate. For the measurement of cytokine production, the dynamic flow cytometry and the Western blot experiments, GEN2.2 cells were separated from the MS-5 feeder cells.

Inhibitors, Antibodies, and Reagents

MEK-1/2 inhibitor PD0325901 obtained from InvivoGen (Toulouse, France) and U0126 obtained from Sigma (Sigma-Aldrich, Lyon, France) were used as recommended by supplier. PD0325901 is a selective non-ATP-competitive allosteric MEK1/2 inhibitor with *in vitro* IC50 0.33 nM, which was shown to be specific against a panel of 70 different kinases at 10 μM range (54). U0126 inhibits MEK 1/2 with an *in vitro* IC50 of 0.5 μM. JNK inhibitor SP600125, TBK1 inhibitor BX795, NF-κB inhibitor Bay11-7082, p38 MAPK inhibitor SB253080, and calcineurin inhibitor FK506 were all purchased from InvivoGen, San Diego, USA. For *in vitro* pDC stimulation assays, CpG-A (ODN 2216), CpG-B (ODN 2006), and PMA (all InvivoGen, San Diego, USA), and BDCA-2 antibody (Miltenyi Biotech, Paris, France), and ILT7 antibody (eBioscience) were used.

In Vitro pDC Stimulation

To determine cytokine production, purified primary human pDCs (in the presence of IL-3) or GEN2.2 cells were kept at a concentration of 10^6 cells/ml aliquoted in 100 μl quantities in 96-well round-bottom culture plates and stimulated with 4 μg/ml CpG-A or CpG-B, 25 ng/ml PMA, 20 μg/ml of BDCA-2 or ILT7 antibody, or 10 HCV geq/cell for 16 h. In some experiments, BDCA-2 or ILT7 antibody-exposed cells were further crosslinked with goat-antimouse $F(ab')_2$ (15 μg/ml) (Jackson ImmunoResearch).

Production and Purification of Cell Culture-Derived HCVcc (JFH-1 3 M), HSV-1, and HCMV Virus Stocks

Hepatitis C virus cc particles were prepared in Huh7.5 cells (55) (kindly provided by APATH L.L.C.) on the basis of plasmid pJFH-1 displaying mutations, F172C and P173S in core and N534K in E2 (56), as described previously (33). The ultracentrifuged virus purified through a cushion of 20% sucrose was resuspended in RPMI 1640 to obtain a 1,000-fold concentrated virus suspension containing 10^7 $FFU_{Huh7.5}/10^{11}$ HCV RNA copies/ml. Stocks of HSV-1, strain Praha, and HCMV, strain AD-169, were prepared as described previously (57, 58).

Preparation of BST2 Expressing HEK293T Cells

The BST2 sequence from pCMV-Sport6-BST2 was cloned into the pRRL.PPT.SF.i2GFPp expression vector to produce a lentiviral vector pRRL-BST2-GFP. HEK293T cells were transduced by the resulting lentivirus construct at MOI = 10 and GFP-positive cells were selected by FACSAria (BD Biosciences). The expression of GFP and BST2 in transduced cells was determined by flow cytometry by LSRII (BD Biosciences).

Determination of *c-FOS* Expression

Total cellular RNA was isolated using RNeasy Mini Kit (Qiagen). cDNA was synthesized using High Capacity cDNA Reverse Transcription Kit (Applied Biosystems). Human *c-FOS* was amplified with SYBR® Green PCR Master Mix (Applied Biosystems) using the following primers: *c-FOS*: forward: 5′-CAAGCGGAGACAGACCAACT-3′and reverse 5′-AGTCAGATCAAGGGAAGCCA-3′; GAPDH: forward: 5′-GCGAGATCCCTCCAAAATCAA-3′and reverse 5′-GTTCACACCCATGACGAACAT-3′. Relative expression levels were calculated using $2^{-\Delta\Delta CT}$ method. *GAPDH* was used as endogenous control.

Determination of ERK and c-FOS by Immunobloting

Total c-FOS and ERK in the whole cell lysate of GEN2.2 cells or primary pDCs were determined by Western blotting by means of rabbit polyclonal c-FOS (sc-52) and ERK1/2 (sc-154) Abs (Santa Cruz Biotechnology, Dallas, USA). Phosphorylation of ERK and c-FOS in the whole cell lysate of GEN2.2 cells was analyzed by Western blotting using phospho-c-FOS-T325 Ab from Abcam (Cambridge, UK) and ERK Ab T202/Y204 (Santa Cruz Biotechnology, Dallas, USA) as described previously (15). After incubation with the appropriate horseradish peroxidase-conjugated secondary antibody, the membranes were washed and the protein bands were detected with Super Signal™ enhanced chemoluminiscent substrate detection reagent (ThermoFisher Scientific, Villebon-sur-Yvette, France). Densitometric analyses were performed using Amersham Imager 600 (GE Healthcare Life Science). Band intensities were normalized to GAPDH or Ponceau red.

Determination of c-FOS by Dynamic Flow Cytometry

To determine total c-FOS by dynamic flow cytometry, 10^6 GEN2.2 cells or 2×10^6 PBMCs per milliliter were kept in the RPMI 1640 medium supplemented with 10% FCS. Aliquots of 10^6 GEN2.2 cells or 8×10^6 PBMCs were stimulated with 4 μg/ml CpG-A, 100 ng/ml PMA, 10 μg/ml of BDCA-2 mAb for 16 hr (GEN2.2 cells) or 4 hr PBMCs. Live/Dead cell discrimination was performed by Zombie Green™ Fixable Viability Kit (BioLegend, San Diego, USA). For flow cytometry analysis of total c-FOS, cells were fixed in 4% formaldehyde for 10 min, permeabilized by 90% methanol for 30 min, and stained by PE conjugated c-FOS (9F6) rabbit mAb (Cell Signaling, Danvers, USA). For determination of c-FOS in primary pDCs, PBMCs were stained by APC-conjugated anti-human CD123 mouse mAb (BD Biosciences, San Jose, USA) and FITC-conjugated anti-human lineage cocktail mouse Abs (BioLegend, San Diego, USA). pDCs in PBMCs population were defined as Lin-, CD123+ cell population. Samples were analyzed using a BD LSR FORTESSA cytometer (BD Biosciences, San Jose, USA) and data were processed using FLOWJO software (Treestar, San Carlos, USA).

Cell Cycle Analysis

For analysis of cell cycle, 10^6 GEN2.2 cells/ml of RPMI 1640 medium supplemented with 10% FCS were aliquoted in 1 ml

quantities in 6-well flat-bottom culture plates and exposed to 1 μM PD0325901, 4 μg/ml CpG-A, and 10 μg/ml of BDCA-2 mAb for 16 h. The cells were then resuspended in the RPMI 1640 medium containing 6 μg/ml Hoechst 33342 Dye (ThermoFischer Scientific) and incubated at 37°C in 5% CO_2 for 30 min and the amount of DNA was determined by flow cytometry. Live/Dead cell discrimination was performed by Zombie Green™ Fixable Viability Kit (BioLegend, San Diego, USA). Samples were analyzed using a BD LSR FORTESSA cytometer (BD Biosciences, San Jose, USA) and data were processed using FLOWJO software (Treestar, San Carlos, USA). Phases of the cell cycle were calculated by Dean-Jett-Fox model.

Determination of Secreted IFN-α, TNF-α, and IL-6

The quantities of total IFN-α, TNF-α, and IL-6 produced by pDCs or GEN2.2 were measured in cell-free supernatants using human ELISA kits (IFN-α and IL-6 from Mabtech, and TNF-α from BD Biosciences). The index of synergism was determined from the following formula: the level of cytokine production after stimulation with the combination of CpG and PD0325901 divided by the sum of cytokine production level after stimulation with CpG and PD0325901 separately. PD0325901 alone did not induce a detectable quantity of respective cytokines. Combinations resulting in an index of synergism >1.5 were considered to be synergistic. The combinations resulting in an index of synergism ≤1.5 and in a 30% increase in stimulation compared to the stimulation observed with either of the two stimulators were considered to be additive.

Statistical Analysis

Quantitative variables are expressed as the mean ± SEM (standard error of the mean). To compare the levels of cytokine production and transcription of c-FOS mRNA by pDCs, we used a Mann–Whitney or a Wilcoxon two-tailed non-parametric tests. For flow cytometry analyses, we used two-tailed *t*-test. Data were analyzed with GraphPad Prism 4 (GraphPad Software, La Jolla, CA). A p value ≤ 0.05 was considered to be significant.

ETHICS STATEMENT

Peripheral blood mononuclear cells (PBMCs) from healthy anonymous donors were obtained from the national blood services (Etablissement Francais du Sang, Marseille, France). Blood samples were obtained after written consent following the approval of the EFS, Marseille, France and the Centre de Recherche en Cancérologie de Marseille (CRCM) in accordance to the convention signed the 20th May 2014.

AUTHOR CONTRIBUTIONS

Contribution: VJ, BA, and AF-H equally performed research, designed research, and analyzed data. TH, KT, and JW performed research and analyzed data. JN, DO, and PD designed research and analyzed data. LC and JP provided essential materials. RS and IH designed research, analyzed data, and wrote the paper.

ACKNOWLEDGMENTS

DO is a scholar of the Institut Universitaire de France. We acknowledge the Imaging Methods Core Facility at BIOCEV for their support with obtaining flow cytometry data presented in this paper.

FUNDING

This work was supported by grants from the Grantova Agentura Ceske Republiky (Czech Science Foundation) grant no. 14-32547S (IH) and by Fondation ARC pour la Recherche sur le Cancer. This work was also supported by institutional grants from the Institut National de la Santé et de la Recherche Médicale, the Centre National de la Recherche Scientifique and Aix-Marseille Université to CRCM, and from Charles University, GAUK-434616 (AFH), SVV 260426. BIOCEV – Biotechnology and Biomedicine Centre of the Academy of Sciences and Charles University (CZ.1.05/1.1.00/02.0109) from the European Regional Development Fund (http://www.biocev.eu/) (IH). Ligue contre le cancer (http://www.ligue-cancer.net/) (BA). Algerian Ministry of Higher Education and Research, and Franco-Algerian Cooperation (BA).

SUPPLEMENTARY MATERIAL

The Supplementary Material for this article can be found online at http://www.frontiersin.org/articles/10.3389/fimmu.2018.00364/full#supplementary-material.

REFERENCES

1. Diebold SS, Kaisho T, Hemmi H, Akira S, Reis e Sousa C. Innate antiviral responses by means of TLR7-mediated recognition of single-stranded RNA. *Science* (2004) 303(5663):1529–31. doi:10.1126/science.1093616
2. Lund J, Sato A, Akira S, Medzhitov R, Iwasaki A. Toll-like receptor 9-mediated recognition of herpes simplex virus-2 by plasmacytoid dendritic cells. *J Exp Med* (2003) 198(3):513–20. doi:10.1084/jem.20030162
3. Diamond MS, Kinder M, Matsushita H, Mashayekhi M, Dunn GP, Archambault JM, et al. Type I interferon is selectively required by dendritic cells for immune rejection of tumors. *J Exp Med* (2011) 208(10):1989–2003. doi:10.1084/jem.20101158
4. Sisirak V, Faget J, Gobert M, Goutagny N, Vey N, Treilleux I, et al. Impaired IFN-alpha production by plasmacytoid dendritic cells favors regulatory t-cell expansion that may contribute to breast cancer progression. *Cancer Res* (2012) 72(20):5188–97. doi:10.1158/0008-5472.CAN-11-3468
5. Conrad C, Gregorio J, Wang YH, Ito T, Meller S, Hanabuchi S, et al. Plasmacytoid dendritic cells promote immunosuppression in ovarian cancer via ICOS costimulation of Foxp3+ T-regulatory cells. *Cancer Res* (2012) 72(20):5240–9. doi:10.1158/0008-5472.CAN-12-2271
6. Ghirelli C, Reyal F, Jeanmougin M, Zollinger R, Sirven P, Michea P, et al. Breast cancer cell-derived GM-CSF licenses regulatory Th2 induction by plasmacytoid predendritic cells in aggressive disease subtypes. *Cancer Res* (2015) 75(14):2775–87. doi:10.1158/0008-5472.CAN-14-2386
7. Leifer CA, Medvedev AE. Molecular mechanisms of regulation of toll-like receptor signaling. *J Leukoc Biol* (2016) 100(5):927–41. doi:10.1189/jlb.2MR0316-117RR
8. Bao M, Liu YJ. Regulation of TLR7/9 signaling in plasmacytoid dendritic cells. *Protein Cell* (2013) 4(1):40–52. doi:10.1007/s13238-012-2104-8
9. Swiecki M, Colonna M. The multifaceted biology of plasmacytoid dendritic cells. *Nat Rev Immunol* (2015) 15(8):471–85. doi:10.1038/nri3865

10. Hirsch I, Caux C, Hasan U, Bendriss-Vermare N, Olive D. Impaired toll-like receptor 7 and 9 signaling: from chronic viral infections to cancer. *Trends Immunol* (2010) 31(10):391–7. doi:10.1016/j.it.2010.07.004
11. Cao W, Rosen DB, Ito T, Bover L, Bao M, Watanabe G, et al. Plasmacytoid dendritic cell-specific receptor ILT7-Fc epsilonRI gamma inhibits toll-like receptor-induced interferon production. *J Exp Med* (2006) 203(6):1399–405. doi:10.1084/jem.20052454
12. Cao W, Zhang L, Rosen DB, Bover L, Watanabe G, Bao M, et al. BDCA2/Fc epsilon RI gamma complex signals through a novel BCR-like pathway in human plasmacytoid dendritic cells. *PLoS Biol* (2007) 5(10):e248. doi:10.1371/journal.pbio.0050248
13. Dzionek A, Sohma Y, Nagafune J, Cella M, Colonna M, Facchetti F, et al. BDCA-2, a novel plasmacytoid dendritic cell-specific type II C-type lectin, mediates antigen capture and is a potent inhibitor of interferon alpha/beta induction. *J Exp Med* (2001) 194(12):1823–34. doi:10.1084/jem.194.12.1823
14. Cao W, Bover L, Cho M, Wen X, Hanabuchi S, Bao M, et al. Regulation of TLR7/9 responses in plasmacytoid dendritic cells by BST2 and ILT7 receptor interaction. *J Exp Med* (2009) 206(7):1603–14. doi:10.1084/jem.20090547
15. Aouar B, Kovarova D, Letard S, Font-Haro A, Florentin J, Weber J, et al. Dual role of the tyrosine kinase syk in regulation of toll-like receptor signaling in plasmacytoid dendritic cells. *PLoS One* (2016) 11(6):e0156063. doi:10.1371/journal.pone.0156063
16. Hirsch I, Janovec V, Stranska R, Bendriss-Vermare N. Cross talk between inhibitory immunoreceptor tyrosine-based activation motif-signaling and toll-like receptor pathways in macrophages and dendritic cells. *Front Immunol* (2017) 8:394. doi:10.3389/fimmu.2017.00394
17. Martinelli E, Cicala C, Van Ryk D, Goode DJ, Macleod K, Arthos J, et al. HIV-1 gp120 inhibits TLR9-mediated activation and IFN-{alpha} secretion in plasmacytoid dendritic cells. *Proc Natl Acad Sci U S A* (2007) 104(9):3396–401. doi:10.1073/pnas.0611353104
18. Xu Y, Hu Y, Shi B, Zhang X, Wang J, Zhang Z, et al. HBsAg inhibits TLR9-mediated activation and IFN-alpha production in plasmacytoid dendritic cells. *Mol Immunol* (2009) 46(13):2640–6. doi:10.1016/j.molimm.2009.04.031
19. Florentin J, Aouar B, Dental C, Thumann C, Firaguay G, Gondois-Rey F, et al. HCV glycoprotein E2 is a novel BDCA-2 ligand and acts as an inhibitor of IFN production by plasmacytoid dendritic cells. *Blood* (2012) 120(23):4544–51. doi:10.1182/blood-2012-02-413286
20. Healy S, Khan P, Davie JR. Immediate early response genes and cell transformation. *Pharmacol Ther* (2013) 137(1):64–77. doi:10.1016/j.pharmthera.2012.09.001
21. Chambard JC, Lefloch R, Pouyssegur J, Lenormand P. ERK implication in cell cycle regulation. *Biochim Biophys Acta* (2007) 1773(8):1299–310. doi:10.1016/j.bbamcr.2006.11.010
22. Monje P, Marinissen MJ, Gutkind JS. Phosphorylation of the carboxyl-terminal transactivation domain of c-Fos by extracellular signal-regulated kinase mediates the transcriptional activation of AP-1 and cellular transformation induced by platelet-derived growth factor. *Mol Cell Biol* (2003) 23(19):7030–43. doi:10.1128/MCB.23.19.7030-7043.2003
23. Deng T, Karin M. c-Fos transcriptional activity stimulated by H-Ras-activated protein kinase distinct from JNK and ERK. *Nature* (1994) 371(6493):171–5. doi:10.1038/371171a0
24. Kaiser F, Cook D, Papoutsopoulou S, Rajsbaum R, Wu X, Yang HT, et al. TPL-2 negatively regulates interferon-beta production in macrophages and myeloid dendritic cells. *J Exp Med* (2009) 206(9):1863–71. doi:10.1084/jem.20091059
25. Chaperot L, Blum A, Manches O, Lui G, Angel J, Molens JP, et al. Virus or TLR agonists induce TRAIL-mediated cytotoxic activity of plasmacytoid dendritic cells. *J Immunol* (2006) 176(1):248–55. doi:10.4049/jimmunol.176.1.248
26. Kim T, Pazhoor S, Bao M, Zhang Z, Hanabuchi S, Facchinetti V, et al. Aspartate-glutamate-alanine-histidine box motif (DEAH)/RNA helicase A helicases sense microbial DNA in human plasmacytoid dendritic cells. *Proc Natl Acad Sci U S A* (2010) 107(34):15181–6. doi:10.1073/pnas.1006539107
27. Li J, Du Q, Hu R, Wang Y, Yin X, Yu H, et al. Death receptor 6 is a novel plasmacytoid dendritic cell-specific receptor and modulates type I interferon production. *Protein Cell* (2016) 7(4):291–4. doi:10.1007/s13238-015-0239-0
28. Kim TW, Hong S, Lin Y, Murat E, Joo H, Kim T, et al. Transcriptional repression of IFN regulatory factor 7 by MYC is critical for type I IFN production in human plasmacytoid dendritic cells. *J Immunol* (2016) 197(8):3348–59. doi:10.4049/jimmunol.1502385
29. Bao M, Wang Y, Liu Y, Shi P, Lu H, Sha W, et al. NFATC3 promotes IRF7 transcriptional activity in plasmacytoid dendritic cells. *J Exp Med* (2016) 213(11):2383–98. doi:10.1084/jem.20160438
30. Pauls E, Shpiro N, Peggie M, Young ER, Sorcek RJ, Tan L, et al. Essential role for IKKbeta in production of type 1 interferons by plasmacytoid dendritic cells. *J Biol Chem* (2012) 287(23):19216–28. doi:10.1074/jbc.M112.345405
31. Rao S, Liu X, Freedman BD, Behrens EM. Spleen tyrosine kinase (Syk)-dependent calcium signals mediate efficient CpG-induced exocytosis of tumor necrosis factor alpha (TNFalpha) in innate immune cells. *J Biol Chem* (2013) 288(18):12448–58. doi:10.1074/jbc.M113.454405
32. Shiina M, Rehermann B. Cell culture-produced hepatitis C virus impairs plasmacytoid dendritic cell function. *Hepatology* (2008) 47(2):385–95. doi:10.1002/hep.21996
33. Gondois-Rey F, Dental C, Halfon P, Baumert TF, Olive D, Hirsch I. Hepatitis C virus is a weak inducer of interferon alpha in plasmacytoid dendritic cells in comparison with influenza and human herpesvirus type-1. *PLoS One* (2009) 4(2):e4319. doi:10.1371/journal.pone.0004319
34. Rock J, Schneider E, Grun JR, Grutzkau A, Kuppers R, Schmitz J, et al. CD303 (BDCA-2) signals in plasmacytoid dendritic cells via a BCR-like signalosome involving Syk, Slp65 and PLCgamma2. *Eur J Immunol* (2007) 37(12):3564–75. doi:10.1002/eji.200737711
35. Pellerin A, Otero K, Czerkowicz JM, Kerns HM, Shapiro RI, Ranger AM, et al. Anti-BDCA2 monoclonal antibody inhibits plasmacytoid dendritic cell activation through Fc-dependent and Fc-independent mechanisms. *EMBO Mol Med* (2015) 7(4):464–76. doi:10.15252/emmm.201404719
36. Schuster P, Donhauser N, Pritschet K, Ries M, Haupt S, Kittan NA, et al. Co-ordinated regulation of plasmacytoid dendritic cell surface receptors upon stimulation with herpes simplex virus type 1. *Immunology* (2010) 129(2):234–47. doi:10.1111/j.1365-2567.2009.03176.x
37. Varani S, Cederarv M, Feld S, Tammik C, Frascaroli G, Landini MP, et al. Human cytomegalovirus differentially controls B cell and T cell responses through effects on plasmacytoid dendritic cells. *J Immunol* (2007) 179(11):7767–76. doi:10.4049/jimmunol.179.11.7767
38. Sjolin H, Robbins SH, Bessou G, Hidmark A, Tomasello E, Johansson M, et al. DAP12 signaling regulates plasmacytoid dendritic cell homeostasis and down-modulates their function during viral infection. *J Immunol* (2006) 177(5):2908–16. doi:10.4049/jimmunol.177.8.5748-b
39. Xing J, Zhang A, Zhang H, Wang J, Li XC, Zeng MS, et al. TRIM29 promotes DNA virus infections by inhibiting innate immune response. *Nat Commun* (2017) 8(1):945. doi:10.1038/s41467-017-00101-w
40. Bao M, Hanabuchi S, Facchinetti V, Du Q, Bover L, Plumas J, et al. CD2AP/SHIP1 complex positively regulates plasmacytoid dendritic cell receptor signaling by inhibiting the E3 ubiquitin ligase Cbl. *J Immunol* (2012) 189(2):786–92. doi:10.4049/jimmunol.1200887
41. Christian SL, Zu D, Licursi M, Komatsu Y, Pongnopparat T, Codner DA, et al. Suppression of IFN-induced transcription underlies IFN defects generated by activated Ras/MEK in human cancer cells. *PLoS One* (2012) 7(9):e44267. doi:10.1371/journal.pone.0044267
42. Chen Y, Chen J, Wang H, Shi J, Wu K, Liu S, et al. HCV-induced miR-21 contributes to evasion of host immune system by targeting MyD88 and IRAK1. *PLoS Pathog* (2013) 9(4):e1003248. doi:10.1371/journal.ppat.1003248
43. Heikenwalder M, Polymenidou M, Junt T, Sigurdson C, Wagner H, Akira S, et al. Lymphoid follicle destruction and immunosuppression after repeated CpG oligodeoxynucleotide administration. *Nat Med* (2004) 10(2):187–92. doi:10.1038/nm987
44. Tomasello E, Pollet E, Vu Manh TP, Uze G, Dalod M. Harnessing mechanistic knowledge on beneficial versus deleterious IFN-I effects to design innovative immunotherapies targeting cytokine activity to specific cell types. *Front Immunol* (2014) 5:526. doi:10.3389/fimmu.2014.00526
45. Centlivre M, Legrand N, Steingrover R, van der Sluis R, Grijsen ML, Bakker M, et al. Altered dynamics and differential infection profiles of lymphoid and myeloid cell subsets during acute and chronic HIV-1 infection. *J Leukoc Biol* (2011) 89(5):785–95. doi:10.1189/jlb.0410231
46. McMichael AJ, Borrow P, Tomaras GD, Goonetilleke N, Haynes BF. The immune response during acute HIV-1 infection: clues for vaccine development. *Nat Rev Immunol* (2010) 10(1):11–23. doi:10.1038/nri2674
47. Wursthorn K, Lutgehetmann M, Dandri M, Volz T, Buggisch P, Zollner B, et al. Peginterferon alpha-2b plus adefovir induce strong cccDNA decline

and HBsAg reduction in patients with chronic hepatitis B. *Hepatology* (2006) 44(3):675–84. doi:10.1002/hep.21282
48. Lucifora J, Xia Y, Reisinger F, Zhang K, Stadler D, Cheng X, et al. Specific and nonhepatotoxic degradation of nuclear hepatitis B virus cccDNA. *Science* (2014) 343(6176):1221–8. doi:10.1126/science.1243462
49. Jaeckel E, Cornberg M, Wedemeyer H, Santantonio T, Mayer J, Zankel M, et al. Treatment of acute hepatitis C with interferon alfa-2b. *N Engl J Med* (2001) 345(20):1452–7. doi:10.1056/NEJMoa011232
50. Fuertes MB, Kacha AK, Kline J, Woo SR, Kranz DM, Murphy KM, et al. Host type I IFN signals are required for antitumor CD8+ T cell responses through CD8{alpha}+ dendritic cells. *J Exp Med* (2011) 208(10):2005–16. doi:10.1084/jem.20101159
51. Labidi-Galy SI, Sisirak V, Meeus P, Gobert M, Treilleux I, Bajard A, et al. Quantitative and functional alterations of plasmacytoid dendritic cells contribute to immune tolerance in ovarian cancer. *Cancer Res* (2011) 71(16):5423–34. doi:10.1158/0008-5472.CAN-11-0367
52. Decalf J, Fernandes S, Longman R, Ahloulay M, Audat F, Lefrerre F, et al. Plasmacytoid dendritic cells initiate a complex chemokine and cytokine network and are a viable drug target in chronic HCV patients. *J Exp Med* (2007) 204(10):2423–37. doi:10.1084/jem.20070814
53. Dental C, Florentin J, Aouar B, Gondois-Rey F, Durantel D, Baumert TF, et al. Hepatitis C virus fails to activate NF-kappaB signaling in plasmacytoid dendritic cells. *J Virol* (2011) 86(2):1090–6. doi:10.1128/JVI.05444-11
54. Bain J, Plater L, Elliott M, Shpiro N, Hastie CJ, McLauchlan H, et al. The selectivity of protein kinase inhibitors: a further update. *Biochem J* (2007) 408(3):297–315. doi:10.1042/BJ20070797
55. Blight KJ, McKeating JA, Marcotrigiano J, Rice CM. Efficient replication of hepatitis C virus genotype 1a RNAs in cell culture. *J Virol* (2003) 77(5):3181–90. doi:10.1128/JVI.77.5.3181-3190.2003
56. Delgrange D, Pillez A, Castelain S, Cocquerel L, Rouille Y, Dubuisson J, et al. Robust production of infectious viral particles in Huh-7 cells by introducing mutations in hepatitis C virus structural proteins. *J Gen Virol* (2007) 88(Pt 9):2495–503. doi:10.1099/vir.0.82872-0
57. Suchankova A, Hirsch I, Kremar M, Vonka V. Determination of herpes simplex virus type-specific antibodies by solid-phase RIA on helix pomatia lectin-purified antigens. *J Infect Dis* (1984) 149(6):964–72. doi:10.1093/infdis/149.6.964
58. Boguszakova L, Hirsch I, Brichacek B, Faltyn J, Fric P, Dvorakova H, et al. Absence of cytomegalovirus, Epstein-Barr virus, and papillomavirus DNA from adenoma and adenocarcinoma of the colon. *Acta Virol* (1988) 32(4):303–8.

Conflict of Interest Statement: The authors declare that this research was conducted in the absence of any commercial or financial relationships that could be construed as a potential conflict of interest.

frontiers in Immunology

ORIGINAL RESEARCH
published: 12 March 2018
doi: 10.3389/fimmu.2018.00489

Computational Insight Into the Structural Organization of Full-Length Toll-Like Receptor 4 Dimer in a Model Phospholipid Bilayer

*Mahesh Chandra Patra[1], Hyuk-Kwon Kwon[2], Maria Batool[1] and Sangdun Choi[1]**

[1] Department of Molecular Science and Technology, Ajou University, Suwon, South Korea, [2] Department of Orthopaedics and Rehabilitation, Yale School of Medicine, New Haven, CT, United States

Toll-like receptors (TLRs) are a unique category of pattern recognition receptors that recognize distinct pathogenic components, often utilizing the same set of downstream adaptors. Specific molecular features of extracellular, transmembrane (TM), and cytoplasmic domains of TLRs are crucial for coordinating the complex, innate immune signaling pathway. Here, we constructed a full-length structural model of TLR4—a widely studied member of the interleukin-1 receptor/TLR superfamily—using homology modeling, protein–protein docking, and molecular dynamics simulations to understand the differential domain organization of TLR4 in a membrane-aqueous environment. Results showed that each functional domain of the membrane-bound TLR4 displayed several structural transitions that are biophysically essential for plasma membrane integration. Specifically, the extracellular and cytoplasmic domains were partially immersed in the upper and lower leaflets of the membrane bilayer. Meanwhile, TM domains tilted considerably to overcome the hydrophobic mismatch with the bilayer core. Our analysis indicates an alternate dimerization or a potential oligomerization interface of TLR4-TM. Moreover, the helical properties of an isolated TM dimer partly agree with that of the full-length receptor. Furthermore, membrane-absorbed or solvent-exposed surfaces of the toll/interleukin-1 receptor domain are consistent with previous X-ray crystallography and biochemical studies. Collectively, we provided a complete structural model of membrane-bound TLR4 that strengthens our current understanding of the complex mechanism of receptor activation and adaptor recruitment in the innate immune signaling pathway.

Keywords: full-length TLR, TLR4, plasma membrane, molecular dynamics simulation, signal transduction, adaptor recruitment

OPEN ACCESS

Edited by:
Moncef Zouali, INSERM U1132, Paris Diderot University, France

Reviewed by:
Lubka T. Roumenina, INSERM UMRS1138 Centre de Recherche des Cordeliers, France
James Noble Arnold, King's College London, United Kingdom

****Correspondence:***
Sangdun Choi
sangdunchoi@ajou.ac.kr

Specialty section:
This article was submitted to Molecular Innate Immunity, a section of the journal Frontiers in Immunology

Received: *12 January 2018*
Accepted: *26 February 2018*
Published: *12 March 2018*

Citation:
Patra MC, Kwon HK, Batool M and Choi S (2018) Computational Insight Into the Structural Organization of Full-Length Toll-Like Receptor 4 Dimer in a Model Phospholipid Bilayer. Front. Immunol. 9:489. doi: 10.3389/fimmu.2018.00489

INTRODUCTION

Toll-like receptors (TLRs) are key components of the vertebrate innate immune system and play a dominant role in the activation of the adaptive immune system (1–3). They are pattern recognition receptors that recognize exogenous pathogen-associated molecular patterns or endogenous damage-associated molecular patterns to initiate a complex cascade of signal transduction to produce pro-inflammatory cytokines and interferons (IFNs) (4). TLRs are found in the plasma membrane (TLR1, 2, 4, 5, 6, and 10) as well as in the endosomal membrane (TLR3, 7, 8, and 9), recognizing distinct categories of ligands (5). Specifically, triacyl lipopeptides (Pam_3CSK_4) are recognized by TLR1/2

(6), diacyl lipopeptides (Pam_2CSK_4) by TLR2/6 (7), viral double-stranded RNA by TLR3 (8, 9), lipopolysaccharides (LPS) by TLR4 (10–12), bacterial flagellin by TLR5 (13), viral single-stranded RNA by TLR7 and TLR8 (14, 15), and bacterial CpG-containing DNA by TLR9 (16). Ligands recognized by TLR10 are unknown; however, evidence indicates that TLR10 can recognize viral or bacterial components (17, 18).

Ligand-induced TLR dimerization results in the recruitment of the downstream adaptor, myeloid differentiation primary response gene 88 (MyD88), or in the case of TLR3, toll/interleukin-1 receptor (TIR) domain-containing adapter-inducing interferon β (TRIF). TLR4 also initiates TRIF-dependent immune signaling from the endosomal membrane. Therefore, TLR4 is most unique one among TLRs, as it can trigger LPS-induced MyD88- and TRIF-dependent signal transduction from both the plasma membrane and endosomal membrane, respectively. In the MyD88 pathway, activated TLRs recruit MyD88 through TIR domain interactions. MyD88, in turn, recruits the interleukin-1 receptor-associated kinase 4 (IRAK4) through death domain interactions. IRAK4 phosphorylates IRAK1, which brings tumor necrosis factor receptor-associated factor 6 to the receptor complex (19). The TLR-MyD88-IRAK4-IRAK1/2 supercomplex is termed myddosome, whose actual stoichiometry is still under debate (20, 21). Subsequently, a number of phosphorylation and ubiquitination events occur that eventually activate nuclear factor kappa-light-chain-enhancer of activated B cells (NF-κB). Similarly, the TRIF-dependent pathway employs a different set of adaptors and kinases to activate IFN regulatory factor 3 (IRF3)—a transcription factor. Activated NF-κB and IRF3 translocate to the nucleus and assist in the transcription of pro-inflammatory cytokines: interleukin-1 (IL-1), IL-6, IL-10, IFN1β, and IFNγ (22).

Structurally, TLRs show a tripartite domain architecture with an extracellular ligand binding domain (ECD) containing leucine-rich repeats (LRR), a single transmembrane (TM) domain, and an intracellular TIR domain (ICD). Agonist binding induces homo- or heterodimerization of TLRs that laterally translocate in the membrane until the recruitment of downstream adaptors. TLR4-ECD is tightly associated with a co-receptor, myeloid differentiation protein 2 (MD2), which traps agonists (such as LPS) in its large hydrophobic cavity and plays a significant role in the activation of the receptor. Conformational changes in TIR domains provide a platform for adaptors that then propagate signal transduction. Several studies have been conducted to uncover the three-dimensional structures of proteins involved in this complex pathway. TLR structural biology has been reviewed in detail elsewhere (23). The extracellular domains of all TLRs (6, 7, 9, 13, 16, 24–26), except TLR10, and the TIR domains of some TLRs (27–29) have been solved through X-ray crystallography. The TM domains of TLR3 (30) and TLR4 (31) have been recently solved through NMR spectroscopy, suggesting a hypothetical model for full-length TLR4. However, experimental or computational studies elucidating the full-length structure of TLRs with an intact ECD-TM-ICD organization have not been reported so far. A complete understanding of full-length TLRs would aid identification of receptor micro-domains that participate in membrane association and orientation of individual domains in physiological environments. Such regions could be targeted using novel activators or inhibitors for modulating different functional properties of TLRs to obtain the desired therapeutic outcomes (32–38).

In this study, we predicted the putative structural organization of full-length TLR4 in a membrane-mimetic environment. The prediction provided several key insights into the orientation and interaction of ECD, TM, and TIR domains with respect to the membrane bilayer. Since these domains are independent and well-validated drug-targets, detailed understanding of their interactions with the plasma membrane and dimeric counterparts is a prerequisite for the development of peptide- or small-molecule-based therapeutics.

MATERIALS AND METHODS

Construction of a Full-Length TLR4-MD2-LPS Homo-Heterodimer and Individual TIR and TM Homodimers

The construction of a full-length TLR4 dimer was completed in five successive stages. First, the dimeric LPS-bound ECD structure was obtained from the protein data bank (PDB ID: 3FXI). Missing residues were modeled *via* homology modeling using the SWISS-MODEL server (39), followed by energy minimization using GROMACS software version 5.1.4 (40). Second, the TM domain (residues 630–660) was modeled as a single α-helix, followed by protein–protein docking using the ZDOCK server (41) to obtain a dimeric structure. Energy minimization was performed to optimize interatomic distances and angles. Third, the TIR domain was modeled by homology modeling using the crystal structure of TLR10 (PDB ID: 2J67) that was solved in physiological dimeric conditions (28). Consecutive superimposition of monomeric TLR4-TIR over the two subunits of dimeric TLR10-TIR resulted in a dimeric TLR4-TIR domain. Energy minimization was performed to remove steric conflicts between atoms. Fourth, all three individual domains were aligned on a straight axis and peptide bonds were patched between the extreme C- and N-terminal residues of adjacent domains using Discovery Studio Visualizer 4.0 (DSV 4.0) program (Dassault Systèmes, San Diego, CA, USA). Another round of energy minimization was performed to correct interatomic conflicts within the full-length TLR4 dimer. Finally, the residues around the constructed peptide bonds were optimized using the ModLoop webserver (42).

In addition, individual TIR and TM dimers were constructed using the protein–protein docking approach. For TLR4-TIR, two different models were created based on the dimer packing information available in the literature (28, 37, 43, 44). The first TIR dimer was created by successive superimposition of TLR4-TIR monomers over those of the dimeric TLR10-TIR. The second TIR dimer was obtained by performing protein–protein docking using the BB loop of one subunit and the helix αE of the other as binding regions. The TM domain dimer was constructed using an automated protein–protein docking approach with the ZDOCK program. The best scoring predictions were selected for further study.

Construction of Lipid Bilayers and Insertion of TLR4 Into the Bilayer

TLR4 was simulated in two separate dipalmitoylphosphatidylcholine (DPPC) bilayers with 574 lipids to observe if dynamic properties of both TLR4 and the membrane are replicated. Initially, a pre-equilibrated lipid bilayer of 128 DPPC molecules was obtained from the Peter Tieleman website.[1] The bilayer was replicated in *X* and *Y* directions using the GROMACS *gmx conf* tool to accommodate TLR4-ECD in lateral directions. The resultant bilayer was energy minimized and simulated for 100 ns. TLR4 was inserted inside the DPPC bilayer by aligning the hydrophobic segments of TLR4-TM with that of the membrane. InflateGRO methodology was used for the packing of lipids around TLR4 (45).

Molecular Dynamics (MD) Simulation Parameters for Modeled TLR4 Dimers in Phospholipid Bilayers

A hybrid force field was created by combining Gromos96-54a7 and Berger-lipid parameters for simulating the TLR4-MD2-LPS system. An appropriate amount of simple point charge (SPC) water molecules and counterions (Na^+/Cl^-) were added to the simulation system. Energy minimization was carried out using the steepest descent algorithm in GROMACS. Temperature and pressure couplings were performed for 100 ps each using Nose–Hoover and Parrinello–Rahman methods, respectively, with positional restraints on the backbone heavy atoms. The production run was carried out for 100 ns using the NPT ensemble (constant pressure, constant temperature) without backbone restraints. Short-range van der Waals and electrostatic interactions were calculated using a 12 Å distance cutoff. Long-range electrostatic interactions were handled using the particle mesh Ewald method. Periodic boundary condition was applied to the simulation system and all bonds were constrained using the linear constraint solver algorithm. Structural snapshots were saved at 2 ps time intervals. Trajectory data analysis was performed using visual molecular dynamics (VMD) (46), PyMOL (Schrödinger, LLC, New York, NY, USA), DSV 4.0, XMgrace,[2] and built-in GROMACS tools. LPS topology was computed using the automated topology builder server (47) which uses a hybrid quantum mechanics/molecular mechanics method for assigning partial charges to atoms. The volume of the MD2 hydrophobic cavity was computed using *trj_cavity_v2.0* program (48).

MD Simulation of Isolated TLR4-TIR Dimers

Two separate MD simulations were performed for the isolated TLR4-TIR dimers in two different dimeric orientations, as reported in the literature (37, 43, 44, 49). The models were solvated with SPC water molecules inside separate cubic boxes. Counterions (Na^+/Cl^-) were added and energy minimization was performed using Gromos96-54a7 force field and steepest descent algorithm. Temperature and pressure equilibrations were carried out using V-rescale and Parrinello-Rahman coupling schemes, respectively. Remainder of the parameters were the same as described for TLR4-membrane simulations.

MD Simulation of an Isolated TLR4-TM Dimer

A separate MD simulation was carried out for the isolated TM segment of TLR4 (residues 630–660) in a pre-equilibrated DPPC bilayer. The dimeric TM domain was placed inside the hydrophobic core of a DPPC membrane. The simulation was performed for 100 ns using the same set of parameters described for TLR4 in the previous section.

Electrostatic Potential Calculation

The molecular electrostatic potential surfaces were calculated using the adaptive Poisson–Boltzmann solver and PyMOL *apbsplugin* tool.[3] The solvent accessible surface area was computed using a linearized Poisson–Boltzmann equation with a bulk solvent radius of 1.4 Å. The isosurfaces (positive and negative spheres) were viewed using a contour (kT/e) value of 1.

Free Energy Landscape (FEL)

The FEL was calculated to obtain lowest energy conformations of the modeled TLR4, which were then evaluated for stereochemical accuracy using ProSA-Web (50) and the Rampage servers (51). The FEL was calculated using the GROMACS *gmx sham* tool and the landscape was plotted using the demo version of Mathematica software (version 11.2; Wolfram Research, Inc., Champaign, IL, USA).

Molecular Docking of the TAK-242 Ligand With TLR4-TIR Dimers

The chemical structure of TAK-242 was obtained from the PubChem database (CID: 11703255). Then, the structure was protonated and energy minimized using the molecular operating environment program (52). The binding site was defined around the C747 residue and docking was performed using the London-DG scoring function and MMFF94x force field optimization. A total of 30 different docked conformations were generated and the best pose was selected based on the binding affinity (*S*) score.

Binding Free Energy Calculation of TIR Dimer and TIR-TAK-242 Complexes

The molecular mechanics/Poisson–Boltzmann surface area (MM/PBSA) method (53) was employed to calculate the binding free energies between different components. The method is summarized by Eq. 1,

$$\Delta G_{\text{bind}} = \left\langle \Delta G_{\text{complex}} \right\rangle - \left\langle \Delta G_{\text{protein}} \right\rangle - \left\langle \Delta G_{\text{ligand}} \right\rangle \quad (1)$$

where G_{bind} denotes the binding free energy and G_{complex}, G_{protein}, and G_{ligand} represent the free energy of individual states. The free energy of each state is calculated by Eq. 2,

$$G = G_{\text{bond}} + G_{\text{ele}} + G_{\text{vdW}} + G_{\text{pol}} + G_{\text{npol}} - \text{TS} \quad (2)$$

[1] http://www.ucalgary.ca/tieleman/.

[2] http://plasma-gate.weizmann.ac.il/Grace/.

[3] https://pymolwiki.org/index.php/Apbsplugin.

where G_{bond} (bonded, angle, and dihedral), G_{ele}, and G_{vdW} are bonded, electrostatic, and van der Waals interaction energies derived from molecular mechanics energy calculations, respectively. G_{pol} and G_{npol} represent the polar and nonpolar solvation energies obtained by solving the Poisson–Boltzmann equation and solvent accessible surface area methods. The entropic contribution, TS (absolute temperature T multiplied by entropy S), is generally estimated by normal mode analysis. However, the *g_mmpbsa* program (54, 55), which we used for binding free energy calculation, ignores entropic contribution to improve computational efficiency. In computational binding free energy calculations, the computation of the entropic term often overestimates obtained binding free energy, resulting in misleading outcomes (56).

RESULTS

The Full-Length TLR4-MD2 Complex Tilts and Wraps Over the Membrane Surface

To understand the structural organization of an intact TLR4, we performed two separate MD simulations of a full-length TLR4-MD2-LPS homo-heterodimer (residues 24–839) solvated inside a phospholipid bilayer for 100 ns durations (**Figure 1**). We observed that TLR4 experienced a significant rotation and structural transition in the membrane bilayer (simulation 1). The ECD progressively became inclined over the membrane to the left of the bilayer normal (*Z*-axis) and ultimately placed its N-terminal subdomain (LRR-NT) and LRR1-3 into the polar headgroups of the bilayer surface (**Figures 1A,B**). Meanwhile, the TM helices exhibited a substantial orientation that tilted with respect to the average helical axes due to hydrophobic mismatch with the bilayer core. Likewise, the TIR domains gradually moved upward and were partially immersed in the lower leaflet of the bilayer. In the final MD simulation snapshot, TLR4 was found completely wrapped around both upper and lower surfaces of the membrane in a slanted manner (**Figure 1B**). To confirm the dynamic behavior of TLR4 within the membrane bilayer, we repeated the MD simulation with a marginally upward (~2 Å) placement of the TM helices in the bilayer (simulation 2). TLR4-ECD of simulation 2 showed a similar behavior to simulation 1 by inclining over the membrane, where the LRR-NT was completely buried inside the phospholipid headgroups (**Figures 1C,D**). The TM helices were comparatively linear with respect to the bilayer normal; however, the first 10 residues of subunit A lost helicity. The helical tilt angle was visibly smaller than that of TLR4 in simulation 1, indicating that the placement of TM helices in simulation 1 was more precise. Finally, the TIR domain was partially absorbed into the bilayer lower leaflet, but slightly to the right of the *Z*-axis.

The TLR4-MD2 Homo-Heterodimer Is Stable in the Phospholipid Bilayer During MD Simulation

Before studying the detailed structural properties of membrane-bound TLR4-MD2-LPS homo-heterodimers, we checked the stability of both protein subunits and phospholipids as a function of simulation time. The root mean square deviation (RMSD) of the backbone (N-Cα-C) atoms indicated that both TLR4 chains reached an equilibrium plateau shortly after ~40 ns of MD simulation (**Figure 2A**). The backbone RMSD of MD2 showed an exceptional stability oscillating around ~2 Å throughout the simulation. The root mean square fluctuation (RMSF) of Cα atoms showed that the TIR domain residues were highly flexible throughout the simulation, in that the C-terminal residues of TLR4* (chain B) reached an RMSF higher than 20 Å (**Figure 2C**). On the other hand, local fluctuation of MD2 residues was largely restricted, indicating a stable molecular structure. Similarly, the radius of gyration (Rg) values indicated that MD2 maintained a compact architecture throughout the simulation. However, TLR4 showed an elevated Rg value of 50 Å toward the end of MD simulation, probably due to its extended molecular geometry spanning through the membrane (**Figure 2E**). The secondary structures of individual subunits of the TLR4-MD2 dimeric complex were largely conserved during MD simulation.

The quality of our TLR4 model was validated by calculating the Φ and Ψ dihedral angles using the Rampage server. For this task, a representative low energy structure was extracted from the Gibbs FEL (Figure S1A in Supplementary Material) using the *get_timestamp.py* script.[4] The Ramachandran plot showed that >90% of both TLR4 and TLR4* residues fell under the most favorable and allowed regions of the plot (Figures S1C,D in Supplementary Material; **Table 1**). A few residues located in the flexible loops were found to have outlier dihedrals. The *Z*-score obtained from the ProSA-web server indicated that both subunits of TLR4 occupy a region defined for X-ray crystallographic structures (Figures S1E,F in Supplementary Material).

Next, we analyzed key biophysical properties of the membrane bilayer to confirm its consistency throughout MD simulations. Density profiles of various membrane components revealed low and high densities at the hydrophobic and hydrophilic regions, respectively (**Figure 2D**). Water density at the hydrophobic core ($Z = 0$) of the bilayer was 0. The distance between headgroup densities was 37–38 Å, which is the approximate thickness of the bilayer (57). The density of tailgroups was higher than that of headgroups. Phosphorous atom (P8) density showed a good correlation with that of the headgroups. Altogether, the symmetric density of the lipids indicated a well-organized bilayer holding the dimeric TLR4. The area per lipid (A/L) of both top and bottom leaflets of the bilayer were calculated to be 58.2 ± 1, consistent with previous simulations of DPPC membranes and experimental A/L values for DPPC bilayers (58–60). Order parameters ($-S_{CD}$) of the *sn1* and *sn2* chains of DPPC lipids showed a plateau at ~0.2 for carbon atoms 34–39 and 17–22, respectively (**Figure 2B**), consistent with experimental measurements (58, 61). The mean square displacement plot of lipids (lateral diffusion) exhibited a linear curve, indicating that phospholipid movements within the bilayer were natural (**Figure 2F**). The stability and stereochemical parameters of TLR4-DPPC system of simulation 2 are shown in **Table 1**, Figures S1 and S2 in Supplementary Material. Altogether,

[4]http://nmr.chem.uu.nl/~adrien/course/molmod/get_timestamp.py.

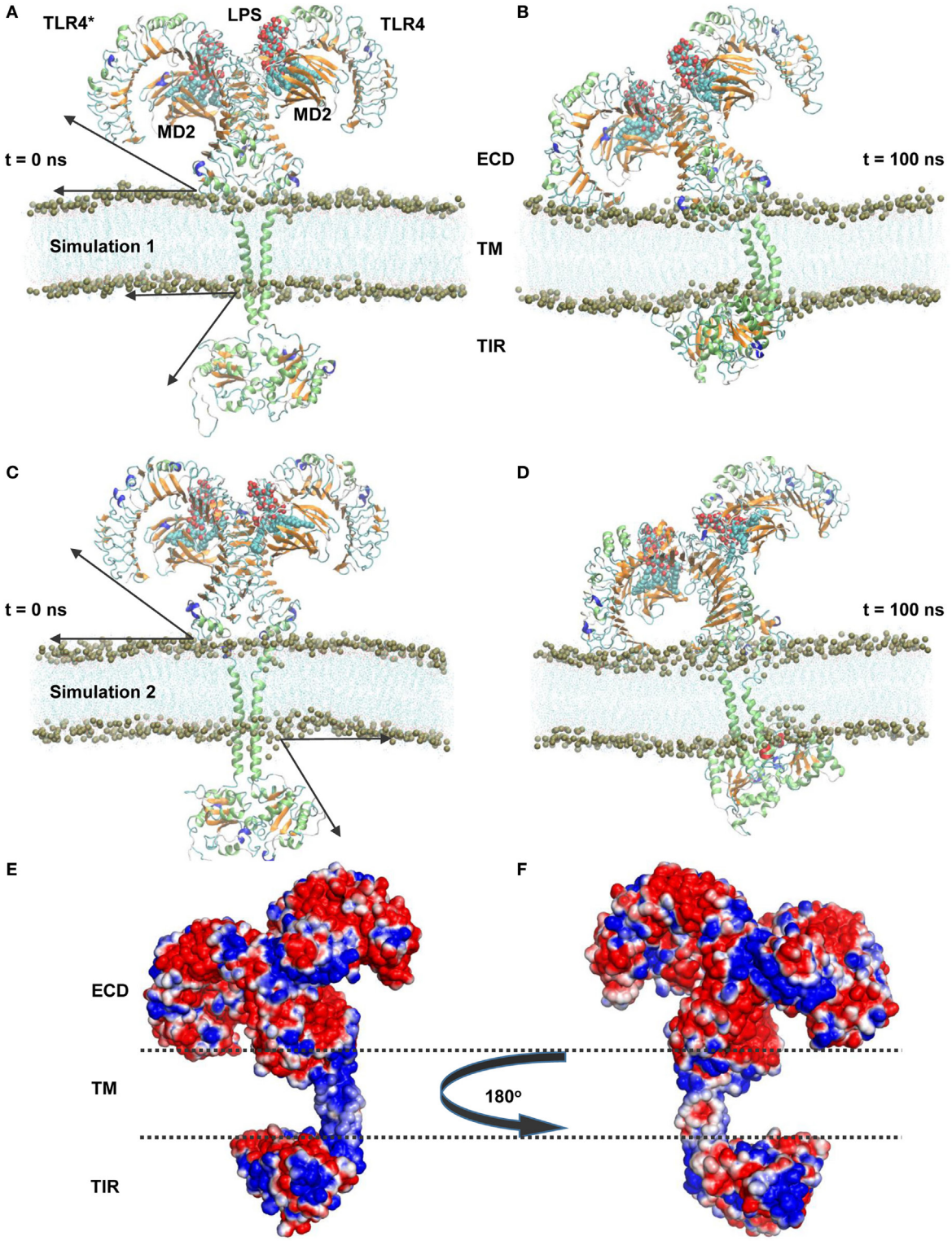

FIGURE 1 | Overall structural organization of full-length TLR4-myeloid differentiation protein 2 (MD2)-lipopolysaccharides (LPS) homo-heterodimers in a membrane-embedded condition. **(A,C)** Initial models of the TLR4-MD2-LPS complex in a dipalmitoylphosphatidylcholine membrane. **(B,D)** Final snapshots of the TLR4-MD2-LPS complex after 100 ns of molecular dynamics simulation. **(A,B)** represent simulation 1, while **(C,D)** represent simulation 2. For TLR4 and MD2, the lime color represents the α-helix, orange color represents the β sheets, and LPS is illustrated as a calotte model. Arrows indicate the approximate distance traveled by extracellular and intracellular domains above and below the membrane from their starting positions. Phospholipids are indicated by lines, while phosphorous (P8) atoms are represented by mauve beads. **(E,F)** Electrostatic potential surface around the TLR4-MD2-LPS complex. The transmembrane region is marked by dashed lines.

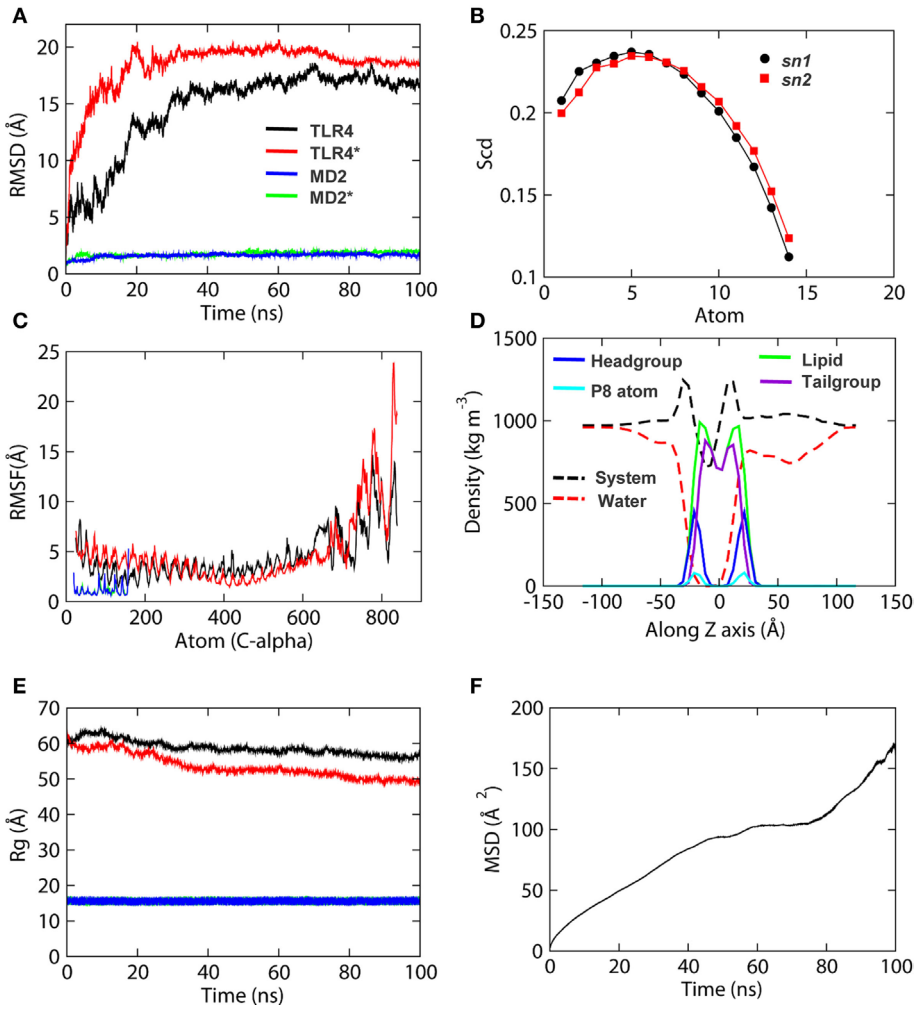

FIGURE 2 | Stability parameters of the TLR4-myeloid differentiation protein 2 (MD2) complex and dipalmitoylphosphatidylcholine (DPPC) membrane of simulation 1 as a function of time. **(A)** Root mean square deviation. **(B)** Order parameters for lipid acyl chains. **(C)** Root mean square fluctuation. **(D)** Density profiles of various components of the membrane. **(E)** Radius of gyration. **(F)** Lateral diffusion of lipid head groups, also known as mean square displacement (MSD) of lipids. MSD values are based on diffusion of DPPC headgroup P8 atoms. "*" indicates chain B of TLR4 and MD2.

TABLE 1 | Model validation scores of representative TLR4 models from two separate molecular dynamics simulations.

Subunit	Ramachandran plot[a]			ProSA-web *Z*-score
	Favored region	Allowed region	Outliers region	
Simulation 1				
TLR4	726 (89.2%)	64 (7.9%)	24 (2.9%)	−7.25
TLR4*	730 (89.7%)	62 (7.2%)	22 (2.7%)	−7.99
Simulation 2				
TLR4	719 (88.3%)	76 (9.3%)	19 (2.3%)	−7.01
TLR4*	720 (88.5%)	80 (9.8%)	14 (1.7%)	−7.07

[a]*Distribution of non-glycine and non-proline amino acids in the Ramachandran plot.*
**Indicates subunit B of TLR4.*
% represents total number of non-glycine and non-proline residues in the protein.

we concluded that the modeled, full-length TLR4 can be considered for further in-depth structural analysis.

The ECD Conserves Key Molecular Features While Inclining Over the Membrane

During MD simulation, the horseshoe-like architecture of TLR4-ECD was intact in the membrane-aqueous environment with a leftward tilt due to electrostatic attraction between LRR-NT and DPPC headgroups (**Figure 3A**). Analysis of amino acid composition of the membrane-absorbed portion of ECD revealed the LRR-NT and LRR1-3 contain several polar and aromatic-polar residues (**Figure 3C**) that provide charge complementarity for association with the zwitterionic DPPC membrane surface. The

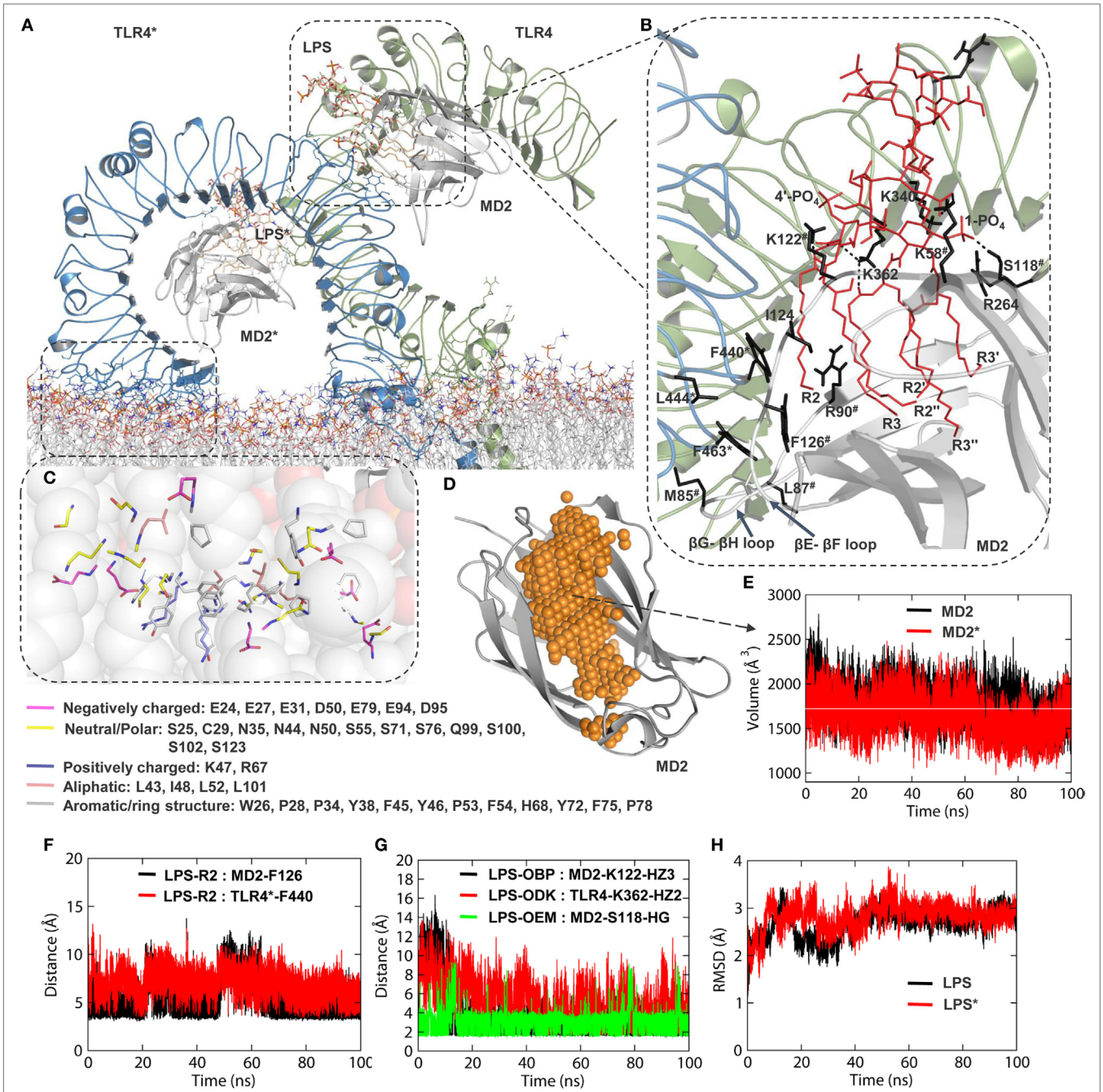

FIGURE 3 | Structural properties of TLR4-extracellular ligand binding domain (ECD) and myeloid differentiation protein 2 (MD2) during molecular dynamics simulation. **(A)** Inclination of ECD over the membrane surface, as seen in the representative low energy model obtained at 94.702 ns. **(B)** Interaction of lipopolysaccharides (LPS) with the hydrophobic pocket of MD2. "*" on TLR4 residues indicates chain B and "#" represents MD2 residues. **(C)** Interaction of N-terminal region of the leucine-rich repeat domain [leucine rich repeats (LRR)-NT; residues 24–51] and LRR1-3 with phospholipid headgroups. **(D)** An illustration of the hydrophobic cavity of MD2. **(E)** Volume of the MD2 hydrophobic cavity as a function of time. The horizontal white line indicates the average value. **(F)** Distance of the R2 chain terminal $-CH_3$ group from the F126 of MD2 and F440 of TLR4. **(G)** Distance of LPS interacting atoms from K122 (MD2), K362 (TLR4), and S118 (MD2). **(H)** Root mean square deviation of LPS in both subunits of MD2 as a function of time. "*" indicates LPS in chain B of MD2.

electrostatic potential surface around TLR4 also showed that the membrane-absorbed portions of ECD comprised a zwitterionic patch as found on the DPPC surface (**Figures 1E,F**), supporting the charge-dependent tilting action of ECD on the bilayer.

Comparisons with the X-ray crystallographic structure (PDB ID: 3FXI) revealed that the dimerization interface between TLR4 and MD2 was completely conserved; this interface involved LRR15-17 of the C-terminal subdomain, as well as A and B

patches provided by the N- and C-terminal regions of TLR4-ECD, respectively (12). TLR4 formed direct interactions with LPS and F126 (βG-βH strands) and the L87 loops (βE-βF strands) of MD2 (**Figure 3B**). The interaction of LPS within the β-cup-fold structure of MD2 is in agreement with the X-ray crystal structure. Specifically, all five acyl chains (R3, R2″, R2′, R3″, and R3′) of LPS are buried deep inside the MD2 pocket, while the R2 chain is partially exposed to the hydrophobic interface formed by F440, F463, and L444 of TLR4* and V82, M85, L87, I124, and F126 of MD2. The distances between the R2 chain terminal $–CH_3$ group and the benzyl rings of F440 (TLR4*) and F126 (MD2) were consistent throughout the simulation (**Figure 3F**). The two phosphate groups of lipid A were anchored to a positively charged cluster of lysine and arginine from both TLR4 and MD2, providing dimerization support; specifically, K112 of MD2 and K362 of TLR4 were involved in a consistent hydrogen bond (H-bond) interaction with the phosphate oxygen atoms of lipid A throughout the MD simulation (**Figure 3G**). The phosphate oxygen of 1-PO_4 forms a strong H-bond with the –OH group of S118 (**Figure 3G**). Overall, we observed that the effect of LPS binding and charge on the membrane led to localized changes in TLR4-ECD that allowed it to bend over the membrane surface at an approximate 45° angle.

Next, we monitored the volume of the MD2 large hydrophobic cavity to validate if membrane-bound TLR4-ECD possesses a physiologically relevant LPS-MD2 conformation. The LPS binding cavity of MD2 is highly flexible and can expand or shrink depending on the presence, absence, or size of the ligand. The LPS-bound MD2 cavity was reported to have a volume of ~1,710 $Å^3$ (62). Our calculation revealed that the average volume of MD2 was approximately 1,700 $Å^3$ value throughout the simulation (**Figures 3D,E**). This observation was supported by a stable RMSD of LPS as a function of simulation time (**Figure 3H**). Thus, MD2 maintains a steady interaction with LPS inside an intact cavity during the dynamic condition, where ECD tilts and adjusts itself on the membrane surface. Overall, we found the modeled TLR4 structure was reasonably accurate in mimicking the physiologically active state.

TM Helices Tilt and Bend to Overcome Hydrophobic Mismatches

We analyzed and compared the helical properties of TM bundles in two separate MD simulations. The TM domain in simulation 1 showed an axis-length of ~20 Å and a tilt angle of ~15° with respect to the average helical axis. In contrast, the TM domain in simulation 2 tilted between 8 and 10° with an axis-length of ~40 Å (**Figures 4A,D**). The shorter helical axis of the TM bundle in simulation 1 indicates a greater curvature than the TM bundle in simulation 2. The tilt angles of individual TM helices suggest that chain A largely contributes to the orientation of the whole TM domain (**Figures 4B,C**). During these tilting and bending processes, individual TM helices maintained a per-residue twist angle close to 100° (**Figures 4E,F**), a value usually obtained for ideal α-helices.

The dimer interface of TLR4-TM was studied in two different TLR4 models obtained from separate MD simulations. In model 1, the dimer interface can be divided into two regions, interface I with mostly aliphatic residues, namely I633, V636, V641, V644, and A648, and interface II containing both aliphatic and aromatic residues, namely V649, Y652, F656, and L660 (**Figure 4G**). Aromatic stacking was observed between Y652 and F656 of both monomers. S640 of interface I forms electrostatic interactions with backbone amide atoms of the other monomer residues. We found that residues V636, L639, V643, and V647—previously reported to form the dimer interface (31)—are exposed to the hydrophobic core of the bilayer (**Figure 4H**). This suggests the existence of an alternate dimer interface or a possible oligomerization interface of TLR4-TM, as reported for TLR3-TM (30). In model 2, we found some additional residues, namely I634, S637, and S645 of interface I and M659 of interface II, were involved in dimer formation (**Figure 4I**). However, the distance between the axis centers of the two helices in model 2 (~6.5 Å) was found to be larger than that of model 1 (~5 Å) (Figure S3A in Supplementary Material). This indicates that the tilt and curvature observed in model 1 indeed provides a stronger dimer packing between TM helices. Furthermore, we carried out a separate MD simulation of the isolated TM dimer (residues 630–660) by solvating it inside a DPPC membrane. Our analysis revealed that helical properties of the isolated TM dimer partly correlate with that of the full-length TLR4; specifically, the helical bundle tilts up to an angle of >40° with an axis-length of ~15 Å, much shorter than that of the full-length TLR4 (Figures S3D,F in Supplementary Material). While the twist angles remained close to 100° (Figure S3E in Supplementary Material), chain A contributed the most to the overall tilting behavior of the whole dimer (Figure S3C in Supplementary Material). However, distances between axis centers were found to be >10 Å (Figure S3B in Supplementary Material), indicating that isolated TMs tend to form a loose dimer in the membrane-bound condition.

TIR Domains Are Partially Immersed Into the Lower Surface of the Membrane

During MD simulations, we observed that the TIR domains were partially absorbed into the lower leaflet of the bilayer, owing to electrostatic attraction by the polar headgroups supplemented by bending or tilting actions of both ECD and TM domains. The helix αA and AB loop of one subunit and the helix αB, CD loop, and C-terminal tail of the other subunit-mediated interactions with membrane phospholipids, while the BB loop was situated underneath the membrane (**Figure 5A**). The BB loop is considered the site of TIR dimerization and adaptor attachment (38), thus solvent exposure of this segment throughout MD simulation validates its functional significance. The DD loop, helix αE, and CD loops of TLR4-TIR were also situated adjacent to the membrane, but most residues from these segments remained directed toward the solvent. The C-terminal tail of one subunit is situated at the opposite end of the membrane closely spaced to helix αE. TIR domain residues that make direct contacts with phospholipids are shown in **Table 2**. The dimer interface mediated by the BB loop and helix αC of both monomers was found to be intact. Overall, the TIR dimer rotated up to 90° and moved upward before being absorbed into the membrane during MD simulation. All subdomains that contacted phospholipids in simulation 1 showed a similar behavior in simulation 2

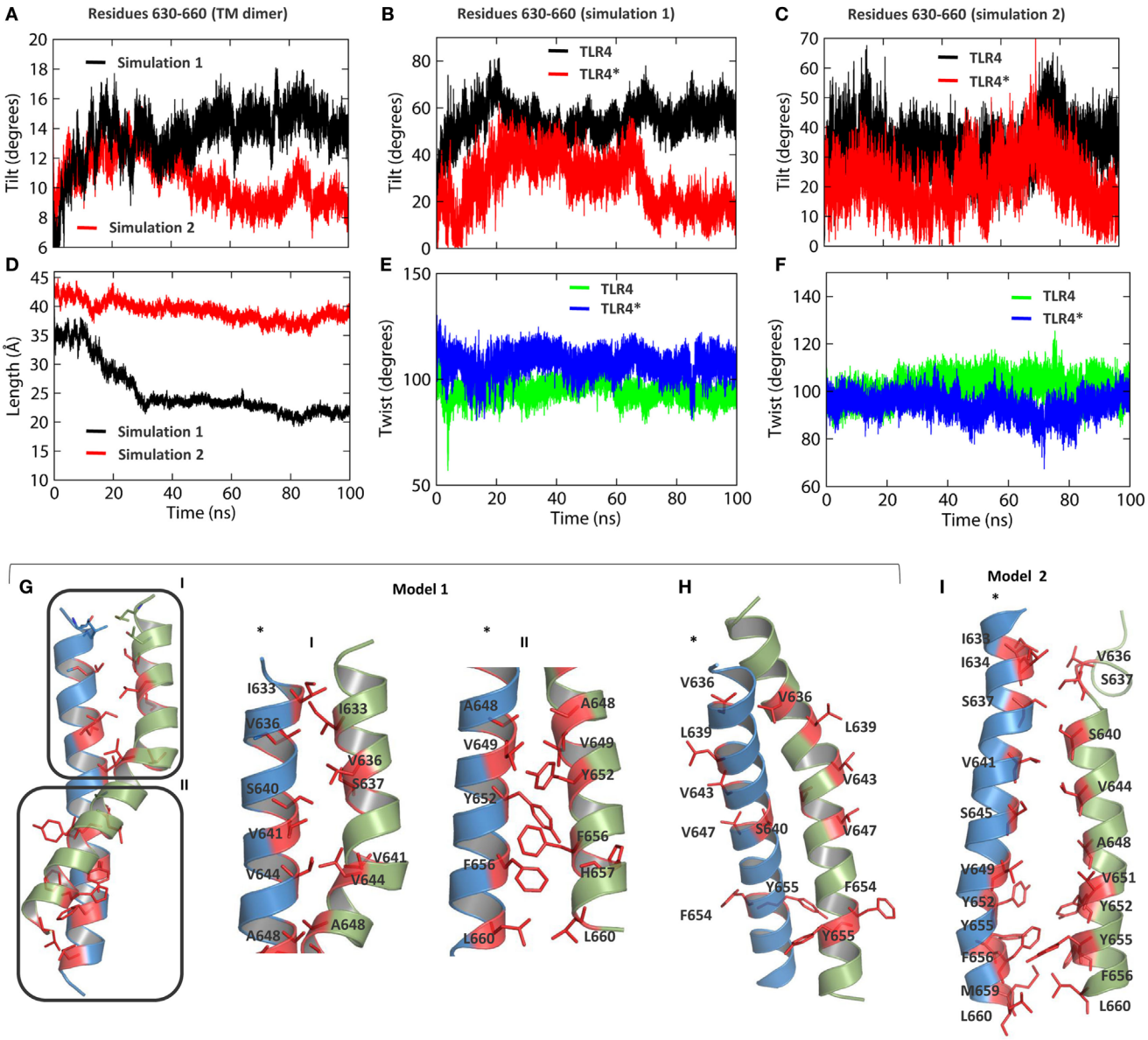

FIGURE 4 | Helical properties of TLR4-transmembrane (TM). **(A)** Tilt angle of the TM dimer as a function of time. The black and red lines represent simulation 1 and simulation 2, respectively. **(B)** Tilt angles of individual helices in simulation 1. **(C)** Tilt angles of individual helices in simulation 2. **(D)** Length of the helical axis in both simulations. **(E)** Twist angle of TM residues in simulation 1. **(F)** Twist angle of TM residues in simulation 2. **(G)** Dimer packing interactions between residues of TM helices in simulation 1. **(H)** Solvent-exposed residues of the TM domain in simulation 1, indicating a possible alternate dimerization surface. **(I)** Dimer packing interactions between residues of TM helices in simulation 2.

(**Figure 5B**; **Table 2**). The electrostatic potential surface around the TIR domain indicated that the juxtamembrane region mostly contains positively charged residues; other surfaces bordering the membrane contain a mixture of positively and negatively charged patches that form polar contacts with the phosphate oxygen atoms of the DPPC headgroups (**Figure 5C**). Calculated electrostatic isosurfaces indicated that surfaces of the helix αA and CD loop were more negatively charged due to the presence of glutamic acids E685 and E691 in helix αA, and E750 and E752 in the CD loop (**Figure 5D**). Altogether, these analyses reveal that TLR4-TIR surfaces are potentially membrane-absorbed and solvent-exposed for interactions with other proteins.

TAK-242 Binding Pockets Display Different Shapes in Isolated TIR and in Full-Length TLR4

TAK-242 is a well-known small molecular weight TLR4 antagonist that interacts with the amino acid, C747, situated in helix αC of the TIR domain. In our TLR10-TIR-based dimeric model, the BB

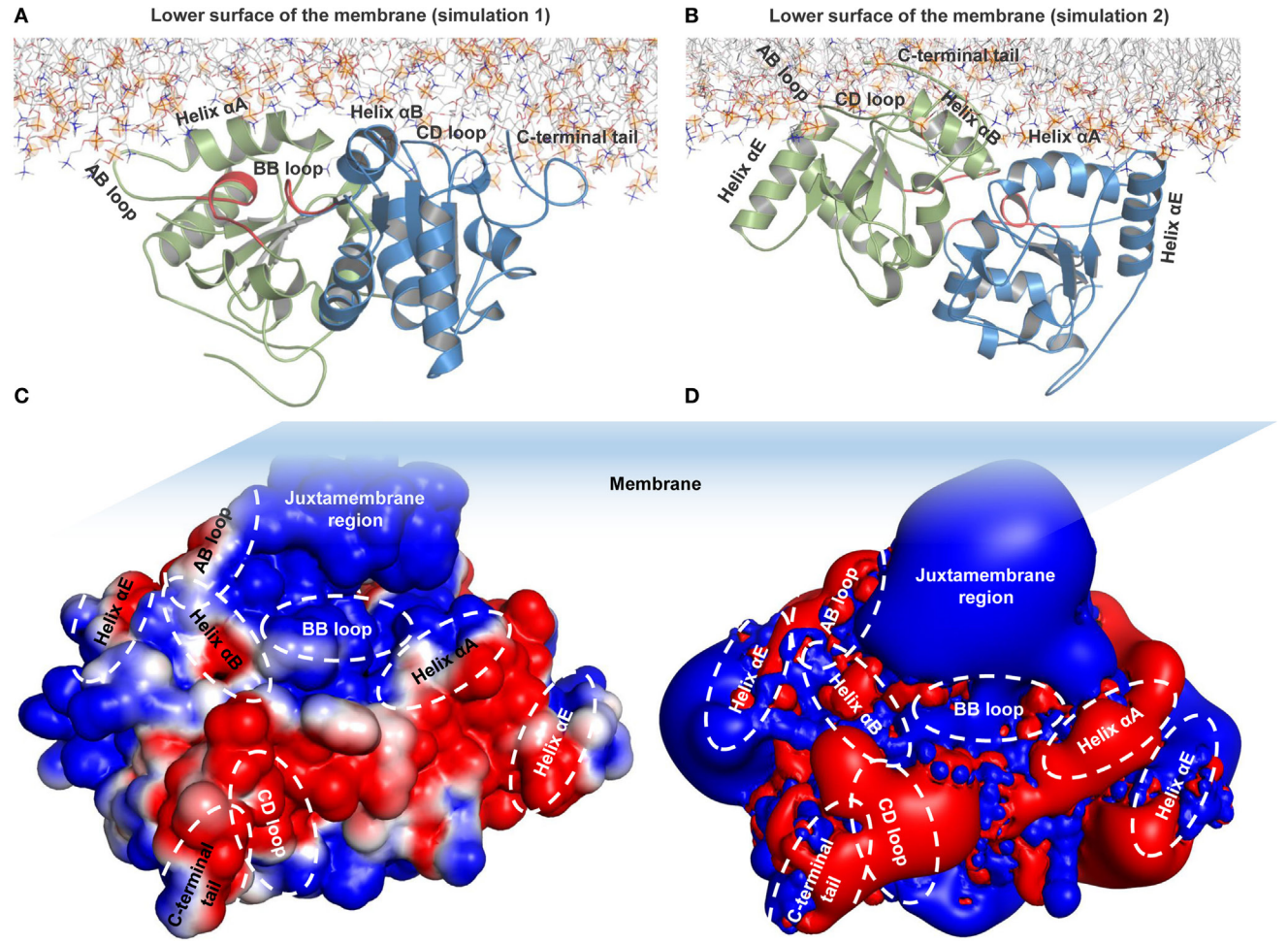

FIGURE 5 | Membrane interaction and surface electrostatic properties of toll/interleukin-1 receptor (TIR) domains. **(A)** TIR-membrane interaction in simulation 1. **(B)** TIR-membrane interaction in simulation 2. **(C)** Electrostatic potential surface of the TIR domain in simulation 1. **(D)** Electrostatic isosurface showing only the most dominant positively and negatively charged surfaces of TIR domains.

TABLE 2 | Amino acids of the TLR4-TIR domain that interact with the model phospholipid bilayer.

Simulation 1		Simulation 2	
Region	**Residues**	**Region**	**Residues**
Helix αA	Q683, E685, D686, W687, R689, N690, E691, K694	Helix αA*	D686, R689, N690, E691, K694, N695, E697
AB loop	E697, E698, V700, P701, Q704	AB loop	G699, V700, P701, P702, F703, Q704
Helix αB*	N721, H724, E725, H728, K729	Helix αB	A720, N721, H724, E725, H728, K729, S730
CD loop*	E750, Y751, E752, I753, A754, W757, Q758, F759, S762, R763	CD loop	A754, Q755, T756, W757, Q758, F757, S762, R763, A764
C-terminal tail*	T829, C831, N832, S838, I839	Helix αE	R809, R812, K813, L816, V800*, L802*, R804*, H805*, R812*
BB loop	Y9, R10	C-terminal tail	D817, K819, E824, C831, N832, W833, E835, A836, A837, S838, I839

**Indicates subunit B of TLR4.*

loop and helix αC from one subunit form a dimerization interface with the corresponding segments from the other subunit, while C747 of each monomer faces each other creating a pocket for TAK-242 binding (Figures S4A,C in Supplementary Material) (63). We found that the opening of the TAK-242 binding cavity was lined with several bulkier amino acids, namely Y751, R780, L778, H740, and Q782, that partially blocked the cavity opening in both full-length TLR4 models (**Figures 6A,B**). However, in the isolated TIR dimer, these residues faced discrete directions providing a relatively exposed cavity for smoother ligand entry (**Figure 6C**). When a docked conformation TAK-242 inside an isolated TIR dimer was visualized after 100 ns of MD simulation,

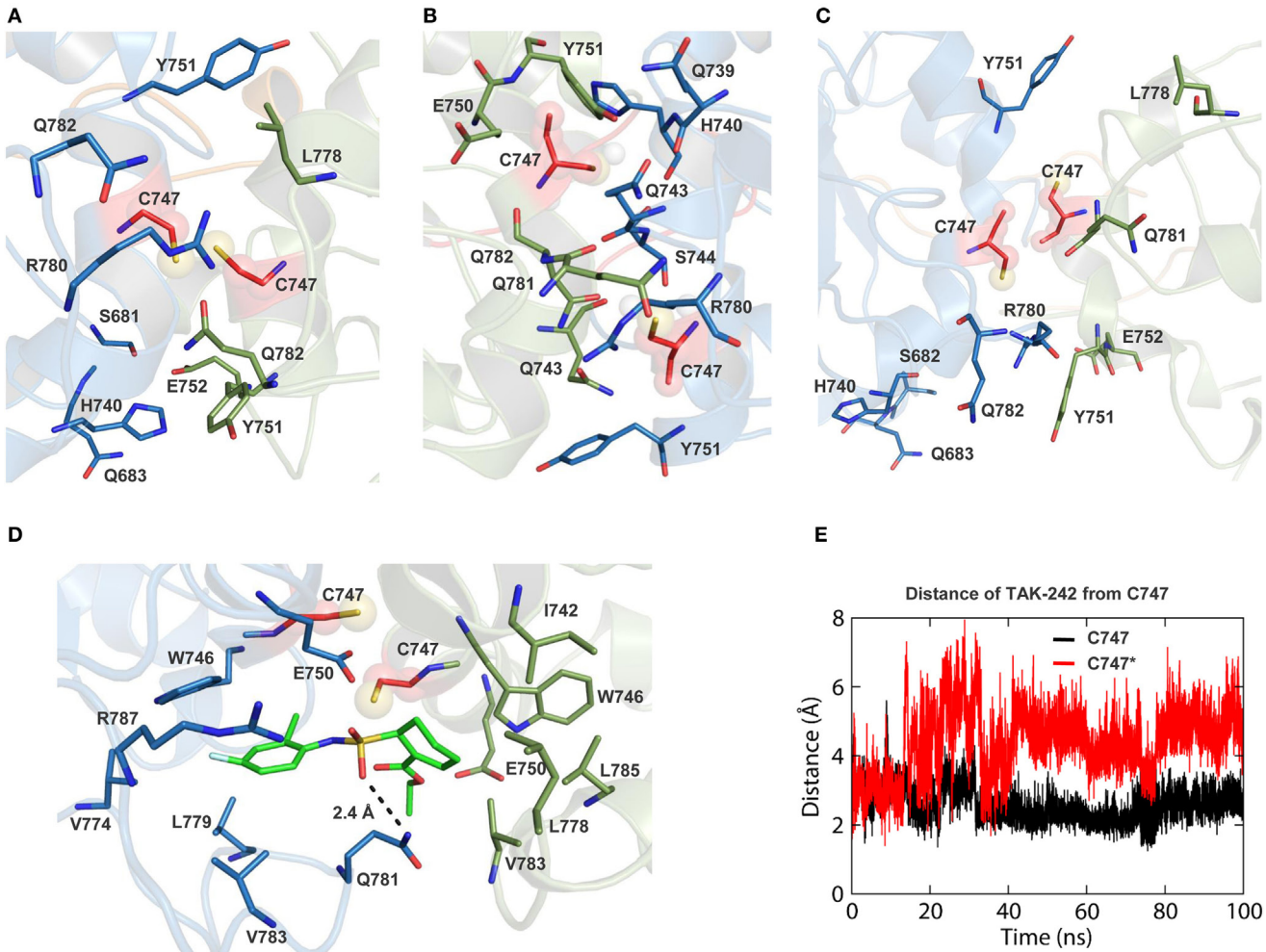

FIGURE 6 | Views of TAK-242 binding cavities of different toll/interleukin-1 receptor (TIR) dimer models. **(A)** TAK-242 binding pocket of TIR dimer in simulation 1. **(B)** TAK-242 binding pocket of TIR dimer in simulation 2. **(C)** TAK-242 binding pocket of isolated TIR dimer. **(D)** Interaction of TAK-242 with the TIR domain dimer residues. **(E)** Distance between the TAK-242 cyclohexane ring and the $–SH_2$ group of C747 of both TIR monomers.

we found that the TAK-242 cyclohexane ring remained ~2.5 Å away from the –SH group of C747 throughout the simulation (**Figure 6E**). An H-bond was observed between the SO_2-oxygen and nitrogen atoms of the Q781 side chain (**Figure 6D**). Interestingly, the residues surrounding C747 in unliganded TIRs did not interact with TAK-242, except for Q781. This suggests that TAK-242 induces conformational alterations in the residues neighboring C747 for its antagonistic interaction with TLR4. In an alternate TIR4-TIR dimeric model proposed by Toshchakov et al. (37), dimerization is governed by helix αE and the BB loop of either monomer (Figure S4B in Supplementary Material); this model shows that helix αC from both monomers is located at opposite surfaces of the TIR dimer with a solvent-exposed C747 (Figure S4D in Supplementary Material). Calculated binding affinities between TIR monomers revealed that αC-αC dimers were comparatively more stable than αE-BB dimers (**Table 3**). Furthermore, the binding affinity of TAK-242 for αC-αC dimers was found to be greater than that of TAK-242 for αE-BB dimers. Altogether, this indicates that the αC-αC orientation is the likely physiological dimeric state of TLR4-TIR domains.

DISCUSSION

An agonist-mediated dimeric state is the basic functional unit of TLRs; nevertheless, oligomeric states have lately been hypothesized (30, 64). Owing to a recent interest in TLR structural biology, NMR/X-ray crystal structures of almost all TLR individual domains have been solved. Although these experimental structures facilitated numerous mechanistic and rational drug development studies, the complete structural organization of ECD, TM, and TIR is yet to be studied as a single membrane-bound receptor unit (65). Here, we describe structural properties of a full-length TLR4 homo-heterodimer containing LPS-bound MD2 subunits in a membrane-aqueous environment that theoretically mimics the activated receptor in physiological conditions. Two independent MD simulations were performed and the

TABLE 3 | Comparison of binding affinities (kJ·mol^{-1}) between different toll/interleukin-1 receptor (TIR) dimer models and TIR-TAK-242 complexes.

TIR interface	Δ_{vdW}[a]	Δ_{elec}[b]	Δ_{ps}[c]	Δ_{SASA}[d]	Δ_{Total}[e]
Helix αC-αC	−437.952 (2.8)	−461.041 (3.6)	666.160 (5.4)	−62.136 (3.3)	−294.969 (4.6)
Helix αE-BB loop	−237.209 (1.8)	−581.003 (8.0)	665.111 (1.0)	−26.933 (4.6)	−180.035 (5.1)
TAK-242-αC-αC	−66.875 (2.3)	−72.790 (3.4)	101.001 (5.7)	−7.901 (1.9)	−46.566 (2.1)
TAK-242-αE-BB	−146.588 (1.4)	−181.268 (2.3)	328.178 (3.8)	−17.622 (1.0)	−17.299 (2.1)

[a]*Van der Waals energy.*
[b]*Electrostatic energy.*
[c]*Polar solvation energy.*
[d]*Solvent accessible surface area energy.*
[e]*Total binding free energy.*
SD are indicated in brackets.

most reasonable simulation showing stable receptor dynamics was described in detail. The rationale behind this is that the TM and TIR domains—with the exception of TLR4-ECDs—in simulation 2 displayed considerably dissimilar properties than those of simulation 1. We reason that due to a slightly different membrane placement of the TM bundle in simulation 2, the helical properties of the TM domain were partly distorted, causing the differential orientation of TIR domains. Therefore, we consider simulation 1 TLR4 as the most stable and acceptable model that describes various structural properties reliably. However, the observed tilt of TLR4 domains in simulation 1 might not be specific, since the juxtamembrane loops at the top and bottom layers of the membrane are highly flexible and mobile; therefore, the ECD and TIR domains can tilt to either direction of the membrane normal (*Z*-axis).

We found that the flexible juxtamembrane regions of full-length TLR4 allow for simultaneous tilting or bending actions of ECD and TIR domains on the membrane. As the ECD gradually inclined over the membrane surface, the LRR-NT of one monomer (TLR*) was partially absorbed into the upper leaflet of the bilayer. The inclination of ECD toward one particular direction of the bilayer surface was due to charge-dependent interactions of phospholipid headgroups with ECD amino acids facilitated by the cooperative actions of both TM and TIR domains. During this process, the LPS-bound MD2* (chain B of MD2) approached the membrane surface closely. It is possible that MD2 increased ECD bulkiness leading to its inclination over the membrane for stability. Interestingly, this dynamic behavior of ECD had little effect on the interaction between LPS and MD2. LPS was stable inside the large hydrophobic pocket of MD2—with an approximate volume of 1,700 Å^3 (62)—and interacted consistently with both TLR4 and MD2. Earlier works have shown that the hexaacylated LPS tail prompts reorientation of the MD2 F126 aromatic side chain from an open to a closed conformation; this induces stable agonist binding prior to association with TLR4 (10, 66). The open conformation of F126 in agonist-free states of activated receptor dimers acts as a molecular switch that destabilizes the relative arrangement of TM and TIR domains (10). Throughout our simulation, F126 maintained a steady interaction distance with the LPS R2 chain that kept F126 in a closed conformation. This indicates that the observed dynamic properties of TLR4-ECD in the presence of the membrane bilayer do not destabilize interactions between different TLR4-MD2-LPS homo-heterodimer subunits.

TLR4, including all TLR members, has a typical type I membrane protein structure; a bulky ECD, a single narrow TM helix, and a small TIR domain. By observing this architecture, it is reasonable to accept that homo or heterodimerization is required to maintain stability at the TM region. This stability is important for the efficient adaptor recruitment platform provided by TIR domains in the cytoplasm. Studies on TLR-TM are sparse compared with ECD and TIR; however, the literature suggests that isolated TLR-TM segments can form stable homo/heterodimeric or oligomeric assemblies (30, 31, 64, 67). TLR4-TM (residues 630–650) along with the juxtamembrane region (residues 651–660) forms a continuous helix of 32 residues that extends beyond the nonpolar region of the membrane bilayer lower leaflet. This results in a hydrophobic mismatch between the nonpolar segments of the bilayer and the TM domain. Therefore, the TM domain tilts and bends considerably to overcome the energetic penalty incurred during dynamic conditions. More recently, the dimeric state of TLR4-TM was solved through an NMR spectroscopy study (31), showing a continuous helix that includes a portion of the ICD juxtamembrane region. Protein–protein docking was then applied to obtain a dimeric TM model that showed resides V636, L639, V643, and V647 from each monomer defining the potential dimer interface. Structures of TLR4 and TLR3-TM domains were determined by a synthetic TM construct that may not reflect the precise side chain orientations of a full-length TLR surrounded by membrane phospholipids. After a 100 ns-long MD simulation of full-length TLR4, we found that the residues reported by Mineev et al. (31) were directed toward the hydrophobic core of the bilayer; this points to the possibility of an alternate homodimerization or homooligomerization interface of TLR4-TM, as was found for other type I TM proteins, including TLR3-TM (30, 68). The strong interaction between aromatic residues of both TM monomers in interface II may result in helix bending at the center. These helical properties of TM domains of the full-length TLR4 are consistent with observations of other bitopic membrane proteins, where the specific lipid-TM and TM–TM interactions stabilize functionally relevant receptor conformations (69).

Inflammatory signaling and host defense downstream of membrane-bound TLRs involve several transient interactions between TIR domain-containing proteins (19). Functional TIR domain interactions are largely specific, in that a given set of TIRs tend to only associate with each other; however, some TIR domain-containing proteins interact with multiple partners giving rise to overlaps in the signal transduction cascade (22).

Despite considerable efforts, the molecular basis of TIR domain specificities has not been completely unraveled. We observed that the TIR domains were gradually absorbed into the lower surface of the membrane bilayer due to electrostatic interactions and the bending or twisting actions of ECD and TM domains. Along with the juxtamembrane region, the upper surface of the TIR domain was partially immersed into the polar, lower face of the membrane. Of note, the primary contact surface between the membrane and both TIR domains is governed by helices αA and αB. Polar residues of the AB loop, CD loop, and C-terminal tail of one subunit made partial contacts with the membrane for stability, while the same regions of the other subunit remained completely solvent-exposed. The BB loop motif was situated right underneath the membrane bilayer as its Y709 and R710 residues formed H-bonds with phospholipid headgroups. The functionally important helix αE—thought to form an alternate dimerization surface by interacting with the BB loop (37)—remained solvent-exposed throughout the simulation, suggesting that helix αE might potentially form the TLR4 oligomerization interface. This indicates that our MD simulation accurately described physiological folding of membrane-bound TLR4. The interaction between TIR residues and membrane phospholipids or partial immersion of amino acid side chains into the polar region of the bilayer is unlikely to preclude these segments from contacting adaptor or other binding components. Decoy peptides from the helix αA and juxtamembrane region of TLR4-TIR were able to inhibit agonist-induced cytokine production by targeting their site of origin (37). This indicates that the polar region of the membrane, containing partially absorbed TIR residues, can accommodate other signaling components or external peptide antagonists. The MyD88 protein is sorted to TLR4-TIR by the membrane anchored adaptor, TIR domain-containing adaptor protein (TIRAP) (70, 71); therefore, it is most likely that the activated receptor complex formed by TLR4-TIRAP-MyD88 is in close proximity to membrane phospholipids (72). Moreover, it is likely that polar phospholipid headgroups provide the necessary charged environment for surface-exposed hydrophilic residues of the receptor or adaptors, thus stabilizing the supercomplex.

Next, we compared the small-molecule antagonist binding cavity of the TIR domain in both full-length TLR4 and isolated conditions. We considered TAK-242 as it is the most potent small-molecule antagonist reported to date that blocks recruitment of downstream adaptors by activated TLR4 (73). TAK-242 has been reported to bind to the conserved C747, located in the helix αC, of the TIR domain and prevents adaptor recruitment without affecting receptor homodimerization (63). In the absence of a commonly accepted TLR4-TIR dimerization model, we constructed two possible homodimerization interfaces, as reported in the literature. The first model was created based on the widely accepted view that helix αC and the BB loop of both subunits form the dimer interface (43, 44, 49). This model is based on the solved crystal structure of TLR10-TIR homodimer with one symmetric and one asymmetric subunits (28). We used the αC-αC model for completing our full-length TLR4 homodimer as well as for studying TAK-242 interactions. On the other hand, an alternative dimerization model has also been proposed using a decoy peptide approach (37). This model exposes helix αC toward the solvent and places helix αE and the BB loop in between the dimer interface. Our estimated binding free energy revealed that the αC-αC dimer has a greater binding affinity than the αE-BB dimer. Moreover, the affinity of TAK-242 for αC-αC dimers was stronger than for αE-BB dimers. This indicates that the αC-αC/BB-BB model might represent the physiological dimeric interface of TLR4. Remarkably, in the full-length TLR4, the TAK-242 binding cavity was partially blocked by neighboring residues that precluded C747 from contacting TAK-242. Possibly, due to the rotation and upward movement of the TIR dimer of full-length TLR4, the side chains of C747 neighboring residues covered the opening of the ligand binding cavity after coming in contact with rapidly moving water molecules. This phenomenon was also observed in a separate simulation of full-length TLR4. Thus, TAK-242 binding deep inside the TIR dimer cavity remains speculative, particularly in the absence of a cocrystallized ligand with the TIR dimer. Since TAK-242 does not interfere with LPS binding to MD2 and receptor dimerization, but prevents adaptor recruitment, it is tempting to state that C747 interacts with the ligand on the solvent accessible surface of the domain. An X-ray/NMR structure of TAK-242 bound to the dimeric TLR4-TIR is required to clarify this issue.

In this study, we proposed a full-length dimeric model of membrane-bound TLR4 containing two subunits of MD2-LPS complexes that represents the agonist-induced activated state. The structural properties of ECD, TM, and TIR domains of intact TLR4 are consistent with X-ray crystallography/NMR structures determined in isolated conditions. Lipid–protein and protein–protein interactions of the TM and TIR domains were crucial for shaping the biophysical properties behind the signaling-competent form of intact TLR4 homo-heterodimers (see Data Sheet 1 in Supplementary Material). Of note, caution should be exercised while using the proposed model in any study in the current form. Although we performed a detailed analysis and validation of its various structural properties in the membrane through multiple MD simulations, experiments with atomic force microscopy or cryo-electron microscopy on liposomes with inserted full-length TLR4-MD2-LPS complexes could only illustrate the exact conformation.

AUTHOR CONTRIBUTIONS

MP and HKK conceptualized the study. MP designed and performed the experiments. MP, HKK, and MB analyzed the results. MP, HKK, MB, and SC wrote the manuscript.

FUNDING

This work was supported by the National Research Foundation of Korea (NRF-2015R1A2A2A09001059, NRF 2012–0006687).

SUPPLEMENTARY MATERIAL

The Supplementary Material for this article can be found online at http://www.frontiersin.org/articles/10.3389/fimmu.2018.00489/full#supplementary-material.

REFERENCES

1. Iwasaki A, Medzhitov R. Toll-like receptor control of the adaptive immune responses. *Nat Immunol* (2004) 5(10):987–95. doi:10.1038/ni1112
2. Iwasaki A, Medzhitov R. Regulation of adaptive immunity by the innate immune system. *Science* (2010) 327(5963):291–5. doi:10.1126/science.1183021
3. Iwasaki A, Medzhitov R. Control of adaptive immunity by the innate immune system. *Nat Immunol* (2015) 16(4):343–53. doi:10.1038/ni.3123
4. Akira S, Takeda K. Toll-like receptor signalling. *Nat Rev Immunol* (2004) 4(7):499–511. doi:10.1038/nri1391
5. Gay NJ, Symmons MF, Gangloff M, Bryant CE. Assembly and localization of toll-like receptor signalling complexes. *Nat Rev Immunol* (2014) 14(8):546–58. doi:10.1038/nri3713
6. Jin MS, Kim SE, Heo JY, Lee ME, Kim HM, Paik SG, et al. Crystal structure of the TLR1-TLR2 heterodimer induced by binding of a tri-acylated lipopeptide. *Cell* (2007) 130(6):1071–82. doi:10.1016/j.cell.2007.09.008
7. Kang JY, Nan X, Jin MS, Youn SJ, Ryu YH, Mah S, et al. Recognition of lipopeptide patterns by toll-like receptor 2-toll-like receptor 6 heterodimer. *Immunity* (2009) 31(6):873–84. doi:10.1016/j.immuni.2009.09.018
8. Alexopoulou L, Holt AC, Medzhitov R, Flavell RA. Recognition of double-stranded RNA and activation of NF-kappaB by toll-like receptor 3. *Nature* (2001) 413(6857):732–8. doi:10.1038/35099560
9. Liu L, Botos I, Wang Y, Leonard JN, Shiloach J, Segal DM, et al. Structural basis of toll-like receptor 3 signaling with double-stranded RNA. *Science* (2008) 320(5874):379–81. doi:10.1126/science.1155406
10. Paramo T, Piggot TJ, Bryant CE, Bond PJ. The structural basis for endotoxin-induced allosteric regulation of the toll-like receptor 4 (TLR4) innate immune receptor. *J Biol Chem* (2013) 288(51):36215–25. doi:10.1074/jbc.M113.501957
11. Park BS, Lee JO. Recognition of lipopolysaccharide pattern by TLR4 complexes. *Exp Mol Med* (2013) 45:e66. doi:10.1038/emm.2013.97
12. Park BS, Song DH, Kim HM, Choi BS, Lee H, Lee JO. The structural basis of lipopolysaccharide recognition by the TLR4-MD-2 complex. *Nature* (2009) 458(7242):1191–5. doi:10.1038/nature07830
13. Yoon SI, Kurnasov O, Natarajan V, Hong M, Gudkov AV, Osterman AL, et al. Structural basis of TLR5-flagellin recognition and signaling. *Science* (2012) 335(6070):859–64. doi:10.1126/science.1215584
14. Guiducci C, Gong M, Cepika AM, Xu Z, Tripodo C, Bennett L, et al. RNA recognition by human TLR8 can lead to autoimmune inflammation. *J Exp Med* (2013) 210(13):2903–19. doi:10.1084/jem.20131044
15. Heil F, Hemmi H, Hochrein H, Ampenberger F, Kirschning C, Akira S, et al. Species-specific recognition of single-stranded RNA via toll-like receptor 7 and 8. *Science* (2004) 303(5663):1526–9. doi:10.1126/science.1093620
16. Ohto U, Shibata T, Tanji H, Ishida H, Krayukhina E, Uchiyama S, et al. Structural basis of CpG and inhibitory DNA recognition by toll-like receptor 9. *Nature* (2015) 520(7549):702–5. doi:10.1038/nature14138
17. Lee SM, Kok KH, Jaume M, Cheung TK, Yip TF, Lai JC, et al. Toll-like receptor 10 is involved in induction of innate immune responses to influenza virus infection. *Proc Natl Acad Sci U S A* (2014) 111(10):3793–8. doi:10.1073/pnas.1324266111
18. Nagashima H, Iwatani S, Cruz M, Jimenez Abreu JA, Uchida T, Mahachai V, et al. Toll-like receptor 10 in *Helicobacter pylori* infection. *J Infect Dis* (2015) 212(10):1666–76. doi:10.1093/infdis/jiv270
19. O'Neill LA, Bowie AG. The family of five: TIR-domain-containing adaptors in toll-like receptor signalling. *Nat Rev Immunol* (2007) 7(5):353–64. doi:10.1038/nri2079
20. Valkov E, Stamp A, Dimaio F, Baker D, Verstak B, Roversi P, et al. Crystal structure of toll-like receptor adaptor MAL/TIRAP reveals the molecular basis for signal transduction and disease protection. *Proc Natl Acad Sci U S A* (2011) 108(36):14879–84. doi:10.1073/pnas.1104780108
21. Lin SC, Lo YC, Wu H. Helical assembly in the MyD88-IRAK4-IRAK2 complex in TLR/IL-1R signalling. *Nature* (2010) 465(7300):885–90. doi:10.1038/nature09121
22. Kawai T, Akira S. The role of pattern-recognition receptors in innate immunity: update on toll-like receptors. *Nat Immunol* (2010) 11(5):373–84. doi:10.1038/ni.1863
23. Botos I, Segal DM, Davies DR. The structural biology of toll-like receptors. *Structure* (2011) 19(4):447–59. doi:10.1016/j.str.2011.02.004
24. Ohto U, Fukase K, Miyake K, Shimizu T. Structural basis of species-specific endotoxin sensing by innate immune receptor TLR4/MD-2. *Proc Natl Acad Sci U S A* (2012) 109(19):7421–6. doi:10.1073/pnas.1201193109
25. Tanji H, Ohto U, Shibata T, Miyake K, Shimizu T. Structural reorganization of the toll-like receptor 8 dimer induced by agonistic ligands. *Science* (2013) 339(6126):1426–9. doi:10.1126/science.1229159
26. Zhang Z, Ohto U, Shibata T, Krayukhina E, Taoka M, Yamauchi Y, et al. Structural analysis reveals that toll-like receptor 7 is a dual receptor for guanosine and single-stranded RNA. *Immunity* (2016) 45(4):737–48. doi:10.1016/j.immuni.2016.09.011
27. Jang TH, Park HH. Crystal structure of TIR domain of TLR6 reveals novel dimeric interface of TIR-TIR interaction for toll-like receptor signaling pathway. *J Mol Biol* (2014) 426(19):3305–13. doi:10.1016/j.jmb.2014.07.024
28. Nyman T, Stenmark P, Flodin S, Johansson I, Hammarstrom M, Nordlund P. The crystal structure of the human toll-like receptor 10 cytoplasmic domain reveals a putative signaling dimer. *J Biol Chem* (2008) 283(18):11861–5. doi:10.1074/jbc.C800001200
29. Xu Y, Tao X, Shen B, Horng T, Medzhitov R, Manley JL, et al. Structural basis for signal transduction by the toll/interleukin-1 receptor domains. *Nature* (2000) 408(6808):111–5. doi:10.1038/35040600
30. Mineev KS, Goncharuk SA, Arseniev AS. Toll-like receptor 3 transmembrane domain is able to perform various homotypic interactions: an NMR structural study. *FEBS Lett* (2014) 588(21):3802–7. doi:10.1016/j.febslet.2014.08.031
31. Mineev KS, Goncharuk SA, Goncharuk MV, Volynsky PE, Novikova EV, Aresinev AS. Spatial structure of TLR4 transmembrane domain in bicelles provides the insight into the receptor activation mechanism. *Sci Rep* (2017) 7(1):6864. doi:10.1038/s41598-017-07250-4
32. Allette YM, Kim Y, Randolph AL, Smith JA, Ripsch MS, White FA. Decoy peptide targeted to toll-IL-1R domain inhibits LPS and TLR4-active metabolite morphine-3 glucuronide sensitization of sensory neurons. *Sci Rep* (2017) 7(1):3741. doi:10.1038/s41598-017-03447-9
33. Couture LA, Piao W, Ru LW, Vogel SN, Toshchakov VY. Targeting toll-like receptor (TLR) signaling by toll/interleukin-1 receptor (TIR) domain-containing adapter protein/MyD88 adapter-like (TIRAP/Mal)-derived decoy peptides. *J Biol Chem* (2012) 287(29):24641–8. doi:10.1074/jbc.M112.360925
34. Ke Y, Li W, Wang Y, Yang M, Guo J, Zhan S, et al. Inhibition of TLR4 signaling by Brucella TIR-containing protein TcpB-derived decoy peptides. *Int J Med Microbiol* (2016) 306(6):391–400. doi:10.1016/j.ijmm.2016.05.003
35. Piao W, Shirey KA, Ru LW, Lai W, Szmacinski H, Snyder GA, et al. A decoy peptide that disrupts TIRAP recruitment to TLRs is protective in a murine model of influenza. *Cell Rep* (2015) 11(12):1941–52. doi:10.1016/j.celrep.2015.05.035
36. Piao W, Vogel SN, Toshchakov VY. Inhibition of TLR4 signaling by TRAM-derived decoy peptides in vitro and in vivo. *J Immunol* (2013) 190(5):2263–72. doi:10.4049/jimmunol.1202703
37. Toshchakov VY, Szmacinski H, Couture LA, Lakowicz JR, Vogel SN. Targeting TLR4 signaling by TLR4 Toll/IL-1 receptor domain-derived decoy peptides: identification of the TLR4 Toll/IL-1 receptor domain dimerization interface. *J Immunol* (2011) 186(8):4819–27. doi:10.4049/jimmunol.1002424
38. Toshchakov VY, Vogel SN. Cell-penetrating TIR BB loop decoy peptides a novel class of TLR signaling inhibitors and a tool to study topology of TIR-TIR interactions. *Expert Opin Biol Ther* (2007) 7(7):1035–50. doi:10.1517/14712598.7.7.1035
39. Biasini M, Bienert S, Waterhouse A, Arnold K, Studer G, Schmidt T, et al. SWISS-MODEL: modelling protein tertiary and quaternary structure using evolutionary information. *Nucleic Acids Res* (2014) 42(Web Server issue):W252–8. doi:10.1093/nar/gku340
40. Abraham MJ, Murtola T, Schulz R, Páll S, Smith JC, Hess B, et al. GROMACS: high performance molecular simulations through multi-level parallelism from laptops to supercomputers. *SoftwareX* (2015) 1–2:19–25. doi:10.1016/j.softx.2015.06.001
41. Pierce BG, Hourai Y, Weng Z. Accelerating protein docking in ZDOCK using an advanced 3D convolution library. *PLoS One* (2011) 6(9):e24657. doi:10.1371/journal.pone.0024657
42. Fiser A, Sali A. ModLoop: automated modeling of loops in protein structures. *Bioinformatics* (2003) 19(18):2500–1. doi:10.1093/bioinformatics/btg362
43. Bovijn C, Ulrichts P, De Smet AS, Catteeuw D, Beyaert R, Tavernier J, et al. Identification of interaction sites for dimerization and adapter recruitment in toll/interleukin-1 receptor (TIR) domain of toll-like receptor 4. *J Biol Chem* (2012) 287(6):4088–98. doi:10.1074/jbc.M111.282350

44. Guven-Maiorov E, Keskin O, Gursoy A, VanWaes C, Chen Z, Tsai CJ, et al. The architecture of the TIR domain signalosome in the toll-like receptor-4 signaling pathway. *Sci Rep* (2015) 5:13128. doi:10.1038/srep13128
45. Kandt C, Ash WL, Tieleman DP. Setting up and running molecular dynamics simulations of membrane proteins. *Methods* (2007) 41(4):475–88. doi:10.1016/j.ymeth.2006.08.006
46. Humphrey W, Dalke A, Schulten K. VMD: visual molecular dynamics. *J Mol Graph* (1996) 14(1):33–8. doi:10.1016/0263-7855(96)00018-5
47. Koziara KB, Stroet M, Malde AK, Mark AE. Testing and validation of the automated topology builder (ATB) version 2.0: prediction of hydration free enthalpies. *J Comput Aided Mol Des* (2014) 28(3):221–33. doi:10.1007/s10822-014-9713-7
48. Paramo T, East A, Garzon D, Ulmschneider MB, Bond PJ. Efficient characterization of protein cavities within molecular simulation trajectories: trj_cavity. *J Chem Theory Comput* (2014) 10(5):2151–64. doi:10.1021/ct401098b
49. Nunez Miguel R, Wong J, Westoll JF, Brooks HJ, O'Neill LA, Gay NJ, et al. A dimer of the toll-like receptor 4 cytoplasmic domain provides a specific scaffold for the recruitment of signalling adaptor proteins. *PLoS One* (2007) 2(8):e788. doi:10.1371/journal.pone.0000788
50. Wiederstein M, Sippl MJ. ProSA-web: interactive web service for the recognition of errors in three-dimensional structures of proteins. *Nucleic Acids Res* (2007) 35(Web Server issue):W407–10. doi:10.1093/nar/gkm290
51. Bhattacharya A, Tejero R, Montelione GT. Evaluating protein structures determined by structural genomics consortia. *Proteins* (2007) 66(4):778–95. doi:10.1002/prot.21165
52. Molecular Operating Environment (MOE), 2016.08; Chemical Computing Group ULC, 1010 Sherbooke St. West, Suite #910, Montreal, QC, Canada, H3A 2R7 (2018).
53. Genheden S, Ryde U. The MM/PBSA and MM/GBSA methods to estimate ligand-binding affinities. *Expert Opin Drug Discov* (2015) 10(5):449–61. doi:10.1517/17460441.2015.1032936
54. Baker NA, Sept D, Joseph S, Holst MJ, McCammon JA. Electrostatics of nanosystems: application to microtubules and the ribosome. *Proc Natl Acad Sci U S A* (2001) 98(18):10037–41. doi:10.1073/pnas.181342398
55. Kumari R, Kumar R; Open Source Drug Discovery Consortium, Lynn A. g_mmpbsa – a GROMACS tool for high-throughput MM-PBSA calculations. *J Chem Inf Model* (2014) 54(7):1951–62. doi:10.1021/ci500020m
56. Genheden S, Ryde U. Will molecular dynamics simulations of proteins ever reach equilibrium? *Phys Chem Chem Phys* (2012) 14(24):8662–77. doi:10.1039/c2cp23961b
57. Leekumjorn S, Sum AK. Molecular simulation study of structural and dynamic properties of mixed DPPC/DPPE bilayers. *Biophys J* (2006) 90(11):3951–65. doi:10.1529/biophysj.105.076596
58. Lupyan D, Mezei M, Logothetis DE, Osman R. A molecular dynamics investigation of lipid bilayer perturbation by PIP2. *Biophys J* (2010) 98(2):240–7. doi:10.1016/j.bpj.2009.09.063
59. Nagle JF. Area/lipid of bilayers from NMR. *Biophys J* (1993) 64(5):1476–81. doi:10.1016/S0006-3495(93)81514-5
60. Taylor J, Whiteford NE, Bradley G, Watson GW. Validation of all-atom phosphatidylcholine lipid force fields in the tensionless NPT ensemble. *Biochim Biophys Acta* (2009) 1788(3):638–49. doi:10.1016/j.bbamem.2008.10.013
61. Petrache HI, Dodd SW, Brown MF. Area per lipid and acyl length distributions in fluid phosphatidylcholines determined by (2)H NMR spectroscopy. *Biophys J* (2000) 79(6):3172–92. doi:10.1016/S0006-3495(00)76551-9
62. Ohto U, Fukase K, Miyake K, Satow Y. Crystal structures of human MD-2 and its complex with antiendotoxic lipid IVa. *Science* (2007) 316(5831):1632–4. doi:10.1126/science.1139111
63. Takashima K, Matsunaga N, Yoshimatsu M, Hazeki K, Kaisho T, Uekata M, et al. Analysis of binding site for the novel small-molecule TLR4 signal transduction inhibitor TAK-242 and its therapeutic effect on mouse sepsis model. *Br J Pharmacol* (2009) 157(7):1250–62. doi:10.1111/j.1476-5381.2009.00297.x
64. Godfroy JI III, Roostan M, Moroz YS, Korendovych IV, Yin H. Isolated toll-like receptor transmembrane domains are capable of oligomerization. *PLoS One* (2012) 7(11):e48875. doi:10.1371/journal.pone.0048875
65. Song DH, Lee JO. Sensing of microbial molecular patterns by toll-like receptors. *Immunol Rev* (2012) 250(1):216–29. doi:10.1111/j.1600-065X.2012.01167.x
66. Yu L, Phillips RL, Zhang D, Teghanemt A, Weiss JP, Gioannini TL. NMR studies of hexaacylated endotoxin bound to wild-type and F126A mutant MD-2 and MD-2.TLR4 ectodomain complexes. *J Biol Chem* (2012) 287(20):16346–55. doi:10.1074/jbc.M112.343467
67. Nishiya T, Kajita E, Miwa S. Ligand-independent oligomerization of TLR4 regulated by a short hydrophobic region adjacent to the transmembrane domain. *Biochem Biophys Res Commun* (2006) 341(4):1128–34. doi:10.1016/j.bbrc.2006.01.074
68. Bocharov EV, Lesovoy DM, Pavlov KV, Pustovalova YE, Bocharova OV, Arseniev AS. Alternative packing of EGFR transmembrane domain suggests that protein-lipid interactions underlie signal conduction across membrane. *Biochim Biophys Acta* (2016) 1858(6):1254–61. doi:10.1016/j.bbamem.2016.02.023
69. Bocharov EV, Mineev KS, Pavlov KV, Akimov SA, Kuznetsov AS, Efremov RG, et al. Helix-helix interactions in membrane domains of bitopic proteins: specificity and role of lipid environment. *Biochim Biophys Acta* (2017) 1859(4):561–76. doi:10.1016/j.bbamem.2016.10.024
70. Kagan JC, Medzhitov R. Phosphoinositide-mediated adaptor recruitment controls toll-like receptor signaling. *Cell* (2006) 125(5):943–55. doi:10.1016/j.cell.2006.03.047
71. Bonham KS, Orzalli MH, Hayashi K, Wolf AI, Glanemann C, Weninger W, et al. A promiscuous lipid-binding protein diversifies the subcellular sites of toll-like receptor signal transduction. *Cell* (2014) 156(4):705–16. doi:10.1016/j.cell.2014.01.019
72. Ve T, Vajjhala PR, Hedger A, Croll T, DiMaio F, Horsefield S, et al. Structural basis of TIR-domain-assembly formation in MAL- and MyD88-dependent TLR4 signaling. *Nat Struct Mol Biol* (2017) 24(9):743–51. doi:10.1038/nsmb.3444
73. Kawamoto T, Ii M, Kitazaki T, Iizawa Y, Kimura H. TAK-242 selectively suppresses toll-like receptor 4-signaling mediated by the intracellular domain. *Eur J Pharmacol* (2008) 584(1):40–8. doi:10.1016/j.ejphar.2008.01.026

Conflict of Interest Statement: The authors declare that the research was conducted in the absence of any commercial or financial relationships that could be construed as a potential conflict of interest.

frontiers in Immunology

ORIGINAL RESEARCH
published: 19 March 2018
doi: 10.3389/fimmu.2018.00523

Astrocytic Interleukin-15 Reduces Pathology of Neuromyelitis Optica in Mice

*Zhiguo Li[1,2], Jinrui Han[1], Honglei Ren[1], Cun-Gen Ma[3], Fu-Dong Shi[1,2,4], Qiang Liu[1,4] and Minshu Li[1,2]**

[1] Department of Neurology, Tianjin Neurological Institute, Tianjin Medical University General Hospital, Tianjin, China, [2] Center for Neuroinflammation, Beijing Tiantan Hospital, Capital Medical University, Beijing, China, [3] Shanxi University of Traditional Chinese Medicine, Taiyuan, China, [4] Department of Neurology, Barrow Neurological Institute, St. Joseph's Hospital and Medical Center, Phoenix, AZ, United States

Astrocyte loss induced by neuromyelitis optica (NMO)-IgG and complement-dependent cytotoxicity (CDC) is the hallmark of NMO pathology. The survival of astrocytes is thought to reflect astrocyte exposure to environmental factors in the CNS and the response of astrocytes to these factors. However, still unclear are how astrocytes respond to NMO-IgG and CDC, and what CNS environmental factors may impact the survival of astrocytes. In a murine model of NMO induced by intracerebral injection of NMO-IgG and human complement, we found dramatic upregulation of IL-15 in astrocytes. To study the role of astrocytic IL-15 in NMO, we generated a transgenic mouse line with targeted expression of IL-15 in astrocytes (IL-15^{tg}), in which the expression of IL-15 is controlled by a glial fibrillary acidic protein promoter. We showed that astrocyte-targeted expression of IL-15 attenuates astrocyte injury and the loss of aquaporin-4 in the brain. Reduced blood–brain barrier leakage and immune cell infiltration are also found in the lesion of IL-15^{tg} mice subjected to NMO induction. IL-15^{tg} astrocytes are less susceptible to NMO-IgG-mediated CDC than their wild-type counterparts. The enhanced resistance of IL-15^{tg} astrocytes to cytotoxicity and cell death involves NF-κB signaling pathway. Our findings suggest that IL-15 reduces astrocyte loss and NMO pathology.

Keywords: astrocytes, complement-dependent cytotoxicity, neuromyelitis optica-IgG, IL-15, neuromyelitis optica

OPEN ACCESS

Edited by:
Antonio La Cava, University of California, Los Angeles, United States

Reviewed by:
Nina Ivanovska, Institute of Microbiology (BAS), Bulgaria
Yinghong Hu, Emory University, United States

***Correspondence:**
Minshu Li
minshuli2012@163.com

Specialty section:
This article was submitted to Molecular Innate Immunity, a section of the journal Frontiers in Immunology

Received: *11 January 2018*
Accepted: *28 February 2018*
Published: *19 March 2018*

Citation:
Li Z, Han J, Ren H, Ma C-G, Shi F-D, Liu Q and Li M (2018) Astrocytic Interleukin-15 Reduces Pathology of Neuromyelitis Optica in Mice. Front. Immunol. 9:523. doi: 10.3389/fimmu.2018.00523

INTRODUCTION

Neuromyelitis optica (NMO) is a severe autoimmune disease in the central nervous system that predominantly affects the optic nerves and spinal cord (1, 2). Binding of NMO-IgG to water channel aquaporin-4 (AQP4), primarily expressed at the end-feet of astrocytes, initiates complement-dependent cell cytotoxicity (CDCC) on astrocytes, followed by blood–brain barrier breakdown, recruitment of granulocytes and macrophages and cytokine secretion, which result in secondary oligodendrocyte injury, demyelination, and neuronal injury (3–6). In NMO disease, death of astrocytes is thought to be pivotal because it initiates a cascade of inflammatory responses that further exacerbate CNS injury. Astrocytes could play an active role in regulating CNS inflammation and brain homeostasis *via* producing inflammatory mediators, energy and oxidative precursors, as well as scavenging extracellular cytotoxic substances in a variety of neurological diseases (7–9). Although it has long been known that astrocytes are targets of NMO-IgG and CDC, how astrocytes respond to NMO-IgG and CDC are still poorly understood.

The survival of astrocytes depends on their exposure and receptiveness to CNS environmental factors. Interleukin-15 is a proinflammatory cytokine that impacts the homeostasis and intensity

of immune response in autoimmune diseases. In the periphery, studies have demonstrated that IL-15 contributes to the immunopathology of several inflammatory diseases, such as rheumatoid arthritis and inflammatory bowel disease (10, 11). In the CNS, IL-15 is minimally expressed in physiological conditions, but the level of IL-15 in the brain is upregulated after CNS injuries. Astrocytes have been found as a major source of IL-15 in the CNS after injuries (12–16). Previous studies suggest that IL-15 would either aggravate or attenuate inflammation and neural injuries depending on timing, disease stage and types (17, 18). However, the role of IL-15 in NMO pathology remains unknown. In a murine model of NMO, we found that IL-15 is dramatically upregulated in astrocytes. To test the potential role of astrocytic IL-15 in NMO, we generated a transgenic mouse line with targeted expression of IL-15 in astrocytes (IL-15^{tg} mice) and examined NMO pathology in these mice.

MATERIALS AND METHODS

Mice

The study was performed in accordance with the National Institutes of Health Guide for the Care and Use of Laboratory Animals. All experimental procedures were approved by Animal Care and Use Committees of Barrow Neurological Institute (AZ, USA) and Tianjin Neurological Institute (Tianjin, China). IL-15^{tg} mice were developed by Genetically Engineered Mouse Models Core at Univercity of Arizona (Tuscon, AZ, USA), the method of IL-15^{tg} mice development and genotype identification was done as previously described (13–15). IL-15^{tg} mice were backcrossed to the C57BL/6 background for at least 10 generations before experiments were performed. All mice were kept in specific pathogen-free conditions and kept at a standard 21°C with a 12 h light/dark cycle at the animal facility of the Barrow Neurological Institute or Tianjin Neurological Institute.

NMO Animal Model Procedure

Weight-matched adult female mice, aged 8–12 weeks old IL-15^{tg} mice and WT littermates, were used in our experiments. NMO mouse model is induced by intra-parenchymal injections of NMO-IgG [recombinant antibody (rAb-53)], AQP4-specific IgG, which is cloned from intrathecal plasma cells in early NMO (19) and human complement (HC). In brief, mice were anesthetized by inhaling 3.5% isoflurane and maintained by inhalation of 1.0–2.0% isoflurane in 70% N_2O and 30% O_2 by a face mask, then mounted in a stereotactic frame. A midline scalp incision was made to expose bregma and lambda, a burr hole was made 2 mm to the right of the bregma. A 26-gauge needle attached to 10 µl gas-tight glass syringe (Hamilton) was inserted 3-mm deep to infuse 8 µl PBS containing 2 µg NMO-IgG (rAb-53) and 3 µl HC to the parenchymal tissue at a rate of 0.5 µl/min. During the entire procedure, rectal temperature was maintained at 37°C with a heating lamp.

Neuroimaging

Neuromyelitis optica lesions and BBB permeability were detected using a 7T small animal, 30-cm horizontal-bore magnet and BioSpec Advance III spectrometer (Bruker, Billerica, MA, USA) with a 116-mm high power gradient set (600 mT/m) and a 72-mm whole-body mouse transmit/surface receive coil configuration. T2-weighted images were acquired at day 3 after NMO induction. Scan parameters and T2-weigthed acquisition were as we described previously (13–15, 20). Axial 2D multi slice T2-weighted images of brain were acquired with TR = 4,000 ms, TE = 60 ms, FOV = 19.2 mm × 19.2 mm, matrix 192 mm × 192 mm. In order to assess BBB permeability, the post-contrast T1 was obtained 10 min after the administration of gadopentetate dimeglumine (Gd-DTPA) (Magnevist) with dosage of 0.2 mmol/kg bodyweight, as described (13–15, 21). Axial 2D multi slice T1-weighted images of brain were acquired with TR = 322 ms, TE = 10.5 ms, FOV = 28 mm × 28 mm, matrix 256 mm × 256 mm. During MRI scan, the animal's respiration was continually monitored by a small animal monitoring and gating system (SA Instruments) *via* a pillow sensor positioned under the abdomen. Mice were placed on a heated circulating water blanket (Bruker) and the normal body temperature (36–37°C) was maintained. The MRI data were analyzed with Image J software (NIH).

Cell Isolation and Flow Cytometry

Quantitative analysis of immune cell subsets and cell apoptosis were prepared from brain tissue and stained with fluorochrome-conjugated antibodies as described (13–15, 22). At day 3 after NMO, we isolated single cell suspension from the brain. Briefly, mice were deeply anesthetized and brain was removed immediately after perfusion with PBS. For CNS immune cell infiltration, brain tissue was cut into small pieces and digested with 1 mg/ml collagenase in 10 mM Hepes/NaOH buffer at 37°C for 1 h. The cell pellet was re-suspended in 70% percoll, then overlaid with 30% percoll. After centrifugation, the cell monolayer between 30 and 70% percoll interface was harvested as mononuclear cells. For astrocyte and cell death analysis, we harvested the brain and homogenized with 70 µm nylon cell strainers in PBS, then, we removed the myelin using 30% percoll with the centrifuge at 700 *g* for 10 min. The cell pellet was collected for analysis of Caspase3 and IL-15 expression.

We used flow cytometry to analyze leukocyte subsets and neural cell apoptosis. Single cell suspensions were stained with antibodies and appropriate isotype controls. All antibodies were purchased from BD Bioscience or eBioscience, Inc. unless otherwise indicated. The procedure of cell staining followed the manual protocol. The following antibodies were used: CD3 (145-2C11), NK1.1 (PK136), CD8 (53-6.72), CD45 (30-F11), CD11b (M1/70), CD4 (GK1.4), Ly6G/C (RB6-8C5), glial fibrillary acidic protein (GFAP) (GA5), Caspase 3 (3G2). Flow cytometric data were acquired on a FACSAria flow cytometer (BD Bioscience) and analyzed with Flow Jo software version 7.6.1.

Immunofluorescence and H&E Staining

Mice were terminally anesthetized and perfused with PBS followed by 4% PFA. Brains were removed and embedded in paraffin. 5-µm thick coronal sections were deparaffinized and rehydrated in serial ethanol. For immunofluorescence staining, sections were permeabilized with 0.3% TritonX-100 for 15 min, then incubated with blocking solution consisting of 5% donkey serum,

followed by incubating with antibodies against GFAP (Abcam), AQP4 (Santa Cruz), Claudin5 (Life Tech) at 4°C overnight. After washing with PBS, slices were incubated with appropriate fluorochrome conjugated secondary antibodies: donkey anti-rabbit 488 (Invitrogen), donkey anti-goat 594 (Invitrogen), donkey anti-rabbit 546 (Invitrogen), respectively, at room temperature for 1 h. Finally, all slices were incubated with fluoro-shield mounting medium with DAPI (Abcam). Images were taken with a fluorescence microscope (model BX-61, Olympus). To get the image with the whole lesion in each slice, we took 10–15 visual fields in a row under a × 40 field of microscope around the lesion site (GFAP and AQP4 loss), then merged these images into a bigger one using the photoshop7.0 software. For H&E Staining, tissue sections were stained with hematoxylin and eosin. Images were taken with a microscope (model BX-61, Olympus). The data were quantified using ImageJ.

Primary Astrocytes Culture

Primary cortical astrocytes were prepared as previously described (13–15). Briefly, mixed cortices were removed from 1 to 3 days old WT and IL-15^{tg} pups and minced with scissors in ice-cold HBSS (Gibco), then digested with 0.25% trypsin solution (Gibco) at 37°C for 30 min. The dissociated cells were rinsed and resuspended in high glucose DMEM and counted. Cells were plated in 35-mm culture dishes at a density of 2.5×10^4 cells/cm^2. After 2 days, the medium [High glucose DMEM (Gibco) + 10% heat-inactivated FBS (Gibco) + 1% Penicillin/Streptomycin (Gibco)] was changed to remove cell debris. 7–8 days later, we passaged the first split astrocyte population at the appropriate cell concentration for the experiment. The purity of astrocytes was up to 95%.

Complement–Dependent Cytotoxicity (CDC)

Cultured astrocyte were plated onto 96-well microplates at 20,000 cells/well and grown at 37°C/5% CO_2 for 18–24 h. Cells were washed with PBS for three times and incubated on ice with 50 µl of rAb-53 for 30 min in DMEM (Gibco). Thereafter, 2.5 µl pooled normal HC serum (Innovative Research) was added to the cells and cultured for additional 60 min at 37°C. Cytotoxicity was measured by lactate dehydrogenase (LDH) release assay using a commercial kit (Sigma) according to the manufacturer's instructions (23). LDH release from cells was calculated as a percentage of total LDH in each sample.

Western Blot

Cells were lysed with cell lysis buffer (Cell Signaling Technology) containing protease inhibitor cocktail (Sigma-Aldrich) and phosphatase inhibitor mixture (Sigma-Aldrich) for 30 min on ice. The samples were centrifuged at 14,000 rpm for 15 min at 4°C to remove cell debris. Protein concentration was determined using a BCA protein assay kit (Pierce). Proteins were subjected to SDS-PAGE gel (Bio-Rad) and transferred to a PVDF membrane (Millipore). The membrane was blocked with 5% non-fat milk in TBS solution containing 0.05% Tween-20 for 1 h at room temperature. Then the membrane was incubated with antibodies against GAPDH (1:1,000), IκB (1:500, Cell signaling pathway), and pIκB (1:500, Cell signaling pathway) overnight at 4°C. After washing three times with TBST solution, the membrane was incubated with HRP-conjugated goat anti-rabbit (1:2,000; Zymed) for 1 h at room temperature. Immuno-reactive bands were detected using enhanced chemiluminescence (Thermo Scientific) and captured with an Odyssey Fc Imager (Li-cor biosciences Inc.). Western blot data were analyzed with ImageJ software.

Statistics

We determined each sample size by power analysis using a significance level of $\alpha = 0.05$ with 80% power to detect statistical differences. SAS 9.1 software (SAS Institute Inc., Cary, NC, USA) was used for power analysis and sample-size calculations. All values are expressed as mean ± SE. Statistical data analyses were performed using Graphpad Primes 6 software. Two-tailed unpaired Student's *t*-test was used to analyze the statistical significance of two groups. Where appropriate, One-way ANOVA were used for three or more groups. Values of $p < 0.05$ will be considered significant.

RESULTS

Astrocyte-Targeted Expression of IL-15 Is Upregulated in NMO Mice

Astrocytic IL-15 is inducible and has a dual role on brain injury in different CNS diseases (17, 18), to assess whether astrocytic IL-15 level was increased in NMO, we compared the expression of IL-15 in astrocytes in the brain tissue from the ipsilateral hemisphere to the contralateral hemisphere or sham control at day 3 after injection of recombinant NMO-IgG (rAb-53) and HC. Flow cytometry data show that the amount of IL-15 in astrocytes is much higher after NMO (**Figures 1A,B**), indicating that astrocytic IL-15 expression is related to NMO progression.

Astrocyte-Targeted Expression of IL-15 Reduces Lesion Size in NMO Mice

To investigate the effect of astrocytic IL-15 in NMO, we adopted IL-15^{tg} mice in which IL-15 expression is controlled by a GFAP promotor, as we previously reported (13–15). The expression level of IL-15 in astrocytes is prominently higher in IL-15^{tg} mice as compared to WT littermates. Importantly, these transgenic mice develop normally without showing any abnormal behavior or infertility, and the current transgenic mice show normal nerve cell properties and immune system, no inflammatory infiltrates were seen in brain tissues of normal IL-15^{tg} mice.

To further understand whether astrocyte-derived IL-15 affects NMO lesion severity, we induced an animal NMO model through intracerebral injection of HC and recombinant NMO-IgG (rAb-53) in IL-15^{tg} mice and WT littermates. At day 3, 7T-MRI scans combined with conventional immunofluorescence staining for AQP4 and GFAP were used to evaluate NMO lesion size. MRI data show that the group of IL-15^{tg} mice have markedly reduced NMO lesion size as compared to WT littermates (IL-15^{tg} vs WT: 2.40 ± 0.58 vs 5.23 ± 0.45 mm^3) (**Figures 2A,B**), corresponding to less loss of GFAP and AQP4 immunostaining in the region of injection site (IL-15^{tg} vs WT: 9.00 ± 2.1% vs 17.24 ± 1.9%)

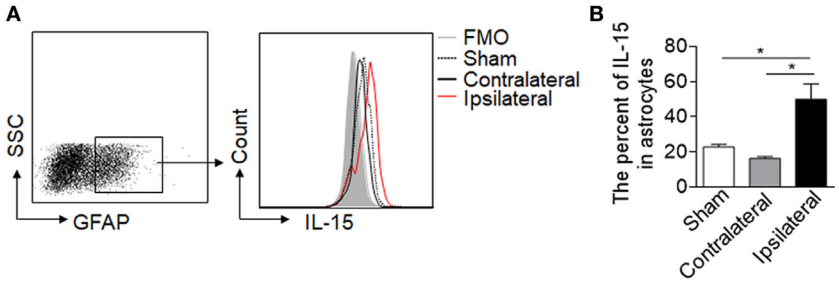

FIGURE 1 | Upregulation of IL-15 in astrocytes after neuromyelitis optica (NMO) induction. Mouse brains were injected with 2 μg rAb-53 plus 3 μl human complement. At day 3 after NMO induction, the brain tissues were harvested for flow cytometry analysis. **(A,B)** The data show expression of IL-15 in astrocytes from the tissue of the ipsilateral and contralateral hemisphere, as well as sham control, $n = 4$ mice/group. Data represent the mean ± SE, $^*p < 0.05$.

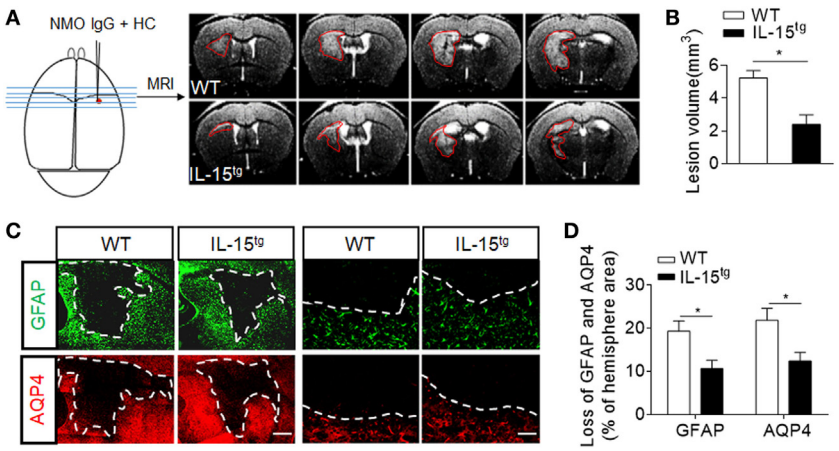

FIGURE 2 | Reduced brain lesion severity and astrocytes loss in IL-15^{tg} mice subjected to injection of neuromyelitis optica (NMO)-IgG (rAb-53) and human complement (HC). Mouse brains were injected with 2 μg rAb-53 plus 3 μl HC. At day 3 after NMO induction, visualization and quantification of NMO lesion size were taken with T2-weighted images obtained with a 7 T MRI scanner. Representative of sequential MRI images of NMO lesion in the brain from WT littermates and IL-15^{tg} mice **(A)**. The left schematic view of brain denotes the injection position (red dot) and the region of brain corresponding to the MRI image in the right. Red lines in the MRI images indicate the NMO lesion area. Quantification of NMO lesion volumes in MRI images **(B)**, $n = 12$ mice/group. **(C)** Immunostaining of glial fibrillary acidic protein (GFAP) and aquaporin-4 (AQP4) in NMO lesion at day 3 after NMO induction. Image of whole lesion area (left panel) represented by loss of GFAP and AQP4 immunostaining. High magnification of immunostaining of GFAP and AQP4 around NMO lesion was shown in the right panel. White dashed line represents lesion area. Scale bar = 1mm (left panel) and 100 μm (right panel). **(D)** Quantification of the NMO lesion size with GFAP and AQP4 loss in the sections of WT and IL-15^{tg} mice, $n = 5$ mice/group. Data represent the mean ± SE, $^*p < 0.05$.

(**Figures 2C,D**). A higher magnification of the lesion shows the characteristics of AQP4 and GFAP loss and reactive astrocytes existing around the lesion area (**Figure 2C**). These results indicate that astrocytic IL-15 may attenuate brain injury after NMO.

Astrocyte-Targeted Expression of IL-15 Attenuates BBB Leakage and Tight-Junction Loss in NMO Mice

Astrocytes, the target of NMO-IgG, are essential for the formation and maintenance of the BBB. The findings that astrocytic IL-15 attenuates astrocyte loss, prompted us to consider that BBB integrity may be preserved in IL-15^{tg} mice. As we expected, BBB permeability is more prominent in WT mice than that in IL-15^{tg} mice, as measured by T1 MRI scan (**Figures 3A,B**). The protein level of claudin 5, a tight junction protein, is also much higher in IL-15^{tg} mice as compared to WT littermates (**Figures 3C,D**). These data further supported that astrocyte-specific expression of IL-15 could prevent BBB damage.

Astrocyte-Targeted Expression of IL-15 Reduces Brain Infiltration of Immune Cell Subsets in NMO Mice

Injection of NMO-IgG and HC in mouse brain produces marked inflammation. Leukocyte infiltration and microglia activation contribute to the brain inflammation in NMO development. IL-15, as an inflammatory cytokine, has functions on a wide range of immune cells. To investigate the inflammation and immune response in the brain of WT and IL-15^{tg} mice, we used H&E staining (**Figures 4A,B**) and flow cytometry to detect the subsets of leukocytes, as well as microglia, the gating strategy as in **Figure 4C**. We did not observe a significant difference in the

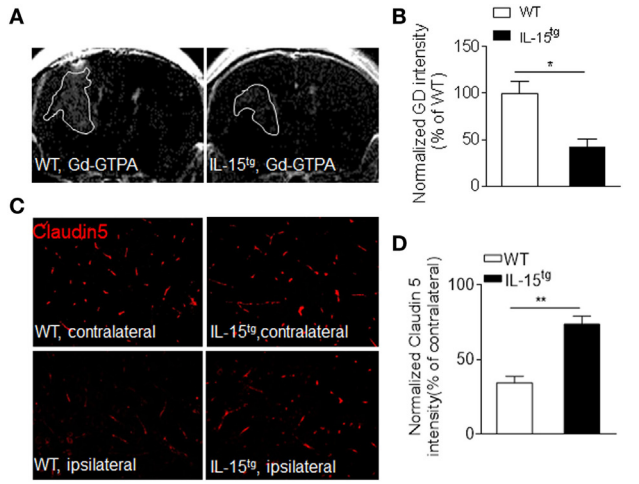

FIGURE 3 | Reduced blood–brain barrier permeability in IL-15^{tg} mice subjected to neuromyelitis optica (NMO) induction. **(A,B)** T1-weighted MRI were performed to visualize and quantify Gd-DTPA leakage into the brain parenchyma in the indicated groups at day3 after NMO induction. White line indicates Gd-GTPA leakage area. **(C,D)** Immunostaining of tight junction protein, Claudin5, in ipsilateral NMO lesion area and contralateral corresponding normal area and the quantification of the intensity. $n = 10$ sections from three mice/group. Data represent the mean ± SE, $^*p < 0.05$, $^{**}p < 0.01$.

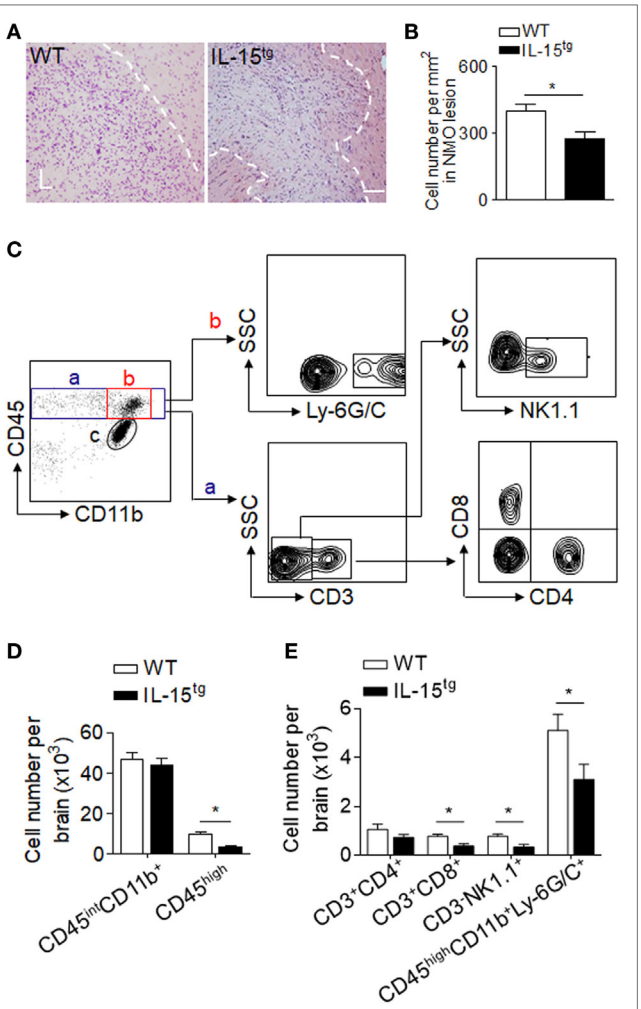

FIGURE 4 | Astrocyte-targeted expression of IL-15 reduced CNS infiltration of immune cells. **(A,B)** H&E stains showed less cell density in neuromyelitis optica (NMO) lesions in IL-15^{tg} mice as compared to WT mice at day 3 after NMO induction. $n = 5$ mice/group. **(C–E)** CNS-invading immune cell subsets and microglia cell numbers were analyzed using flow cytometry at day 3 after NMO induction. Gating strategy of immune cells including macrophage and neutrophils (CD45^{high}CD11b$^+$ly6G/C$^+$), microglia (CD11b$^+$CD45^{inter}), CD4$^+$ T cells (CD45^{high}CD3$^+$CD4$^+$), CD8$^+$ T cells (CD45^{high} CD3$^+$CD8$^+$), NK cells (CD45^{high}CD3$^-$NK1,1$^+$) **(C)**. Cell number of microglia, CNS-invading immune cells (CD45^{high}), and immune cell subsets decreased in IL-15^{tg} mice as compared to WT mice after NMO induction **(D,E)**, $n = 5$ mice/group. Data represent the mean ± SE, $^*p < 0.05$.

number of CD45^{int}/CD11b$^+$ (microglia) in the brain between WT and IL-15^{tg} mice after NMO induction. In contrast, accumulation of CD45^{high} and Ly6G/C (macrophage and neutrophil), the prominent immune cells in lesions of patients with NMO, was markedly decreased in IL-15^{tg} mice (**Figure 4D**). In addition, IL-15^{tg} mice exhibited significantly reduced cell numbers of CD3, CD8, and NK cells in the brain as compared to WT littermates (**Figure 4E**). These data show that IL-15^{tg} mice have extensively decreased leukocyte infiltration in the brain compared to WT littermates, indicating that the contribution of astrocytic IL-15 to brain inflammation is likely dependent on BBB damage and astrocyte loss.

IL-15 Promotes the Survival of Astrocytes From CDC-Induced Cell Death

CDC-mediated astrocyte injury is the key event during NMO development, which initiates secondary inflammation and NMO lesion development. Our findings that astrocytic IL-15 reduces astrocyte loss and BBB damage indicate that IL-15 may have the function of inhibiting astrocyte injury induced by CDC. To answer this question, we analyzed the cell apoptosis of astrocytes in the brain after NMO induction. We found that both the percent and cell number of astrocytes expressing caspase3 is significantly reduced in IL-15^{tg} mice, suggesting that astrocytic IL-15 may have a function of resistance to CDC-mediated cell death (**Figure 5A**). While, there is no significant difference of astrocyte apoptosis in the contralateral hemisphere between WT and IL-15^{tg} mice after NMO (data not shown). To further confirm the protective role of astrocytic IL-15, we incubated primary cultured astrocytes from the brain of WT and IL-15^{tg} mice with 10 or 20 μg/ml NMO-IgG and 5% HC respectively. Cell viability was measured by LDH assay. The data show that cell death of astrocytes from IL-15^{tg} mice were reduced as compared to that from WT littermates when cultured with 10 or 20 μg/ml NMO IgG (**Figure 5B**). These findings demonstrate that IL-15 might be a survival factor for astrocytes from CDC induced by NMO-IgG and HC.

IL-15 Protects Astrocytes Against CDC *via* NF-κB Signaling Pathway

NF-κB pathway has been reported to be responsible for nucleated cells resistant to CDC-dependent cytotoxicity (24). To determine whether NF-κB is involved in CDC resistance of astrocytic

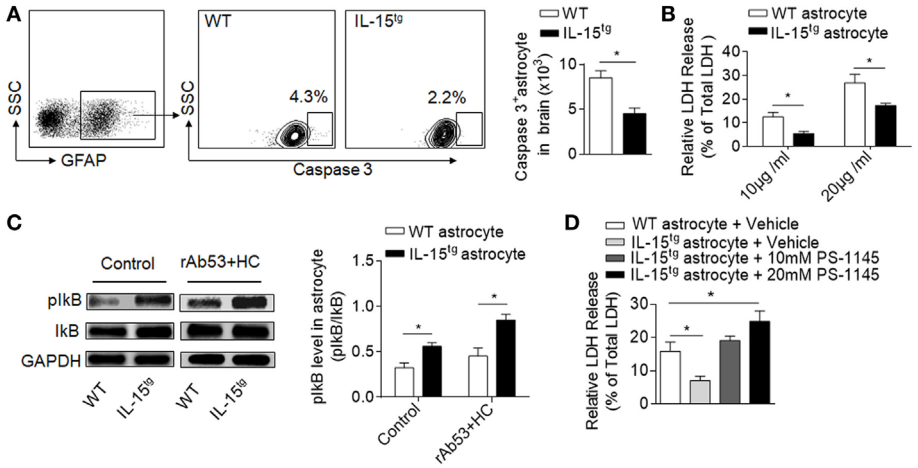

FIGURE 5 | IL-15 protects astrocyte from CDC-mediated astrocyte injury. **(A)** Gating strategy of astrocytes expressing Caspase 3 and quantification of cell number of Caspase 3+ astrocytes in WT and IL-15tg neuromyelitis optica (NMO) mice at day 3 (n = 5 mice/group). **(B)** Quantification of lactate dehydrogenase (LDH) release in cultured astrocytes isolated from WT littermates and IL-15tg mice incubated with recombinant NMO-IgG (rAb-53) (10 or 20 μg/ml) and 5% human complement (HC) for 60 min, cell viability was determined by LDH assay. Data represent the mean (±SE) of three independent experiments. **(C)** Western blot were performed to test activation of NF-κB signaling pathway in astrocytes treated with 10 μg/ml rAb-53 and 5% HC for 60 min, pIκB values are relative to IκB (three independent experiments). **(D)** PS-1145, a NF-κB pathway inhibitor, could attenuate the protection of astrocytic IL-15 on CDC-mediated cell damage *in vitro*. Data represent the mean (±SE) of three independent experiments, $^*p < 0.05$.

IL-15, we compared the protein levels of phosphorylated IκB in astrocytes. The data show that the level of pIκB is much higher in astrocytes from IL-15tg mice than in WT littermates when incubated with NMO-IgG with HC (**Figure 5C**), suggesting that IL-15 or NMO-IgG binding could activate NF-κB signaling pathway. To further demonstrate whether NF-κB is responsible for CDC resistance, we treated astrocytes with PS-1145, which specifically blocks NF-κB activation by inhibiting phosphorylation of IκB. The data show that pretreatment of PS-1145 make the astrocytes from IL-15tg mice more sensitive to complement-dependent necrosis (**Figure 5D**). These results together suggest that NF-κB pathway may contribute to the protective role of astrocytic IL-15 on CDC resistance after NMO.

DISCUSSION

The current study provides the first evidence that astrocyte-derived IL-15 can protect against NMO pathology. As documented here, astrocytic IL-15 can be a survival factor to attenuate astrocytes loss induced by CDC, together with attenuated BBB injury and CNS inflammation. IL-15 augments the survival of astrocytes against CDC *via* NF-κB signaling. In all, our results reveal IL-15 as a key factor to reduce astrocyte loss and CNS inflammation in NMO.

The finding that IL-15 is upregulated in astrocytes in NMO mice suggest that astrocytes can respond to NMO-IgG and CDC and modulate CNS inflammation. This is consistent with previous reports showing that astrocytes undergo dramatic changes of immune profiles including upregulation of chemokines and cytokines after the binding of NMO-IgG (25, 26). In particular, blockade of these factors could reduce cytotoxicity and preserve AQP4 protein level in cultured astrocytes (25). In contrast to the proinflammatory factors reported in this study, we found that astrocytic IL-15 reduces NMO severity and CNS inflammation, suggesting that astrocytes could play an active role in NMO pathology.

IL-15 is an inflammatory cytokine with a function on a wide range of immune cells (27, 28). Much evidence demonstrated that IL-15 can boost immune cells to exacerbate disease progression such as rheumatoid arthritis and stroke (13–15, 29). However, there are still documents, which demonstrated that IL-15 is beneficial to experimental autoimmune encephalomyelitis (17, 18). In NMO mice, we found that IL-15 is dramatically upregulated in astrocytes. Using genetic manipulation, we demonstrated that astrocyte-specific expression of IL-15 could attenuate NMO pathology severity. These discrepancies between the roles of IL-15 in different CNS diseases may contribute to the setting of these diseases and the pleiotropic function of IL-15. In the setting of NMO, CDC-mediated astrocytes loss plays a vital role in NMO progression, which, to large extent, determines the BBB integrity and immune cell infiltration. Less astrocytes damage in IL-15tg mice is likely to produce less immune cell infiltration. Additionally, it is noteworthy that IL-15 is also beneficial to neuron growth and development (30), whether IL-15 has the direct protective function on neuron survival or enhancing neurodegeneration needs further investigation.

The finding that IL-15 reduces NMO severity in mice and protects astrocytes against CDC has clinical relevance. As above described, CDC-induced astrocytes damage plays a key role in NMO pathology. As such, the use of IL-15 could be a candidate for further advanced studies to test its effectiveness to reduce NMO pathology. However, it is also noteworthy that the effect of exogenous IL-15 may be different from endogenous IL-15 as trans-presentation may be needed for the elaboration of IL-15 efficacy. In addition, the efficacy of IL-15 may vary depending

on injected doses and their availability to various cell types that express IL-15 receptors. Future more advanced investigations are needed to better understand the role of IL-15 in NMO pathology. Although treatments targeting the CDC process have been investigated including complement inhibitor or NMO-IgG mutant (31, 32), no treatments are available to directly boost astrocyte survival and reduce CNS inflammation. Our results in this study suggest that IL-15 may serve as a potential therapy or at least a complementary approach to attenuate NMO pathology.

There are also limitations in this study. First, we induced NMO in mice by direct injection of NMO-lgG and HC into brain parenchyma, which may not fully mimic the scenario of pathological events in patients with NMO, such as the trigger of BBB breakdown, neuroinflammation, and peripheral immune response (33–35). Therefore, future studies are needed to verify our findings in other NMO animal models. Second, the beneficial role of IL-15 might be related to multiple cellular targets including CNS intrinsic cells and peripheral immune cell subsets. Because different doses of IL-15 may show different influences in nerve cells or immune cells, it is needed to define whether the protection of astrocytic IL-15 in NMO depends on available IL-15 concentration. Third, IL-15 receptors are widely expressed by CNS cell types such as neural progenitors. Therefore, the role of IL-15 in neuronal function or neurorepair warrant further investigations in future studies.

In conclusion, our studies provide novel insight astrocytic IL-15 in NMO pathology.

ETHICS STATEMENT

The study was performed in accordance with the National Institutes of Health Guide for the Care and Use of Laboratory Animals. All experimental procedures were approved by Animal Care and Use Committees of Barrow Neurological Institute (Arizona, USA) and Tianjin Neurological Institute (Tianjin, China).

AUTHOR CONTRIBUTIONS

ML, QL, and F-DS formulated the study concept and wrote the paper. ZL, JH, and HR performed experiments. ML, ZL, and C-GM analyzed the data, interpreted the results, and assisted preparation of the manuscript.

ACKNOWLEDGMENTS

We would like to thank Dr. Jeffrey L. Bennett for providing us recombinant monoclonal NMO-IgG (rAb-53), and thank Kristofer Wood for editorial assistance. This study was supported in part by National Science Foundation of China grants 91642205, 81471535, and 81701176; The Science and Technology Development Fund of Tianjin Education Commission for higher Education 2016YD04; and National Multiple Sclerosis Society research grant RG-1507-05318.

REFERENCES

1. Hinson SR, Lennon VA, Pittock SJ. Autoimmune AQP4 channelopathies and neuromyelitis optica spectrum disorders. *Handb Clin Neurol* (2016) 133:377–403. doi:10.1016/B978-0-444-63432-0.00021-9
2. Wingerchuk DM, Lennon VA, Lucchinetti CF, Pittock SJ, Weinshenker BG. The spectrum of neuromyelitis optica. *Lancet Neurol* (2007) 6:805–15. doi:10.1016/S1474-4422(07)70216-8
3. Lucchinetti CF, Mandler RN, McGavern D, Bruck W, Gleich G, Ransohoff RM, et al. A role for humoral mechanisms in the pathogenesis of Devic's neuromyelitis optica. *Brain* (2002) 125:1450–61. doi:10.1093/brain/awf151
4. Jarius S, Wildemann B. AQP4 antibodies in neuromyelitis optica: diagnostic and pathogenetic relevance. *Nat Rev Neurol* (2010) 6:383–92. doi:10.1038/nrneurol.2010.72
5. Lennon VA, Kryzer TJ, Pittock SJ, Verkman AS, Hinson SR. IgG marker of optic-spinal multiple sclerosis binds to the aquaporin-4 water channel. *J Exp Med* (2005) 15(202):473–7. doi:10.1084/jem.20050304
6. Sabater L, Giralt A, Boronat A, Hankiewicz K, Blanco Y, Llufriu S, et al. Cytotoxic effect of neuromyelitis optica antibody (NMO-IgG) to astrocytes: an in vitro study. *J Neuroimmunol* (2009) 30(215):31–5. doi:10.1016/j.jneuroim.2009.07.014
7. Colombo E, Farina C. Astrocytes: key regulators of neuroinflammation. *Trends Immunol* (2016) 37:608–20. doi:10.1016/j.it.2016.06.006
8. Vaknin-Dembinsky A, Karussis D, Avichzer J, Abramsky O. NMO spectrum of disorders: a paradigm for astrocyte-targeting autoimmunity and its implications for MS and other CNS inflammatory diseases. *J Autoimmun* (2014) 54:93–9. doi:10.1016/j.jaut.2014.05.004
9. Yang JF, Tao HQ, Liu YM, Zhan XX, Liu Y, Wang XY, et al. Characterization of the interaction between astrocytes and encephalitogenic lymphocytes during the development of experimental autoimmune encephalitomyelitis (EAE) in mice. *Clin Exp Immunol* (2012) 170:254–65. doi:10.1111/j.1365-2249.2012.04661.x
10. McInnes IB, Leung BP, Sturrock RD, Field M, Liew FY. Interleukin-15 mediates T cell-dependent regulation of tumor necrosis factor-alpha production in rheumatoid arthritis. *Nat Med* (1997) 3:189–95. doi:10.1038/nm0297-189
11. Sakai T, Kusugami K, Nishimura H, Ando T, Yamaguchi T, Ohsuga M, et al. Interleukin 15 activity in the rectal mucosa of inflammatory bowel disease. *Gastroenterology* (1998) 114:1237–43. doi:10.1016/S0016-5085(98)70430-5
12. Gomez-Nicola D, Valle-Argos B, Pita-Thomas DW, Nieto-Sampedro M. Interleukin 15 expression in the CNS: blockade of its activity prevents glial activation after an inflammatory injury. *Glia* (2008) 56:494–505. doi:10.1002/glia.20628
13. Li HD, Li M, Shi E, Jin WN, Wood K, Gonzales R, et al. A translocator protein 18 kDa agonist protects against cerebral ischemia/reperfusion injury. *J Neuroinflammation* (2017) 28(14):151. doi:10.1186/s12974-017-0921-7
14. Li M, Li Z, Ren H, Jin WN, Wood K, Liu Q, et al. Colony stimulating factor 1 receptor inhibition eliminates microglia and attenuates brain injury after intracerebral hemorrhage. *J Cereb Blood Flow Metab* (2017) 37:2383–95. doi:10.1177/0271678X16666551
15. Li M, Li Z, Yao Y, Jin WN, Wood K, Liu Q, et al. Astrocyte-derived interleukin-15 exacerbates ischemic brain injury via propagation of cellular immunity. *Proc Natl Acad Sci U S A* (2017) 17(114):E396–405. doi:10.1073/pnas.1612930114
16. Saikali P, Antel JP, Pittet CL, Newcombe J, Arbour N. Contribution of astrocyte-derived IL-15 to CD8 T cell effector functions in multiple sclerosis. *J Immunol* (2010) 15(185):5693–703. doi:10.4049/jimmunol.1002188
17. Gomez-Nicola D, Spagnolo A, Guaza C, Nieto-Sampedro M. Aggravated experimental autoimmune encephalomyelitis in IL-15 knockout mice. *Exp Neurol* (2010) 222:235–42. doi:10.1016/j.expneurol.2009.12.034
18. Wu X, Pan W, He Y, Hsuchou H, Kastin AJ. Cerebral interleukin-15 shows upregulation and beneficial effects in experimental autoimmune encephalomyelitis. *J Neuroimmunol* (2010) 223:65–72. doi:10.1016/j.jneuroim.2010.04.001
19. Bennett JL, Lam C, Kalluri SR, Saikali P, Bautista K, Dupree C, et al. Intrathecal pathogenic anti-aquaporin-4 antibodies in early neuromyelitis optica. *Ann Neurol* (2009) 66:617–29. doi:10.1002/ana.21802
20. Liu Q, Jin WN, Liu Y, Shi K, Sun H, Zhang F, et al. Brain ischemia suppresses immunity in the periphery and brain via different neurogenic innervations. *Immunity* (2017) 21(46):474–87. doi:10.1016/j.immuni.2017.02.015

21. Bell JC, Liu Q, Gan Y, Liu Q, Liu Y, Shi FD, et al. Visualization of inflammation and demyelination in 2D2 transgenic mice with rodent MRI. *J Neuroimmunol* (2013) 15(264):35–40. doi:10.1016/j.jneuroim.2013.09.008
22. Ren H, Kong Y, Liu Z, Zang D, Yang X, Wood K, et al. Selective NLRP3 (pyrin domain-containing protein 3) inflammasome inhibitor reduces brain injury after intracerebral hemorrhage. *Stroke* (2018) 49:184–92. doi:10.1161/STROKEAHA.117.018904
23. Liu Q, Tang Z, Gan Y, Wu W, Kousari A, La Cava A, et al. Genetic deficiency of beta2-containing nicotinic receptors attenuates brain injury in ischemic stroke. *Neuroscience* (2014) 3(256):170–7. doi:10.1016/j.neuroscience.2013.10.049
24. Gancz D, Lusthaus M, Fishelson Z. A role for the NF-kappaB pathway in cell protection from complement-dependent cytotoxicity. *J Immunol* (2012) 15(189):860–6. doi:10.4049/jimmunol.1103451
25. Haruki H, Sano Y, Shimizu F, Omoto M, Tasaki A, Oishi M, et al. NMO sera down-regulate AQP4 in human astrocyte and induce cytotoxicity independent of complement. *J Neurol Sci* (2013) 15(331):136–44. doi:10.1016/j.jns.2013.05.035
26. Howe CL, Kaptzan T, Magana SM, Ayers-Ringler JR, LaFrance-Corey RG, Lucchinetti CF. Neuromyelitis optica IgG stimulates an immunological response in rat astrocyte cultures. *Glia* (2014) 62:692–708. doi:10.1002/glia.22635
27. Ma A, Koka R, Burkett P. Diverse functions of IL-2, IL-15, and IL-7 in lymphoid homeostasis. *Annu Rev Immunol* (2006) 24:657–79. doi:10.1146/annurev.immunol.24.021605.090727
28. Waldmann TA. The biology of interleukin-2 and interleukin-15: implications for cancer therapy and vaccine design. *Nat Rev Immunol* (2006) 6:595–601. doi:10.1038/nri1901
29. Diaz-Torne C, Ortiz de Juana MA, Geli C, Canto E, Laiz A, Corominas H, et al. Rituximab-induced interleukin-15 reduction associated with clinical improvement in rheumatoid arthritis. *Immunology* (2014) 142:354–62. doi:10.1111/imm.12212
30. Huang YS, Cheng SN, Chueh SH, Tsai YL, Liou NH, Guo YW, et al. Effects of interleukin-15 on neuronal differentiation of neural stem cells. *Brain Res* (2009) 22(1304):38–48. doi:10.1016/j.brainres.2009.09.009
31. Phuan PW, Zhang H, Asavapanumas N, Leviten M, Rosenthal A, Tradtrantip L, et al. C1q-targeted monoclonal antibody prevents complement-dependent cytotoxicity and neuropathology in in vitro and mouse models of neuromyelitis optica. *Acta Neuropathol* (2013) 125:829–40. doi:10.1007/s00401-013-1128-3
32. Tradtrantip L, Zhang H, Saadoun S, Phuan PW, Lam C, Papadopoulos MC, et al. Anti-aquaporin-4 monoclonal antibody blocker therapy for neuromyelitis optica. *Ann Neurol* (2012) 71:314–22. doi:10.1002/ana.22657
33. Bradl M, Lassmann H. Experimental models of neuromyelitis optica. *Brain Pathol* (2014) 24:74–82. doi:10.1111/bpa.12098
34. Jones MV, Collongues N, de Seze J, Kinoshita M, Nakatsuji Y, Levy M. Review of Animal models of neuromyelitis optica. *Mult Scler Relat Disord* (2012) 1:174–9. doi:10.1016/j.msard.2012.06.003
35. Li M, Yan Y. Experimental models of neuromyelitis optica: current status, challenges and future directions. *Neurosci Bull* (2015) 31:735–44. doi:10.1007/s12264-015-1552-6

Conflict of Interest Statement: The authors declare that the research was conducted in the absence of any commercial or financial relationships that could be construed as a potential conflict of interest.

frontiers in Immunology

ORIGINAL RESEARCH
published: 04 April 2018
doi: 10.3389/fimmu.2018.00634

Semaphorin3A: A Potential Therapeutic Tool for Lupus Nephritis

*Jacob Bejar[1], Ofra Kessler[2], Adi D. Sabag[3], Edmond Sabo[4], Ofer Ben Itzhak[4], Gera Neufeld[2] and Zahava Vadasz[3]**

[1] The Department of Pathology, Bnai-Zion Medical Center, Haifa, Israel, [2] The Bruce Rappaport Medical School, Technion – Israel Institute of Technology, Haifa, Israel, [3] The Division of Allergy and Clinical Immunology, Bnai-Zion Medical Center, Haifa, Israel, [4] The Department of Pathology, RAMBAM Medical Center, Haifa, Israel

Background: The immune regulatory properties of semaphorin3A (sema3A) (both innate and adaptive) are well established in many *in vitro* studies. The injection of sema3A into a mice model of rheumatoid arthritis was proven to be highly beneficial, both in attenuating clinical symptoms and in decreasing inflammatory mechanisms.

Objectives: This study was designed in order to assess the possible therapeutic benefits of sema3A following its injection into female NZB/W mice.

Methods: Forty-eight NZB/W mice were recruited for this study. Thirty mice were treated as a "prevention group" and 18 were used as a "treatment group." Eight-week-old mice were acclimated and then divided into the two abovementioned groups.

Results: The injection of sema3A into young mice (at week 12) before the onset of disease (the prevention group) delayed the appearance of proteinuria. Here, the median time to severe proteinuria was 110 days, 95% CI: 88–131. However, in mice in which the empty vector was injected, the median time to severe proteinuria was 63 days, 95% CI: 0–139. sema3A treatment, significantly reduced renal damage, namely, it prevented the deposition of immune complexes in the glomeruli. When sema3A was injected at the onset of proteinuria (the treatment group), aiming to treat rather than to prevent disease in these mice, survival was increased and the deterioration of proteinuria was delayed.

Conclusion: Semaphorin3A is highly beneficial in reducing lupus nephritis in NZB/W mice. It delays the appearance and deterioration of proteinuria, and increases the survival rates in these mice. The regulatory mechanisms of sema3A involve both innate and adaptive immune responses. Further studies will establish the idea of applying sema3A in the treatment of lupus nephritis.

Keywords: semaphorin3A, NZB mice model, immune regulation, innate immunity, lupus nephritis

OPEN ACCESS

Edited by:
Moncef Zouali, Institut National de la Santé et de la Recherche Médicale (INSERM), France

Reviewed by:
Nina Ivanovska, Institute of Microbiology (BAS), Bulgaria
Jue Hou, Virginia Mason Medical Center, United States

****Correspondence:***
Zahava Vadasz
zahava.vadas@b-zion.org.il

Specialty section:
This article was submitted to Molecular Innate Immunity, a section of the journal Frontiers in Immunology

Received: *15 January 2018*
Accepted: *14 March 2018*
Published: *04 April 2018*

Citation:
Bejar J, Kessler O, Sabag AD, Sabo E, Itzhak OB, Neufeld G and Vadasz Z (2018) Semaphorin3A: A Potential Therapeutic Tool for Lupus Nephritis. Front. Immunol. 9:634. doi: 10.3389/fimmu.2018.00634

INTRODUCTION

Systemic lupus erythematosus (SLE) is a multi-system autoimmune disease, which involves the skin, synovia, kidneys, and the brain. Long-lasting organ damage mainly, the kidneys, is associated with a high rate of morbidity and mortality. Standard therapy (steroids and immune-suppressive drugs) though beneficial and improving survival, is associated with frequent and sometimes severe side effects. Therefore, safe and better focused therapies are continuously being developed. Of these,

belimumab (anti-B cell activating factor) is considered to be beneficial in milder cases of SLE (1); however, more therapies are definitely required. In this respect, the possibility of targeting regulatory cells or regulatory molecules aiming to reduce inflammation and restore self-tolerance have recently been suggested to be a beneficial strategy in the field of autoimmunity. Semaphorins are widely reported to be involved in the regulation of inflammatory immune responses. Special attention has been given to semaphorin3A (sema3A) since it is valued as one of the important regulators in suppressing immune-mediated inflammation (2). The expression of sema3A and its operative receptors, namely, neuropilin-1 (NP-1), NP-2, and plexins were reported to be increased on differentiating macrophages as well as on T regulatory cells, thereby resulting in the inhibition of T cell proliferation and pro-inflammatory cytokine secretion (3, 4). Recently, we reported that sema3A was highly expressed on B regulatory cells (CD19+CD25highCD1dhigh) suggesting that it was a possible marker for this subset of cells (5). Assuming that sema3A is involved in the pathogenesis of SLE, we designed a study where the serum level of sema3A was analyzed. Low sema3A levels were found to be negatively correlated with SLE disease activity, renal involvement, and the detection of specific autoantibodies. In this study, we were able to demonstrate increased sema3A expression on B regulatory (B reg) cells, namely, CD19+CD25high CD1dhigh. As expected, the expression of sema3A on B reg cells was significantly lower in SLE patients when compared to those in healthy individuals, thereby suggesting that this finding is partially responsible for B cell auto-reactivity in SLE (6). The overexpression of TLR-9 and increased production of pro-inflammatory cytokines such as IL-6 and IFNs is highly typical for autoreactive B cells in SLE. In many studies, these markers were reported to be positively associated with SLE disease activity as well as with increased titers of anti-dsDNA antibodies. Since it was considered to be a potent immune regulator, sema3A was cocultured with activated B cells, isolated from SLE patients, with the goal of evaluating its ability to lower TLR-9 expression. The addition of sema3A to activated B cells in culture downregulated TLR-9 expression, which raised the possibility of applying sema3A as a therapeutic option for SLE treatment (7). B-cell overactivity was also shown to be also regulated by the expression of CD72 on B cells. Following the ligation of CD72, suppressive signals are induced and B cell receptor positive signaling is downregulated, maintaining by this, self-tolerance. Keeping this in mind, we conducted a study, which sought to compare the expression of CD72 on activated B cells from SLE patients with that from healthy individuals. The expression of CD72 on B cells from SLE patients was significantly lower when compared to that in the controls. Decreased CD72 expression was inversely correlated with SLE disease activity, specifically with lupus nephritis, with high titers of anti-dsDNA antibodies and with low levels of complement (8). Here again, when purified B cells were co-cultured with recombinant sema3A, we noticed a significant upregulation of CD72 in both the normal controls and SLE patients (though they were lower than in the normal controls), suggesting its beneficial usage in many autoimmune diseases (9). The expression of sema3A was also assessed in the glomeruli and tubuli of suffering from lupus nephritis and found to be in inverse correlation with renal function assays. These findings suggested that sema3A is involved in lupus glomerulonephritis and could have a protective role (10). Taking into account all of the above factors, we designed this *in vivo* study with the aim of assessing the beneficial effect of injecting sema3A into female NZB/W mice.

Our results will show that sema3A has both therapeutic and preventive properties.

MATERIALS AND METHODS

Mice Strains

Forty-eight female NZB/W mice were recruited for this study. Thirty mice were studied as a "prevention group" and 18 mice as a "treatment group." Eight-week-old mice were acclimated and then were divided into the two above mentioned groups. The study was approved by the Israeli Ethical Committee for designing studies on animal models. The study was given the approval number of IL-15-12-360.

Study Design

Prevention Group

Fifteen mice were injected with a recombinant human sema3A containing plasmid and another 15 were injected with empty vector cDNA and followed as a control group. Both groups were injected at the age of 12 weeks (before the appearance of proteinuria), every 3 weeks, for a total of three injections. They were followed until proteinuria appeared and when proteinuria persisted in the range of +3 (>300 mg/ml) they were sacrificed.

Treatment Group

Eight mice were injected with a recombinant human sema3A plasmid and eight were injected with empty vector cDNA and used as a control group. In this case, mice were injected when proteinuria was +2 (>100 mg/ml) (around 25–27 weeks of age) every 3 weeks, for a total of three injections. They were followed for the extent of proteinuria, weight loss, and their natural survival rate until they died.

Expression Plasmids

The following specific primers were used to construct an expression vector cDNA containing human sema3A: 5′-aacgggggcttttcatcc 3′-cccttctcacatcactcatgct. The sema3A cDNA was cloned from HUVEC (human umbilical vein endothelial cells) mRNA using RT-PCR, following sub-cloning into the NSPI-CMV-myc-his lentiviral expression vector. A FLAG epitope tag was added upstream to the stop codon of sema3A as described (11).

Hydroporation Method of Injection

Fifty micrograms of cDNA (recombinant human sema3A or empty vector) was injected in 2 ml of PBS per mouse. The injection was performed rapidly (during 5–7 s, as was described earlier) (12). In brief, a rapid injection of a large volume (above 10% of body weight) of solution (with or without any substance dissolved in it) *via* the tail vein can cause the accretion of the injected solution in the inferior vena cava. This is caused by the injection protocol of a large volume that exceeds the pump capacity of the mouse's heart.

As a result of this failure, high pressure develops in the venous region, and this causes a retrograde movement of the solution into the liver. The reason for this retrograde movement is the direct vascular connection of the liver to the inferior vena cava. As a result of this, the pore sizes of the liver fenestrae are enlarged and the membrane of the hepatocytes is permeabilized, allowing for the delivery of the injected material into the hepatocytes and over time trapping it inside. This method of hydroporation allows hepatocytes to become a source for the production of the injected recombinant protein of interest, and its gradual release into the blood's circulation. Serum levels of human sema3A were analyzed in all mice after 4 weeks of injection and were found detectable when this was compared to mice in which empty vector was injected (data not shown). Therefore, all of the mice were injected every 3 weeks for a total three injections.

Immunohistochemistry

In the prevention group, mice were sacrificed when proteinuria was +3 (above 300 mg/24 h). Formalin-Fixed paraffin-embedded kidney biopsies were subjected to hematoxylin–eosin [Periodic Acid-Schiff (PAS)—for evaluation of polysaccharides (especially glycogen), neutral mucus substances (glycoproteins, glycolipids, and neutral mucins), and tissue basement membranes]. We also stained kidneys with silver staining (this staining is used for highlighting the basement membrane of the glomerulus in the kidney. The periodic acid oxidizes the carbohydrate components of the basement membrane that produce aldehydes. The released aldehydes reduce the silver to visible metallic silver). The extent of glomeruli and tubule inflammation was assessed by two expert pathologists.

Immunofluorescence

Frozen kidney biopsies were additionally assessed by immunofluorescence for the detection of IgG and C3 deposits in the glomeruli of scarified mice. The extent and intensity of these deposits was determined by two expert pathologists. The intensity and extent of staining was scored as "+3" as the highest score of immune-complex deposition and "0" as negative score.

Statistical Methods

Survival and time to severe proteinuria progression analysis was performed using the Kaplan–Meier Analysis Curve. The difference between groups was tested using the Log-Rank test. A p-value of 0.05 or less was considered to be statistically significance.

RESULTS

The Prevention Group

Proteinuria

All mice were injected at the age of 12 weeks, before the appearance of proteinuria. Proteinuria was assessed every 4 days in all mice and was cataloged as follows: in the control sub-group, proteinuria of +1 to +2 was noticed in all mice between weeks 19 and 20. In two mice, it approached +3 (>300 mg/ml) at week 22, and in another two mice, this was documented at week 25. In six mice, proteinuria was measured +3 at weeks 30–32, and in the last five mice, it reached +3 at week 35 of age. In this group (treated with empty vector), the median time to severe proteinuria was 63 days, 95% CI: 0–139. In contrast to this, in mice in which human sema3A cDNA was injected, the time to the appearance of proteinuria was significantly longer: in the first mouse, it approached +3 (>300 mg/ml) only at week 28, and in another three mice, at week 30 of age. In four mice, proteinuria of +3 developed at 31–33 weeks of age, and in four mice, only at weeks 35–38. The remaining mice were scarified at week 40 without the appearance of any proteinuria. In this group, the median time to severe proteinuria was 110 days, 95% CI: 88–131 (**Figure 1**).

Renal Histopathology

Mice from both groups (sema3A-treated and control-treated) were scarified when proteinuria reached +3 and renal biopsies were assessed: mice in which empty vector was injected, developed severe inflammation in both the interstitium and in glomeruli (see hematoxylin–eosin staining, **Figure 2**). The damage was noticed as paucity of blood capillaries and diffused mesangial proliferation (left panel). In sema3A-treated mice, these findings were minimal (right panel). In control-treated mice, profound glycoprotein deposits in both the mesangium and the tubuli were demonstrated using PAS staining (**Figures 2B,C**, left panels). This deposition was minimal in sema3A-treated mice (**Figures 2B,C**, right panels). When silver staining was used, a typical railway pattern was demonstrated in the glomeruli of control-treated mice (highly characteristic of lupus nephritis) (**Figure 3A**, left panel). In contrast, all treated mice in which sema3A was injected remained protected with minimal glomerular inflammation (**Figure 3A**, right panel).

Renal Immunofluorescence

The glomerular deposition of immunoglobulin's (IgG) was evaluated using immunofluorescence techniques. Increased IgG deposition was significant in control-treated mice (**Figure 3B**, left panel). However, in sema3A-treated mice, IgG deposition was minimal (**Figure 3B**, right panel) ($p < 0.01$). We similarly assessed C3 deposition and found it increased in control-treated

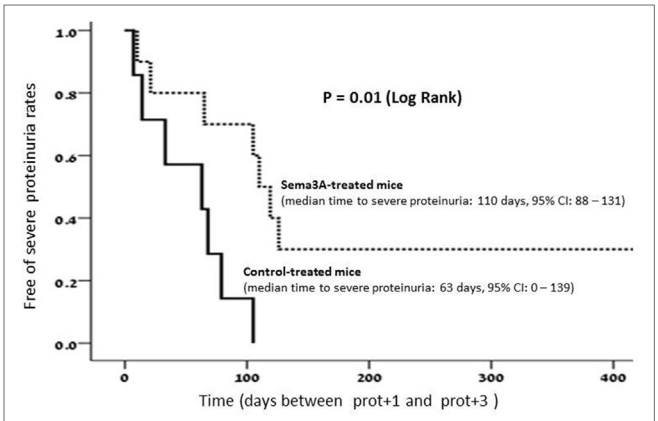

FIGURE 1 | In semaphorin3A (sema3A)-treated mice, the median time to severe proteinuria was 110 days, 95% CI: 88–131. Whereas in control-treated mice, the median time to severe proteinuria was 63 days, 95%, CI: 0–139.

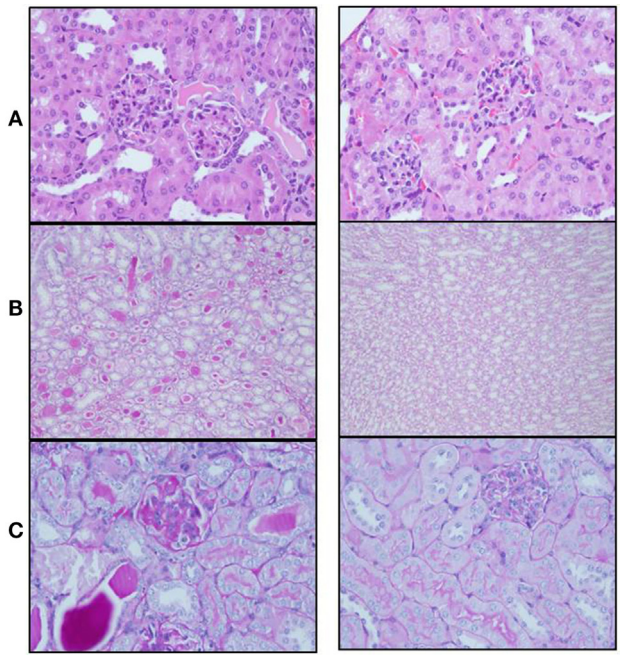

FIGURE 2 | **(A)** Hematoxylin–eosin staining shows paucity of blood capillaries and diffuse mesangial proliferation in control-treated mice (left panel). These findings were minimal in semaphorin3A (sema3A)-treated mice (right panel). **(B)** PAS staining demonstrates profound glycoprotein deposits in the tubuli of control-treated mice (left panel) and minimal deposits in sema3A-treated mice (right panel). **(C)** Increased glycoprotein deposits are seen in the mesangium of control-treated mice (left panel) and minimal in sema3A-treated mice (right panel).

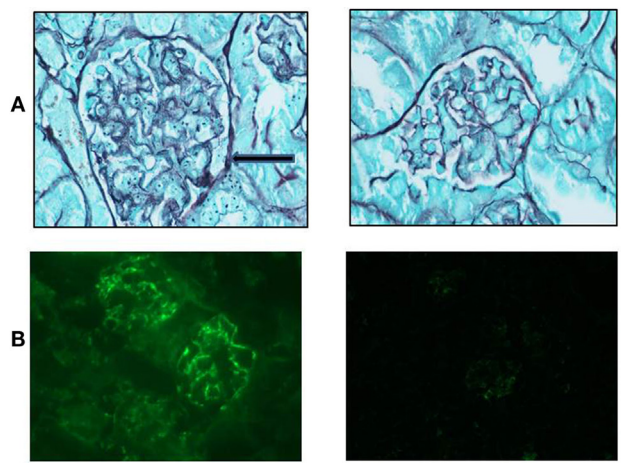

FIGURE 3 | **(A)** Silver staining shows a typical railway pattern in the glomeruli of control-treated mice (left panel, black arrow). Semaphorin3A (sema3A)-treated mice remained protected with minimal glomerular damage (right panel). **(B)** Increased IgG deposition is significant in the glomeruli of control-treated mice (left panel) and is minimal in sema3A-treated mice ($p < 0.01$).

mice when compared to that of sema3A-treated mice. In this case, we could not show statistical significance due to the small number of studied mice.

Treatment Group

Proteinuria

The rate of proteinuria progression from +2 to +3 was notably rapid in mice in which empty vector was injected. The time it took to progress to severe proteinuria in this group of mice was 10.2 ± 2.3 days. However, the deterioration to a proteinuria of +3 was much slower in mice in which sema3A was injected and was 18.3 ± 3.4 days ($p < 0.2$). Though indeed slower but did not reach statistical significance due to the small number of studied mice.

Survival

The survival rate in the sema3A-treated vs control (empty-vector) treated mice was higher. At the end of the study, 3 out of the 8 (30%) sema3A-treated mice were still alive, whereas all the eight control-treated mice died (log rank-0.7). Though impressive, the small number of studied mice did not allow statistical significance of this difference (see **Figure 4**).

DISCUSSION

This is the first study where sema3A is demonstrated to be highly efficient in both treating and preventing glomerular damage in a SLE-mice model. When sema3A was preventively injected into NZB/W mice, they remained free of proteinuria significantly longer than control mice into which empty vector were injected. When sema3A was injected at onset of proteinuria (treatment regimen), the deterioration to severe proteinuria was significantly delayed. In both preventive and treatment regimens, the survival rate was also higher in sema3A treatment mice. By injecting sema3A into NZB/W mice, glomerular and tubular damage were notably protected, in contrast with the control mice in which glomerular inflammation and tubular damage developed quickly, leading to their short survival rate. Finally, increased immune complex deposition, mainly the deposition of IgG and C3 in the glomeruli was found in almost all control (empty-vector treated)

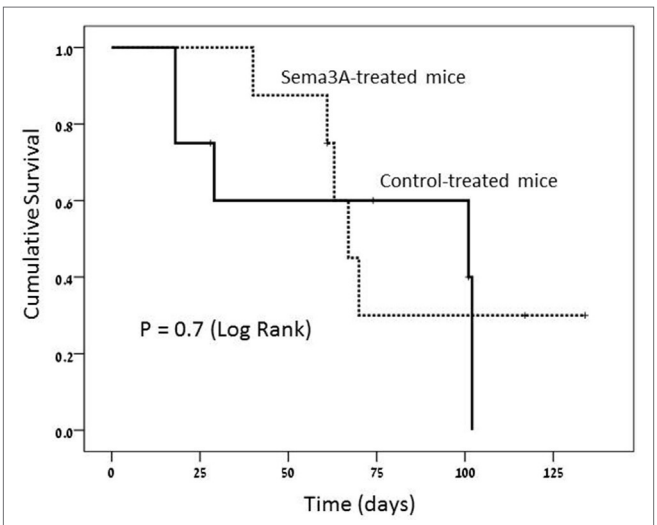

FIGURE 4 | Survival rate is much longer in semaphorin3A (sema3A)-treated mice and shorter in control-treated mice.

mice. However, this deposition was minimal in sema3A-treated mice.

By injecting sema3A to NZB/W mice, glomerular inflammation and immune complex deposition were significantly decreased and the survival of these mice was prolonged. The regulatory/anti-inflammatory effects of sema3A are provided by mechanisms involving both the innate and adaptive immune responses. Aiming to evaluate the effect of sema3A on innate immune responses, dendritic cells (DCs) were incubated with sema3A-rich supernatants. Following their exposure to sema3A, MHC and CD40 expression as well as the production of IL-12 were all downregulated. The suppressive effect of sema3A was also demonstrated by the decreased capability of DCs to activate antigen-specific T cells and the secretion of IFN-γ and IL-2 (13). sema3A has been shown to influence murine DCs migration by signaling through the NP-1/plexin-A1 axis. In this respect, sema3A was further reported to influence human DC migration. By binding DCs, sema3A leads to the reorganization of actin filaments at the plasma membrane, increasing by that their cell deformability and altering their activity in the absence or presence of chemokine CCL19 (3). The role of sema3aA in controlling the function of monocyte-derived macrophages was also assessed. Here, the expression of NP-1, NP-2, and plexin A1 and A2, all of which are receptors for sema3A, were found to be significantly increased during the differentiation and activation of monocyte-derived macrophages, in association with the increased surface binding of sema3A during M2 differentiation. In addition, sema3A was able to induce apoptosis of monocyte-derived macrophages, thereby suggesting that sema3A plays a role in inducing apoptosis of activated macrophages and the modulation of innate inflammation conditions (14). One of the many molecular mechanisms by which sema3A provides its anti-inflammatory effects is by altering TCR-induced proliferation and early signal transduction responses such as ZAP-70 or focal adhesion kinase phosphorylation, resulting in a delayed negative feedback loop and the inhibition of DC-induced T cell proliferation (15). The abovementioned studies support the notion of sema3A being a regulator of innate immune responses. Obviously, these data was more than encouraging and further steps were taken and sema3A was investigated in many *in vivo* models. One of these was assessing the beneficial therapeutic effect of sema3A in a mouse model of collagen-induced arthritis. Following the injection of plasmid DNA encoding sema3A into these mice, disease severity and articular damage were significantly reduced when compared to mice injected with empty plasmid. sema3A treatment reduced the titers of anti-collagen IgG antibodies and the release of pro-inflammatory cytokines such as IL-17 and IFN-γ. In addition, sema3A treatment increased the serum level of the anti-inflammatory cytokine IL-10. In respect to this, the expression of sema3A and NP-1 on Treg cells of RA patients (appreciated as a source of IL-10) was found to be decreased. In this case, the co-culture of T-cells with sema3A induced the expression of CD4+NP-1+ T cells and increased IL-10 expression, suggesting that sema3A could be highly beneficial in treating RA (16). The expression of sema3A on synovial tissues of RA patients was also investigated, in relation with RA disease activity and synovial histological features. Human synovial tissues from established RA patients and patients suffering from osteoarthritis (OA) were assessed for sema3A, VEGF-A, and NP-1mRNA expression. Protein expression of sema3A was decreased in RA tissues when compared to that of OA, when correlated with the extent of synovial inflammation, namely, with the extent of lymphocyte infiltration ($R = 0.50$; $p = 0.004$) (17). Decreased expression/production of sema3A in the skin of atopic dermatitis as well as in psoriatic patients was found to be associated with itch and disease severity. sema3A replacement was reported to normalize the hyper-innervation in atopic dermatitis, resulting in suppression of itching suggesting sema3A to be a potential therapeutic strategy in a wide spectrum of immune-mediated inflammatory diseases (18–20).

CONCLUSION

Semaphorin3A is a unique regulator of both early and late innate and adaptive immune responses. We demonstrated the high beneficial effect of sema3A in ameliorating lupus nephritis in NZB mice by delaying the appearance and deterioration of proteinuria and increasing the survival rate. Future efforts should focus on establishing *in vivo* mechanisms by which sema3A provides its beneficial effect. In addition, the above data should be supported in a bigger cohort of mice and making sema3A suitable and safe for use in SLE patients and other autoimmune diseases.

AUTHOR CONTRIBUTIONS

ZV conducted this study, wrote the MS, and contributed to the analysis of the results. OK, AS, and GN contributed to the semaphorin3A reagents to this study and assisted to the writing of this MS. ES contributed to the analysis of the pathology results and statistical analysis of results. JB contributed to the analysis of the pathology results. OI contributed to the analysis of the pathology results and immunofluorescence of kidneys.

REFERENCES

1. Touma Z, Sayani A, Pineau CA, Fortin I, Matsos M, Ecker GA, et al. Belimumab use, clinical outcomes and glucocorticoid reduction in patients with systemic lupus erythematosus receiving belimumab in clinical practice settings: results from the OBSErve Canada study. *Rheumatol Int* (2017) 37:865–73. doi:10.1007/s00296-017-3682-9
2. Vadasz Z, Toubi E. Semaphorins: their dual role in regulating immune-mediated diseases. *Clin Rev Allergy Immunol* (2014) 47:17–25. doi:10.1007/s12016-013-8360-4
3. Curreli S, Wong BS, Latinovic O, Konstantopoulos K, Stamatos NM. Class 3 semaphorins induce F-actin reorganization in human dendritic cells: role in cell migration. *J Leukoc Biol* (2016) 100:1323–34. doi:10.1189/jlb.2A1114-534R
4. Catalano A, Cappari P, Moretti S, Faronato M, Tamagnone L, Procopio A. Semaphorin3A is expressed by tumor cells and alters T-cell signal transduction and function. *Blood* (2006) 107:3321–9. doi:10.1182/blood-2005-06-2445
5. Vadasz Z, Haj T, Toubi E. The role of B regulatory cells and semaphorin3A in atopic diseases. *Int Arch Allergy Immunol* (2014) 163:245–51. doi:10.1159/000360477

6. Vadasz Z, Toubi E. Semaphorin3A – a marker for disease activity and a potential putative disease-modifying treatment in systemic lupus erythematosus. *Lupus* (2012) 21:1266–70. doi:10.1177/0961203312456753
7. Vadasz Z, Haj T, Halasz K, Rosner I, Slobodin G, Attias D, et al. semaphorin3A is a marker for disease activity and a potential immunoregulator in systemic lupus erythematosus. *Arthritis Res Ther* (2012) 14:R146. doi:10.1186/ar3881
8. Nakano S, Morimoto S, Suzuki J, Mitsuo A, Nakiri Y, Katagiri Y, et al. Down-regulation of CD72 and increased surface IgG on B cells in patients with lupus nephritis. *Autoimmunity* (2007) 40:9–15. doi:10.1080/08916930601118890
9. Vadasz Z, Haj T, Balbir A, Peri R, Rosner I, Slobodin G, et al. A regulatory role for CD72 expression on B cells in systemic lupus erythematosus. *Semin Arthritis Rheum* (2014) 43:767–71. doi:10.1016/j.semarthrit.2013.11.010
10. Vadasz Z, Ben-Izhak O, Bejar J, Sabo E, Kessel A, Storch S, et al. The involvement of immune semaphorins and neuropilin-1 in lupus nephritis. *Lupus* (2011) 20:1466–73. doi:10.1177/0961203311417034
11. Guttmann-Raviv N, Shraga-Heled N, Varshavsky A, Guimaraes-Sternberg C, Kessler O, Neufeld G. Semaphorin-3A and semaphorin-3F work together to repel endothelial cells and to inhibit their survival by induction of apoptosis. *J Biol Chem* (2007) 282:26294–305. doi:10.1074/jbc.M609711200
12. Zhang G, Gao X, Song YK, Vollmer R, Stolz DB, Gasiorowski JZ, et al. Hydroporation as the mechanism of hydrodynamic delivery. *Gene Ther* (2004) 11:675–82. doi:10.1038/sj.gt.3302210
13. Zhou XL, Huang Y, Wang F, Cai LF, Zhang LH, Shi LY. Effects of sema3A derived from tumor cells on functions of dendritic cells. *Zhejiang Da Xue Bao Yi Xue Ban* (2010) 39:364–9.
14. Ji JD, Park-Min KH, Ivashkiv LB. Expression and function of semaphoring 3A and its receptors in human monocyte-derived macrophages. *Hum Immunol* (2009) 70:211–7. doi:10.1016/j.humimm.2009.01.026
15. Lepelletier Y, Maura IC, Hadj-Slimane R, Renand A, Fiorentino S, Baude C, et al. Immuno-suppressive role of semaphotin-3A on T cell proliferation is mediated by inhibition of actin cytoskeleton reorganization. *Eur J Immunol* (2006) 36:1782–93. doi:10.1002/eji.200535601
16. Catalano A. The neuroimmune semaphorin3A reduces inflammation and progression of experimental autoimmune arthritis. *J Immunol* (2010) 185:6373–83. doi:10.4049/jimmunol.0903527
17. Takagawa S, Nakamura F, Kumagai K, Nagashima Y, Goshima Y, Saito T. Decreased semaphorin3A expression correlates with disease activity and histological features of rheumatoid arthritis. *BMC Musculoskelet Disord* (2013) 14:40. doi:10.1186/1471-2474-14-40
18. Tominaga M, Ogawa H, Takamori K. Decreased production of semaphorin3A in the lesional skin of atopic dermatitis. *Br J Dermatol* (2008) 158:842–4. doi:10.1111/j.1365-2133.2007.08410.x
19. Kou K, Nakamura F, Aihara M, Chen H, Seto K, Komori-Yamaguchi J, et al. Decreased expression of semaphorin3A, a neurite-collapsing factor, is associated with itch in psoriatic skin. *Acta Derm Venereol* (2012) 92:521–8. doi:10.2340/00015555-1350
20. Tominaga M, Takamori K. Itch and nerve fibers with special reference to atopic dermatitis: therapeutic implications. *J Dermatol* (2014) 41:205–12. doi:10.1111/1346-8138.12317

Conflict of Interest Statement: The authors declare that the research was conducted in the absence of any commercial or financial relationships that could be construed as a potential conflict of interest.

frontiers in Immunology

REVIEW
published: 16 May 2018
doi: 10.3389/fimmu.2018.01064

The Interplay Between Innate-Like B Cells and Other Cell Types in Autoimmunity

Gregory J. Tsay[1,2] *and Moncef Zouali*[3,4]*

[1] Division of Immunology and Rheumatology, Department of Internal Medicine, China Medical University Hospital, Taichung, Taiwan, [2] College of Medicine, China Medical University, Taichung, Taiwan, [3] INSERM, U1132, Paris, France, [4] Université Paris Diderot, Université Sorbonne Paris Cité, Paris, France

Studies performed in animal models and in humans indicate that the innate arm of the immune system provides an essential role in the initial protection against potential insults and in maintaining tolerance to self-antigens. In the B cell compartment, several subsets engage in both adaptive and innate functions. Whereas B cell subsets are recognized to play important roles in autoimmune diseases, understanding the intricacies of their effector functions remains challenging. In addition to B-1a cells and marginal zone B cells, the B cell compartment comprises other B cells with innate-like functions, including innate response activator B cells, T-bet positive B cells, natural killer-like B cells, IL-17-producing B cells, and human self-reactive V_H4-34-expressing B cells. Herein, we summarize the functions of recently described B cell populations that can exert innate-like roles in both animal models and humans. We also highlight the importance of the cross talk between innate-like B cells and other adaptive and innate branches of the immune system in various autoimmune and inflammatory diseases. In as much as innate immunity seems to be important in resolving inflammation, it is possible that targeting certain innate-like B cell subsets could represent a novel therapeutic approach for inducing resolution of inflammation of autoimmune and inflammatory responses.

Keywords: innate immunity, autoimmunity, B-1a cell, marginal zone B cell, innate response activator B cell, T-bet positive B cell, natural killer-like B cell, IL-17-producing B cell

OPEN ACCESS

Edited by:
Jagadeesh Bayry, Institut National de la Santé et de la Recherche Médicale (INSERM), France

Reviewed by:
Jorg Hermann Fritz, McGill University, Canada
Mohan Maddur, Pfizer, United States
Juan Li, Rockefeller University, United States

***Correspondence:**
Moncef Zouali
moncef.zouali@wanadoo.fr

Specialty section:
This article was submitted to Molecular Innate Immunity, a section of the journal Frontiers in Immunology

Received: *24 November 2017*
Accepted: *27 April 2018*
Published: *16 May 2018*

Citation:
Tsay GJ and Zouali M (2018) The Interplay Between Innate-Like B Cells and Other Cell Types in Autoimmunity. Front. Immunol. 9:1064. doi: 10.3389/fimmu.2018.01064

INTRODUCTION

The immune system makes use of two branches of cellular and humoral effectors: the innate and the adaptive arms of immune defense that are able to sense the presence of potential threats and to mount protective immune responses. In the adaptive arm, cells must interact, proliferate, and, over time, generate antigen-specific cells and antibodies, and immune memory. To be effective, the innate arm must be recruited quickly to impart immediate protection, and it is increasingly recognized that cells of the innate branch can enforce protective barrier functions by regulating adaptive immunity. In addition, lymphocytes that differ from conventional lymphocytes in both expression of cell-surface markers, behavior and innate-like characteristics are able to support adaptive immune functions in various ways. This includes innate lymphoid cells (ILCs), natural killer (NK) cells, lymphoid-tissue inducer cells, γδ T cells, natural killer T (NKT) cells, but also B cells.

In addition to its potential to produce various cytokines (**Figure 1**), the B cell compartment of the immune system comprises several subsets of innate-like B cells that can produce low-affinity

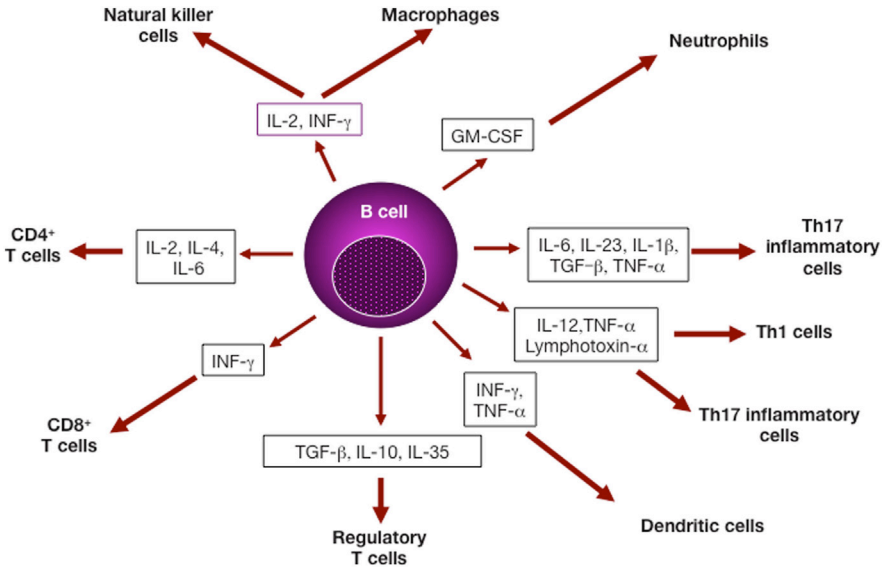

FIGURE 1 | B lymphocytes and cytokine production. Cytokines derived from B cell subsets can impact several cell types of both the adaptive and the immune systems, and affect cell differentiation and/or effector function (3).

antibody responses able to provide a level of immune protection while follicular (FO) B cells are developed to generate high-affinity antibodies with a lag time of about 5 days (1). As outlined in **Table 1**, B cell subsets are recognized to play important roles in autoimmune diseases (2). However, understanding the intricacies of their effector functions remains challenging. Herein, we summarize the functions of several B cell subsets that have been described to exert innate-like roles in both animal models and humans. We also highlight the importance of cross talk between innate-like B cells and other adaptive and innate branches of the immune system in various autoimmune and inflammatory diseases.

TABLE 1 | Antibody-dependent and independent roles of B cells in autoimmune disorders.

- Production of autoantibodies that that form pathogenic immune complexes
- Secretion of autoantibodies that bind *in situ* to target autoantigens
- Generation of autoantibodies that act as catalytic antibodies
- High autoantigen presentation capacity to T cells
- Secretion of pro-inflammatory cytokines and chemokines
- Enhancement of dendritic cell antigen presentation ability
- Provision of cognate help for autoreactive T cells
- Induction of inflammatory Th1 and Th17 cells
- Maintenance of T cell memory
- Inhibition of regulatory T cells
- Organization of tertiary lymphoid tissues and ectopic germinal centers

B cell subsets are endowed with various functions that can contribute to the generation and/or the amplification of autoimmune diseases.

ANTIBODY-INDEPENDENT ROLES OF B CELLS IN INNATE IMMUNITY

Neutralizing antibodies produced by B cells are a hallmark of immunity. Less recognized, however, in the fact that B cells also play critical functions as regulators of innate immunity. Initial protection is provided by the innate immune system, including natural antibodies (NAbs), macrophages, NK cells, neutrophils, and cytokines, in particular type I interferons whose production is regulated by lymphotoxin-β derived from hematopoietic cells. Remarkably, splenic B cells represent a copious source of lymphotoxin-β that can act on potentially infected stromal cells to drive IFN-β production, leading to early protection against infection (4). Since these events occur very rapidly after infection, B cells, independently of antibody production, can be considered as key regulators of early innate immunity to various insults. This is, for example, illustrated in studies of vesicular stomatitis virus infection in the mouse. In this experimental model, B cell-derived lymphotoxin-b is required for splenic $CD169^+$ macrophage organization and viral capture, further establishing an antibody-independent role for B cells in antiviral immunity (5). Consistently, in the absence of B cells, lymph node macrophages do not allow virus replication (6). In this experimental system, B cells, but not antibodies, are required for macrophage-dependent type I interferon production and for protection against infection. Together with other converging observations, B cells are indispensable for promoting IFN production and protective immunity (7).

B CELL SUBSETS IN THE PERIPHERAL B CELL COMPARTMENT

Within the mature peripheral B cell compartment, three distinct subsets that engage in different branches of the immune response have been described: FO B cells, marginal zone (MZ) B cells, and B-1 cells. The majority of mature B lymphocytes are FO recirculating B cells that can home mainly to B cell

follicles in secondary lymphoid organs. In follicles located adjacent to T cell zones, FO B cells participate essentially in T cell-dependent (TD) immune responses to protein antigens, but are less responsive to toll-like receptor (TLR) agonists than MZ B cells or B-1 cells.

In contrast to other B cell subsets, which are produced throughout life in the bone marrow, B-1 cells are generated early in ontogeny from progenitors that are present in the fetal bone marrow (8). They represent the major B cell subpopulation in the pleural and peritoneal cavities but are less represented in the spleen (9). B-1 cells are the main producers of NAbs that have been demonstrated to be important in early protection against various infectious insults (10). They respond vigorously to lipopolysaccharide stimulation and take part in the T cell-type-2 independent (TI-2) responses to bacterial capsular polysaccharides (**Table 2**).

This B-1 cell population comprises two subsets: B-1a ($CD5^+$) cells and B-1b ($CD5^-$) cells that seem to exert distinct functions. For example, in experiments involving rechallenge with *Borrelia hermsii*, B-1b cells, but not B-1a cells, have been shown to generate TI memory B cells (11). After immunization with the model TI-2 antigen NP-Ficoll and the pneumococcal capsular polysaccharide, B-1b cells can also give rise to long-lived memory plasma cells in a thymus-independent manner (12). In addition, they play a prominent role in the immune response against mucosal pathogens and produce IgA in a thymus-independent manner (13, 14).

MECHANISMS THAT MEDIATE B-1 CELL REPOSITIONING

Within secondary lymphoid organs, B-1 cells participate in innate-like immune responses. Following a threatening insult, B-1 cells migrate from their initial location, i.e., the peritoneal and pleural cavities, to secondary lymphoid tissues, i.e., the spleen and the lymph nodes, where they secrete antibodies of the IgM isotype. Thus, during influenza virus infection, B-1 cells were demonstrated to relocate to regional mediastinal lymph nodes (MedLN) and to become a primary source of locally secreted IgM (15). To determine the mechanisms that trigger activated B-1 cells to migrate to secondary lymphoid organs and to subsequently differentiate to antibody-secreting cells, the redistribution of these innate-like B cells to regional MedLN was recently investigated in an experimental model of infection (16). The data showed that type I IFN receptor signaling leads to the accumulation of B-1 cells in MedLN, and is facilitated by activation of an integrin family member (CD11b) known to regulate leukocyte adhesion and migration and to mediate inflammatory responses. Specifically, a gradient of innate cytokines elaborated in response to a local threat leads to activation of CD11b on body cavity B-1 cells, promoting their rapid accumulation in inflamed lymph nodes. Since the peripheral blood contains significant numbers of B-1 cells, it is likely that, even in the absence of insults, body cavity B-1 cells represent reservoirs of innate lymphocytes that can rapidly reposition and continuously home to and from body cavities to peripheral tissues *via* the peripheral blood.

TABLE 2 | Functional dichotomy in B cell subsets.

	Adaptive	Innate-like	
	FO cells	B-1a cells	MZ B cells
Recirculation in lymph	+	–	–
T-dependent responses	+	+/–	+
T-independent responses	+	+++	+++
Antigen presentation *in vitro*	+	+++	+++
Favorite isotypes produced	γ1	μ, γ3, α	μ, γ3
Time to peak cell cycle	Long	Short	Short
Proliferation to lipopolysaccharide	+	+++	+++
Proliferation to anti-IgM Ab	+	–	–
CD9 expression	–	+	+

Shown are the main properties of follicular (FO), B-1a, and marginal zone (MZ) B cells in the mouse.

SIGNALS THAT DRIVE B1 CELL HOMING

The mechanisms that underlie the maturation and expansion of B-1 cells remain under study, but there is evidence that antigen encounters during fetal development lead to positive selection. Studies performed in both wild-type mice and in mice raised in germ-free environments suggest that the selection is triggered by endogenous self-antigens (17). For example, it has been suggested that the repertoire of B-1 cells is selected to bind to evolutionarily important epitopes, such as oxidation-specific epitopes (OSEs) that are a major target of innate NAbs in both mice and humans (18, 19). NAbs represent an important component of innate immunity, and it is generally accepted that they often target OSEs (10, 18).

Oxidation-specific epitopes are neo-self OSEs present on dying cells and damaged proteins that result from the oxidative damage of lipids present in membranes or lipoproteins. Whereas progress has been made in understanding how lipid homeostasis impacts lymphocyte function, the influence of lipid metabolism on B cell-specific responses remains unclear, and the factors that regulate B cell homing into dedicated compartments are not clearly understood. Among the proteins that influence cellular cholesterol homeostasis, the sterol ATP-binding cassette transporter G1 (ABCG1) is an ATPase that promotes unidirectional, net cholesterol efflux to lipoprotein particles. In a relevant study, loss of ABCG1 was found to result in the accumulation of specific oxidized sterols and phospholipids, and to elicit a lung-specific immune response (20). Remarkably, the lungs and pleural cavities of *Abcg1*$^{-/-}$ mice contained increased levels of B-1a cells. There was a niche-specific increase in B-1 cells in the lungs and pleural cavities of the knockout mice that was associated with parallel increases in IgM and antibodies that recognize oxidized phospholipid, indicating an increased NAb production. This site-specific expansion of B-1 cells in response to the accumulation of an oxidized lipid antigen could suggest that ABCG1-dependent control of intracellular lipid homeostasis represents a mechanism for the regulation of B-1 cell homing. It is thus tempting to propose that changes in the lipid content of the lung could alter B cell homing pathways. Overall, the demonstration of a niche-specific expansion of B-1 cells in response to oxidized

lipid antigens, together with the increase in titers of NAbs that reflect an enhanced innate immunity suggest that loss of ABCG1 results in accumulation of both sterols and phospholipids. Once oxidized, some of these lipids can trigger movement signals for B-1 cells that lead them to home into the lungs and pleural cavity. These oxidized lipids and OSEs could also drive B-1 cell expansion and increased secretion of NAbs.

SELF-RENEWAL AND REPOPULATION POTENTIALS OF B-1a CELLS

The origin of B-1a cells remains the focus of investigation with two competing models (8, 21–23). In the "lineage model," the decision to become either a B-1a or a B-2 cell is made before the expression of surface B cell antigen receptor (BCR). By contrast, in the "selection model," entry into the B-1a versus B-2 fate starts after BCR engagement, implying that cell fate decision is made after expression of surface IgM and is based on BCR specificity.

To further resolve hematopoietic lineage relationships in B cells, the impact of developmental timing on acquisition of a B-1a potential was recently investigated using cellular barcoding. This innovative biology tool is based on heritable tagging of individual cells with unique DNA identifiers. It allows identification of the progeny of individual cells *in vivo.* The technology is based on heritable tagging of individual cells with unique DNA identifiers. In immunology, it enables simultaneous tracking the burst sizes of multiple distinct responding cells in transplanted animals (24). This experimental approach allowed tracing fetal hematopoietic stem cells (HSCs) clones across serial transplantations. It demonstrated that serially transplantable fetal liver HSCs give rise to B-1a cells as well as to B-2 cells *in vivo,* and that the B-1a potential is lost over time (25). In contrast to other studies suggesting that definitive HSCs lack B-1a potential (26), this observation showing a developmental shift in HSC state links the attenuation of B-1a potential to developmental changes in HSC fate. These developmental changes in lineage potential also indicate that the B-1a potential can be reinitiated by expression of Lin28b, a protein thought to regulate stem cell self-renewal, in a polyclonal fashion that coincides with the reversal to a fetal-like HSC state (25).

In parallel, a transcription factor necessary for the generation and homeostasis of B-1a cells was recently identified (27). This factor, called Bhlhe41, is a member of the basic helix-loop-helix family. It acts as an inhibitor of negative regulators of BCR activation. Whereas Bhlhe41 is important for normal development and function of B-1a cells, it is not essential for that of B-2 cells. In the absence of Bhlhe41, mice show an altered B-1a cell repertoire and a B cell loss that includes lymphocytes expressing self-reactive BCRs known to recognize phosphatidylcholine. In previous studies, the development of B-1a cells had been described to involve multiple positive regulators of BCR signaling, but Bhlhe41 is a remarkable regulator because it is expressed differentially in developing fetal B cells relative to bone marrow B cells. The observation that the survival of B-1a cells with certain BCRs requires the expression of an amplifier of BCR signals, i.e., Bhlhe41, which is highly expressed in fetal lineage B cells as compared with adult lineage B cells, has led to the speculation that cells of the fetal lineage are able to support the maturation of cells with a self-reactive repertoire, but that rearrangement of the same immunoglobulin (Ig) genes in developing B cells derived from HSCs would not survive receptor engagement (23). This proposal accords with the view that the B cell repertoire is critical in determining the phenotype of mature B cells and with the idea that lineage commitment determines cell fate.

COMMITMENT TO THE MZ B CELL FATE

Marginal zone B cells occupy a unique positioning in the spleen where they surround the follicles and, hence, are frequently exposed to blood-borne antigens. Such frequent encounters enable MZ B cells to provide immunosurveillance and to shuttle antigens to FO dendritic cells (1, 28). Following exposure to antigens, MZ B cells can present antigen and promote T cell activation, but also differentiate into plasmablasts. Compared with FO B cells, MZ B cells exhibit higher expression of surface IgM, the complement receptors CD35 and CD21, and the lipid antigen-presenting molecule CD1d. Together with an elevated TLR expression, the presence of these receptors allows rapid immune responses to blood-borne pathogens, such as encapsulated bacteria. Gene-expression profiling also allows distinguishing MZ and FO B cells, with differences in their transcriptomes contributing to their differential development, localization and function (29). For example, the transcription factor IRF4 limits the MZ B cell pool size and regulates the positioning of cells in the MZ, and the transmembrane receptor Notch2 seems to be necessary for promoting MZ B cell fate. Because they reside between the marginal sinus and the red pulp of the spleen, MZ B cells are located at the first line of defense against blood-borne particulate pathogens (28). By shuttling between the MZ and the follicles, MZ B cells are able to deliver blood-borne antigen to FO dendritic cells (30). In addition, they can act as potent antigen-presenting cells for the activation of NKT cells by virtue of high expression of the antigen-presenting molecule CD1d (31).

Recent studies revealed that commitment of transitional B cells to the MZ B cell fate is a complex process. Immature B cells receive signals *via* the receptor Notch2 from one of its ligands, Delta-like 1, expressed by fibroblastic reticular stromal cells in the spleen (32). In addition, signals from the BCR are important for accessing the MZ B cell fate (33). Specifically, following BCR signaling *via* the serine-threonine kinase Taok3, the transmembrane metalloprotease ADAM10 translocates from intracellular vesicles to the cell surface. This translocation leads to a cleavage step that frees the intracellular domain of Notch, and the fragment generated can translocate to the nucleus where it will drive the MZ cell fate-determining transcriptional program (33). In addition to Taok3 signaling (33), the RNA-binding protein ZFP36L1 was identified to play an indispensable role in determining the identity of MZ B cells by promoting their proper localization and survival (34). In its absence, MZ B cells are mislocalized and die. Further investigation is required to determine whether such mechanism could contribute to shaping of the B cell repertoire.

MZ B CELL FATE AND IMMUNE TOLERANCE

This molecular pathway that links BCR signaling and Notch2 signaling in driving the MZ B cell fate after contact with stromal cells expressing a Notch ligand (33) could have advantages in shaping the MZ B cell repertoire. For example, autoreactive immature B cells that encounter self-antigen, but do not rapidly come into contact with the appropriate stromal cells, would not develop into MZ B cells. By contrast, B cells reactive with non-self-antigens, i.e., microbiota-derived antigens that can be present in the peripheral blood, would be exposed to both proper BCR and Notch2 signaling, which would drive them into the MZ B cell fate. Such a mechanism would be advantageous for the immune system because it would provide protection against microbial infection and allow negative peripheral selection of autoreactive B cells.

Since the gut is a key interface between the immune system and the environment, it has become clear that the mucosal immune system of the gut plays a chief role in maturation of the immune system, in shaping the T cell and B cell repertoires, and in induction of immune tolerance to food antigens and to microbiota-derived antigens. This recent insight is being used in investigation of the pathogenesis of various diseases, including type-1 diabetes (T1D). Gut microbes are known to release the short-chain fatty acids (SCFAs) acetate and butyrate from specialized diets. Since the NOD mouse develops symptoms of spontaneous diabetes with a number of similarities to human T1D, it can be used to investigate the importance of the SCFA microbial metabolites acetate and butyrate in this autoimmune form of diabetes. A recent comprehensive study disclosed that SCFA-rich diets had substantial effects on the immune system through different modes of action (35). Interestingly, the acetate diet resulted in a decreased number of splenic B cells, particularly transitional and MZ B cells. By contrast, the butyrate diet was associated with an increased number and function of regulatory T cells. While the SCFA-enriched diets had a clear effect on B cells, especially MZ B cells, which were markedly reduced in number and function (35), it remains unknown whether SCFAs had an impact on plasma cells or on mucosal IgA-producing B cells. Further investigation of these beneficial effects could have potential therapeutic applications, not only in this form of diabetes, but also in other autoimmune diseases.

MULTI-WAY INTERACTIONS AMONG HUMAN INNATE CELLS

The phenotype of MZ B cells differs in mice versus humans. In the mouse, MZ B cells form a population of $IgM^{+}IgD^{lo}CD^{21hi}CD23^{lo}$ B cells that do not recirculate and that are thought to be a lineage separate from FO B cells. By contrast, human MZ B cells recirculate and are often somatically hypermutated, suggesting a memory B cell origin. However, high-throughput V_H sequencing of human B cell subsets indicates that IgM memory and MZ B cells constitute two distinct entities (36). Given such differences, it remains unclear if MZ B cells play similar conserved roles in both species.

For their activation, MZ B cells rely on unconventional sources of stimulation, such as TLRs, which contrasts with the requirement of FO B cells. To become fully activated, these latter cells receive a first signal delivered trough antigen recognition by the BCR followed by a T cell-derived second signal. In fact, it appears that there is a complex set of intercellular interactions that facilitate antibody production by MZ B cells in both TI type 1 settings and TI type 2 settings, and that require a small subset of ILCs that reside mainly in the MZ of the human spleen (37). These cells express CD127 (IL-7 receptor), CD117 (stem-cell factor receptor), and the transcription factor RORγt. In response to IL-1β and IL-23, they produce IL-22, which places them in the mucosal cell-like ILC3 category. These MZ ILCs are located in the vicinity of stromal cells expressing the integrin ligand MAdCAM-1, suggesting that they represent the human equivalent of mouse marginal reticular cells (MRCs) that express TLR3, TLR4, and TLR9.

Intriguingly, interactions between MRCs and ILCs can synergistically amplify a signal from TLR ligands that enhances human MZ B cell activation and differentiation into antibody-secreting cells (37). Furthermore, neutrophils that reside in the MZ can be activated by ILCs, which will further boost MZ B cell stimulation (38). These observations have potential implications for our understanding of immune tolerance to self. Since these events take place in the absence of BCR engagement, they are reminiscent of polyclonal TI type 1 responses. This cellular interactive web could lower the threshold of MZ B cell activation to TI antigens, which would increase their responsiveness to foreign threats and simultaneously maintain tolerance to self-antigens.

T-bet^{+} AGE-ASSOCIATED B CELLS (ABCs)

A novel subset of B cells, termed ABCs, has recently been identified in mouse models. ABCs express high levels of CD11c and the transcription factor T-bet, which distinguishes them from other B cell subsets (39). Subsequently, T-bet was found to be necessary and sufficient for the appearance of this subset, and triggering of the BCR, IFN-γ receptor, and TLR7 on B cells induces high levels of T-bet expression. Since ABCs exhibit a unique T-bet driven transcriptional program, they differ substantially from other B cell subsets in their activation requisites, functional capacities, and survival requirements (40). They respond poorly to BCR engagement, but survive, which distinguishes them from FO and MZ B cells. Remarkably, ABCs express the canonical BAFF receptors BR3 and TACI, but do not rely on BAFF for survival, another feature that distinguishes them from FO and MZ B cells. Following simulation with either TLR9 or TLR7 agonists, either alone or in combination with BCR ligation, they proliferate vigorously and produce the regulatory cytokines IL-10 and IFN-g. Overall, these functional properties suggest that ABCs could have profound effects on the dynamics and homeostasis of peripheral B cell subsets.

Since ABCs are potent antigen-presenting cells, they could play a role in autoimmune responses by presenting self-antigen

to autoreactive T cells. Consistently, T-bet$^+$ ABCs appear in autoimmune-prone mice and in autoimmune patients. Thus, several groups have reported the presence of T-bet-expressing B cells in autoimmune-prone mice and in autoimmune patients, including rheumatoid arthritis (RA) and scleroderma patients (41). B cells with a similar phenotype (CD21$^-$CD19^{hi}CD11c$^+$) have also been found to be enriched in the blood of common variable immunodeficiency patients with autoimmune cytopenia, systemic lupus erythematous (SLE), RA, and Sjögren's syndrome. Importantly, several groups have recently reported the appearance of T-bet$^+$ B cells in autoimmune patients suffering from SLE (42), multiple sclerosis (43), and Crohn's disease (44). More recently, investigators demonstrated that T-bet expression in B cells is critical for the rapid initiation and progression of autoimmune responses, end-organ damage, and early mortality during lupus-like autoimmunity (45). They also have shown that ABCs are located at the T cell/B cell border in the spleen, which could increase the likelihood of contact between Ag-specific T cells and antigen-presenting ABCs. Remarkably, their BCRs are autoreactive, suggesting that ABCs are precursors for autoantibody production. All these features indicate that ABCs will be ideal presenters of autoantigens to T cells. Together, these observations suggest that T-bet-dependent activation of autoreactive B cells is important for the development and/or the progression of human autoimmunity, and it has been suggested that T-bet$^+$ B cells represent promising targets for treatment of human autoimmunity (39). However, other investigators found that during the remission phase of collagen-induced arthritis (CIA), an experimental model for RA, MZ B cells express an elevated level of T-bet (46), thereby confirming the existence of IL-10/T-bet co-expressing cells. These observations, suggesting that T-bet could contribute to the remission of CIA by facilitating the regulatory potential of IL-10$^+$ MZ B cells, does not militate in favor of targeting T-bet$^+$ B cells for therapeutic purposes. They also raise questions regarding the functional relationships between T-bet$^+$ B cells, MZ B cells, and regulatory B cells.

NK-LIKE B CELLS

Recently, a separate subpopulation of innate B cells, termed NKB cells, was identified in mice, and in human (47). They exhibit CD19$^+$NK1.1$^+$ signature markers and reside mainly in the spleen and mesenteric lymph nodes. Their identity seems unique and is distinct from that of NK and B cells. NKB cells can produce large amounts of interleukin-18 (IL-18) and IL-12, and, consequently, are able to activate type 1 innate lymphoid cells (ILC1s) and NK cells to initiate innate immunity against invading microorganisms. Unlike other cell lineages, NKB cells are postulated to harbor unique fate-decision transcription factors that could specifically drive their progenitors to differentiate into mature NKB cells (47). It is possible that NKB cells act as a separate subset of innate B cells and play a critical role in the early stage of innate immune responses.

Reminiscent of B-1 cells and MZ B cells, which express a limited diversity of germline-encoded BCRs and are rapidly activated upon challenge with innate stimuli, NKB cells exhibit a non-Gaussian distribution of the length of their Ig heavy-chain third hypervariable region (47), suggesting that NKB cells display a restricted BCR repertoire. The fact that they harbor a low-diversity BCR repertoire different from that of B cells suggests a restricted recognition of antigens. However, the antigen repertoire of NKB cells needs to be better delineated to determine if they can recognize self- and non-self-antigens. In addition, further studies are required to determine whether these NKB cells represent a *bona fide* separate subset of innate B cells that are distinct from conventional B cells and to decipher their potential role in inflammatory and autoimmune conditions. Since NKB cells can produce substantial amounts of IL-18 and IL-12 that lead to activation of innate lymphocytes, and in as much as IL-18 is also an inflammatory factor responsible for promotion of autoimmune diseases, future studies should investigate whether NKB cells are implicated in the pathogenesis of autoimmune diseases.

HUMAN INNATE-LIKE, SELF-REACTIVE V_H4-34-EXPRESSING B CELLS

In humans, V_H4-34-B cell clones expressing the germline Ig variable heavy-chain 4-34 (V_H4-34) gene are common in the naive B cell repertoire, but are rarely found in IgG memory B cells from healthy individuals. Several groups showed that the V_H4-34 gene codes for autoantibodies that recognize I/i carbohydrates expressed by red blood cells with a specific motif in their framework region 1 (FWR1) (48, 49). In recent studies of patients exhibiting a genetic deficiency in IRAK4 or MYD88, which mediate the function of TLRs except TLR3, CD27$^+$IgG$^+$ B cells comprised V_H4-34-expressing clones and showed decreased somatic hypermutation frequencies (50). Importantly, whereas V_H4-34-encoded IgGs from healthy donors harbored FWR1 mutations abrogating self-reactivity, their counterparts from IRAK4- and MYD88-deficient patients often displayed an unmutated FWR1 motif, which enables these antibodies to recognize I/i antigens present on erythrocytes. Paradoxically, this self-reactivity was associated with a potential of these V_H4-34-encoded IgG clones to bind commensal bacterial antigens.

It is possible that germline-encoded self-reactive V_H4-34$^+$ antibodies recognizing I/i carbohydrates expressed on erythrocytes and the corresponding B cell clones exert beneficial functions through their cross-reactivity with antigens present on commensal bacteria that reach the circulation. This view is in line with the proposal that B cells expressing germline-encoded self-reactive V_H4-34 antibodies may represent an innate-like B cell population specialized in the containment of commensal bacteria when gut barriers are breached (50). Other studies described human V_H4-34-expressing B cells that are anergic, a state that precludes them from being recruited into B cell follicles (51–53). Consistently, the fact that the majority of V_H4-34-expressing IgG$^+$ B cells isolated from healthy donors were described to acquire mutations that abolish self-reactivity to I/i antigens (50) supports the contention that V_H4-34$^+$ B cells are *bona fide* anergic. It will be important to determine the interrelationship between the innate-like function and the anergic state of human V_H4-34$^+$ B cells.

IL-17-PRODUCING B CELLS AND INNATE IMMUNITY

Other investigations have identified B cells as a chief source of rapid, innate-like production of IL-17 in response to infection, and, remarkably, IL-17$^+$ B cells outnumbered inflammatory Th17 cells (54). In addition, the IL-17$^+$ B cells had a plasmablast phenotype (CD19$^+$B220^{dim}GL7$^-$CD138$^+$), suggesting that, in addition to antibody secretion, IL-17 production may represent an additional key effector function for plasma cells during infection. Consistent with that idea, B cell-intrinsic production of IL-17A was required for efficient control of parasitemia and regulation of inflammatory responses. The IL-17 B cell production in response to infection occurred *via* a previously unknown pathway involving a trans-sialidase. Through the use of inhibitors and genetic models, a requirement for both Src and Btk-Tec kinases was demonstrated in B cells (54). Genetic deletion or pharmacological blockade of CD45 abrogated IL-17 B cell production, suggesting that the trans-sialidase can trigger CD45 compartmentalization or oligomerization, and initiate an IL-17 transcriptional program that operates independently of key candidate receptors on the B cell surface. It is possible that this enzyme is able to modify the B cell-surface protein CD45, triggering Src and Btk kinase intracellular signaling. Importantly, this signaling program operated in both mouse primary B cells and human primary B cells.

Overall, these observations may indicate that the generation of IL-17$^+$ B cells represents an unappreciated arm of the innate immune response required for pathogen control. Since both B cells and IL-17 have been linked to a range of autoimmune diseases, it will be important to determine the potential role(s) of IL-17$^+$ B cells in candidate autoimmune disorders.

INNATE RESPONSE ACTIVATOR (IRA) B CELLS

In a related experimental study, peritoneal B-1a cells were found to give rise to a population of B cells, called IRA B cells, that produce the growth factor GM-CSF (55). This IRA B cell population arises in the mouse peritoneum and accumulates in large numbers in the splenic red pulp. In additional studies, pleural B cells were demonstrated to migrate from the pleural space and to relocate to the lung parenchyma where they produce abundant natural IgM Abs that bind to bacteria and neutralize them (56). It is of note that the Abs that recognize oxidized phospholipids (20) also bind *S. pneumoniae* and provide optimal protection to mice from this pathogen (56). This innate immune mechanism is able to clear bacteria and to protect against pneumonia, and the B cell-derived GM-CSF is the autocrine instructor required for IgM production. This early appearance of a unique GM-CSF-producing B cell is intriguing. It suggests that IRA B cells are able to educate other cell subsets, such as myeloid cells. It will be important to elucidate the precise molecular and cellular events that link GM-CSF signaling to IgM production.

These observations may have implications toward our understanding of the pathogenesis of autoimmune diseases. A growing body of evidence suggests that autoimmunity in patients is initiated outside the tissue that is targeted by the autoimmune attack. In RA, for example, serum autoantibodies are detectable years before the development of the initial joint symptoms, and mucosal tissues, including the lung and the oral cavity, have been implicated as potential initiating sites for disease development (57).

As occurs in other organs, immunologic lung diseases develop when the normal mechanisms of immune self-tolerance are disrupted. In the lung, macrophages and lymphocytes are the key cells involved in the initiation and perpetuation of undesirable immune responses. Macrophages can ingest and degrade the inhaled antigens and serve as scavenger cells. In addition, they can act as antigen-presenting cells for T cells. Even tough lymphocytes are present in low numbers in the normal lung parenchyma, a subset of lymphocytes that have been triggered by relevant antigens in the surrounding lymphoid tissues are able to migrate to the lung and participate in inflammatory responses. This could account for the fact that systemic autoimmune diseases frequently involve the lung, the pleura, pulmonary parenchyma, or airway. The observation that pleural space B cells control the early responses to insults broadens our understanding of the immune system's spatio-cellular dynamics. The identification of the GM-CSF–IgM axis could have implications for our understanding of autoimmune diseases in human.

THE INTERPLAY BETWEEN INNATE-LIKE B CELLS AND OTHER CELL TYPES IN AUTOIMMUNITY

B lymphocytes are known to exert crucial non-redundant roles in the innate and adaptive arms of the immune system through both antibody-dependent and antibody-independent mechanisms. For example, during acute infection, B lymphocytes play a role in the early innate immune response, where they aid in mounting an efficient and protective inflammatory response (55). Even in the inflammatory response secondary to other forms of acute injury, experimental studies uncovered a key role for B cells in production of CCL7, previously called monocyte-chemotactic protein 3, or MCP3 (58). In that setting, B cells are able to produce Ccl7 and to induce a Ly6C^{hi} monocyte mobilization from the bone marrow and recruitment to the heart, leading to enhanced tissue injury and deterioration of myocardial function. Remarkably, high circulating concentrations of CCL7 and the B cell longevity factor BAFF in patients with acute myocardial infarction predict increased risk of death or recurrent myocardial infarction (58). The precise B cell subset involved in this setting remains to be examined in more detail. However, the results indicate that this pathogenic effect of B cells depends in part on BAFF-R signaling, a finding reminiscent of observations showing that BAFF-R deficiency or B cell depletion can reduce the development of atherosclerotic lesions in several experimental models (59). Since atherosclerosis can be considered an auto-inflammatory disease associated with inflammatory factors characterized by lipoprotein metabolism alterations that lead to immune system activation with the consequent

proliferation of smooth muscle cells, narrowing arteries, and atheroma formation, the contribution of various B cell subsets to post-ischemic injury is likely to be important.

During atherosclerosis, several studies consistently demonstrated that B lymphocytes play prominent roles (60, 61). Thus, natural IgM antibodies derived from B-1 cells have been found to be atheroprotective, and B-2 cell responses were demonstrated to promote atherogenesis chiefly by supporting proatherogenic T cells. The contribution of adaptive FO B cells to the development of atherosclerosis can be inferred from their roles in the support of proatherogenic T follicular helper (TFH) cells and germinal center responses. In addition, the contribution of innate-like MZ B cells to regulation of the immune response in atherosclerosis was investigated in mice. In that setting, MZ B cells were found to activate a homeostatic program in response to high-cholesterol diet (HCD) and to regulate the differentiation and accumulation of TFH cells (62). In mice fed with a HCD diet, MZ B cells upregulated surface expression of the immunoregulatory ligand PDL1 and increased the interaction between MZ B cells and pre-TFH cells, which led to PDL1-mediated suppression of TFH cell motility, alteration of TFH cell differentiation, reduced TFH abundance and suppression of the proatherogenic TFH response. This MZ B cell role in controlling the TFH-germinal center response to a cholesterol-rich diet is critical in limiting exaggerated adaptive immune responses and in substantially reducing the development and progression of atherosclerosis (62). In the absence of MZ B cells, there is an excessive accumulation of suboptimally differentiated TFH cells and increased levels of T helper and T effector memory cells. However, the signals that instruct MZ B cells to leave the MZ and guide them to TFH cells remain unclear.

Similarly, various cell types play a role in the autoimmune disease T1D, but the trigger mechanisms involved in the early stages of disease pathogenesis remain under investigation. In early studies, the number of circulating $CD5^+$ B cells was reportedly higher in children with recent onset T1D, as compared with patients with long-term disease or controls (63). In addition, as has been observed in other autoimmune disease, an altered BCR signaling threshold has been disclosed in patients with T1D as compared with healthy controls (64, 65). In diabetes-prone NOD mice, an elevated frequency of self-reactive B cells is detectable, as compared with C57BL/6 and BALB/c mice (66), and peritoneal B-1a cells were demonstrated to participate in T1D development in NOD mice (67). In further studies of young female NOD mice, physiological beta-cell death was found to induce the recruitment and activation of B-1a cells, neutrophils, and plasmacytoid dendritic cells (pDCs) to the pancreas (68). Experiments based on depletion of cell subsets indicated that B-1a cells, neutrophils, and IFN-α-producing pDCs are required for the initiation of the diabetogenic T cell response and T1D development (68), suggesting that an innate immune cell dialog that starts in the pancreas of young NOD mice can lead to the initiation of T1D. This IFN-α production would create an inflammatory milieu favorable for a diabetogenic adaptive response that leads to autoimmune diabetes. It is possible that the interplay between B-1a cells, neutrophils and pDCs represents a common feature of other autoimmune diseases.

DISCUSSION

Studies performed in animal models and in humans indicate that the innate arm of the immune system provides an essential role in the initial protection against potential insults and in maintaining tolerance to self-antigens. Investigations of innate-like lymphocytes, including γδ T cells and NKT cells, suggest that there are no tight boundaries between innate and adaptive immunity. As discussed above, the existence of several B cell subsets with distinct effector functions enables production of pathogenic autoantibodies and promotion of inflammatory cascades that involve various other cell types (**Table 3**). Within inflammatory lesions, there is a complex and dynamic cross talk between B cells and other cell types.

In as much as innate immunity seems to be important in resolving inflammation (69), it is possible that targeting certain innate-like B cell subsets could represent a novel therapeutic approach for inducing resolution of inflammation of auto-inflammatory responses. However, it remains uncertain whether observations made in mice will translate meaningfully to the extent of human subjects. In addition, some of the newly described B cell subsets need a more detailed characterization using novel methodical approaches.

Throughout the years, categorization of B cells has relied on immunophenotyping by flow cytometry, which allows identification of cells in suspension by expression of cell-surface receptors and intracellular cytokines. However, the census of B cells remains incomplete because, depending on environmental encounters, each B cell can be at a different stage of activation or differentiation. In addition, the same cell subset can be present in different locations of the organism, but in distinct phenotypes that result from adaptation to the tissue of residence. Furthermore, B cells are endowed with particular antigen receptor sequences, and, therefore, are clonal in nature, which creates a unique genetic diversity into these cells.

In recent years, development of single-cell genomics and spatial profiling methods is enabling genome-wide quantification of

TABLE 3 | Principal B cell subsets with innate-like functions.

B cell subset	B-1a cells	Marginal zone B cells	T-bet positive B cells	Innate response activator B cells	Natural killer-like B cells	IL-17-producing B cells	Human self-reactive V_H4-34-expressing B cells
Associated pathology	Type-1 diabetes (T1D), rheumatoid arthritis (RA)	Atherosclerosis, T1D	RA, scleroderma, systemic lupus erythematous	Under investigation	Under investigation	Under investigation	Under investigation

molecules in thousands of individual cells, and multiplex spatial analysis of proteins and RNA *in situ* (70). These new approaches can quantify subtle changes in gene expression between individual cells and dynamic expression modifications during an immune response. The power of single-cell genomics to identify previously unidentified subpopulations is illustrated by recent studies of cells of the immune system. For example, studies using human DCs have revealed previously unknown DC subsets and provided insight into the complexity of the lineage of these cells (71, 72). In parallel, similar approaches led to characterize variations within Th17 cells, and to describe a spectrum of cell subsets with distinct levels of pathogenicity, that, upon adoptive transfer, are able to induce symptoms of autoimmune disease in animal models (73, 74).

For B lymphocytes, single-cell techniques are ideal to study the antigen receptor repertoire, and its relation to the B cell subtype and state. It is likely that these new approaches will lead to a more precise characterization of B cell subsets and their effector functions. They should considerably enhance our understanding of the complexity of the B cell compartment and its innate-like functions within the immune system, and beyond. It is possible that combining B cell repertoire analysis, single-cell genomics, new emerging spatial approaches, and multiplex immunophenotyping could lead to a novel generation of diagnostics and therapeutic approaches.

ETHICS STATEMENT

The work is exempt from ethical approval procedures.

AUTHOR CONTRIBUTIONS

Both authors made substantive intellectual contributions to this study to qualify as authors. MZ designed and drafted the manuscript. GT contributed discussion and re-drafted parts of the manuscript.

FUNDING

MZ is funded by INSERM and University of Paris Diderot. GT is funded by the Ministry of Science and Technology, Taiwan: MOST-103-2314-B-039-039, MOST-104-2314-B-039-045, MOST-105-2911-I-039-504, MOST-105-2314-B-039-047, MOST-106-2911-I-039-501, and DMR-107-173, CMUH, Taichung, Taiwan.

REFERENCES

1. Cerutti A, Cols M, Puga I. Marginal zone B cells: virtues of innate-like antibody-producing lymphocytes. *Nat Rev Immunol* (2013) 13:118–32. doi:10.1038/nri3383
2. Viau M, Zouali M. B-lymphocytes, innate immunity, and autoimmunity. *Clin Immunol* (2005) 114:17–26. doi:10.1016/j.clim.2004.08.019
3. Harris DP, Haynes L, Sayles PC, Duso DK, Eaton SM, Lepak NM, et al. Reciprocal regulation of polarized cytokine production by effector B and T cells. *Nat Immunol* (2000) 1:475–82. doi:10.1038/82717
4. Schneider K, Loewendorf A, De Trez C, Fulton J, Rhode A, Shumway H, et al. Lymphotoxin-mediated crosstalk between B cells and splenic stroma promotes the initial type I interferon response to cytomegalovirus. *Cell Host Microbe* (2008) 3:67–76. doi:10.1016/j.chom.2007.12.008
5. Honke N, Shaabani N, Cadeddu G, Sorg UR, Zhang DE, Trilling M, et al. Enforced viral replication activates adaptive immunity and is essential for the control of a cytopathic virus. *Nat Immunol* (2011) 13:51–7. doi:10.1038/ni.2169
6. Moseman EA, Iannacone M, Bosurgi L, Tonti E, Chevrier N, Tumanov A, et al. B cell maintenance of subcapsular sinus macrophages protects against a fatal viral infection independent of adaptive immunity. *Immunity* (2012) 36:415–26. doi:10.1016/j.immuni.2012.01.013
7. Vinuesa CG, Chang PP. Innate B cell helpers reveal novel types of antibody responses. *Nat Immunol* (2013) 14:119–26. doi:10.1038/ni.2511
8. Hayakawa K, Hardy RR, Herzenberg LA, Herzenberg LA. Progenitors for Ly-1 B cells are distinct from progenitors for other B cells. *J Exp Med* (1985) 161:1554–68. doi:10.1084/jem.161.6.1554
9. Montecino-Rodriguez E, Leathers H, Dorshkind K. Identification of a B-1 B cell-specified progenitor. *Nat Immunol* (2006) 7:293–301. doi:10.1038/ni1301
10. Zouali M. Antibodies. *eLS*. Chichester, UK: John Wiley & Sons, Ltd (2016). doi:10.1002/9780470015902.a0000906.pub3
11. Alugupalli KR, Leong JM, Woodland RT, Muramatsu M, Honjo T, Gerstein RM. B1b lymphocytes confer T cell-independent long-lasting immunity. *Immunity* (2004) 21:379–90. doi:10.1016/j.immuni.2004.06.019
12. Defrance T, Taillardet M, Genestier L. T cell-independent B cell memory. *Curr Opin Immunol* (2011) 23:330–6. doi:10.1016/j.coi.2011.03.004
13. Macpherson AJ, Gatto D, Sainsbury E, Harriman GR, Hengartner H, Zinkernagel RM. A primitive T cell-independent mechanism of intestinal mucosal IgA responses to commensal bacteria. *Science* (2000) 288:2222–6. doi:10.1126/science.288.5474.2222
14. Fagarasan S, Honjo T. Intestinal IgA synthesis: regulation of front-line body defences. *Nat Rev Immunol* (2003) 3:63–72. doi:10.1038/nri982
15. Choi YS, Baumgarth N. Dual role for B-1a cells in immunity to influenza virus infection. *J Exp Med* (2008) 205:3053–64. doi:10.1084/jem.20080979
16. Waffarn EE, Hastey CJ, Dixit N, Soo Choi Y, Cherry S, Kalinke U, et al. Infection-induced type I interferons activate CD11b on B-1 cells for subsequent lymph node accumulation. *Nat Commun* (2015) 6:8991. doi:10.1038/ncomms9991
17. Hardy RR, Wei CJ, Hayakawa K. Selection during development of VH11+ B cells: a model for natural autoantibody-producing CD5+ B cells. *Immunol Rev* (2004) 197:60–74. doi:10.1111/j.0105-2896.2004.0100.x
18. Pluddemann A, Neyen C, Gordon S. Macrophage scavenger receptors and host-derived ligands. *Methods* (2007) 43:207–17. doi:10.1016/j.ymeth.2007.06.004
19. Chou MY, Fogelstrand L, Hartvigsen K, Hansen LF, Woelkers D, Shaw PX, et al. Oxidation-specific epitopes are dominant targets of innate natural antibodies in mice and humans. *J Clin Invest* (2009) 119:1335–49. doi:10.1172/JCI36800
20. Baldan A, Gonen A, Choung C, Que X, Marquart TJ, Hernandez I, et al. ABCG1 is required for pulmonary B-1 B cell and natural antibody homeostasis. *J Immunol* (2014) 193:5637–48. doi:10.4049/jimmunol.1400606
21. Berland R, Wortis HH. Origins and functions of B-1 cells with notes on the role of CD5. *Annu Rev Immunol* (2002) 20:253–300. doi:10.1146/annurev.immunol.20.100301.064833
22. Rajewsky K. The Herzenberg lecture: how to make a B-1 cell? *Ann N Y Acad Sci* (2015) 1362:6–7. doi:10.1111/nyas.12767
23. Wortis HH. To B-1 or not to B-1. *Nat Immunol* (2017) 18:365–6. doi:10.1038/ni.3715
24. Krueger A, Zietara N, Lyszkiewicz M. T cell development by the numbers. *Trends Immunol* (2017) 38:128–39. doi:10.1016/j.it.2016.10.007
25. Kristiansen TA, Jaensson Gyllenback E, Zriwil A, Bjorklund T, Daniel JA, Sitnicka E, et al. Cellular barcoding links B-1a B cell potential to a fetal hematopoietic stem cell state at the single-cell level. *Immunity* (2016) 45:346–57. doi:10.1016/j.immuni.2016.07.014
26. Ghosn EE, Waters J, Phillips M, Yamamoto R, Long BR, Yang Y, et al. Fetal hematopoietic stem cell transplantation fails to fully regenerate the B-lymphocyte compartment. *Stem Cell Reports* (2016) 6:137–49. doi:10.1016/j.stemcr.2015.11.011
27. Kreslavsky T, Vilagos B, Tagoh H, Poliakova DK, Schwickert TA, Wohner M, et al. Essential role for the transcription factor Bhlhe41 in regulating the development, self-renewal and BCR repertoire of B-1a cells. *Nat Immunol* (2017) 18:442–55. doi:10.1038/ni.3694

28. Martin F, Kearney JF. Marginal-zone B cells. *Nat Rev Immunol* (2002) 2:323–35. doi:10.1038/nri799
29. Kleiman E, Salyakina D, De Heusch M, Hoek KL, Llanes JM, Castro I, et al. Distinct transcriptomic features are associated with transitional and mature B-cell populations in the mouse spleen. *Front Immunol* (2015) 6:30. doi:10.3389/fimmu.2015.00030
30. Cinamon G, Zachariah MA, Lam OM, Foss FW Jr, Cyster JG. Follicular shuttling of marginal zone B cells facilitates antigen transport. *Nat Immunol* (2008) 9:54–62. doi:10.1038/ni1542
31. Zietara N, Lyszkiewicz M, Krueger A, Weiss S. ICOS-dependent stimulation of NKT cells by marginal zone B cells. *Eur J Immunol* (2011) 41:3125–34. doi:10.1002/eji.201041092
32. Fasnacht N, Huang HY, Koch U, Favre S, Auderset F, Chai Q, et al. Specific fibroblastic niches in secondary lymphoid organs orchestrate distinct Notch-regulated immune responses. *J Exp Med* (2014) 211:2265–79. doi:10.1084/jem.20132528
33. Hammad H, Vanderkerken M, Pouliot P, Deswarte K, Toussaint W, Vergote K, et al. Transitional B cells commit to marginal zone B cell fate by Taok3-mediated surface expression of ADAM10. *Nat Immunol* (2017) 18:313–20. doi:10.1038/ni.3657
34. Newman R, Ahlfors H, Saveliev A, Galloway A, Hodson DJ, Williams R, et al. Maintenance of the marginal-zone B cell compartment specifically requires the RNA-binding protein ZFP36L1. *Nat Immunol* (2017) 18:683–93. doi:10.1038/ni.3724
35. Marino E, Richards JL, McLeod KH, Stanley D, Yap YA, Knight J, et al. Gut microbial metabolites limit the frequency of autoimmune T cells and protect against type 1 diabetes. *Nat Immunol* (2017) 18:552–62. doi:10.1038/ni.3713
36. Bagnara D, Squillario M, Kipling D, Mora T, Walczak AM, Da Silva L, et al. A reassessment of IgM memory subsets in humans. *J Immunol* (2015) 195:3716–24. doi:10.4049/jimmunol.1500753
37. Magri G, Miyajima M, Bascones S, Mortha A, Puga I, Cassis L, et al. Innate lymphoid cells integrate stromal and immunological signals to enhance antibody production by splenic marginal zone B cells. *Nat Immunol* (2014) 15: 354–64. doi:10.1038/ni.2830
38. Puga I, Cols M, Barra CM, He B, Cassis L, Gentile M, et al. B cell-helper neutrophils stimulate the diversification and production of immunoglobulin in the marginal zone of the spleen. *Nat Immunol* (2011) 13:170–80. doi:10.1038/ni.2194
39. Rubtsov AV, Marrack P, Rubtsova K. T-bet expressing B cells – novel target for autoimmune therapies? *Cell Immunol* (2017) 321:35–9. doi:10.1016/j.cellimm.2017.04.011
40. Rubtsova K, Rubtsov AV, Cancro MP, Marrack P. Age-associated B cells: a T-bet-dependent effector with roles in protective and pathogenic immunity. *J Immunol* (2015) 195:1933–7. doi:10.4049/jimmunol.1501209
41. Rubtsov AV, Rubtsova K, Fischer A, Meehan RT, Gillis JZ, Kappler JW, et al. Toll-like receptor 7 (TLR7)-driven accumulation of a novel CD11c(+) B-cell population is important for the development of autoimmunity. *Blood* (2011) 118:1305–15. doi:10.1182/blood-2011-01-331462
42. Becker AM, Dao KH, Han BK, Kornu R, Lakhanpal S, Mobley AB, et al. SLE peripheral blood B cell, T cell and myeloid cell transcriptomes display unique profiles and each subset contributes to the interferon signature. *PLoS One* (2013) 8:e67003. doi:10.1371/journal.pone.0067003
43. Claes N, Fraussen J, Vanheusden M, Hellings N, Stinissen P, Van Wijmeersch B, et al. Age-associated B cells with proinflammatory characteristics are expanded in a proportion of multiple sclerosis patients. *J Immunol* (2016) 197: 4576–83. doi:10.4049/jimmunol.1502448
44. Wang Z, Wang Z, Wang J, Diao Y, Qian X, Zhu N. T-bet-expressing B cells are positively associated with Crohn's disease activity and support Th1 inflammation. *DNA Cell Biol* (2016) 35:628–35. doi:10.1089/dna.2016.3304
45. Rubtsova K, Rubtsov AV, Thurman JM, Mennona JM, Kappler JW, Marrack P. B cells expressing the transcription factor T-bet drive lupus-like autoimmunity. *J Clin Invest* (2017) 127:1392–404. doi:10.1172/JCI91250
46. Huber K, Sarmay G, Kovesdi D. MZ B cells migrate in a T-bet dependent manner and might contribute to the remission of collagen-induced arthritis by the secretion of IL-10. *Eur J Immunol* (2016) 46:2239–46. doi:10.1002/eji.201546248
47. Wang S, Xia P, Chen Y, Huang G, Xiong Z, Liu J, et al. Natural killer-like B cells prime innate lymphocytes against microbial infection. *Immunity* (2016) 45:131–44. doi:10.1016/j.immuni.2016.06.019
48. Pascual V, Victor K, Lelsz D, Spellerberg MB, Hamblin TJ, Thompson KM, et al. Nucleotide sequence analysis of the V regions of two IgM cold agglutinins. Evidence that the VH4-21 gene segment is responsible for the major cross-reactive idiotype. *J Immunol* (1991) 146:4385–91.
49. Grillot-Courvalin C, Brouet JC, Piller F, Rassenti LZ, Labaume S, Silverman GJ, et al. An anti-B cell autoantibody from Wiskott-Aldrich syndrome which recognizes i blood group specificity on normal human B cells. *Eur J Immunol* (1992) 22:1781–8. doi:10.1002/eji.1830220717
50. Schickel JN, Glauzy S, Ng YS, Chamberlain N, Massad C, Isnardi I, et al. Self-reactive VH4-34-expressing IgG B cells recognize commensal bacteria. *J Exp Med* (2017) 214:1991–2003. doi:10.1084/jem.20160201
51. Ekland EH, Forster R, Lipp M, Cyster JG. Requirements for follicular exclusion and competitive elimination of autoantigen-binding B cells. *J Immunol* (2004) 172:4700–8. doi:10.4049/jimmunol.172.8.4700
52. Cappione A III, Anolik JH, Pugh-Bernard A, Barnard J, Dutcher P, Silverman G, et al. Germinal center exclusion of autoreactive B cells is defective in human systemic lupus erythematosus. *J Clin Invest* (2005) 115:3205–16. doi:10.1172/JCI24179
53. Zouali M. Immunological tolerance: mechanisms. *eLS*. Chichester, UK: John Wiley & Sons, Ltd (2014). doi:10.1002/9780470015902.a0000950.pub3
54. Bermejo DA, Jackson SW, Gorosito-Serran M, Acosta-Rodriguez EV, Amezcua-Vesely MC, Sather BD, et al. Trypanosoma cruzi trans-sialidase initiates a program independent of the transcription factors RORgammat and Ahr that leads to IL-17 production by activated B cells. *Nat Immunol* (2013) 14:514–22. doi:10.1038/ni.2569
55. Rauch PJ, Chudnovskiy A, Robbins CS, Weber GF, Etzrodt M, Hilgendorf I, et al. Innate response activator B cells protect against microbial sepsis. *Science* (2012) 335:597–601. doi:10.1126/science.1215173
56. Weber GF, Chousterman BG, Hilgendorf I, Robbins CS, Theurl I, Gerhardt LM, et al. Pleural innate response activator B cells protect against pneumonia via a GM-CSF-IgM axis. *J Exp Med* (2014) 211:1243–56. doi:10.1084/jem.20131471
57. Mikuls TR, Payne JB, Deane KD, Thiele GM. Autoimmunity of the lung and oral mucosa in a multisystem inflammatory disease: the spark that lights the fire in rheumatoid arthritis? *J Allergy Clin Immunol* (2016) 137:28–34. doi:10.1016/j.jaci.2015.10.024
58. Zouggari Y, Ait-Oufella H, Bonnin P, Simon T, Sage AP, Guerin C, et al. B lymphocytes trigger monocyte mobilization and impair heart function after acute myocardial infarction. *Nat Med* (2013) 19:1273–80. doi:10.1038/nm.3284
59. Ait-Oufella H, Herbin O, Bouaziz JD, Binder CJ, Uyttenhove C, Laurans L, et al. B cell depletion reduces the development of atherosclerosis in mice. *J Exp Med* (2010) 207:1579–87. doi:10.1084/jem.20100155
60. Kyaw T, Tipping P, Bobik A, Toh BH. Protective role of natural IgM-producing B1a cells in atherosclerosis. *Trends Cardiovasc Med* (2012) 22:48–53. doi:10.1016/j.tcm.2012.06.011
61. Tsiantoulas D, Sage AP, Mallat Z, Binder CJ. Targeting B cells in atherosclerosis: closing the gap from bench to bedside. *Arterioscler Thromb Vasc Biol* (2015) 35:296–302. doi:10.1161/ATVBAHA.114.303569
62. Nus M, Sage AP, Lu Y, Masters L, Lam BYH, Newland S, et al. Marginal zone B cells control the response of follicular helper T cells to a high-cholesterol diet. *Nat Med* (2017) 23:601–10. doi:10.1038/nm.4315
63. De Filippo G, Pozzi N, Cosentini E, Cavalcanti M, Carel JC, Tamasi S, et al. Increased CD5+CD19+ B lymphocytes at the onset of type 1 diabetes in children. *Acta Diabetol* (1997) 34:271–4. doi:10.1007/s005920050087
64. Hasler P, Zouali M. B cell receptor signaling and autoimmunity. *FASEB J* (2001) 15:2085–98. doi:10.1096/fj.00-0860rev
65. Habib T, Funk A, Rieck M, Brahmandam A, Dai X, Panigrahi AK, et al. Altered B cell homeostasis is associated with type I diabetes and carriers of the PTPN22 allelic variant. *J Immunol* (2012) 188:487–96. doi:10.4049/jimmunol.1102176
66. Thomas JW, Kendall PL, Mitchell HG. The natural autoantibody repertoire of nonobese diabetic mice is highly active. *J Immunol* (2002) 169:6617–24. doi:10.4049/jimmunol.169.11.6617
67. Kendall PL, Woodward EJ, Hulbert C, Thomas JW. Peritoneal B cells govern the outcome of diabetes in non-obese diabetic mice. *Eur J Immunol* (2004) 34:2387–95. doi:10.1002/eji.200324744

68. Diana J, Simoni Y, Furio L, Beaudoin L, Agerberth B, Barrat F, et al. Crosstalk between neutrophils, B-1a cells and plasmacytoid dendritic cells initiates autoimmune diabetes. *Nat Med* (2013) 19:65–73. doi:10.1038/nm.3042
69. Rauber S, Luber M, Weber S, Maul L, Soare A, Wohlfahrt T, et al. Resolution of inflammation by interleukin-9-producing type 2 innate lymphoid cells. *Nat Med* (2017) 23:938–44. doi:10.1038/nm.4373
70. Donati G. The niche in single-cell technologies. *Immunol Cell Biol* (2016) 94:250–5. doi:10.1038/icb.2015.107
71. Villani AC, Satija R, Reynolds G, Sarkizova S, Shekhar K, Fletcher J, et al. Single-cell RNA-seq reveals new types of human blood dendritic cells, monocytes, and progenitors. *Science* (2017) 356:eaah4573. doi:10.1126/science.aah4573
72. See P, Dutertre CA, Chen J, Gunther P, McGovern N, Irac SE, et al. Mapping the human DC lineage through the integration of high-dimensional techniques. *Science* (2017) 356:eaag3009. doi:10.1126/science.aag3009
73. Gaublomme JT, Yosef N, Lee Y, Gertner RS, Yang LV, Wu C, et al. Single-cell genomics unveils critical regulators of Th17 cell pathogenicity. *Cell* (2015) 163:1400–12. doi:10.1016/j.cell.2015.11.009
74. Wang C, Yosef N, Gaublomme J, Wu C, Lee Y, Clish CB, et al. CD5L/AIM regulates lipid biosynthesis and restrains Th17 cell pathogenicity. *Cell* (2015) 163:1413–27. doi:10.1016/j.cell.2015.10.068

Conflict of Interest Statement: The authors declare that the research was conducted in the absence of any commercial or financial relationships that could be construed as a potential conflict of interest.

The handling Editor declared a shared affiliation, though no other collaboration, with one of the authors MZ.

frontiers in Immunology

PERSPECTIVE
published: 06 July 2018
doi: 10.3389/fimmu.2018.01497

Potential Chronotherapeutic Optimization of Antimalarials in Systemic Lupus Erythematosus: Is Toll-Like Receptor 9 Expression Dependent on the Circadian Cycle in Humans?

*Erika Aurora Martínez-García[1,2,3], Maria Guadalupe Zavala-Cerna[4], Andrea Verónica Lujano-Benítez[1], Pedro Ernesto Sánchez-Hernández[2,5], Beatriz Teresita Martín-Márquez[1,3], Flavio Sandoval-García[1,6,7] and Mónica Vázquez-Del Mercado[1,3,8]**

[1] Instituto de Investigación en Reumatología y del Sistema Músculo Esquelético, Centro Universitario de Ciencias de la Salud, Universidad de Guadalajara, Guadalajara, Mexico, [2] Departamento de Fisiología, Centro Universitario de Ciencias de la Salud, Universidad de Guadalajara, Guadalajara, Mexico, [3] UDG-CA-703, Inmunología y Reumatología, Centro Universitario de Ciencias de la Salud, Universidad de Guadalajara, Guadalajara, Mexico, [4] Immunology Research Laboratory, Programa Internacional de Medicina, Universidad Autonoma de Guadalajara, Guadalajara, Mexico, [5] Laboratorio de Inmunología, Centro Universitario de Ciencias de la Salud, Universidad de Guadalajara, Guadalajara, Mexico, [6] Departamento de Clínicas Médicas, Centro Universitario de Ciencias de la Salud, Universidad de Guadalajara, Guadalajara, Mexico, [7] UDG CA-701, Inmunometabolismo en Enfermedades Emergentes (GIIEE), Centro Universitario de Ciencias de la Salud, Universidad de Guadalajara, Guadalajara, Mexico, [8] Hospital Civil de Guadalajara "Juan I. Menchaca", Servicio de Reumatología, Programa Nacional de Posgrados de Calidad (PNPC), Consejo Nacional de Ciencia y Tecnología (CONACYT), Guadalajara, Mexico

OPEN ACCESS

Edited by:
Moncef Zouali, Institut National de la Santé et de la Recherche Médicale (INSERM), France

Reviewed by:
Peter Korsten, Universitätsmedizin Göttingen, Germany
Sally Ishizaka, Eisai, United States

***Correspondence:**
Mónica Vázquez-Del Mercado
dravme@hotmail.com

Specialty section:
This article was submitted to Molecular Innate Immunity, a section of the journal Frontiers in Immunology

Received: *12 January 2018*
Accepted: *15 June 2018*
Published: *06 July 2018*

Citation:
Martínez-García EA, Zavala-Cerna MG, Lujano-Benítez AV, Sánchez-Hernández PE, Martín-Márquez BT, Sandoval-García F and Vázquez-Del Mercado M (2018) Potential Chronotherapeutic Optimization of Antimalarials in Systemic Lupus Erythematosus: Is Toll-Like Receptor 9 Expression Dependent on the Circadian Cycle in Humans? Front. Immunol. 9:1497. doi: 10.3389/fimmu.2018.01497

Toll-like receptor 9 (TLR9) belongs to the group of endosomal receptors of the innate immune system with the ability to recognize hypomethylated CpG sequences from DNA. There is scarce information about TLR9 expression and its association with the circadian cycle (CC). Different patterns of TLR9 expression are regulated by the CC in mice, with an elevated expression at Zeitgeber time 19 (1:00 a.m.); nevertheless, we still need to corroborate this in humans. In systemic lupus erythematosus (SLE), the inhibitory effect of chloroquine (CQ) on TLR9 is limited. TLR9 activation has been associated with the presence of some autoantibodies: anti-Sm/RNP, anti-histone, anti-Ro, anti-La, and anti-double-stranded DNA. Treatment with CQ for SLE has been proven to be useful, in part by interfering with HLA-antigen coupling and with TLR9 ligand recognition. Studies have shown that TLR9 inhibitors such as antimalarial drugs are able to mask TLR9-binding sites on nucleic acids. The data presented here provide the basic information that could be useful for other clinical researchers to design studies that will have an impact in achieving a chronotherapeutic effect by defining the ideal time for CQ administration in SLE patients, consequently reducing the pathological effects that follow the activation of TLR9.

Keywords: toll-like receptor 9, systemic lupus erythematosus, circadian cycle, chronotherapy, chloroquine

INTRODUCTION

The main role of the immune system is to identify and eliminate health threats through mechanisms of both adaptive and innate immunity (1, 2). The adaptive immune system specifically recognizes pathogens through T cell receptors and B cell receptors, while for the innate immune system, the use of pattern-recognition receptors (PRRs) has long been identified to help recognize pathogen-associated

molecular patterns (PAMPs) and damage-associated molecular patterns (3). Toll-like receptor 9 (TLR9) is a PRR that recognizes hypomethylated CpG-DNA sequences in bacteria, viruses, and host DNA, which favor TLR9 signaling when they are included in immune complexes (4–7). Moreover, it has been proposed that TLR9 might be responsible for the initiation of autoimmunity, particularly in systemic lupus erythematosus (SLE), where the production of autoantibodies against double-stranded DNA (dsDNA) is a common characteristic (8). Historically, the use of antimalarial drugs (AMDs) such as chloroquine (CQ) and its analogs has been shown to be effective in the treatment of autoimmune diseases such as SLE (9–11). In general, it has been suggested that CQ could inhibit the endosomal acidification that is necessary for intracellular antigen processing and presentation (12). However, for the inhibition of TLR9 activation, acidification might not be the most important factor, since TLR9 requires contact with its ligand, and CQ has been shown to interfere by masking the TLR9-binding sites on the ligands. Therefore, this pathway has been described as one of the mechanisms through which CQ decreases the inflammatory response (13). It has been widely reported that cells and proteins of the immune system are regulated by the circadian cycle (CC) (14, 15); however, there are few studies that describe the impact of TLR9 circadian regulation and the therapeutic repercussions for SLE. This perspective deals with the evidence of TLR9 expression patterns related to CC and the interference of CQ in TLR9 activation, suggesting that in theory, it is possible to improve the benefit of CQ treatment based on its chronotherapeutic effect, and this might be exploited to reduce the activation of TLR9 that includes the production of autoantibodies and inflammatory cytokines in SLE. This information will be useful to conduct future clinical studies to achieve the best treatment results with CQ.

TOLL-LIKE RECEPTOR 9

Toll-like receptor 9 identification occurred during homology structure studies on different Toll-Like Receptors (TLRs) (4, 16–18). TLRs are highly conserved proteins by means of positive selection induced *via* gene duplication (19–22). The human *TLR9* (*hTLR9*) gene is localized on chromosome 3p21.3 and consists of two exons that encode for 1,032 amino acids (aa) (18). There are five reported isoforms of TLR9, produced by alternative splicing: TLR9A to TLR9E, with variable expression in B and T cells (18, 23, 24). The protein structure of TLR9 has three domains: (1) an extracellular domain with leucine-rich repeats that recognizes pathogens, (2) a single transmembrane domain, and (3) an intracellular toll-interleukin 1 receptor (TIR) domain for signal transduction (25).

According to various studies, hTLR9 expression is predominant in the spleen, lymph nodes, tonsil, skin (keratinocytes), kidney, and peripheral blood leukocytes [dendritic cells (DCs), B cells, macrophages, neutrophils, eosinophils, natural killer, and T cells] (26–34). In all of them, TLR9 elicits their activation after engaging PAMPs. Despite the typical intracellular localization of TLR9 in endosomes, two additional sites of expression were described: (1) the cell surface of human and mouse neutrophils, intestinal epithelial cells (IEC), mouse colonic tissue, and hepatocellular carcinoma cells (35–37) and (2) a soluble form in bacterial pleural effusions and human embryonic kidney 293 cells (**Figure 1A**) (38, 39). The different localizations of TLR9 possibly have a role in its function (40), a concept that will be discussed in detail in the following section.

TLR9: THE PATH TO ENDOSOMES FOR LIGAND IDENTIFICATION AND ACTIVATION

Endosomes or phagosomes are cell structures that contain PAMPs derived from phagocytosed pathogens. Inside these structures is where TLR9 engages targets and elicits cell activation (41, 42). Importantly, in studies performed with laser scanning confocal microscopy, it was found that before TLR9 interacts with endosomes or lysosomes, it is located in its full-length form (immature) inside the endoplasmic reticulum and/or the Golgi apparatus (GA) (43, 44) (**Figure 1B**). TLR9 is then translocated with unc-93 homolog B1 (UNC93B1), a facilitator protein, from the GA toward the cell surface, where it is associated with an adaptor protein complex 2 for internalization to endosomes (45–47). The binding between TLR9 and UNC93B1 depends on the presence of a specific sequence of aa located in the juxtamembrane region of TLR9. This finding became evident after the observation that mutated proteins with changes in the aa residues from Asp^{812} to Ser (D812S) and from Glu^{813} to Thr (E813T) in mice avoided the interaction between TLR9 and UNC93B1 and disrupted the continuous trafficking of TLR9 toward the endosome (48). There is still missing information as to whether this intracellular trafficking is required for other TLRs since, in the case of TLR7, for example, although it interacts with UNC93B1 protein, transportation from the GA to endosomes occurs without cell surface expression (46, 49). Once TLR9 is located in endosomes, it undergoes proteolytic cleavage performed by cathepsins (50, 51), generating a protein of 80 kDa, which is required for the adequate functioning of the receptor (52). Other proteolytic cleavage sites by cathepsins have been described in the aminoterminal region ($NH_3$1-723 aa) of TLR9, producing a protein of 100 kDa that lacks the transmembrane and TIR domains, i.e., a soluble form retained in endosomes that inhibits TLR9 signaling (39). Importantly, the proteolytic function of cathepsins and other enzymes involved in the activation and signaling of TLR9 within the endosome microenvironment are carried out at an acidic pH (5.0 ± 0.2) (50, 53, 54). It is clear that the endosomal pH is an important factor for the activation of TLR9; however, when referring to TLR9 being expressed on the cell surface, there are no conclusive studies on its function or form of activation. However, one study performed in human hepatocellular carcinoma cell lines concluded that the expression of TLR9 on hepatocyte cell surface promotes tumorigenesis and cancer progression by promoting cellular proliferation and cell survival after receptor stimulation with CpG-oligodeoxynucleotides (CpG-ODNs) (55). Other studies suggest that cell surface expression of TLR9 is a rescue mechanism for the activation of neutrophils when their ligands are not internalized to endosomes or when intracellular TLR9 shows resistance to activation (35). Once endosomal TLR9 is sensitized by its ligand, it triggers MyD88-dependent signaling that induces the production of pro-inflammatory cytokines after activation of NF-kB (56–59).

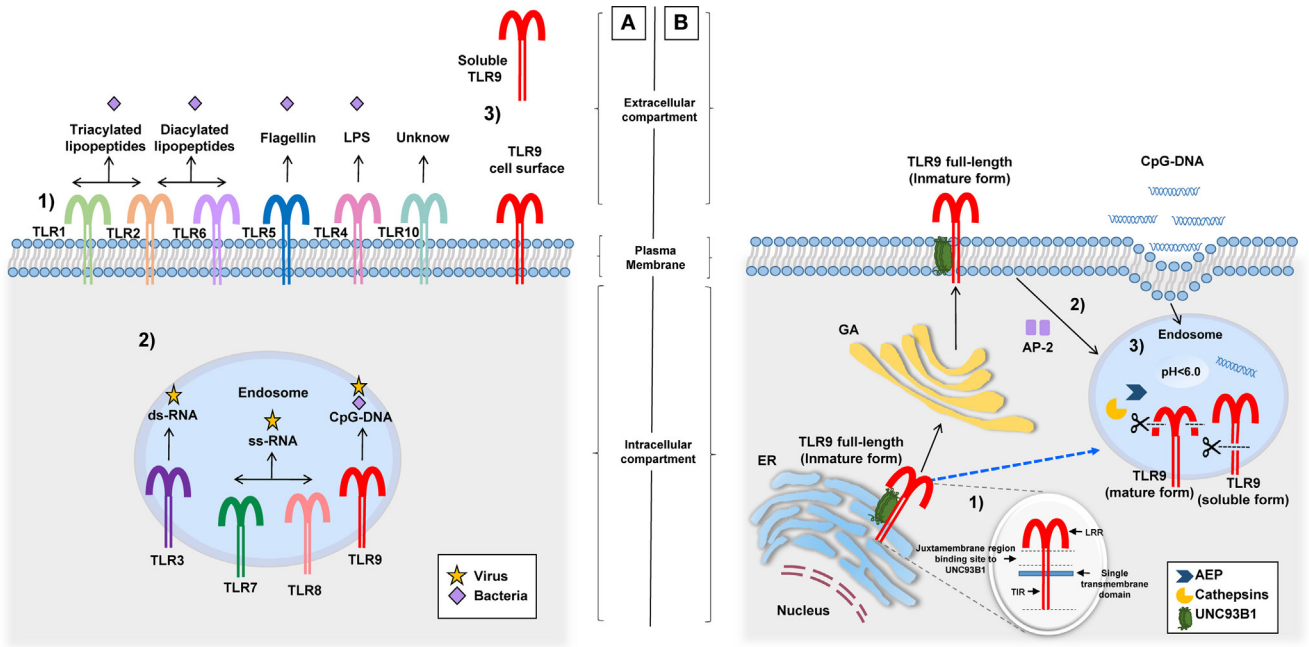

FIGURE 1 | Different locations of TLRs and the TLR9 signaling route. **(A)** (1) TLRs (and their respective ligand) expressed on the cell surface: TLR1/TLR2 (triacylated lipopeptides), TLR2/TLR6 (diacylated lipopeptides), TLR5 (flagellin), TLR4 (LPS), and TLR10 (unknown). (2) TLRs expressed in endosomes: TLR3 (ds-RNA), TLR7/TLR8 (ss-RNA), and TLR9 (CpG-DNA). (3) TLR9 cell surface expression related to their signaling route and soluble form identified in pleural effusions and HEK 293 cells, although its production and functions are unknown. **(B)** Before TLR9 is located inside the endosome, it can be identified in the ER, the GA, and lysosomes. (1) Inside the ER, the juxtamembrane region of TLR9 interacts with UNC93B1, a facilitator protein that allows the exit of TLR9 toward the cell surface or directly to endosomes (dotted blue line). (2) Once on the cell surface, TLR9 becomes associated with AP-2 for cell internalization through the interaction with phagosomes or endosomes. (3) In this location, TLR9 modifies its structure by the action of AEP and cathepsins generating a mature form (80 kDa) and a soluble form (100 kDa) without transmembrane and TIR domains, this form is retained in the endosome and prevents the activation of TLR9. Abbreviations: ER, endoplasmic reticulum; GA, Golgi apparatus; LPS, lipopolysaccharide; HEK 293, human embryonic kidney 293; UNC93B1, unc-93 homolog B1; AP-2, adaptor protein complex 2; AEP, asparagine endopeptidase; TLR9, toll-like receptor 9; TIR, toll-interleukin 1 receptor; LRR, Leucine-rich repeats.

SLE, AMDs, AND THE INHIBITION OF TLR9

Loss of immunological tolerance in SLE is responsible for the secretion of circulating autoantibodies against cellular components such as nucleosomes, histones, ribonucleoproteins, DNA, and RNA helicase A, among others (60–63). One of the theories for autoantibody generation in SLE is the inefficient removal of cellular debris after apoptosis and neutrophil extracellular traps, two different processes in origin that could lead to an increased amount of free DNA and RNA when there is a defective removal of debris by macrophages (64–69). The principal autoantibodies associated with impaired clearance of cellular antigens in SLE are Sm/RNP, histone, Ro/La, and dsDNA (70–72). Artificial autoantibody production against nuclear antigens was described with the use of hydralazine. The mechanism proposed was the inhibition of the ERK signaling pathway with hydralazine, which caused a downregulation of the DNA methyltransferase 1 (*DNMT1*) mRNA, necessary for DNA methylation (73–75). It is important to acknowledge that hypomethylated DNA is a PAMP recognized by TLR9. In addition, both in humans and mice, TLR9 is involved in inflammation *via* the synthesis of inflammatory cytokines and activation of autoreactive B cells, contributing to autoantibody production and the subsequent clinical development of autoimmune features (76). In murine models of lupus-prone and mixed bone marrow chimeras, it became evident that when there was a lack of expression of endosomal TLRs, autoantibody production was absent. In the absence of TLR7, mice failed to generate anti-Sm/RNP autoantibodies and mice lacking TLR9 failed to produce anti-dsDNA autoantibodies (77, 78). The mRNA expression of *TLR7* and *TLR9* in SLE patients was associated with testing positive for anti-extractable nuclear antigens and anti-dsDNA, respectively (79). In addition, in kidney biopsies from patients with lupus nephritis (LN), there was evidence of TLR3, TLR7, and TLR9 overexpression with a positive correlation between TLR9 expression and high activity, measured by renal-systemic lupus erythematosus (R-SLEDAI) (80). Furthermore, SNPs in the *TLR9* gene, such as rs352140, were associated with LN (81).

In recent studies performed on peripheral blood mononuclear cells (PBMCs) from SLE patients and healthy individuals, there was evidence of elevated expression of TLR9 protein and mRNA, with a positive correlation to antinuclear antibodies titers (82–84). Therefore, previous studies have proposed that the modulation or inhibition of TLR9 is a potential tool for SLE treatment (85, 86). CQ was introduced as one of the AMDs that later proved to be beneficial for rheumatic diseases, mainly owing

to an anti-inflammatory, immunosuppressive, and skin photoprotective effect (9, 87, 88). The administration of AMDs in SLE patients is indicated when there are no major organ manifestations (89), without standardized time for the prescription of this drug. The lipophilic non-protonated form of CQ is diffused in a passive way to endosomes, lysosomes, or Golgi vesicles, where it is protonated and retained by ion trapping (90, 91), suggesting that this protonated form of CQ could change the acidic medium necessary for the proteolytic processing of TLR9 in endosomes. However, the cleavage of TLR9 is not inhibited by AMDs. Studies have shown that TLR9 inhibitors such as CQ are able to mask TLR9-binding sites on nucleic acids (13). It is important to explore whether CQ, in addition to the findings mentioned above, has other mechanisms related to the inhibition of TLR9. In this respect, in a mouse model of sepsis, CQ administration induced decreased expression of TLR9 in the spleen, which was associated with increased survival and reduction of renal injury; interestingly, the same effect was evident in the absence of TLR9 (TLR9-deficient mice) (92). Nonetheless, this effect has not been acknowledged in autoimmune diseases or other immune system-related pathologies.

TLR9 CIRCADIAN BEHAVIOR AND SYNCHRONIZATION WITH CQ ADMINISTRATION

The CC is known to regulate the main biological processes (physiological, metabolic, and behavioral) in living organisms, originated by oscillations of light and dark conditions within a 24-h period, which is aligned with the rotation of the earth on its own axis (93–95). Recently, the importance of the CC has been highlighted by the recipients of the Nobel Prize in Physiology and Medicine 2017: Jeffrey Hall, Michael Rosbash, and Michael Young. These investigators stated that the CC is a molecular genetic mechanism that directs various functions in *Drosophila melanogaster* (96–100), and knowledge of this has had an impact on the clinical course and treatment of the human diseases. The master regulator of the CC is localized in the suprachiasmatic nucleus (SCN) of the hypothalamus and the activity of this regulator depends on the received light through photoreceptors in the retina of both eyes (101–104). The SCN is also synchronized with other peripheral circadian clocks such as the hypothalamic–pituitary–adrenal axis and the immune system (105, 106). The molecular mechanisms of these peripheral circadian clocks are autonomous and controlled by a transcriptional–translation feedback loop in clock genes (107, 108). Some of these clock genes include the heterodimer circadian locomotor output cycles kaput gene and brain and muscle aryl hydrocarbon receptor nuclear translocator 1 gene (*Clock*:*Bmal1)* (109–111). This heterodimer functions as a transcriptional factor for the Period (*Per*) and Cryptochrome (*Cry*) genes (112, 113), whose proteins then become transcriptional repressors of the *Clock:Bmal1* heterodimer, allowing repeating of the cycle (114).

An experimental analysis performed in mouse tissues (aorta, adrenal gland, brainstem, fat, cerebellum, heart, hypothalamus, kidney, liver, lung, and skeletal muscle) demonstrated that the patterns of gene expression in 43% of the entire mouse genome had a circadian behavior (115). Particularly when referring to the immune system and the CC, it was observed that the number and functions of leukocytes are controlled by clock genes; therefore, they are subjects of this CC (116). Furthermore, after analyzing mouse peritoneal macrophages by microarray, 8.1% of expressed genes in these cells had circadian control, including *Bmal1, Clock, Per1, Per2, Cry1,* and *Cry2*, among others (117). There is evidence that the expression of these clock genes in mouse macrophages, DCs, and B cells is observed at two peaks every 12-h under light–dark conditions (118). More specifically, the percentage of neutrophils and their phagocytic function increase after dark conditions, a phenomenon that occurs in a cyclic manner (119).

Silver et al. in 2012 published their results describing that peritoneal macrophages derived from *Per2*-mutant mice ($mPer2^{Brdm1}$) that were subject to conditions of 12-h light/12-h darkness and challenged with CpG-ODNs (TLR9 ligand) at different times, had a fluctuation in the expression of *TLR9* mRNA, with peaks at Zeitgeber time (ZT) 11 (5:00 p.m.), which correlated with the production of low cytokine levels (TNF-α and IL-12); yet, this circadian behavior was not observed in TLR1, 2, 3, 4, 5, 6, and 7 (120). In addition, they reported an increase in the expression of *TLR9* mRNA and median fluorescence intensity at ZT19 (1:00 a.m.) in spleen cells compared with that at ZT7 (1:00 p.m.) (120). Moreover, the mRNA expression of *TLR1–TLR5* and *TLR9* (not *TLR6* and *TLR7*) in IEC presents a circadian pattern with higher levels at ZT0 (6:00 a.m.) vs. ZT12 (6:00 p.m.) and is dependent on the presence of retinoic acid receptor-related orphan receptor-α (121). There is a gap in the knowledge of circadian TLR9 expression. We consider that it would be interesting to research this concept in mice in depth. However, the studies performed so far have not been examined in the context of human SLE, either in the lupus-prone NZBxNZW or pristane-induced lupus models, to evaluate the role of circadian expression of TLR9 in autoimmunity.

All these results on TLR9 expression confirm the existence of circadian behavior in other organs, independent of the SCN action. A possible candidate for other anatomical regions capable of capturing the external light that entails circadian pathways in humans is the skin (122–124). In a scenario of autoimmunity, such as that in SLE, injury to the skin is the second most frequent clinical feature, which might even induce lupus flares (125). One of the main environmental factors associated with a lupus flare is UV light exposure (126), which causes DNA damage and subsequent apoptosis of keratinocytes (sunburn cells), being a source of nuclear autoantigens that undergo relocalization of autoantigens such as Ro (125–128). In this respect, *in vivo* studies showed that erythema induced after fixed doses of UV light exposure caused an exacerbated inflammatory response in the morning in comparison with that in the afternoon (129), suggesting that the skin inflammation processes depends on a CC and not entirely on UV light exposure. Other autoimmune rheumatic diseases associated with environmental triggering factors are the idiopathic inflammatory myopathies that are more prevalent near equatorial zones (130) since UV light exposure seems to be one important factor associated with its clinical

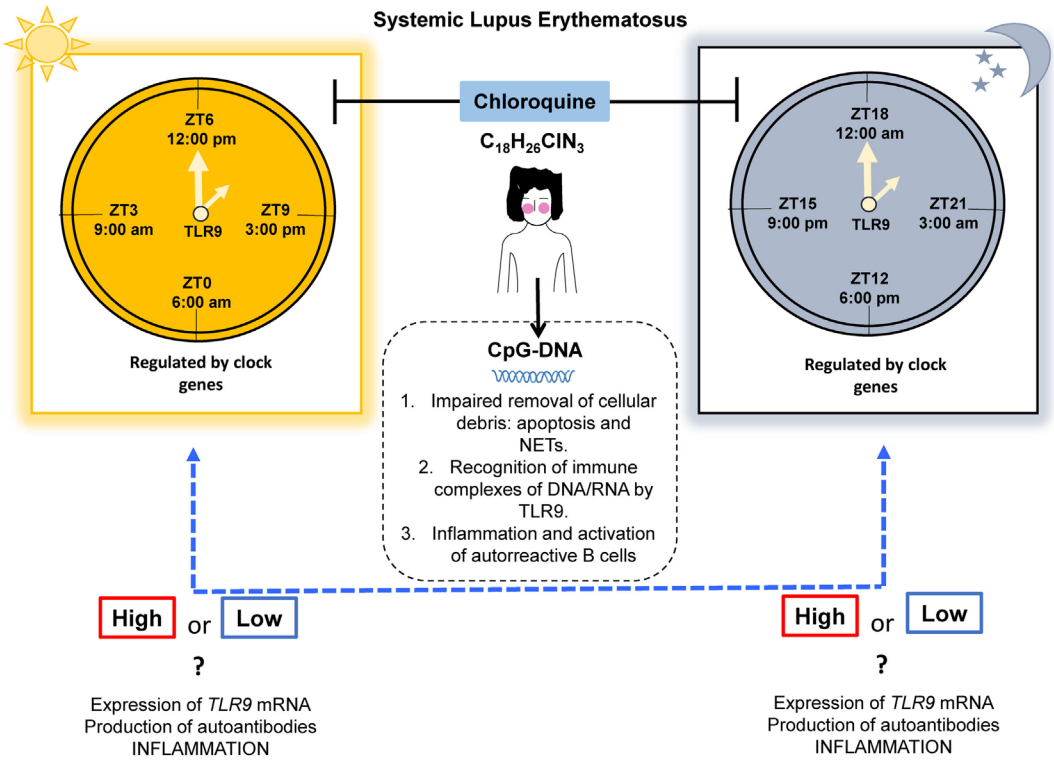

FIGURE 2 | Proposal for a chronotherapeutic effect in SLE patients receiving CQ treatment. Ligands for TLR9 include CpG-DNA, which might originate during impaired clearance of cellular debris. The expression of TLR9 has shown circadian behavior in mice, with higher expression at ZT19 (1:00 a.m.) and lower expression at ZT7 (1:00 p.m.) and this is regulated by clock genes. However, in humans, this information is lacking. CQ acts as an inhibitor of TLR9 by masking its binding sites for nucleic acids. We propose that the chronotherapeutic optimization of CQ would make it more beneficial if it is prescribed when there is maximal expression of TLR9 in SLE that possibly leads to a reduction in the expression of TLR9, autoantibodies production, and inflammation (dotted blue line). Abbreviations: CQ, chloroquine; SLE, systemic lupus erythematosus; ZT, Zeitgeber time; NETs, neutrophil extracellular traps; TLR9, toll-like receptor 9.

presentation. Indeed, our group has reported the high prevalence of anti-Mi-2 antibodies in these subsets of autoimmune rheumatic diseases (131).

On the other hand, it is well known that the CC influences the pharmacodynamics of drugs (132, 133), which gives rise to the term chronotherapy, defined as the administration of drugs according to biological clocks: daily, monthly, seasonal, or yearly, leading to the maximum benefit and reduction of adverse effects (134). Perhaps the best clinical example is the optimization of glucocorticoid (GC) doses in patients with autoimmune conditions, including SLE, where the production of cortisol by the host allows a decrease in GC demands, therefore, providing a chronotherapeutic effect (101, 133, 135, 136). In malaria patients, the influence of CQ in the development of the parasite in erythrocytes, manifestations of the disease, and the timing effect of the drug were demonstrated in 1991, highlighting its chronotherapeutic effect for the elimination of the parasite (137).

CONCLUSION AND PERSPECTIVES

It would be extremely interesting to verify whether time-restricted expression of TLR9 and clock gene regulation is present in human beings. These findings could be demonstrated with clock-adjusted gene expression analysis in PBMCs, which might support this chronotherapeutic regimen in SLE, by increasing the modulating effect of autoantibody production and inflammation (**Figure 2**). Also, we propose to study the TLR9 expression and signaling pathways in non-lupus prone mouse strains such as the pristane-induced murine lupus model, owing to its feasibility. Here, we provided the basic evidence that different expression patterns of TLR9 are sustained in association with the CC in mice. Nevertheless, this finding still needs to be addressed in humans, taking into account the following key points: (1) the expression of TLR9 is controlled by the CC, (2) inflammatory cytokine production correlates with the expression of TLR9, (3) CQ has an anti-inflammatory effect by disrupting the signaling of intracellular TLR9, and (4) CQ is already used as monotherapy or combination therapy for autoimmune diseases. However, there is no consensus with respect to the ideal time for AMDs prescription.

ETHICS STATEMENT

All cited studies reported in the present perspective where conducted in compliance with relevant Ethical Guidelines. This article does not represent work made by the authors with human or animal subjects.

AUTHOR CONTRIBUTIONS

Conceived and designed the idea: EM-G, MZ-C, AL-B, PS-H, BM-M, FS-G, and MV-DM. Conducted the bibliographic search: EM-G and AL-B. Analysis and discussion of the information: EM-G, MZ-C, AL-B, PS-H, BM-M, and MV-DM. Wrote the paper: EM-G, MZ-C, AL-B, and MV-DM. Figure editing EM-G, AL-B, and FS-G. All the authors declare that they have read and approved the final version of the manuscript and that they are responsible for its content.

REFERENCES

1. Chaplin DD. Overview of the immune response. *J Allergy Clin Immunol* (2010) 125(2 Suppl 2):S3–23. doi:10.1016/j.jaci.2009.12.980
2. Warrington R, Watson W, Kim HL, Antonetti FR. An introduction to immunology and immunopathology. *Allergy Asthma Clin Immunol* (2011) 7(Suppl 1):S1. doi:10.1186/1710-1492-7-S1-S1
3. Delves PJ, Roitt IM. The immune system. First of two parts. *N Engl J Med* (2000) 343(1):37–49. doi:10.1056/NEJM200007063430107
4. Hemmi H, Takeuchi O, Kawai T, Kaisho T, Sato S, Sanjo H, et al. A toll-like receptor recognizes bacterial DNA. *Nature* (2000) 408(6813):740–5. doi:10.1038/35047123
5. Krieg AM, Vollmer J. Toll-like receptors 7, 8, and 9: linking innate immunity to autoimmunity. *Immunol Rev* (2007) 220:251–69. doi:10.1111/j.1600-065X.2007.00572.x
6. Clancy RM, Markham AJ, Buyon JP. Endosomal toll-like receptors in clinically overt and silent autoimmunity. *Immunol Rev* (2016) 269(1):76–84. doi:10.1111/imr.12383
7. Brencicova E, Diebold SS. Nucleic acids and endosomal pattern recognition: how to tell friend from foe? *Front Cell Infect Microbiol* (2013) 3:37. doi:10.3389/fcimb.2013.00037
8. Han S, Zhuang H, Shumyak S, Yang L, Reeves WH. Mechanisms of autoantibody production in systemic lupus erythematosus. *Front Immunol* (2015) 6:228. doi:10.3389/fimmu.2015.00228
9. Lee SJ, Silverman E, Bargman JM. The role of antimalarial agents in the treatment of SLE and lupus nephritis. *Nat Rev Nephrol* (2011) 7(12):718–29. doi:10.1038/nrneph.2011.150
10. Tang C, Godfrey T, Stawell R, Nikpour M. Hydroxychloroquine in lupus: emerging evidence supporting multiple beneficial effects. *Intern Med J* (2012) 42(9):968–78. doi:10.1111/j.1445-5994.2012.02886.x
11. Al-Bari MA. Chloroquine analogues in drug discovery: new directions of uses, mechanisms of actions and toxic manifestations from malaria to multifarious diseases. *J Antimicrob Chemother* (2015) 70(6):1608–21. doi:10.1093/jac/dkv018
12. Fox RI, Kang HI. Mechanism of action of antimalarial drugs: inhibition of antigen processing and presentation. *Lupus* (1993) 2(Suppl 1):S9–12.
13. Kuznik A, Bencina M, Svajger U, Jeras M, Rozman B, Jerala R. Mechanism of endosomal TLR inhibition by antimalarial drugs and imidazoquinolines. *J Immunol* (2011) 186(8):4794–804. doi:10.4049/jimmunol.1000702
14. Curtis AM, Bellet MM, Sassone-Corsi P, O'Neill LA. Circadian clock proteins and immunity. *Immunity* (2014) 40(2):178–86. doi:10.1016/j.immuni.2014.02.002
15. Labrecque N, Cermakian N. Circadian clocks in the immune system. *J Biol Rhythms* (2015) 30(4):277–90. doi:10.1177/0748730415577723
16. Anderson KV, Jurgens G, Nusslein-Volhard C. Establishment of dorsal-ventral polarity in the *Drosophila* embryo: genetic studies on the role of the toll gene product. *Cell* (1985) 42(3):779–89. doi:10.1016/0092-8674(85)90275-2
17. Lemaitre B, Nicolas E, Michaut L, Reichhart JM, Hoffmann JA. The dorsoventral regulatory gene cassette spatzle/toll/cactus controls the potent antifungal response in *Drosophila* adults. *Cell* (1996) 86(6):973–83. doi:10.1016/S0092-8674(00)80172-5
18. Du X, Poltorak A, Wei Y, Beutler B. Three novel mammalian toll-like receptors: gene structure, expression, and evolution. *Eur Cytokine Netw* (2000) 11(3):362–71.
19. Mikami T, Miyashita H, Takatsuka S, Kuroki Y, Matsushima N. Molecular evolution of vertebrate toll-like receptors: evolutionary rate difference between their leucine-rich repeats and their TIR domains. *Gene* (2012) 503(2):235–43. doi:10.1016/j.gene.2012.04.007
20. Song X, Jin P, Qin S, Chen L, Ma F. The evolution and origin of animal toll-like receptor signaling pathway revealed by network-level molecular evolutionary analyses. *PLoS One* (2012) 7(12):e51657. doi:10.1371/journal.pone.0051657
21. Beutler B, Rehli M. Evolution of the TIR, tolls and TLRs: functional inferences from computational biology. In: Beutler B, Wagner H, editors. *Toll-Like Receptor Family Members and Their Ligands*. Heidelberg, Berlin: Springer (2002). p. 1–21.
22. Uematsu S, Akira S. Toll-like receptors (TLRs) and their ligands. In: Bauer S, Hartmann G, editors. *Toll-Like Receptors (TLRs) and Innate Immunity.* Heidelberg, Berlin: Springer (2008). p. 1–20.
23. Chuang TH, Ulevitch RJ. Cloning and characterization of a sub-family of human toll-like receptors: hTLR7, hTLR8 and hTLR9. *Eur Cytokine Netw* (2000) 11(3):372–8.
24. McKelvey KJ, Highton J, Hessian PA. Cell-specific expression of TLR9 isoforms in inflammation. *J Autoimmun* (2011) 36(1):76–86. doi:10.1016/j.jaut.2010.11.001
25. Godfroy JI III, Roostan M, Moroz YS, Korendovych IV, Yin H. Isolated toll-like receptor transmembrane domains are capable of oligomerization. *PLoS One* (2012) 7(11):e48875. doi:10.1371/journal.pone.0048875
26. Kim S, Kaiser V, Beier E, Bechheim M, Guenthner-Biller M, Ablasser A, et al. Self-priming determines high type I IFN production by plasmacytoid dendritic cells. *Eur J Immunol* (2014) 44(3):807–18. doi:10.1002/eji.201343806
27. Simchoni N, Cunningham-Rundles C. TLR7- and TLR9-responsive human B cells share phenotypic and genetic characteristics. *J Immunol* (2015) 194(7):3035–44. doi:10.4049/jimmunol.1402690
28. Schmitz F, Mages J, Heit A, Lang R, Wagner H. Transcriptional activation induced in macrophages by toll-like receptor (TLR) ligands: from expression profiling to a model of TLR signaling. *Eur J Immunol* (2004) 34(10):2863–73. doi:10.1002/eji.200425228
29. József L, Khreiss T, El Kebir D, Filep JG. Activation of TLR-9 induces IL-8 secretion through peroxynitrite signaling in human neutrophils. *J Immunol* (2006) 176(2):1195–202. doi:10.4049/jimmunol.176.2.1195
30. Nagase H, Okugawa S, Ota Y, Yamaguchi M, Tomizawa H, Matsushima K, et al. Expression and function of toll-like receptors in eosinophils: activation by toll-like receptor 7 ligand. *J Immunol* (2003) 171(8):3977–82. doi:10.4049/jimmunol.171.8.3977
31. Duriez M, Quillay H, Madec Y, El Costa H, Cannou C, Marlin R, et al. Human decidual macrophages and NK cells differentially express toll-like receptors and display distinct cytokine profiles upon TLR stimulation. *Front Microbiol* (2014) 5:316. doi:10.3389/fmicb.2014.00316
32. Hammond T, Lee S, Watson MW, Flexman JP, Cheng W, Fernandez S, et al. Toll-like receptor (TLR) expression on CD4+ and CD8+ T-cells in patients chronically infected with hepatitis C virus. *Cell Immunol* (2010) 264(2):150–5. doi:10.1016/j.cellimm.2010.06.001
33. Lebre MC, van der Aar AM, van Baarsen L, van Capel TM, Schuitemaker JH, Kapsenberg ML, et al. Human keratinocytes express functional toll-like receptor 3, 4, 5, and 9. *J Invest Dermatol* (2007) 127(2):331–41. doi:10.1038/sj.jid.5700530
34. Nishimura M, Naito S. Tissue-specific mRNA expression profiles of human toll-like receptors and related genes. *Biol Pharm Bull* (2005) 28(5):886–92. doi:10.1248/bpb.28.886
35. Lindau D, Mussard J, Wagner BJ, Ribon M, Rönnefarth VM, Quettier M, et al. Primary blood neutrophils express a functional cell surface toll-like receptor 9. *Eur J Immunol* (2013) 43(8):2101–13. doi:10.1002/eji.201142143
36. Ewaschuk JB, Backer JL, Churchill TA, Obermeier F, Krause DO, Madsen KL. Surface expression of toll-like receptor 9 is upregulated on intestinal epithelial cells in response to pathogenic bacterial DNA. *Infect Immun* (2007) 75(5):2572–9. doi:10.1128/IAI.01662-06
37. Miyake K, Onji M. Endocytosis-free DNA sensing by cell surface TLR9 in neutrophils: rapid defense with autoimmune risks. *Eur J Immunol* (2013) 43(8):2006–9. doi:10.1002/eji.201343882
38. Yang HB, Xie KQ, Deng JM, Qin SM. Expression of soluble toll-like receptors in pleural effusions. *Chin Med J (Engl)* (2010) 123(16):2225–30. doi:10.3760/cma.j.issn.0366-6999.2010.16.013

39. Chockalingam A, Cameron JL, Brooks JC, Leifer CA. Negative regulation of signaling by a soluble form of toll-like receptor 9. *Eur J Immunol* (2011) 41(8):2176–84. doi:10.1002/eji.201041034
40. Lee BL, Barton GM. Trafficking of endosomal toll-like receptors. *Trends Cell Biol* (2014) 24(6):360–9. doi:10.1016/j.tcb.2013.12.002
41. Gleeson PA. The role of endosomes in innate and adaptive immunity. *Semin Cell Dev Biol* (2014) 31:64–72. doi:10.1016/j.semcdb.2014.03.002
42. Swiecki M, Colonna M. The multifaceted biology of plasmacytoid dendritic cells. *Nat Rev Immunol* (2015) 15(8):471–85. doi:10.1038/nri3865
43. Latz E, Schoenemeyer A, Visintin A, Fitzgerald KA, Monks BG, Knetter CF, et al. TLR9 signals after translocating from the ER to CpG DNA in the lysosome. *Nat Immunol* (2004) 5(2):190–8. doi:10.1038/ni1028
44. Leifer CA, Kennedy MN, Mazzoni A, Lee C, Kruhlak MJ, Segal DM. TLR9 is localized in the endoplasmic reticulum prior to stimulation. *J Immunol* (2004) 173(2):1179–83. doi:10.4049/jimmunol.173.2.1179
45. Kim YM, Brinkmann MM, Paquet ME, Ploegh HL. UNC93B1 delivers nucleotide-sensing toll-like receptors to endolysosomes. *Nature* (2008) 452(7184):234–8. doi:10.1038/nature06726
46. Lee BL, Moon JE, Shu JH, Yuan L, Newman ZR, Schekman R, et al. UNC93B1 mediates differential trafficking of endosomal TLRs. *Elife* (2013) 2:e00291. doi:10.7554/eLife.00291
47. Manoury B. TLR9 regulation by proteolysis: a friend or a foe. *Eur J Immunol* (2011) 41(8):2142–4. doi:10.1002/eji.201141858
48. Kim J, Huh J, Hwang M, Kwon EH, Jung DJ, Brinkmann MM, et al. Acidic amino acid residues in the juxtamembrane region of the nucleotide-sensing TLRs are important for UNC93B1 binding and signaling. *J Immunol* (2013) 190(10):5287–95. doi:10.4049/jimmunol.1202767
49. Petes C, Odoardi N, Gee K. The toll for trafficking: toll-like receptor 7 delivery to the endosome. *Front Immunol* (2017) 8:1075. doi:10.3389/fimmu.2017.01075
50. Park B, Brinkmann MM, Spooner E, Lee CC, Kim YM, Ploegh HL. Proteolytic cleavage in an endolysosomal compartment is required for activation of toll-like receptor 9. *Nat Immunol* (2008) 9(12):1407–14. doi:10.1038/ni.1669
51. Matsumoto F, Saitoh S, Fukui R, Kobayashi T, Tanimura N, Konno K, et al. Cathepsins are required for toll-like receptor 9 responses. *Biochem Biophys Res Commun* (2008) 367(3):693–9. doi:10.1016/j.bbrc.2007.12.130
52. Ewald SE, Lee BL, Lau L, Wickliffe KE, Shi GP, Chapman HA, et al. The ectodomain of toll-like receptor 9 is cleaved to generate a functional receptor. *Nature* (2008) 456(7222):658–62. doi:10.1038/nature07405
53. Tycko B, Maxfield FR. Rapid acidification of endocytic vesicles containing alpha 2-macroglobulin. *Cell* (1982) 28(3):643–51. doi:10.1016/0092-8674(82)90219-7
54. Ewald SE, Engel A, Lee J, Wang M, Bogyo M, Barton GM. Nucleic acid recognition by toll-like receptors is coupled to stepwise processing by cathepsins and asparagine endopeptidase. *J Exp Med* (2011) 208(4):643–51. doi:10.1084/jem.20100682
55. Tanaka J, Sugimoto K, Shiraki K, Tameda M, Kusagawa S, Nojiri K, et al. Functional cell surface expression of toll-like receptor 9 promotes cell proliferation and survival in human hepatocellular carcinomas. *Int J Oncol* (2010) 37(4):805–14. doi:10.3892/ijo_00000730
56. Blasius AL, Beutler B. Intracellular toll-like receptors. *Immunity* (2010) 32(3):305–15. doi:10.1016/j.immuni.2010.03.012
57. Sasai M, Iwasaki A. Love triangle between Unc93B1, TLR7, and TLR9 prevents fatal attraction. *Immunity* (2011) 35(1):3–5. doi:10.1016/j.immuni.2011.07.006
58. Bauer S. Toll-like receptor 9 processing: the key event in toll-like receptor 9 activation? *Immunol Lett* (2013) 149(1–2):85–7. doi:10.1016/j.imlet.2012.11.003
59. Liu XJ, Liu T, Chen G, Wang B, Yu XL, Yin C, et al. TLR signaling adaptor protein MyD88 in primary sensory neurons contributes to persistent inflammatory and neuropathic pain and neuroinflammation. *Sci Rep* (2016) 6:28188. doi:10.1038/srep28188
60. Tsokos GC, Lo MS, Costa Reis P, Sullivan KE. New insights into the immunopathogenesis of systemic lupus erythematosus. *Nat Rev Rheumatol* (2016) 12(12):716–30. doi:10.1038/nrrheum.2016.186
61. La Paglia GMC, Leone MC, Lepri G, Vagelli R, Valentini E, Alunno A, et al. One year in review 2017: systemic lupus erythematosus. *Clin Exp Rheumatol* (2017) 35(4):551–61.
62. Vázquez-Del Mercado M, Palafox-Sánchez CA, Muñoz-Valle JF, Orozco-Barocio G, Oregon-Romero E, Navarro-Hernández RE, et al. High prevalence of autoantibodies to RNA helicase A in Mexican patients with systemic lupus erythematosus. *Arthritis Res Ther* (2010) 12(1):R6. doi:10.1186/ar2905
63. Palafox Sánchez CA, Satoh M, Chan EK, Carcamo WC, Muñoz Valle JF, Orozco Barocio G, et al. Reduced IgG anti-small nuclear ribonucleoprotein autoantibody production in systemic lupus erythematosus patients with positive IgM anti-cytomegalovirus antibodies. *Arthritis Res Ther* (2009) 11(1):R27. doi:10.1186/ar2621
64. Kruse K, Janko C, Urbonaviciute V, Mierke CT, Winkler TH, Voll RE, et al. Inefficient clearance of dying cells in patients with SLE: anti-dsDNA autoantibodies, MFG-E8, HMGB-1 and other players. *Apoptosis* (2010) 15(9):1098–113. doi:10.1007/s10495-010-0478-8
65. Pieterse E, van der Vlag J. Breaking immunological tolerance in systemic lupus erythematosus. *Front Immunol* (2014) 5:164. doi:10.3389/fimmu.2014.00164
66. Podolska MJ, Biermann MH, Maueröder C, Hahn J, Herrmann M. Inflammatory etiopathogenesis of systemic lupus erythematosus: an update. *J Inflamm Res* (2015) 8:161–71. doi:10.2147/JIR.S70325
67. Bai Y, Tong Y, Liu Y, Hu H. Self-dsDNA in the pathogenesis of systemic lupus erythematosus. *Clin Exp Immunol* (2018) 191(1):1–10. doi: 10.1111/cei.13041
68. Radic M. Clearance of apoptotic bodies, NETs, and biofilm DNA: implications for autoimmunity. *Front Immunol* (2014) 5:365. doi:10.3389/fimmu.2014.00365
69. Berthelot JM, Le Goff B, Neel A, Maugars Y, Hamidou M. NETosis: at the crossroads of rheumatoid arthritis, lupus, and vasculitis. *Joint Bone Spine* (2017) 84(3):255–62. doi:10.1016/j.jbspin.2016.05.013
70. Mahajan A, Herrmann M, Munoz LE. Clearance deficiency and cell death pathways: a model for the pathogenesis of SLE. *Front Immunol* (2016) 7:35. doi:10.3389/fimmu.2016.00035
71. Dema B, Charles N. Autoantibodies in SLE: specificities, isotypes and receptors. *Antibodies* (2016) 5(1):2. doi:10.3390/antib5010002
72. Satoh M, Vazquez-Del Mercado M, Chan EK. Clinical interpretation of antinuclear antibody tests in systemic rheumatic diseases. *Mod Rheumatol* (2009) 19(3):219–28. doi:10.1007/s10165-009-0155-3
73. Deng C, Lu Q, Zhang Z, Rao T, Attwood J, Yung R, et al. Hydralazine may induce autoimmunity by inhibiting extracellular signal-regulated kinase pathway signaling. *Arthritis Rheum* (2003) 48(3):746–56. doi:10.1002/art.10833
74. Handler J. Hydralazine-induced lupus erythematosis. *J Clin Hypertens (Greenwich)* (2012) 14(2):133–6. doi:10.1111/j.1751-7176.2011.00573.x
75. Mazari L, Ouarzane M, Zouali M. Subversion of B lymphocyte tolerance by hydralazine, a potential mechanism for drug-induced lupus. *Proc Natl Acad Sci U S A* (2007) 104(15):6317–22. doi:10.1073/pnas.0610434104
76. Christensen SR, Shlomchik MJ. Regulation of lupus-related autoantibody production and clinical disease by toll-like receptors. *Semin Immunol* (2007) 19(1):11–23. doi:10.1016/j.smim.2006.12.005
77. Christensen SR, Shupe J, Nickerson K, Kashgarian M, Flavell RA, Shlomchik MJ. Toll-like receptor 7 and TLR9 dictate autoantibody specificity and have opposing inflammatory and regulatory roles in a murine model of lupus. *Immunity* (2006) 25(3):417–28. doi:10.1016/j.immuni.2006.07.013
78. Jackson SW, Scharping NE, Kolhatkar NS, Khim S, Schwartz MA, Li QZ, et al. Opposing impact of B cell-intrinsic TLR7 and TLR9 signals on autoantibody repertoire and systemic inflammation. *J Immunol* (2014) 192(10):4525–32. doi:10.4049/jimmunol.1400098
79. Chauhan SK, Singh VV, Rai R, Rai M, Rai G. Distinct autoantibody profiles in systemic lupus erythematosus patients are selectively associated with TLR7 and TLR9 upregulation. *J Clin Immunol* (2013) 33(5):954–64. doi:10.1007/s10875-013-9887-0
80. Conti F, Spinelli FR, Truglia S, Miranda F, Alessandri C, Ceccarelli F, et al. Kidney expression of toll like receptors in lupus nephritis: quantification and clinicopathological correlations. *Mediators Inflamm* (2016) 2016:7697592. doi:10.1155/2016/7697592
81. Elloumi N, Fakhfakh R, Abida O, Ayadi L, Marzouk S, Hachicha H, et al. Relevant genetic polymorphisms and kidney expression of toll-like receptor (TLR)-5 and TLR-9 in lupus nephritis. *Clin Exp Immunol* (2017) 190(3):328–39. doi:10.1111/cei.13022
82. Klonowska-Szymczyk A, Wolska A, Robak T, Cebula-Obrzut B, Smolewski P, Robak E. Expression of toll-like receptors 3, 7, and 9 in peripheral blood

mononuclear cells from patients with systemic lupus erythematosus. *Mediators Inflamm* (2014) 2014:381418. doi:10.1155/2014/381418
83. Mortezagholi S, Babaloo Z, Rahimzadeh P, Ghaedi M, Namdari H, Assar S, et al. Evaluation of PBMC distribution and TLR9 expression in patients with systemic lupus erythematosus. *Iran J Allergy Asthma Immunol* (2016) 15(3):229–36.
84. Mortezagholi S, Babaloo Z, Rahimzadeh P, Namdari H, Ghaedi M, Gharibdoost F, et al. Evaluation of TLR9 expression on PBMCs and CpG ODN-TLR9 ligation on IFN-alpha production in SLE patients. *Immunopharmacol Immunotoxicol* (2017) 39(1):11–8. doi:10.1080/08923973.2016.1263859
85. Horton CG, Pan ZJ, Farris AD. Targeting toll-like receptors for treatment of SLE. *Mediators Inflamm* (2010) 2010:1–9. doi:10.1155/2010/498980
86. Capolunghi F, Rosado MM, Cascioli S, Girolami E, Bordasco S, Vivarelli M, et al. Pharmacological inhibition of TLR9 activation blocks autoantibody production in human B cells from SLE patients. *Rheumatology (Oxford)* (2010) 49(12):2281–9. doi:10.1093/rheumatology/keq226
87. Meshnick SR, Dobson MJ. The history of antimalarial drugs. In: Rosenthal PJ, editor. *Antimalarial Chemotherapy Mechanisms of Action, Resistance, and New Directions in Drug Discovery*. Totowa, New Jersey: Springer (2001). 396 p.
88. Rainsford KD, Parke AL, Clifford-Rashotte M, Kean WF. Therapy and pharmacological properties of hydroxychloroquine and chloroquine in treatment of systemic lupus erythematosus, rheumatoid arthritis and related diseases. *Inflammopharmacology* (2015) 23(5):231–69. doi:10.1007/s10787-015-0239-y
89. Bertsias G, Ioannidis JP, Boletis J, Bombardieri S, Cervera R, Dostal C, et al. EULAR recommendations for the management of systemic lupus erythematosus. Report of a task force of the EULAR standing committee for international clinical studies including therapeutics. *Ann Rheum Dis* (2008) 67(2):195–205. doi:10.1136/ard.2007.070367
90. Daniel WA, Bickel MH, Honegger UE. The contribution of lysosomal trapping in the uptake of desipramine and chloroquine by different tissues. *Pharmacol Toxicol* (1995) 77(6):402–6. doi:10.1111/j.1600-0773.1995.tb01050.x
91. Thomé R, Lopes SC, Costa FT, Verinaud L. Chloroquine: modes of action of an undervalued drug. *Immunol Lett* (2013) 153(1–2):50–7. doi:10.1016/j.imlet.2013.07.004
92. Yasuda H, Leelahavanichkul A, Tsunoda S, Dear JW, Takahashi Y, Ito S, et al. Chloroquine and inhibition of toll-like receptor 9 protect from sepsis-induced acute kidney injury. *Am J Physiol Renal Physiol* (2008) 294(5):F1050–8. doi:10.1152/ajprenal.00461.2007
93. Top D, Young MW. Coordination between differentially regulated circadian clocks generates rhythmic behavior. *Cold Spring Harb Perspect Biol* (2017) 1–27. doi:10.1101/cshperspect.a033589
94. Terzibasi-Tozzini E, Martinez-Nicolas A, Lucas-Sanchez A. The clock is ticking. Ageing of the circadian system: from physiology to cell cycle. *Semin Cell Dev Biol* (2017) 70:164–76. doi:10.1016/j.semcdb.2017.06.011
95. Kwon I, Choe HK, Son GH, Kim K. Mammalian molecular clocks. *Exp Neurobiol* (2011) 20(1):18–28. doi:10.5607/en.2011.20.1.18
96. Bargiello TA, Jackson FR, Young MW. Restoration of circadian behavioural rhythms by gene transfer in *Drosophila*. *Nature* (1984) 312(5996):752–4. doi:10.1038/312752a0
97. Rosbash M, Hall JC. The molecular biology of circadian rhythms. *Neuron* (1989) 3(4):387–98. doi:10.1016/0896-6273(89)90199-2
98. Emery P, So WV, Kaneko M, Hall JC, Rosbash M. CRY, a *Drosophila* clock and light-regulated cryptochrome, is a major contributor to circadian rhythm resetting and photosensitivity. *Cell* (1998) 95(5):669–79. doi:10.1016/S0092-8674(00)81637-2
99. Saez L, Derasmo M, Meyer P, Stieglitz J, Young MW. A key temporal delay in the circadian cycle of *Drosophila* is mediated by a nuclear localization signal in the timeless protein. *Genetics* (2011) 188(3):591–600. doi:10.1534/genetics.111.127225
100. Burki T. Nobel prize awarded for discoveries in circadian rhythm. *Lancet* (2017) 390(10104):e25. doi:10.1016/S0140-6736(17)32661-2
101. Spies CM, Straub RH, Cutolo M, Buttgereit F. Circadian rhythms in rheumatology – a glucocorticoid perspective. *Arthritis Res Ther* (2014) 16(Suppl 2):S3. doi:10.1186/ar4687
102. Nader N, Chrousos GP, Kino T. Interactions of the circadian CLOCK system and the HPA axis. *Trends Endocrinol Metab* (2010) 21(5):277–86. doi:10.1016/j.tem.2009.12.011
103. Tognini P, Thaiss CA, Elinav E, Sassone-Corsi P. Circadian coordination of antimicrobial responses. *Cell Host Microbe* (2017) 22(2):185–92. doi:10.1016/j.chom.2017.07.007
104. McMahon DG, Iuvone PM, Tosini G. Circadian organization of the mammalian retina: from gene regulation to physiology and diseases. *Prog Retin Eye Res* (2014) 39:58–76. doi:10.1016/j.preteyeres.2013.12.001
105. Sternberg EM. Neural regulation of innate immunity: a coordinated nonspecific host response to pathogens. *Nat Rev Immunol* (2006) 6(4):318–28. doi:10.1038/nri1810
106. Scheiermann C, Kunisaki Y, Frenette PS. Circadian control of the immune system. *Nat Rev Immunol* (2013) 13(3):190–8. doi:10.1038/nri3386
107. Man K, Loudon A, Chawla A. Immunity around the clock. *Science* (2016) 354(6315):999–1003. doi:10.1126/science.aah4966
108. Takahashi JS. Transcriptional architecture of the mammalian circadian clock. *Nat Rev Genet* (2017) 18(3):164–79. doi:10.1038/nrg.2016.150
109. Gekakis N, Staknis D, Nguyen HB, Davis FC, Wilsbacher LD, King DP, et al. Role of the CLOCK protein in the mammalian circadian mechanism. *Science* (1998) 280(5369):1564–9. doi:10.1126/science.280.5369.1564
110. Huang N, Chelliah Y, Shan Y, Taylor CA, Yoo SH, Partch C, et al. Crystal structure of the heterodimeric CLOCK:BMAL1 transcriptional activator complex. *Science* (2012) 337(6091):189–94. doi:10.1126/science.1222804
111. Partch CL, Green CB, Takahashi JS. Molecular architecture of the mammalian circadian clock. *Trends Cell Biol* (2014) 24(2):90–9. doi:10.1016/j.tcb.2013.07.002
112. Tei H, Okamura H, Shigeyoshi Y, Fukuhara C, Ozawa R, Hirose M, et al. Circadian oscillation of a mammalian homologue of the *Drosophila* period gene. *Nature* (1997) 389(6650):512–6. doi:10.1038/39086
113. van der Horst GT, Muijtjens M, Kobayashi K, Takano R, Kanno S, Takao M, et al. Mammalian Cry1 and Cry2 are essential for maintenance of circadian rhythms. *Nature* (1999) 398(6728):627–30. doi:10.1038/19323
114. Buhr ED, Takahashi JS. Molecular components of the mammalian circadian clock. In: Kramer A, Merrow M, editors. *Circadian Clocks*. Heidelberg, Berlin: Springer (2013). p. 3–27.
115. Zhang R, Lahens NF, Ballance HI, Hughes ME, Hogenesch JB. A circadian gene expression atlas in mammals: implications for biology and medicine. *Proc Natl Acad Sci U S A* (2014) 111(45):16219–24. doi:10.1073/pnas.1408886111
116. Pritchett D, Reddy AB. Circadian clocks in the hematologic system. *J Biol Rhythms* (2015) 30(5):374–88. doi:10.1177/0748730415592729
117. Keller M, Mazuch J, Abraham U, Eom GD, Herzog ED, Volk HD, et al. A circadian clock in macrophages controls inflammatory immune responses. *Proc Natl Acad Sci U S A* (2009) 106(50):21407–12. doi:10.1073/pnas.0906361106
118. Silver AC, Arjona A, Hughes ME, Nitabach MN, Fikrig E. Circadian expression of clock genes in mouse macrophages, dendritic cells, and B cells. *Brain Behav Immun* (2012) 26(3):407–13. doi:10.1016/j.bbi.2011.10.001
119. Hriscu ML. Modulatory factors of circadian phagocytic activity. *Ann N Y Acad Sci* (2005) 1057:403–30. doi:10.1196/annals.1356.032
120. Silver AC, Arjona A, Walker WE, Fikrig E. The circadian clock controls toll-like receptor 9-mediated innate and adaptive immunity. *Immunity* (2012) 36(2):251–61. doi:10.1016/j.immuni.2011.12.017
121. Mukherji A, Kobiita A, Ye T, Chambon P. Homeostasis in intestinal epithelium is orchestrated by the circadian clock and microbiota cues transduced by TLRs. *Cell* (2013) 153(4):812–27. doi:10.1016/j.cell.2013.04.020
122. Campbell SS, Murphy PJ. Extraocular circadian phototransduction in humans. *Science* (1998) 279(5349):396–9. doi:10.1126/science.279.5349.396
123. Campbell SS, Murphy PJ, Suhner AG. Extraocular phototransduction and circadian timing systems in vertebrates. *Chronobiol Int* (2001) 18(2):137–72. doi:10.1081/CBI-100103183
124. Kawara S, Mydlarski R, Mamelak AJ, Freed I, Wang B, Watanabe H, et al. Low-dose ultraviolet B rays alter the mRNA expression of the circadian clock genes in cultured human keratinocytes. *J Invest Dermatol* (2002) 119(6):1220–3. doi:10.1046/j.1523-1747.2002.19619.x
125. Deng GM. Pathogenesis of skin injury of systemic lupus erythematosus. *Curr Rheumatol Rep* (2018) 20(2):5. doi:10.1007/s11926-018-0713-9
126. Fernandez D, Kirou KA. What causes lupus flares? *Curr Rheumatol Rep* (2016) 18(3):14. doi:10.1007/s11926-016-0562-3
127. Deng GM, Tsokos GC. Pathogenesis and targeted treatment of skin injury in SLE. *Nat Rev Rheumatol* (2015) 11(11):663–9. doi:10.1038/nrrheum.2015.106

128. Andrade F, Casciola-Rosen L, Rosen A. Apoptosis in systemic lupus erythematosus. Clinical implications. *Rheum Dis Clin North Am* (2000) 26(2):215–27, v. doi:10.1016/S0889-857X(05)70136-8
129. Guan L, Suggs A, Ahsanuddin S, Tarrillion M, Selph J, Lam M, et al. 2016 arte poster competition first place winner: circadian rhythm and UV-induced skin damage: an in vivo study. *J Drugs Dermatol* (2016) 15(9):1124–30.
130. Thompson C, Piguet V, Choy E. The pathogenesis of dermatomyositis. *Br J Dermatol* (2017) 1–7. doi:10.1111/bjd.15607
131. Petri MH, Satoh M, Martin-Marquez BT, Vargas-Ramírez R, Jara LJ, Saavedra MA, et al. Implications in the difference of anti-Mi-2 and -p155/140 autoantibody prevalence in two dermatomyositis cohorts from Mexico City and Guadalajara. *Arthritis Res Ther* (2013) 15(2):R48. doi:10.1186/ar4207
132. Torres-Ruiz J, Sulli A, Cutolo M, Shoenfeld Y. Air travel, circadian rhythms/hormones, and autoimmunity. *Clin Rev Allergy Immunol* (2017) 53(1): 117–25. doi:10.1007/s12016-017-8599-2
133. Levi F, Okyar A. Circadian clocks and drug delivery systems: impact and opportunities in chronotherapeutics. *Expert Opin Drug Deliv* (2011) 8(12):1535–41. doi:10.1517/17425247.2011.618184
134. Bairy LK. Chronotherapeutics: a hype or future of chronopharmacology? *Indian J Pharmacol* (2013) 45(6):545–6. doi:10.4103/0253-7613.121265
135. Cutolo M. Chronobiology and the treatment of rheumatoid arthritis. *Curr Opin Rheumatol* (2012) 24(3):312–8. doi:10.1097/BOR.0b013e3283521c78
136. Spies CM, Cutolo M, Straub RH, Burmester GR, Buttgereit F. More night than day – circadian rhythms in polymyalgia rheumatica and ankylosing spondylitis. *J Rheumatol* (2010) 37(5):894–9. doi:10.3899/jrheum.091283
137. Cambie G, Caillard V, Beauté-Lafitte A, Ginsburg H, Chabaud A, Landau I. Chronotherapy of malaria: identification of drug-sensitive stage of parasite and timing of drug delivery for improved therapy. *Ann Parasitol Hum Comp* (1991) 66(1):14–21. doi:10.1051/parasite/199166114

Conflict of Interest Statement: The authors report no conflicts of interest. The authors alone are responsible for the content and writing of the paper.

frontiers in Immunology

MINI REVIEW
published: 24 July 2018
doi: 10.3389/fimmu.2018.01647

DICER1: A Key Player in Rheumatoid Arthritis, at the Crossroads of Cellular Stress, Innate Immunity, and Chronic Inflammation in Aging

Aurore De Cauwer[1,2†], Alexandre Mariotte[1,2†], Jean Sibilia[1,2,3], Seiamak Bahram[1,2] and Philippe Georgel[1,2]*

[1] Université de Strasbourg, INSERM, ImmunoRhumatologie Moléculaire UMR_S 1109, Fédération de Médecine Translationnelle de Strasbourg, Faculté de Médecine, Strasbourg, France, [2] Fédération Hospitalo-Universitaire, OMICARE, Centre de Recherche d'Immunologie et d'Hématologie, Strasbourg, France, [3] Centre de Référence des Maladies Autoimmunes Rares, Hôpitaux Universitaires de Strasbourg, Strasbourg, France

OPEN ACCESS

Edited by:
Moncef Zouali, Institut National de la Santé et de la Recherche Médicale (INSERM), France

Reviewed by:
Laura Mandik-Nayak, Lankenau Institute for Medical Research, United States
Erika H. Noss, University of Washington, United States

***Correspondence:**
Philippe Georgel
pgeorgel@unistra.fr

[†]*These authors have contributed equally to this work.*

Specialty section:
This article was submitted to Autoimmune and Autoinflammatory Disorders, a section of the journal Frontiers in Immunology

Received: *09 May 2018*
Accepted: *04 July 2018*
Published: *24 July 2018*

Citation:
De Cauwer A, Mariotte A, Sibilia J, Bahram S and Georgel P (2018) DICER1: A Key Player in Rheumatoid Arthritis, at the Crossroads of Cellular Stress, Innate Immunity, and Chronic Inflammation in Aging. Front. Immunol. 9:1647. doi: 10.3389/fimmu.2018.01647

Loss-of-function or knockout mouse models have established a fundamental role for the RNAse III enzyme DICER1 in development and tissue morphogenesis and/or homeostasis. These functions are currently assumed to result mainly from the DICER1-dependent biogenesis of microRNAs which exhibit important gene expression regulatory properties. However, non-canonical DICER1 functions have recently emerged. These include interaction with the DNA damage response (DDR) pathway and the processing of cytotoxic non-coding RNAs, suggesting that DICER1 might also participate in the regulation of major cellular processes through miRNA-independent mechanisms. Recent findings indicated that reduced *Dicer1* expression, which correlates with worsened symptoms in mouse models of joint inflammation, is also noted in fibroblast-like synoviocytes (FLS) harvested from rheumatoid arthritis (RA) patients, as opposed to FLS cultured from biopsies of osteoarthritic patients. In addition, low DICER1 levels are associated with the establishment of cellular stress and its associated responses, such as cellular senescence. Senescent and/or stressed cells are associated with an inflammatory secretome (cytokines and chemokines), as well as with "find-me" and "eat-me" signals which will attract and activate the innate immune compartment (NK cells, macrophages, and neutrophils) to be eliminated. Failure of this immunosurveillance mechanism and improper restauration of homeostasis could lead to the establishment of a systemic and chronic inflammatory state. In this review, we suggest that reduced DICER1 expression contributes to a vicious cycle during which accumulating inflammation and premature senescence, combined to inadequate innate immunity responses, creates the appropriate conditions for the initiation and/or progression of autoimmune-autoinflammatory diseases, such as RA.

Keywords: Dicer1, inflammation, rheumatoid arthritis, senescence, ageing

BIOLOGICAL ROLES OF DICER1

The Canonical Role of DICER1: MicroRNA (miRNA) Biogenesis

Since its discovery by Bernstein et al. (1), the RNAse III enzyme DICER (encoded by the *DICER1* gene in *H. sapiens* and *Dicer1* in *Mus musculus*, the nomenclature that will be used throughout this review) has been extensively studied and its role in the miRNA biogenesis is today well described [reviewed in Ref. (2)]. miRNA synthesis usually begins with the RNA polymerase II-dependent

transcription of genes encoding primary-miRNAs (pri-miRNAs), which are several kilobase-long stem-loop transcripts. Alternatively, pri-miRNAs can also originate from introns of protein coding genes. Whatever their origin, pri-miRNAs are then processed by the nuclear microprocessor complex DROSHA/DiGeorge syndrome Critical Region 8 (DGCR8) into precursor microRNAs (pre-miRNAs). Those 60–80 nucleotide-long precursors are then exported to the cytoplasm where they are recognized and cleaved by DICER1 into a 20–22 nucleotide-long RNA duplex (**Figure 1**). One miRNA strand is conserved and loaded into the RNA-induced silencing complex (RISC) composed of argonaute proteins. Guided by the miRNA, the RISC complex hybridizes with complementary mRNAs leading to either their degradation or translational inhibition. Therefore, DROSHA, DICER1, and miRNA are core factors of the Post-Transcriptional Gene Silencing process, a key regulatory mechanism of gene expression. In addition, several miRNAs are produced upon non-canonical pathway because their synthesis bypasses some of the aforementioned steps; those are Mirtons (whose synthesis is DROSHA-independent) (3) and miR-451, the only DICER1-independent miRNA described up to now (4, 5).

Interestingly, a study aiming at re-evaluating the contribution of the different key factors in miRNA biogenesis showed that while DROSHA is actually irreplaceable in the canonical miRNA synthesis, some miRNAs are still produced, albeit at reduced levels, without DICER1 (6). These observations, along with ours showing that reduced expression of DICER1 in fibroblast-like synoviocytes (FLS) from rheumatoid arthritis (RA) patients is associated with no more than a modest reduction of miRNA production (7), strongly suggest that other roles, besides miRNAs maturation, might be attributed to DICER1. Indeed, marked phenotypes have been observed in targeted (tissue-specific) *Dicer1* knockout mouse mutants, despite a noticeable preserved (and even sometimes increased) expression of many mature miRNAs.

DICER1 Non-Canonical Roles

Accordingly, multiple reports have now described the existence of non-canonical, miRNA-independent, roles of DICER1

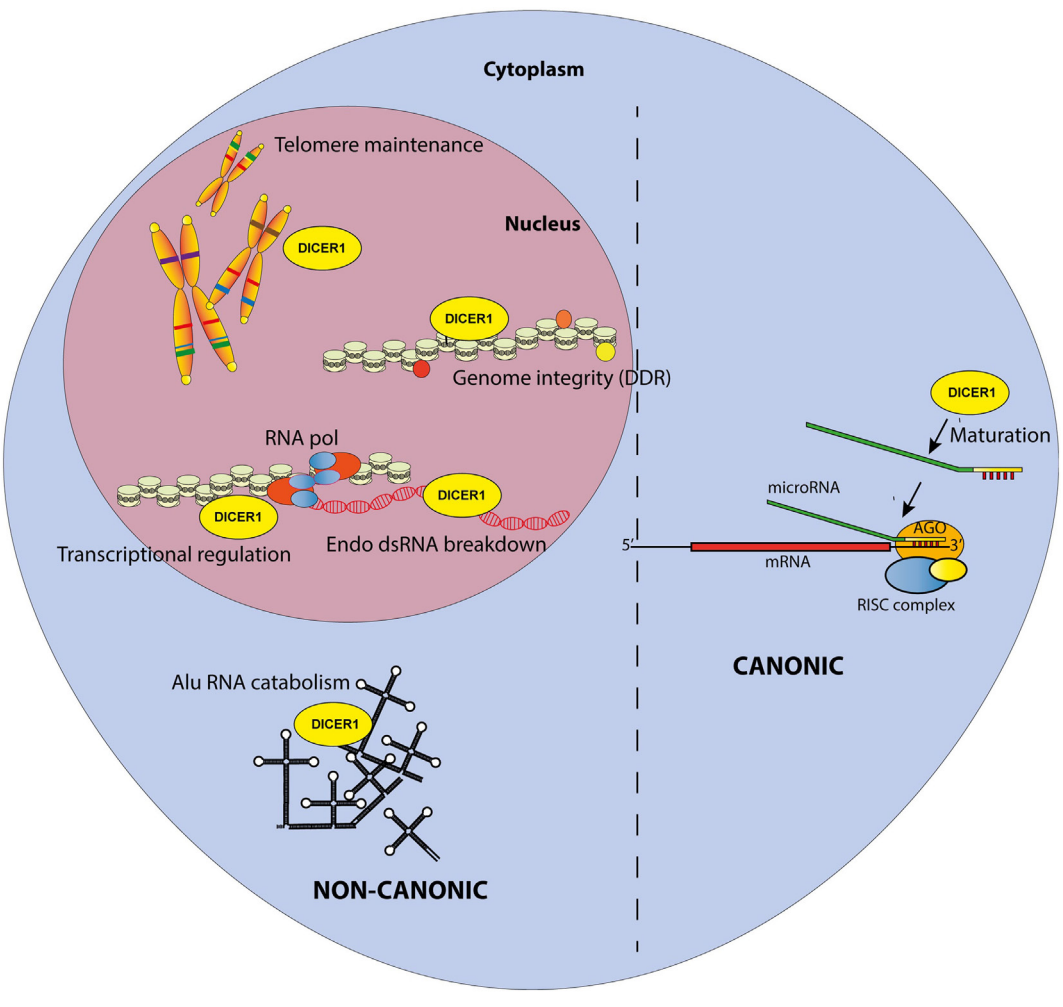

FIGURE 1 | Canonical and non-canonical functions of DICER1 in the nucleus and the cytosol. The canonical function of DICER1 leads to microRNA maturation in the cytoplasm. Others functions are considered non-canonical.

(**Figure 1**). Those functions are essentially implicated in nuclear RNAi and have been thoroughly reviewed elsewhere (8). In brief, DICER1, associated with TAR RNA Binding Protein and Protein activator of protein kinase R (PKR) (TRBP/PACT), was shown to regulate the transcription of a subset of hormone-inducible genes by interacting with their promoters in a dsRNA-dependent manner. Nuclear DICER1 is also implicated in the processing of endogenous dsRNA originating from overlapping transcription units, thereby protecting the cells from interferon (IFN)-mediated apoptosis. In addition, DICER1 plays an essential role in the maintenance of genome integrity (9), especially through interactions with the DNA damage response (DDR) pathway. It has been shown that in response to double-strand breaks in DNA, DICER1-dependent accumulation of break-specific dsRNAs facilitates the recruitment of reparation factors. Interestingly, this mechanism is also needed for the maintenance of telomeres (10).

Furthermore, the cytoplasm is also a major site of DICER1 non-canonical functions, which have been extensively studied over the last decade. A first hint for such roles was discovered in patients with age-related macular degeneration, which exhibit reduced DICER1 expression in retinal pigmented epithelium cells. In these cells, low *Dicer1* (but, importantly, not any of the other genes involved in miRNA production) expression triggered by shRNA knockdown in mice leads to cytotoxic accumulation of non-coding dsRNA formed upon the transcription Alu sequences (repetitive elements abundantly present in the human genome and classified as short interspersed nuclear elements (SINE)—retrotransposon family) (11). Accumulating Alu RNAs lead to a toll-like receptor (TLR)-independent, P2X7- and ROS-dependent activation of the NLRP3 inflammasome. The resulting maturation and secretion of IL-18 induces an MYD88-dependent pathway and caspase-8-mediated cell death, leading to macular degeneration (12–14).

Altogether, these data point to potentially devastating effects of *DICER1* mis-expression which can theoretically affect all steps of gene expression in both nuclear (replication/transcription/splicing) and cytoplasmic (translation) compartments.

DICER1 IN INFLAMMATION

miRNAs in Inflammation: Prominent Roles for miR-155 and -146a

There are 1,917 human miRNA sequences in the most recent miR database. This relatively large number, together with the capacity of every miRNA to target hundreds of mRNAs (15), indicates that they are able to virtually impact every biological function. It is therefore very much expected for miRNAs to be involved in most pathophysiological settings, among which inflammation and associated diseases were particularly scrutinized. In this context, miR-155 and -146a have been extensively described because they clearly exhibit crucial regulatory functions in innate and adaptive immunity. Indeed, miR-146a has been described as a mandatory regulator of the NF-κB pathway in T cells, targeting TRAF6 and IRAK1 (16). miR-146a was also correlated and functionally associated with the control of TNF-α production downstream of several TLRs and to the LPS tolerance phenomenon (17). In this report, it was notably observed that miR-146a is increased in human monocytic cells following LPS re-exposure. Until now, many groups found a pronounced inflammation-limiting role for miR-146a in various inflammatory settings, from atopic dermatitis (18) to sepsis (19). Strong evidence also attests that miR-146a participates in inflammatory disorders such as gout (20, 21) and RA [Ref. (22, 23) and see below].

miR-155, encoded by the *bic* locus, has been described as a major actor in inflammatory responses (24–26). miR-155 is considered a main driver of inflammatory responses through a large array of networks and its down-modulation is associated with termination of acute inflammation, as exemplified in the case of glucocorticoid treatments (27). Interestingly, the inflammatory effects of miR-155 are counteracted by miR-146a, as evidenced by a murine model where the deletion of the former is able to abrogate the inflammation induced by the loss of the latter (28). In essence, miR-155 and -146a, which roles were comprehensively analyzed in mouse knockout models, are considered as major players in the regulation of inflammatory responses.

Interestingly, miRNA biogenesis and the cellular stress response are tightly interconnected (29). This can be illustrated by the reciprocal interactions between type I IFNs-I, cytokines of paramount importance in the resolution of a virus-induced stress, which can modulate *DICER1* gene expression (30). In return, mice carrying a mutation in the *DICER1* gene exhibit an altered transcriptional profile of miRNA-regulated, IFN-stimulates genes (31). It is also noteworthy to observe that miR-124, a major player in the regulation of stress-induced genes in the brain (32), has recently been shown to modulate inflammation in a rat model of arthritis (33).

Non-Canonical Roles of DICER1 in Inflammation

Evidence directly implicating non-canonical roles of DICER1 in inflammatory responses is scarce. To date, only two examples can be mentioned: (1) the DICER1-dependent processing of Alu RNAs which precludes the harmful activation of NLRP3 Inflammasome and the maturation/secretion of pro-inflammatory cytokines IL-1β and IL-18 (11) (see above) and (2) the involvement of nuclear DICER1 in the processing of dsRNA transcripts from overlapping loci, thus preventing an uncontrolled IFN response (34).

Regulation of IFN secretion and IFN-mediated responses are of high interest because excessive production of these cytokines is associated with several autoimmune diseases. Of note, dysregulation of *DICER1* expression has been linked to the modulation IFN responses, a feature which is considered to result from global miRNA deregulation. *DICER1* ablation in endometrial cancer cells was also linked to an increased IFN-β secretion and subsequent upregulation of IFN-stimulated genes (35). However, this response was interpreted as the consequence of cytoplasmic accumulation of pre-miRNAs which are able to trigger the activation of dsRNA sensors, hence leading to an IFN

response. More recently, DICER1's ablation in tumor-associated macrophages was shown to polarize the cells toward an M1-like phenotype associated with hyperactive IFNγ/STAT1 signaling. This observation, described as the result of decreased expression of the let-7 miRNA, can only be partially rescued by transduction with a lentivirus expressing let-7 (36). It is then conceivable that non-canonical roles of DICER1 might also play a role in the M1/M2 macrophage polarization. Nevertheless, this model, whereby unprocessed dsRNAs accumulate in the cytosol upon DICER1 deficiency and drive inflammatory responses, has been poorly explored so far.

Of note, an increase in cytoplasmic Alu RNA following stress promotes disassembly of stress granules (SGs) (37). Since SGs decrease the interactions between DICER1 and its co-factors, thereby reducing its activity (38), a cross-talk between stress-induced pathways and miRNA-independent functions of DICER1 appears also plausible. Furthermore, SGs negatively regulate the production of inflammatory cytokine such as IL-1β by controlling mRNAs stability and decay (39). Hence, impairment of this activity upon Alu RNA accumulation would also contribute to promote inflammation.

DICER1 in Aging

Aging is an important risk factor for the development of inflammatory disorders/diseases (40). In rodents, aging has been associated with a decreased expression of *DICER1* in the adipose tissue (41). In human, octogenarians, compared with centenarians, exhibit global decrease in miRNA expression as well as reduced expression of miRNA biogenesis factors including DICER1 in blood cells (42, 43). However, these observations do not provide mechanistic insights for the contribution of DICER1 in the aging process. Of course, many miRNAs (such as miR-34) targeting emblematic pathways involved in senescence (e.g., P53/P21) have been described (44) and are likely to play a role in aging. Nevertheless, aging is a complex process characterized by nine hallmarks: genomic instability, telomere attrition, epigenetic alterations, loss of proteostasis, deregulated nutrient-sensing, mitochondrial dysfunction, cellular senescence, stem cell exhaustion, and altered intercellular communication (45), all of which are possibly impacted by *DICER1* misexpression, not only through impaired miRNAs maturation but also because non-canonical DICER1 functions may be affected as well.

With regards to genomic instability, the role of DICER1 in the processing of RNAs transcribed from retrotransposons belonging to long- or short-interspersed nuclear elements (line or SINE) families participates in the prevention of retrotransposition deleterious events (46). In addition, accumulation of Alu RNAs was found to restrain "stemcellness" and is associated with persistent DNA damage preventing tissue renewal (47). Their DICER1-dependent elimination is therefore required to maintain tissue homeostasis. Next, DICER1 is implicated in the DDR pathway by processing dsRNA essential for the DNA double-strand break repair. This process seems also to be necessary to prevent a second hallmark of aging, telomere shortening (10). Moreover, *DICER1* deletion has been associated with epigenetic alterations, such as chromatin remodeling, DNA methylation, and histone modification in mammalian cells (48, 49). Evidence in favor of a role of DICER1 in altered nutrient sensing and mitochondrial dysfunction is less documented. However, it was demonstrated that DICER1-depletion in adipocytes (i) overactivates the sensing signaling molecule mTORC1 and (ii) reduces mitochondria numbers, which are also irregularly shaped and associated with reduced oxidative metabolism in response to caloric restriction (50). As mentioned above, senescence has been amply described in relation to modified miRNA expression [e.g., Ref. (51)] but was also linked to Alu RNAs accumulation (47). Finally, downregulation of *Il-8* expression in endothelial cells upon *DICER1* knockdown (52) illustrates the potential impact of this multifunctional enzyme in the last hallmark of aging: cellular communication.

With regards to RA, normal aging of the immune system (immunosenescence) is associated with a higher risk to develop autoimmune disorders, including RA (53, 54). Alternatively, systemic joint inflammation may enhance the progression of immunosenescence and favor the development of comorbidities in RA patients (55).

DICER1 AND MIRNAS ARE MAJOR PLAYERS IN RA

Rheumatoid arthritis is a systemic autoimmune disease affecting around 1% of the global population. This rheumatic disease is characterized by multiple joint swelling, stiffness, and inflammatory pain, mainly in the small joints of hands and feet (56). Although the auto-immune feature of RA is clearly demonstrated, several decades of research have established a major role for the innate immune system and stromal cells in this disease (57). It is now commonly admitted that RA is a multifactorial disease, where its initiation and development requires concomitant participation of genetic, epigenetic, and environmental factors. Among epigenetic players involved in RA, miRNAs have been the focus of intense attention over the past decade (58).

There are presently more than 20 miRNAs, expression of which is deregulated in various cells (T cells, monocytes, and FLS)/compartments (blood and synovial fluid) harvested from RA patients (59, 60), and our lab has contributed to the identification of several of them within the miR-17~92 cluster (61–63). However, likely because RA etiology relies on innate and adaptive immune systems, miR-146a and -155, both of which have been involved in the regulation of adaptive (such as T cells-mediated) and inflammatory (e.g., in monocytes) responses, have been extensively studied in this disease. miR-146a is increased in RA patients (64–66) and is supposed to be integrated in a feedback loop, triggered by the unrestrained inflammation (67). Furthermore, murine models of RA have clearly shown that miR-146a restrains osteoclastogenesis (23). miR-155 is also upregulated in FLS and peripheral blood CD14-positive cells of RA patients (68, 69). In addition, its expression was correlated to the Disease Activity Score on 28 joints (DAS28) (70). Interestingly, miR-155 is also required for the development of the disease in the collagen-induced arthritis model, a commonly used mouse model of autoimmune arthritis (71). In FLS, upregulation of both miR-146a and miR-155 was

correlated to negative regulation of osteoclastogenesis/MMP production. Therefore, this increased expression was interpreted as a way to limit the RA-associated osteoarticular destruction processes (64).

On the other hand, reduced miR-146a and -155 expression in regulatory T cells (Treg) has also been incriminated in RA (22), which illustrates that a global perturbation (driving either an overexpression or a down-modulation) of miRNA production is unlikely to represent a major trigger of RA pathogenesis. Indeed, increased (or decreased) miRs in activated T cells might be compensated by similar alterations in Tregs, and *vice versa*. In this regard, our observations indicating that (i) *Dicer1*-deficient mice exhibit worsened symptoms following experimental (upon K/BxN serum transfer) arthritis induction and (ii) that FLS cultivated from biopsies harvested in RA patients exhibit reduced *DICER1* expression (7) pinpoint to a potential involvement of non-canonical, miRNA-independent activities of DICER1 in joint inflammation. Several possibilities might be considered in line with the abovementioned roles of DICER1 in the processing of Alu sequences. For instance, abolishing DICER1 activity may lead to reduced production of Alu repeat-induced small RNAs (riRNAs) in the nucleus, thereby limiting the proliferative capacities of stem cells (72) and impairing tissue renewal in the joint. Combined with increased DNA damage (73) which is accompanied with the initiation of senescence, reduced DICER1 non-canonical activities might drive the accumulation of aged FLS resistant to apoptotic stimuli (7) and exhibiting pro-inflammatory capabilities [through IL-6, an essential component of the senescence-associated secretory phenotype (SASP) (74)], a dangerous cocktail likely driving their aggressive phenotype observed in RA patients. As mentioned above, *Dicer1* expression is negatively regulated by inflammatory cytokines such as type I IFNs, further aggravating the inflammatory response.

DICER1 AT THE CROSSROADS BETWEEN SENESCENCE AND INFLAMMATION IN RA

These multiple interactions are integrated in the model illustrated in **Figure 2**. We considered three main triggers (or hallmarks) of RA, aging (75), inflammation [through specific cytokines (76)], and stress (77) and their reciprocal interconnections mediated by canonical and non-canonical functions of DICER1. For sake of simplicity, we emphasized only specific miRNAs and other

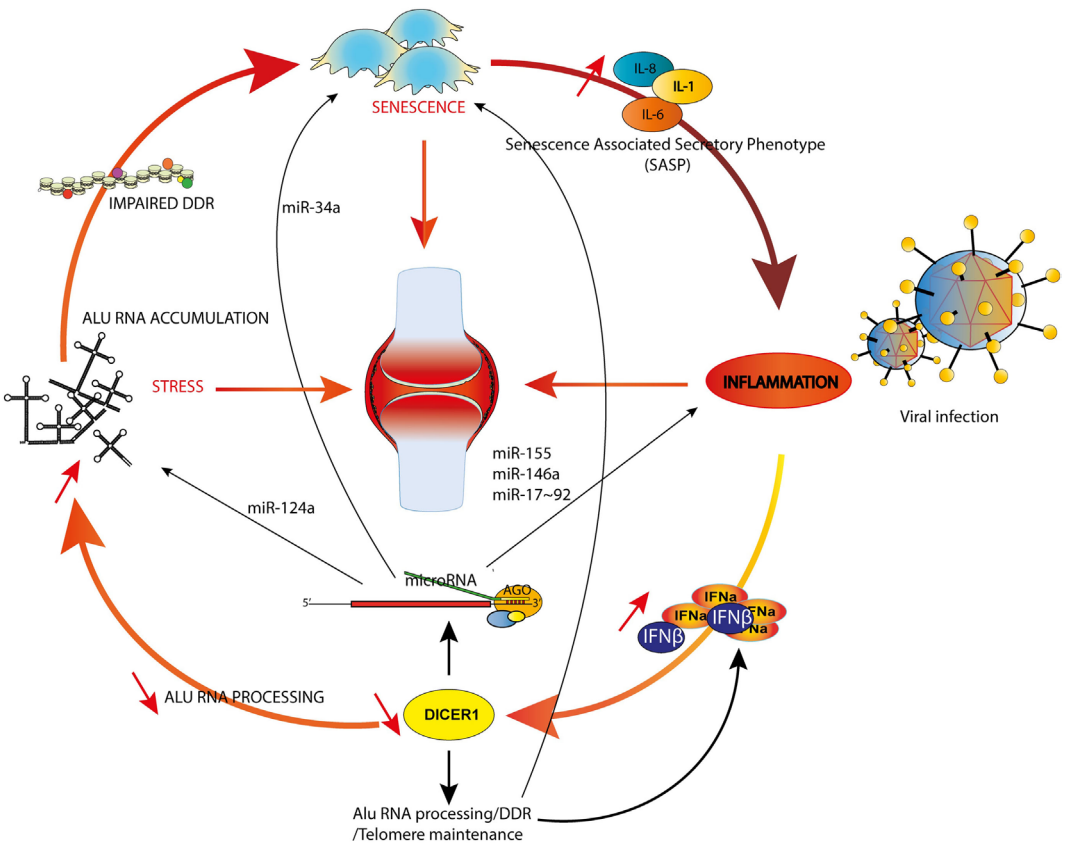

FIGURE 2 | DICER1 functions at the crossroads of inflammation, senescence and aging. Examples of microRNAs involved in both rheumatoid arthritis (RA) and inflammation (miR-155 and -146a), RA and senescence (miR-34a) or RA and stress (miR-124a) are shown. The model illustrates how an initial trigger (e.g., a viral infection) might initiate a vicious circle (see text).

DICER1 ligands (such as Alu RNAs), but nevertheless, our model supports the notion that DICER1 alterations might perturb every trigger of RA and initiate a chain reaction actually driving pathogenesis. Indeed, their interactions create the appropriate conditions to build a vicious circle which can for instance, start with IFN-dependent *DICER1* down-modulation (for example, as a result of a chronic viral infection). This initial event might contribute to accumulation of Alu RNAs and other dsRNAs in the cytoplasm, which favor the survival of senescent cells in which DNA damages are poorly fixed (hence increasing the inflammatory settings through the SASP) and reduced formation of SGs, leading to an impaired degradation of viral RNAs. Viral RNAs and cytoplasmic endogenous dsRNAs will ultimately enhance type I IFN production and amplify the vicious circle. Of course, this model is incomplete and could also, for instance, integrate metabolism (or other environmental factors contributive to RA). Interestingly, interactions between PKR, TRBP, and DICER1 were described, suggesting an additional (miRNA-independent) role for DICER1 in immunometabolism (78).

CONCLUDING REMARKS

Precisely evaluating the various roles of DICER1 appears a challenging task due to its complex and pleiotropic roles. Furthermore, factors that influence *DICER1* gene expression in specific cells and at defined developmental stages are still poorly described. In addition, *DICER1* transcripts and protein levels are not always correlated (79), adding another layer of complexity. Moreover, DICER1 activity appears regulated by post-translational modification such as phosphorylation and SUMOylation (80), and the protein can shuttle between the cytosol and the nucleus and exert different activities in these two compartments, depending on associations with various co-factors. For instance, DICER1-efficient processing activity of Alu RNAs depends on poly(C)-binding protein 2 binding, which is inhibited by iron overload (81).

Here, we provided several examples of reciprocal interactions between DICER1 and mechanisms (stress, inflammation, and aging) that can be either considered as triggers (or inducers of *DICER1* expression) or effectors (i.e., that are able to respond to DICER1-dependent products such as miRNAs or metabolites of Alu or other long non-coding RNAs). We suggest that within this complex network of interactions, DICER1 occupies a central position. In this model, perturbations of these interactions modify homeostasis and drive pathogenesis. The focus of this review has been RA, but this network can be extended to other age-dependent pathological conditions, beyond autoimmune or inflammatory diseases, such as cancer or neurodegeneration.

AUTHOR CONTRIBUTIONS

PG, AC, AM, JS, and SB participated in discussions; drafted and approved the manuscript.

FUNDING

The work in our laboratory is supported by funding from INSERM, Strasbourg University, the Laboratoire d'Excellence TRANSPLANTEX (ANR-11-LABX-0070_TRANSPLANTEX) and the PRTS ANR program (SPIRALE), Institut Universitaire de France and MSD Avenir program AUTOGEN.

REFERENCES

1. Bernstein E, Caudy AA, Hammond SM, Hannon GJ. Role for a bidentate ribonuclease in the initiation step of RNA interference. *Nature* (2001) 409(6818):363–6. doi:10.1038/35053110
2. Bartel DP. Metazoan microRNAs. *Cell* (2018) 173(1):20–51. doi:10.1016/j.cell.2018.03.006
3. Ruby JG, Jan CH, Bartel DP. Intronic microRNA precursors that bypass Drosha processing. *Nature* (2007) 448(7149):83–6. doi:10.1038/nature05983
4. Cheloufi S, Dos Santos CO, Chong MM, Hannon GJ. A dicer-independent miRNA biogenesis pathway that requires Ago catalysis. *Nature* (2010) 465(7298):584–9. doi:10.1038/nature09092
5. Cifuentes D, Xue H, Taylor DW, Patnode H, Mishima Y, Cheloufi S, et al. A novel miRNA processing pathway independent of Dicer requires Argonaute2 catalytic activity. *Science* (2010) 328(5986):1694–8. doi:10.1126/science.1190809
6. Kim YK, Kim B, Kim VN. Re-evaluation of the roles of DROSHA, xport in 5, and DICER in microRNA biogenesis. *Proc Natl Acad Sci U S A* (2016) 113(13):E1881–9. doi:10.1073/pnas.1602532113
7. Alsaleh G, Nehmar R, Bluml S, Schleiss C, Ostermann E, Dillenseger JP, et al. Reduced DICER1 expression bestows rheumatoid arthritis synoviocytes proinflammatory properties and resistance to apoptotic stimuli. *Arthritis Rheumatol* (2016) 68(8):1839–48. doi:10.1002/art.39641
8. Burger K, Gullerova M. Swiss army knives: non-canonical functions of nuclear Drosha and Dicer. *Nat Rev Mol Cell Biol* (2015) 16(7):417–30. doi:10.1038/nrm3994
9. Hawley BR, Lu WT, Wilczynska A, Bushell M. The emerging role of RNAs in DNA damage repair. *Cell Death Differ* (2017) 24(4):580–7. doi:10.1038/cdd.2017.16
10. Rossiello F, Aguado J, Sepe S, Iannelli F, Nguyen Q, Pitchiaya S, et al. DNA damage response inhibition at dysfunctional telomeres by modulation of telomeric DNA damage response RNAs. *Nat Commun* (2017) 8:13980. doi:10.1038/ncomms13980
11. Kaneko H, Dridi S, Tarallo V, Gelfand BD, Fowler BJ, Cho WG, et al. DICER1 deficit induces Alu RNA toxicity in age-related macular degeneration. *Nature* (2011) 471(7338):325–30. doi:10.1038/nature09830
12. Tarallo V, Hirano Y, Gelfand BD, Dridi S, Kerur N, Kim Y, et al. DICER1 loss and Alu RNA induce age-related macular degeneration via the NLRP3 inflammasome and MyD88. *Cell* (2012) 149(4):847–59. doi:10.1016/j.cell.2012.03.036
13. Kim Y, Tarallo V, Kerur N, Yasuma T, Gelfand BD, Bastos-Carvalho A, et al. DICER1/Alu RNA dysmetabolism induces Caspase-8-mediated cell death in age-related macular degeneration. *Proc Natl Acad Sci U S A* (2014) 111(45):16082–7. doi:10.1073/pnas.1403814111
14. Kerur N, Hirano Y, Tarallo V, Fowler BJ, Bastos-Carvalho A, Yasuma T, et al. TLR-independent and P2X7-dependent signaling mediate Alu RNA-induced NLRP3 inflammasome activation in geographic atrophy. *Invest Ophthalmol Vis Sci* (2013) 54(12):7395–401. doi:10.1167/iovs.13-12500
15. Bartel DP. MicroRNAs: target recognition and regulatory functions. *Cell* (2009) 136(2):215–33. doi:10.1016/j.cell.2009.01.002
16. Yang L, Boldin MP, Yu Y, Liu CS, Ea CK, Ramakrishnan P, et al. miR-146a controls the resolution of T cell responses in mice. *J Exp Med* (2012) 209(9):1655–70. doi:10.1084/jem.20112218
17. Nahid MA, Pauley KM, Satoh M, Chan EK. miR-146a is critical for endotoxin-induced tolerance: implication in innate immunity. *J Biol Chem* (2009) 284(50):34590–9. doi:10.1074/jbc.M109.056317
18. Rebane A, Runnel T, Aab A, Maslovskaja J, Ruckert B, Zimmermann M, et al. MicroRNA-146a alleviates chronic skin inflammation in atopic dermatitis

through suppression of innate immune responses in keratinocytes. *J Allergy Clin Immunol* (2014) 134(4):836–47.e11. doi:10.1016/j.jaci.2014.05.022
19. Gao M, Wang X, Zhang X, Ha T, Ma H, Liu L, et al. Attenuation of cardiac dysfunction in polymicrobial sepsis by MicroRNA-146a is mediated via targeting of IRAK1 and TRAF6 expression. *J Immunol* (2015) 195(2):672–82. doi:10.4049/jimmunol.1403155
20. Zhang QB, Qing YF, Yin CC, Zhou L, Liu XS, Mi QS, et al. Mice with miR-146a deficiency develop severe gouty arthritis via dysregulation of TRAF 6, IRAK 1 and NALP3 inflammasome. *Arthritis Res Ther* (2018) 20(1):45. doi:10.1186/s13075-018-1546-7
21. Dalbeth N, Pool B, Shaw OM, Harper JL, Tan P, Franklin C, et al. Role of miR-146a in regulation of the acute inflammatory response to monosodium urate crystals. *Ann Rheum Dis* (2015) 74(4):786–90. doi:10.1136/annrheumdis-2014-205409
22. Zhou Q, Haupt S, Kreuzer JT, Hammitzsch A, Proft F, Neumann C, et al. Decreased expression of miR-146a and miR-155 contributes to an abnormal Treg phenotype in patients with rheumatoid arthritis. *Ann Rheum Dis* (2015) 74(6):1265–74. doi:10.1136/annrheumdis-2013-204377
23. Saferding V, Puchner A, Goncalves-Alves E, Hofmann M, Bonelli M, Brunner JS, et al. MicroRNA-146a governs fibroblast activation and joint pathology in arthritis. *J Autoimmun* (2017) 82:74–84. doi:10.1016/j.jaut.2017.05.006
24. O'Connell RM, Taganov KD, Boldin MP, Cheng G, Baltimore D. MicroRNA-155 is induced during the macrophage inflammatory response. *Proc Natl Acad Sci U S A* (2007) 104(5):1604–9. doi:10.1073/pnas.0610731104
25. O'Connell RM, Kahn D, Gibson WS, Round JL, Scholz RL, Chaudhuri AA, et al. MicroRNA-155 promotes autoimmune inflammation by enhancing inflammatory T cell development. *Immunity* (2010) 33(4):607–19. doi:10.1016/j.immuni.2010.09.009
26. Alivernini S, Gremese E, McSharry C, Tolusso B, Ferraccioli G, McInnes IB, et al. MicroRNA-155-at the critical interface of innate and adaptive immunity in arthritis. *Front Immunol* (2017) 8:1932. doi:10.3389/fimmu.2017.01932
27. Zheng Y, Xiong S, Jiang P, Liu R, Liu X, Qian J, et al. Glucocorticoids inhibit lipopolysaccharide-mediated inflammatory response by downregulating microRNA-155: a novel anti-inflammation mechanism. *Free Radic Biol Med* (2012) 52(8):1307–17. doi:10.1016/j.freeradbiomed.2012.01.031
28. Mann M, Mehta A, Zhao JL, Lee K, Marinov GK, Garcia-Flores Y, et al. An NF-kappaB-microRNA regulatory network tunes macrophage inflammatory responses. *Nat Commun* (2017) 8(1):851. doi:10.1038/s41467-017-00972-z
29. Emde A, Hornstein E. miRNAs at the interface of cellular stress and disease. *EMBO J* (2014) 33(13):1428–37. doi:10.15252/embj.201488142
30. Wiesen JL, Tomasi TB. Dicer is regulated by cellular stresses and interferons. *Mol Immunol* (2009) 46(6):1222–8. doi:10.1016/j.molimm.2008.11.012
31. Ostermann E, Tuddenham L, Macquin C, Alsaleh G, Schreiber-Becker J, Tanguy M, et al. Deregulation of type I IFN-dependent genes correlates with increased susceptibility to cytomegalovirus acute infection of dicer mutant mice. *PLoS One* (2012) 7(8):e43744. doi:10.1371/journal.pone.0043744
32. Sun Y, Luo ZM, Guo XM, Su DF, Liu X. An updated role of microRNA-124 in central nervous system disorders: a review. *Front Cell Neurosci* (2015) 9:193. doi:10.3389/fncel.2015.00193
33. Nakamachi Y, Ohnuma K, Uto K, Noguchi Y, Saegusa J, Kawano S. MicroRNA-124 inhibits the progression of adjuvant-induced arthritis in rats. *Ann Rheum Dis* (2016) 75(3):601–8. doi:10.1136/annrheumdis-2014-206417
34. White E, Schlackow M, Kamieniarz-Gdula K, Proudfoot NJ, Gullerova M. Human nuclear Dicer restricts the deleterious accumulation of endogenous double-stranded RNA. *Nat Struct Mol Biol* (2014) 21(6):552–9. doi:10.1038/nsmb.2827
35. Chiappinelli KB, Haynes BC, Brent MR, Goodfellow PJ. Reduced DICER1 elicits an interferon response in endometrial cancer cells. *Mol Cancer Res* (2012) 10(3):316–25. doi:10.1158/1541-7786.MCR-11-0520
36. Baer C, Squadrito ML, Laoui D, Thompson D, Hansen SK, Kiialainen A, et al. Suppression of microRNA activity amplifies IFN-gamma-induced macrophage activation and promotes anti-tumour immunity. *Nat Cell Biol* (2016) 18(7):790–802. doi:10.1038/ncb3371
37. Berger A, Ivanova E, Gareau C, Scherrer A, Mazroui R, Strub K. Direct binding of the Alu binding protein dimer SRP9/14 to 40S ribosomal subunits promotes stress granule formation and is regulated by Alu RNA. *Nucleic Acids Res* (2014) 42(17):11203–17. doi:10.1093/nar/gku822
38. Emde A, Eitan C, Liou LL, Libby RT, Rivkin N, Magen I, et al. Dysregulated miRNA biogenesis downstream of cellular stress and ALS-causing mutations: a new mechanism for ALS. *EMBO J* (2015) 34(21):2633–51. doi:10.15252/embj.201490493
39. Battu S, Afroz S, Giddaluru J, Naz S, Huang W, Khumukcham SS, et al. Amino acid starvation sensing dampens IL-1beta production by activating riboclustering and autophagy. *PLoS Biol* (2018) 16(4):e2005317. doi:10.1371/journal.pbio.2005317
40. Shaw AC, Goldstein DR, Montgomery RR. Age-dependent dysregulation of innate immunity. *Nat Rev Immunol* (2013) 13(12):875–87. doi:10.1038/nri3547
41. Mori MA, Raghavan P, Thomou T, Boucher J, Robida-Stubbs S, Macotela Y, et al. Role of microRNA processing in adipose tissue in stress defense and longevity. *Cell Metab* (2012) 16(3):336–47. doi:10.1016/j.cmet.2012.07.017
42. Serna E, Gambini J, Borras C, Abdelaziz KM, Belenguer A, Sanchis P, et al. Centenarians, but not octogenarians, up-regulate the expression of microRNAs. *Sci Rep* (2012) 2:961. doi:10.1038/srep00961
43. Borras C, Serna E, Gambini J, Ingles M, Vina J. Centenarians maintain miRNA biogenesis pathway while it is impaired in octogenarians. *Mech Ageing Dev* (2017) 168:54–7. doi:10.1016/j.mad.2017.07.003
44. Munk R, Panda AC, Grammatikakis I, Gorospe M, Abdelmohsen K. Senescence-associated microRNAs. *Int Rev Cell Mol Biol* (2017) 334:177–205. doi:10.1016/bs.ircmb.2017.03.008
45. Lopez-Otin C, Blasco MA, Partridge L, Serrano M, Kroemer G. The hallmarks of aging. *Cell* (2013) 153(6):1194–217. doi:10.1016/j.cell.2013.05.039
46. Heras SR, Macias S, Caceres JF, Garcia-Perez JL. Control of mammalian retrotransposons by cellular RNA processing activities. *Mob Gen Elements* (2014) 4:e28439. doi:10.4161/mge.28439
47. Wang J, Geesman GJ, Hostikka SL, Atallah M, Blackwell B, Lee E, et al. Inhibition of activated pericentromeric SINE/Alu repeat transcription in senescent human adult stem cells reinstates self-renewal. *Cell Cycle* (2011) 10(17):3016–30. doi:10.4161/cc.10.17.17543
48. Haussecker D, Proudfoot NJ. Dicer-dependent turnover of intergenic transcripts from the human beta-globin gene cluster. *Mol Cell Biol* (2005) 25(21):9724–33. doi:10.1128/MCB.25.21.9724-9733.2005
49. Chitale S, Richly H. DICER and ZRF1 contribute to chromatin decondensation during nucleotide excision repair. *Nucleic Acids Res* (2017) 45(10):5901–12. doi:10.1093/nar/gkx261
50. Reis FC, Branquinho JL, Brandao BB, Guerra BA, Silva ID, Frontini A, et al. Fat-specific Dicer deficiency accelerates aging and mitigates several effects of dietary restriction in mice. *Aging* (2016) 8(6):1201–22. doi:10.18632/aging.100970
51. Noren Hooten N, Martin-Montalvo A, Dluzen DF, Zhang Y, Bernier M, Zonderman AB, et al. Metformin-mediated increase in DICER1 regulates microRNA expression and cellular senescence. *Aging Cell* (2016) 15(3):572–81. doi:10.1111/acel.12469
52. Suarez Y, Fernandez-Hernando C, Pober JS, Sessa WC. Dicer dependent microRNAs regulate gene expression and functions in human endothelial cells. *Circ Res* (2007) 100(8):1164–73. doi:10.1161/01.RES.0000265065.26744.17
53. van Onna M, Boonen A. The challenging interplay between rheumatoid arthritis, ageing and comorbidities. *BMC Musculoskelet Disord* (2016) 17:184. doi:10.1186/s12891-016-1038-3
54. Straub RH, Scholmerich J, Cutolo M. The multiple facets of premature aging in rheumatoid arthritis. *Arthritis Rheum* (2003) 48(10):2713–21. doi:10.1002/art.11290
55. Rea IM, Gibson DS, McGilligan V, McNerlan SE, Alexander HD, Ross OA. Age and age-related diseases: role of inflammation triggers and cytokines. *Front Immunol* (2018) 9:586. doi:10.3389/fimmu.2018.00586
56. McInnes IB, Schett G. The pathogenesis of rheumatoid arthritis. *N Engl J Med* (2011) 365(23):2205–19. doi:10.1056/NEJMra1004965
57. Firestein GS, McInnes IB. Immunopathogenesis of rheumatoid arthritis. *Immunity* (2017) 46(2):183–96. doi:10.1016/j.immuni.2017.02.006

58. Ospelt C, Gay S, Klein K. Epigenetics in the pathogenesis of RA. *Semin Immunopathol* (2017) 39(4):409–19. doi:10.1007/s00281-017-0621-5
59. Vicente R, Noel D, Pers YM, Apparailly F, Jorgensen C. Deregulation and therapeutic potential of microRNAs in arthritic diseases. *Nat Rev Rheumatol* (2016) 12(4):211–20. doi:10.1038/nrrheum.2015.162
60. Chen XM, Huang QC, Yang SL, Chu YL, Yan YH, Han L, et al. Role of micro RNAs in the pathogenesis of rheumatoid arthritis: novel perspectives based on review of the literature. *Medicine* (2015) 94(31):e1326. doi:10.1097/MD.0000000000001326
61. Philippe L, Alsaleh G, Suffert G, Meyer A, Georgel P, Sibilia J, et al. TLR2 expression is regulated by microRNA miR-19 in rheumatoid fibroblast-like synoviocytes. *J Immunol* (2012) 188(1):454–61. doi:10.4049/jimmunol.1102348
62. Philippe L, Alsaleh G, Pichot A, Ostermann E, Zuber G, Frisch B, et al. MiR-20a regulates ASK1 expression and TLR4-dependent cytokine release in rheumatoid fibroblast-like synoviocytes. *Ann Rheum Dis* (2013) 72(6):1071–9. doi:10.1136/annrheumdis-2012-201654
63. Alsaleh G, Francois A, Philippe L, Gong YZ, Bahram S, Cetin S, et al. MiR-30a-3p negatively regulates BAFF synthesis in systemic sclerosis and rheumatoid arthritis fibroblasts. *PLoS One* (2014) 9(10):e111266. doi:10.1371/journal.pone.0111266
64. Stanczyk J, Pedrioli DM, Brentano F, Sanchez-Pernaute O, Kolling C, Gay RE, et al. Altered expression of microRNA in synovial fibroblasts and synovial tissue in rheumatoid arthritis. *Arthritis Rheum* (2008) 58(4):1001–9. doi:10.1002/art.23386
65. Nakasa T, Miyaki S, Okubo A, Hashimoto M, Nishida K, Ochi M, et al. Expression of microRNA-146 in rheumatoid arthritis synovial tissue. *Arthritis Rheum* (2008) 58(5):1284–92. doi:10.1002/art.23429
66. Pauley KM, Satoh M, Chan AL, Bubb MR, Reeves WH, Chan EK. Upregulated miR-146a expression in peripheral blood mononuclear cells from rheumatoid arthritis patients. *Arthritis Res Ther* (2008) 10(4):R101. doi:10.1186/ar2493
67. Chan EK, Ceribelli A, Satoh M. MicroRNA-146a in autoimmunity and innate immune responses. *Ann Rheum Dis* (2013) 72(Suppl 2):ii90–5. doi:10.1136/annrheumdis-2012-202203
68. Kurowska-Stolarska M, Alivernini S, Ballantine LE, Asquith DL, Millar NL, Gilchrist DS, et al. MicroRNA-155 as a proinflammatory regulator in clinical and experimental arthritis. *Proc Natl Acad Sci U S A* (2011) 108(27):11193–8. doi:10.1073/pnas.1019536108
69. Long L, Yu P, Liu Y, Wang S, Li R, Shi J, et al. Upregulated microRNA-155 expression in peripheral blood mononuclear cells and fibroblast-like synoviocytes in rheumatoid arthritis. *Clin Dev Immunol* (2013) 2013:296139. doi:10.1155/2013/296139
70. Elmesmari A, Fraser AR, Wood C, Gilchrist D, Vaughan D, Stewart L, et al. MicroRNA-155 regulates monocyte chemokine and chemokine receptor expression in rheumatoid arthritis. *Rheumatology (Oxford)* (2016) 55(11):2056–65. doi:10.1093/rheumatology/kew272
71. Bluml S, Bonelli M, Niederreiter B, Puchner A, Mayr G, Hayer S, et al. Essential role of microRNA-155 in the pathogenesis of autoimmune arthritis in mice. *Arthritis Rheum* (2011) 63(5):1281–8. doi:10.1002/art.30281
72. Hu Q, Tanasa B, Trabucchi M, Li W, Zhang J, Ohgi KA, et al. DICER- and AGO3-dependent generation of retinoic acid-induced DR2 Alu RNAs regulates human stem cell proliferation. *Nat Struct Mol Biol* (2012) 19(11):1168–75. doi:10.1038/nsmb.2400
73. Patchsung M, Settayanon S, Pongpanich M, Mutirangura D, Jintarith P, Mutirangura A. Alu siRNA to increase Alu element methylation and prevent DNA damage. *Epigenomics* (2018) 10(2):175–85. doi:10.2217/epi-2017-0096
74. Munoz-Espin D, Serrano M. Cellular senescence: from physiology to pathology. *Nat Rev Mol Cell Biol* (2014) 15(7):482–96. doi:10.1038/nrm3823
75. Chalan P, van den Berg A, Kroesen BJ, Brouwer L, Boots A. Rheumatoid arthritis, immunosenescence and the hallmarks of aging. *Curr Aging Sci* (2015) 8(2):131–46. doi:10.2174/1874609808666150727110744
76. McInnes IB, Buckley CD, Isaacs JD. Cytokines in rheumatoid arthritis – shaping the immunological landscape. *Nat Rev Rheumatol* (2016) 12(1):63–8. doi:10.1038/nrrheum.2015.171
77. Rahmati M, Moosavi MA, McDermott MF. ER stress: a therapeutic target in rheumatoid arthritis? *Trends Pharmacol Sci* (2018) 39(7):610–23. doi:10.1016/j.tips.2018.03.010
78. Nakamura T, Kunz RC, Zhang C, Kimura T, Yuan CL, Baccaro B, et al. A critical role for PKR complexes with TRBP in immunometabolic regulation and eIF2alpha phosphorylation in obesity. *Cell Rep* (2015) 11(2):295–307. doi:10.1016/j.celrep.2015.03.021
79. Kurzynska-Kokorniak A, Koralewska N, Pokornowska M, Urbanowicz A, Tworak A, Mickiewicz A, et al. The many faces of Dicer: the complexity of the mechanisms regulating Dicer gene expression and enzyme activities. *Nucleic Acids Res* (2015) 43(9):4365–80. doi:10.1093/nar/gkv328
80. Gross TJ, Powers LS, Boudreau RL, Brink B, Reisetter A, Goel K, et al. A microRNA processing defect in smokers' macrophages is linked to SUMOylation of the endonuclease DICER. *J Biol Chem* (2014) 289(18):12823–34. doi:10.1074/jbc.M114.565473
81. Gelfand BD, Wright CB, Kim Y, Yasuma T, Yasuma R, Li S, et al. Iron toxicity in the retina requires Alu RNA and the NLRP3 inflammasome. *Cell Rep* (2015) 11(11):1686–93. doi:10.1016/j.celrep.2015.05.023

Conflict of Interest Statement: The authors declare that the research was conducted in the absence of any commercial or financial relationships that could be construed as a potential conflict of interest.

Advantages of publishing in Frontiers

OPEN ACCESS
Articles are free to read for greatest visibility and readership

FAST PUBLICATION
Around 90 days from submission to decision

HIGH QUALITY PEER-REVIEW
Rigorous, collaborative, and constructive peer-review

TRANSPARENT PEER-REVIEW
Editors and reviewers acknowledged by name on published articles

Frontiers
Avenue du Tribunal-Fédéral 34
1005 Lausanne | Switzerland

Visit us: www.frontiersin.org
Contact us: info@frontiersin.org | +41 21 510 17 00

REPRODUCIBILITY OF RESEARCH
Support open data and methods to enhance research reproducibility

DIGITAL PUBLISHING
Articles designed for optimal readership across devices

FOLLOW US
@frontiersin

IMPACT METRICS
Advanced article metrics track visibility across digital media

EXTENSIVE PROMOTION
Marketing and promotion of impactful research

LOOP RESEARCH NETWORK
Our network increases your article's readership